SOME SPECTROSCOPIC OBSERVATIONS

OF

MICROWAVE AND RADIO-FREQUENCY PLASMAS

BY

SELWYN LESLIE CASTLEDEN

A thesis submitted for the degree of Doctor of Philosophy in the University of London.

Department of Chemistry,
The Imperial College of Science and Technology,
London SW7 2AY

SOME SPECTROSCOPIC OBSERVATIONS

OF

MICROWAVE AND RADIO-FREQUENCY PLASMAS

BY

SELWYN LESLIE CASTLEDEN

ABSTRACT

The radial distribution of spectral emitters within argon-filled temperature controlled electrodeless discharge lamps operated at 2450MHz is investigated using conventional low resolution spectrometry and, for high resolution measurements, a piezoelectric-scanning Fabry-Perot interferometer. The effect of the source operating parameters upon the extent of self-absorption, the excitation temperature and the radial distribution of intensity is described. The existence of two distinct types of intensity distribution is reported and their origin is discussed in terms of the possible processes occurring inside the lamp envelope. The correlation between the type of intensity distribution and the ionization energy of the element employed is outlined.

Measurements made of the strontium line emitted in an inductively coupled plasma operated at 27MHz are described. Possible reasons for the non-linearity of calibration curves are discussed in terms of the relative populations of atom and ion energy levels. Values of the Doppler temperature measured at various viewing heights in the plasma are reported.

The use of the inverse Abel transform to obtain radial information from lateral data is discussed and an improved curve-fitting technique using B-spline functions is described for this application. A FORTRAN computer program is included for performing the inverse Abel transform.

CONTENTS

Abstract 2

Contents 3

Preface 6

CHAPTER 1: Introduction. 8
1.1: Spectroscopy 9
1.2: Plasmas 9
1.3: Electrodeless Discharge Lamps 13
1.4: Inductively-Coupled Radio-Frequency Argon Plasmas 19
1.5: The Scope of this Work 27
1.6: Units 28

CHAPTER 2: General Theory. 30
2.1: The Origin of Atomic Spectral Lines 31
2.1.1: Summary of Electronic Structure and Nomenclature 31
2.1.2: Hyperfine Structure and Isotope Shift 33
2.1.3: Multiplet Intensity Ratios 36
2.2: The Emission and Absorption of Line Radiation 36
2.2.1: The Boltzmann Distribution 36
2.2.2: The Saha-Eggert Ionization Equilibrium 37
2.2.3: The Intensity of a Spectral Line 38
2.2.4: The Absorption Coefficient 40
2.3: The Width and Shape of Spectral Lines 41
2.3.1: Line Profiles 41
2.3.2: Doppler Broadening 42
2.3.3: Pressure Broadening 43
2.3.4: The Zeeman Effect 46
2.3.5: Self-Absorption Broadening 46
2.4: Fabry-Perot Interferometry 50
2.4.1: General Principles 50
2.4.2: Dispersion 53
2.4.3: Scanning 53
2.4.4: Free-Spectral-Range 56
2.4.5: Intensity Distribution 56
2.4.6: Dielectric Plate Coatings 60
2.4.7: The Theoretical Finesse 61
2.4.8: Contrast of the Fringes 63
2.4.9: Resolving Limit and Resolving Power 63
2.4.10: Deviation from the Theoretical Finesse 65
2.4.11: Light-Gathering Power 66
2.4.12: Auxiliary Dispersion 67
2.4.13: The Effect of Stopping Down the Interferometer 68
2.4.14: Reduction of Measurements 68
2.4.15: The Advantages and Disadvantages of the Fabry-Perot Interferometer as an Instrument for High Resolution Spectroscopy 73

CHAPTER 3: Instrumentation. 76
3.1: Optics 77
3.2: The Electronics 81
3.2.1: High Voltage Photomultiplier Tube Supply 81
3.2.2: Scan Generator 81
3.2.3: Signal Processing 82
3.3: Alignment of the Optical System 88
3.4: Operation 90
3.5: The Measurement of the Finesse 91

CHAPTER 4: The Preparation and Operation of Electrodeless Discharge Lamps 93
4.1: The preparation of Electrodeless Discharge Lamps 94
4.1.1: General 94
4.1.2: The Lamp Blank 94
4.1.3: The Vacuum Apparatus 96
4.1.4: Degassing Procedure 97
4.1.5: Fill Material 98
4.2: The Operation of Electrodeless Discharge Lamps 101
4.2.1: Microwave Supply 101
4.2.2: Resonance Cavities 102
4.2.3: Temperature Regulation 104

CHAPTER 5: Some Observations of Electrodeless Discharge Lamps. 111
5.1: Introduction 112
5.2: Studies made Without Spatial Resolution 112
5.3: The Radial Distribution of Intensity from EDL Sources 116
5.3.1: Experimental 116
5.3.2: Processing of Results 116
5.3.3: General Observations 117
5.3.4: The Effect of the Operating Power upon EDL Operation 123
5.3.5: Different Resonance Cavities 125
5.3.6: The Effect of the Operating Temperature 127
5.3.7: Measurements made at Different Wavelengths 132
5.4: Measurements Made of the Intensities of Hyperfine Components 139
5.4.1: Introduction 139
5.4.2: Lead 140
5.4.3: Indium 146
5.4.4: Mercury 149
5.5: The Measurement of Excitation Temperatures in an Indium EDL 151
5.5.1: Theoretical 151
5.5.2: Procedure 154
5.5.3: Results 154

5.6: Discussion 160
5.6.1: Sputtering 160
5.6.2: The Electrical Skin Depth 161
5.6.3: Self-Absorption in the Centre of the Lamp 163
5.6.4: The Possible Reason for the Existence of the Type B Discharge 165
5.6.5: The Type A Discharge 171

CHAPTER 6: The Measurement of the Strontium Line Half-Width in the Radio-Frequency Plasma. 175
6.1: Introduction 176
6.2: Apparatus 177
6.2.1: Plasma Instrumentation 177
6.2.2: The Optical Arrangement 179
6.3: The Hyperfine Structure of the 407.771nm Sr II Line 181
6.4: Results 183
6.4.1: Calibration Curves for Strontium 183
6.4.2: Line Profile Measurements Made With Lateral Resolution 184
6.4.3: Line Profile Measurements Made With Vertical Resolution 188
6.4.4: Measurement of the Doppler Temperature at Different Viewing Heights 189
6.5: Discussion 195

CHAPTER 7: The Transformation of Lateral to Radial Distributions of Intensity 202
7.1: Introduction 203
7.2: The Abel Integral 204
7.3: Curve Fitting Techniques 207
7.4: The Integration Procedure 212
7.5: A Computer Program to Perform the Inverse Abel Transform 213
7.6: Obtaining Radial Information in the Absence of Symmetry 215

CHAPTER 8: Conclusions and Suggestions for Further Work. 216

Appendix: A Computer Program for the Inverse Abel Transform. 223

References 239

PREFACE

The work described in this thesis was carried out in the Chemistry Department of The Imperial College of Science and Technology between October 1975 and August 1978. It is entirely original except where due reference is made,and no part has been submitted previously for any other degree.

I wish to thank my supervisor,Doctor G.F.Kirkbright, for his constant advice and encouragement throughout this work. Gratitude is also expressed to the Science Research Council for their financial support.

Acknowledgement is due to my colleagues and friends in the Chemistry Department,in particular R.M.Bombelka, J.C.Burgess,D.L.Millard and R.D.Snook,for their helpful suggestions.

'Well,in our country,'said Alice,still panting a little, 'you'd generally get to somewhere else- if you ran very fast for a long time,as we've been doing.'

'A slow sort of country!'said the Queen. 'Now,here,you see,it takes all the running you can do,to keep in the same place. If you want to get to somewhere else,you must run at least twice as fast as that!'

Through the Looking Glass,
LEWIS CARROLL.

CHAPTER ONE

INTRODUCTION.

1.1 Spectroscopy 9

1.2 Plasmas 9

1.3 Electrodeless Discharge Lamps 13

1.4 Inductively-Coupled Radio-Frequency Argon Plasmas 19

1.5 The Scope of this Work 27

1.6 Units 28

1.1 SPECTROSCOPY.

Although spectroscopy was conceived by Newton in his publication[1] of 1704 it was not envisaged for many years that it would be possible to determine the identity, the environment and the structure of atoms and molecules by analysing the radiation emitted or absorbed by these species. It was not until about 1860 that Bunsen and Kirchhoff[2-4] confirmed the link between particular atoms and particular wavelengths of radiation.

When the radiation emitted by atoms is analysed by wavelength it is found to consist of discrete lines and bands which may lie superimposed upon a continuum. The appearance of a particular line or band establishes the presence of the species of which it is characteristic. Therefore, a study of the wavelengths present identifies the species present whilst a study of their relative intensities establishes concentrations.

The establishment of the physical properties of the radiating gas or plasma is important because these physical properties affect the wavelength and intensity distributions.

1.2 PLASMAS.

The familiar states of matter on the surface of the Earth are the solid, the liquid and the gas. Chemical reactions are the most common energy releasing processes and temperatures of up to ca. 5000K may result, corresponding to an average thermal energy of ca. 0.5electron-volts. Natural phenomena of higher energy than this are observed only relatively infrequently. The atmospheric lightning

discharge is one example in which ionization of a gas takes place as the result of very large electric fields. The ions and electrons thus produced allow a flow of charge to take place. Following the discharge,when the charge flow is complete,there is recombination between the ions and electrons. In 1879 Sir William Crookes suggested that the ionized gas present during the discharge constituted a fourth state of matter. Later,Langmuir,amongst others,used the term plasma to describe this state.[5]

The term plasma has a general meaning which is used to describe a hot gas,regardless of its degree of ionization. The precise definition of a plasma requires that it is distinguished from a hot gas by the importance of collective effects. The overall charge of the plasma must be zero as it can easily be shown[6] that net charge would require a potential of many thousand volts between freely moving particles. Therefore it is necessary to consider very small distances before the random thermal motion of ions and electrons results in any momentary inbalance of charge. This distance,which is known as the Debye shielding radius, is a characteristic of a particular plasma and corresponds to the distance to which the electric field of an individual ion or electron extends before it is effectively screened by adjacent particles of opposite charge. Therefore,one criterion for the existence of a plasma is that the Debye shielding radius is much smaller than the physical dimensions of the plasma.

Another important parameter in specifying the magnitude of collective effects is the plasma frequency.

The plasma frequency is the resonance frequency for the collective oscillations of the free electrons about their equilibrium positions. These collective oscillations tend to disappear if the motions of the electrons are randomized by collisions. Therefore,a necessary condition for the existence of a plasma frequency is that the collision frequency must be much smaller than the classical resonance frequency.

When the temperature of a gas is increased the kinetic energy of the atoms and molecules increases. Further increases in the temperature result in molecules dissociating into atoms, atoms becoming excited and eventually ionizing. Even further increases in the temperature result in more advanced stages of ionization,species being excited to higher energy states and the kinetic energy of the free electrons increasing. The distribution of kinetic energy between particles is given by the Maxwell distribution[7] and the distribution of population between quantized energy levels is given by the Boltzmann equation. The Saha equation gives the relative populations in different stages of ionization if the system is in equilibrium. These equations are discussed in greater detail in Section 2.2.

There are essentially two distinct types of process by which energy may be transferred to or from an atom or ion: by collision or by radiative transfer.These processes are outlined diagrammatically in Figure 1.1,in which energy is transferred between energy levels E_1 and E_2,having population densities of N_1 and N_2 respectively.

Each form of energy distribution is characterized by

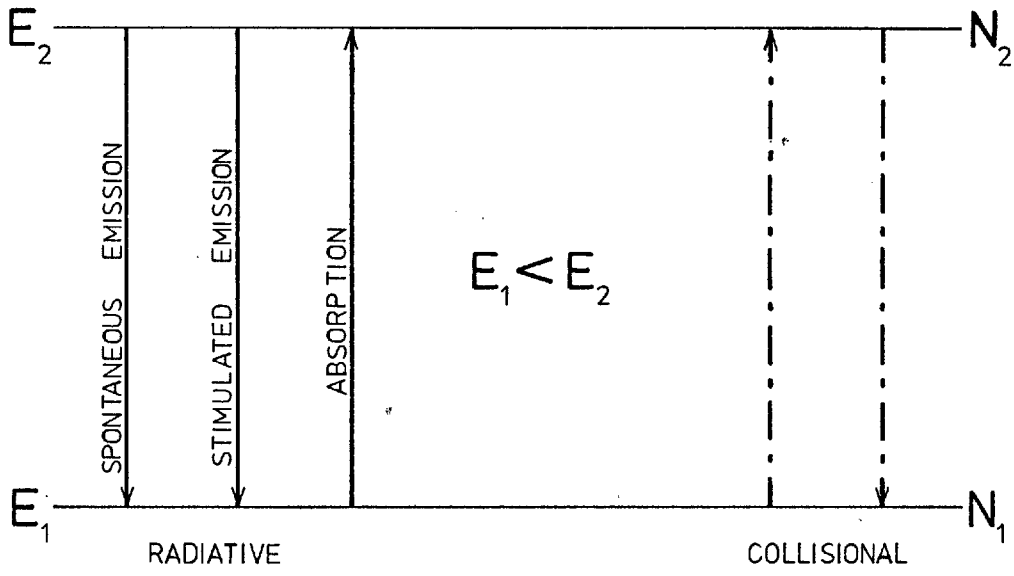


Figure 1.1: Energy transfer processes.

a temperature specified by the appropriate equation mentioned above. However, it may happen that one particular equilibrium process will have a different temperature from another. For example, the ionization temperature specified by Saha's equation for the measured number densities may not agree with the kinetic temperature of the gas. For a system to be in complete thermodynamic equilibrium all the individual equilibria must be characterized by the same temperature. For every particle undergoing spontaneous or stimulated emission there must also be a particle absorbing radiation. The number of collisional energy transfer events between E_2 and E_1 in Figure 1.1 must be balanced for both directions. In this situation, because there would be no net emission or absorption, the plasma would be invisible. Clearly, this is not possible in practice although the conditions for complete equilibrium could be approached if the radiative energy losses were small in comparison

with the total energy of the system. In addition, line spectra could not be observed because radiative equilibrium requires the plasma to be optically thick at all wavelengths.

It is possible for a plasma to be in local thermodynamic equilibrium (LTE) when there is not radiative equilibrium. In this case collisional processes dominate radiative transfers and a single temperature specifies the equilibria given by the Maxwell, Boltzmann and Saha equations for the gas kinetic distribution and the populations of excited and ionized states. The probability of a species in an excited state being de-excited must be much greater by an inelastic collision than by spontaneous emission of radiation.

In a corona the electron temperature is high and the electron density is low resulting in the electrons having enough energy to cause excitation by a single inelastic collision and a relatively large mean-free-path so that the excited species has a high probability of undergoing spontaneous emission. The density of radiation is also low so that excitation and ionization take place primarily by collision and de-excitation takes place by spontaneous emission.

1.3 ELECTRODELESS DISCHARGE LAMPS.

The electrodeless discharge lamp (EDL) consists of a sealed silica bulb containing a metal or metal compound and filled with a noble gas at a pressure of a few torr. The construction and operation of these lamps will be discussed further in Chapter Four.

The use of an electrodeless discharge lamp was first mentioned by Hittorf[8] in 1884 and they were subsequently used by physicists as atomic spectral sources. In 1946 Wiens, Meggers et al.[9-12] used an EDL to investigate the suitability of the 546.07nm line of ^{198}Hg as a wavelength standard and an ultimate standard of length. However, this line was not successful in competition with the orange line of ^{86}Kr (605.78nm), which was chosen as a wavelength standard in 1960.

In 1964 Winefordner and Staab[13] reported the use of electrodeless discharge lamps to excite atomic fluorescence for analytical purposes.

Table 1.1 shows the elements for which electrodeless discharge lamps have been prepared and where these lamps have been used in an analytical application, either in atomic fluorescence or atomic absorption spectroscopy. Electrodeless discharge lamps have been used to the greatest extent in atomic fluorescence spectroscopy[14-37] because of their high intensity and relative freedom from self-absorption compared with hollow cathode lamps and high intensity hollow cathode lamps. In atomic fluorescence spectroscopy the requirement is for a high intensity and stable source emitting a spectrum relatively free from lines due to the filler gas and contamination. The latter point is important in making measurements with non-dispersive equipment. The atomic fluorescence signal is directly proportional to the incident radiation intensity, although the narrowness of the spectral lines emitted is less important than in atomic absorption spectroscopy.

TABLE 1.1: Elements for which EDL's have been prepared.

																	He
Li	¶ Be[14,15]																Ne
Na	¶ Mg[16,17]											¶ Al[18]	¶ Si[19]	P § [28]	S[28] § [41]	Cl†	Ar
K	¶ Ca[16]	Sc	¶ Ti[18]	¶ V[18]	¶ Cr[16]	¶ Mn[16,20]	¶ Fe[16,21]	¶ Co[16,22]	¶ Ni[16]	Cu	¶ Zn[16]	¶ Ga[16,23]	¶ Ge[24]	¶ α As § α	¶ β Se § β	Br†	
Rb	¶ Sr[16]		¶ Zr[18]		¶ Mo[18]				Pd	¶ Ag[16]	¶ Cd[16]	¶ In[28]	¶ Sn[29]	¶ Sb[16,30]	¶ Te[16,31]	I § γ	
Cs	Ba		Hf						Pt	¶ Au[16]	¶ δ Hg § δ	¶ Tl[16,32]	¶ Pb[34] §	¶ ε Bi			

Th		U	

¶ EDL has been used in analysis by atomic fluorescence spectrometry.
§ EDL has been used in analysis by atomic absorption spectrometry.
† Lamps containing chlorine and bromine have been prepared by the Author but they have produced only molecular band spectra.

α 25,42,43
β 26,27,16,42
γ 28,44,45
δ 16,32,33,46
ε 16,35,36,37

The numbers are references in the Bibliography.

There will be a maximum of fluorescence yield when the line profile of the source matches the profile of the absorption coefficient in the fluorescence cell.

Electrodeless discharge lamps have become more important recently in atomic absorption spectroscopy, especially for those elements for which hollow cathode lamps have proven difficult to prepare or where a satisfactory signal-to-noise ratio has been difficult to achieve.[38,39] In atomic absorption spectroscopy an important requirement is that the half-width of the source emission line is much smaller than the profile of the absorption coefficient in the analyte cell. This produces the requirement for an absolute minimum of self-absorption in the source, although a reduction in the emission of the source is acceptable if the signal-to-noise ratio is not degraded.

Apart from the multitude of papers describing the preparation and operation of electrodeless discharge lamps, and the review by Haarsma *et al.*[50] some more recent papers[47-49] have discussed the benefits that may be obtained by operating lamps in a temperature controlled environment.

The ability of the EDL to produce relatively narrow spectral lines has been attributed[51,52] to the presence of a *skin* just inside the inner surface of the lamp from which the most intense emission occurs. This theory would predict that any self-absorption would be small because of the short path length travelled by the radiation before escaping from the lamp. However, this prediction

was not substantiated experimentally. Browner and Winefordner[47] measured the lateral distribution of intensity for mercury, manganese, thallium and zinc lamps but they did not make any corrections for the optical depth viewed. They observed that zinc, manganese and thallium lamps showed a skin discharge under certain operating conditions whilst a mercury lamp did not.

Avni and Winefordner[53] measured various plasma parameters using double floating electric probes and evaluated the line reversal temperature of thallium atoms. They also deduced that, although the plasma was operating under steady-state conditions, it was not in LTE and appeared to have a small positive space charge.

Busch and Vickers[54] have measured plasma parameters in a low pressure microwave-induced plasma and postulated some possible excitation mechanisms. They suggested that an ionization-radiative recombination would lead to two groups of electrons: one of high energy and low density and the other of low energy and high density, both having different Maxwellian velocity distributions. Therefore, there would be two characteristic electron temperatures.

$$\text{IONIZATION} \qquad M + e \rightarrow M^{+} + e + e$$

$$\text{RADIATIVE RECOMBINATION} \qquad M^{+} + e \rightarrow M^{*} + h\nu_{\text{continuum}},$$

where M* represents an excited atom.

These workers suggested that their measurements of the spectroscopic temperature relate to the average energy of

the low-energy electron group whilst their probe measurements of the electron temperature relate to the high energy group. The role of metastable argon atoms was also discussed. The possibility of direct excitation by collisions of the second kind between metastable argon atoms and metal atoms, vis.,

$$M + Ar_{metastable} \rightarrow M^* + Ar + \text{kinetic energy},$$

was discounted because of the large energy difference between the colliding partners resulting in a low probability of fruitful collisions taking place. It was also suggested that metastable argon atoms might be important in the ionization process via the Penning ionization reaction,

$$Ar_{metastable} + M \rightarrow Ar + M^+ + e.$$

In a more recent paper Kawaguchi, Atsuya and Vallee [55] suggested that both dissociation of a metal halide and ionization of the metal occurs simultaneously rather than stepwise. They considered the following reactions in a helium microwave plasma at low pressure,

$$MCl + e \rightarrow M^+ + Cl + e + e$$

and

$$He_{metastable} + MCl \rightarrow He + M^+ + Cl + e,$$

where M is a metal, MCl is a metal chloride and $He_{metastable}$ is a metastable helium atom.

In an extension of the work by Busch and Vickers,[54]

Brassem and Maessen[55,56] measured the electron temperatures and electron densities in monatomic and polyatomic gas plasmas operating in the pressure range 0.05 to 2 torr. They observed that the electron temperature and the electron density both decreased as the pressure increased; the electron temperature reached very high values at 0.5 torr. Whilst the electron temperature appeared to be independent of the operating microwave power, the electron density was found to increase with power.

Analysis performed by sealing a sample in an electrodeless discharge lamp and observing the atomic emission was reported by Aldous et al.[57], and subsequently by Agterdenbos et al.[58-60] More recently Agterdenbos et al.,[61] reported the detection of $1\text{-}10^3$ pg cm^{-3} of some metals with a relative standard deviation of ca.10% using this technique. Hydrogen was used as the filler gas and the use of BiI_3 and CsI as excitation buffers was discussed. A similar study was carried out by Eckert,[62] who used spherical lamps of 35mm and 46mm internal diameter operated at 27MHz by inductive coupling. Temperatures measured by the two-line method were found to vary in the range 4000 to 8500K.

1.4 INDUCTIVELY-COUPLED RADIO-FREQUENCY ARGON PLASMAS.

The results of Babat's research into electrodeless discharges produced by alternating magnetic fields were published in 1942.[63,64] Amongst other conclusions he decided that it was necessary for the wavelength of the exciting oscillation, i.e. the electromagnetic field, to

exceed the smallest dimension of the cell containing the plasma. It was also found that the amount of power required to sustain a plasma decreased as the frequency was increased.

In the early 1960's Reed[65] developed a silica torch which could maintain an inductively-coupled plasma (ICP) operated at 4MHz and 10kW in pure argon and argon mixtures. Although Reed had realized the potential usefulness of the ICP as a spectroscopic source for optical emission spectroscopy, the initial analytical evaluation and development was carried out by Greenfield et al.[66-68] in England and by Fassel et al.[69-73] in Iowa, U.S.A. These studies have been extended by these and other authors [74-113] and reviews have been published.[114/5] A list of the elements which have been determined by optical emission spectroscopy with an ICP source is given in Table 1.2.

A number of authors have recently measured temperatures and electron densities in the argon ICP with the intention of increasing understanding of the excitation mechanism for analyte species in this source.†

Alder and Mermet[79] measured C_2 rotational temperatures in a methane-argon plasma (10%CH_4) and reported values of 6100K ±700K. Argon excitation temperatures were also found to be in the range 5000-7000K ±400K, but the authors were unable to draw any firm conclusions regarding the extent of thermal equilibrium. The necessity of using the inverse Abel transform to obtain radial temperature distributions was also discussed. In the spectral region 280-600nm all the expected Ar I and hydrogen lines were

†[79, 81, 80, 85, 86, 87, 94, 106, 111]

TABLE 1.2: Elements analysed by ICP optical emission spectroscopy.

							*	*									
Li	Be											B	*	*	*	*	*
Na	Mg											Al	Si	P	S	*	*
K	Ca	Sc	Ti	V	Cr	Mn	Fe	Co	Ni	Cu	Zn	Ga	Ge	As	Se	*	*
*	Sr	Y	Zr	Nb	Mo	*	Ru	Rh	Pd	Ag	Cd	In	Sn	Sb	Te	*	*
*	Ba	La	Hf	Ta	W	Re	Os	Ir	Pt	Au	Hg	Tl	Pb	Bi	*	*	*
*	*	*															

Ce	Pr	Nd	Pm	Sm	Eu	Gd	Tb	Dy	Ho	Er	Tm	Yb	Lu
Th	*	U	*	*	*	*	*	*	*	*	*	*	*

observed but there was a complete absence of Ar II emission. The highest level from which emission was observed was at about 15.4eV above the ground state of Ar I whilst the lowest levels from which Ar II lines could have been observed are at ca. 19.2eV above the ground state of Ar II. From these pieces of information, and assuming that electrons alone were responsible for excitation, the deduction was made that there must be an upper limit of about 19eV to the kinetic energy of the electrons in the plasma.

Kornblum and de Galan[81] described an experimental arrangement which permitted the measurement of axial and radial distributions of temperature, electron density and element concentrations in an ICP source operated at 50MHz and 2kW. Desolvation of the sample aerosol by the method previously described by Fassel et al.[73] was also used. Results were presented for a series of elements showing the lateral distributions of intensity. Radial distributions of electron density, derived from continuum measurements, and temperatures for argon excitation were also presented as well as rotational and vibrational temperatures from the OH band emission around 310nm. The effect of the introduction of the sample stream into the plasma was also discussed. The temperature and the electron density measured without the sample flow were found to exhibit a "smooth shape". The introduction of the sample stream caused a considerable decrease in the temperature measured in the middle of the plasma and this connected the visually observed "doughnut" shape with a measured

temperature distribution. The sample introduction was also found to cause a constriction of the plasma between the sample stream and the walls, resulting in the power being concentrated in a smaller volume than before and hence producing higher temperatures. Zinc and argon excitation temperatures were found to be higher than the values of the OH-rotational temperature. The authors did not feel able to draw firm conclusions regarding the extent of LTE; further observations were thought to be necessary.

Scott et al.,[80] discussed the optimum relationship between the operating frequency, ν, and the plasma radius, r. They used the well known relationship between the skin depth, s, i.e. the depth in the plasma at which the induced annular current density has decreased to 1/e th., of its surface value, and the frequency,

$$s(cm) = 5.03/\sqrt{(\mu\sigma\nu)}.$$

In this expression μ is the relative permeability and σ is the specific electrical conductivity ($\Omega^{-1}cm^{-1}$) of the plasma. The desired relationship between the frequency and the plasma radius was obtained as,

$$\nu r^2 = 128/\mu\sigma .$$

The figures obtained were as follows:

Frequency	27MHz
RF power	1kW
Argon coolant flow	$10 dm^3 min^{-1}$
σ	$10\ \Omega^{-1}cm^{-1}$
Skin depth	0.03cm
Plasma radius	0.8cm.

Temperature measurements were also made;the plasma was assumed to be in LTE. A calibration curve for copper indicated negligible self-absorption up to an analyte concentration of ca. 1000μg cm^{-3}. Greenfield et al.;[88] have demonstrated that the central channel in the plasma can be produced just as easily in a plasma at 7MHz as in one at 36MHz and have produced photographs showing the two resulting annular plasmas to be very similar. The latter authors have expressed the opinion that the tunnel-effect is more a function of injector gas flow rate than of skin-depth and the application of the "optimum frequency to radius ratio" [80] has sometimes led to plasma instability.

Mermet[85] found that the excitation temperatures measured for Ar I lines did not match the ionization temperatures calculated using the Saha equation and measured values of the electron density. The observation was made that LTE did not exist in the plasma under these operating conditions.

Barnes and Schleicher[86] developed models of the ICP for conditions important in spectrochemical analysis. These models accounted for the spatial distribution of gas properties,major energy loss processes,realistic gas flows and sample particle motion and decomposition. Computer simulations based upon these models were used to provide spatial temperature,gas velocity,sample concentration and radiation distributions for a number of different sets of experimental conditions. Other papers have also been published by Barnes et al., on this subject.[112,113]

In 1975 Fassel et al.;[87] made spatially resolved

temperature measurements in more detail and with better precision than those previously reported by Kornblum and de Galan.[81] Iron (Fe I) was used as the thermometric species because it is a typical analyte and its transition probabilities are more accurately known than for many other elements. The existence of LTE was assumed but no attempt was made to justify this in their particular experimental system.

Zeeman et al.,[94] also made spatially resolved temperature measurements, but this time in an argon-hydrogen ICP. Measurements were made at the Hβ (486.1nm), Hγ (434.0nm) and Hδ (410.2nm) lines using the two-line temperature method for the pairs Hβ/Hγ, Hγ/Hδ and Hβ/Hδ. The values of the temperature obtained using these pairs differed considerably, resulting in the conclusion that the plasma was not in LTE.

Boumans and DeBoer[107] made measurements of the intensity ratios of ionic and atomic lines of various elements and compared them with values of the excitation temperature for zinc and a literature value of 10^{16} cm^{-3} for the electron density. The conclusion was reached that departure from LTE in the argon ICP was observed under analytical conditions. The departure from LTE was suggested to be the principal ground for some of the favourable analytical properties of the ICP, e.g. the high sensitivity of ionic lines and the small extent of ionization interference. The suggestion was made that both of these characteristics are inter-related with an overpopulation of metastable argon levels resulting from

the mixing of cold (injector gas) and hot argon. The metastable argon atoms would be responsible for the production of a population of ionic levels,by Penning ionization,being higher than predicted by thermal population. The same cause would also result in an higher electron density than the value predicted by assuming the ionization to be purely the result of electron impact. The relatively small interference effects caused by the introduction of easily ionized elements could be explained by the electron density being higher than expected. However,it remains to be shown experimentally that a large overpopulation of metastable argon levels exists and that Penning ionization is a dominant process.

Mermet et al.[110] recently made more measurements of the physical properties of the ICP source and comparisons were made with literature values. Some of these results are given in Table 1.3. Other authors were also criticised for the non-rigorous use of the Saha and Boltzmann equations in non-LTE plasmas. The significant difference between the values of the ionization and excitation temperatures is reported to confirm the absence of complete LTE in the ICP source.

TABLE 1.3: Some physical properties of ICP sources.

OPERATING FREQUENCY	TEMPERATURE IONIZATION	TEMPERATURE EXCITATION	ELECTRON DENSITY
40MHz	6800-7300K	4800K	5.5×10^{14} cm^{-3}
5MHz	8600K	6200K	3.5×10^{15} cm^{-3}

Montaser and Fassel[96] demonstrated the use of an ICP source as an atomization cell for atomic fluorescence spectrometry. The atomic fluorescence signals for cadmium and zinc were found not to be affected by the presence of 10000μg cm^{-3} of 17 different species. The atomic fluorescence detection limits were found to be superior to those obtained by atomic emission by a factor of 2-8 for cadmium, zinc and mercury.

Human and Scott[95] made measurements of the temperature in the ICP source derived from Doppler half-widths. At observation heights of 20mm and above, the ICP source was found to resemble a flame with a layer of absorbing atoms around the central emission region. Low in the plasma, the core was assumed to be a predominantly absorbing region whilst emission originated from an annulus around the core. The possibility of the effects of self-absorption and self-ionization counteracting each other and producing a linear calibration graph was suggested.

Kornblum and deGalan[106] used values of the Doppler half-width to calculate temperatures, avoiding the need to use transition probabilities.

1.5 THE SCOPE OF THIS WORK.

Chapter Two of this thesis consolidates the theory, which will be of use in later chapters. The nature of spectroscopy is such that a surfeit of mathematics is almost inevitable for its discussion. In Chapter Two an attempt has been made to limit the number of equations to those which will be required and to those which are

deemed necessary for a satisfactory explanation. Chapter Two has been divided into four main sections dealing with the origin of atomic spectral lines and, especially, hyperfine multiplets; the total energy emitted in an atomic spectral line; the frequency distribution of the emitted energy and the theory of interferometry.

Chapter Three describes the instrumental manifestation of the interferometric measurements whilst Chapter Four concerns the preparation of electrodeless discharge lamps used in this work and their operation under temperature control.

Chapters Five and Six relate to the observations made of the electrodeless discharge lamps and the radio-frequency inductively-coupled argon plasma.

Chapter Seven discusses the problems involved in obtaining radial information from the lateral observation of spectral sources.

1.6 UNITS.

As far as is possible and sensible the units used in this work conform to the S.I. convention. Exceptions to the pedantic application of this policy have been made where other units are more useful and appropriate. The electron-volt (eV) is often used as a unit of energy in spectroscopy because of its more suitable magnitude compared with the Joule. In the current literature the electron density is quoted in cm^{-3} instead of in m^{-3}, gas pressures are quoted in p.s.i. instead of Pascals and the Kayser (cm^{-1}) is used as a unit of wavenumber.

Although wavelength has been used in discussions where its use is appropriate,most expressions have been derived either in terms of the frequency or the wavenumber. The avoidance of wavelength facilitates many simplifications in expressions relating to interferometry.

CHAPTER TWO

GENERAL THEORY.

2.1 The Origin of Atomic Spectral Lines 31
- 2.1.1 Summary of Electronic Structure and Nomenclature 31
- 2.1.2 Hyperfine Structure and Isotope Shift 33
- 2.1.3 Multiplet Intensity Ratios 36

2.2 The Emission and Absorption of Line Radiation 36
- 2.2.1 The Boltzmann Distribution 36
- 2.2.2 The Saha-Eggert Ionization Equilibrium 37
- 2.2.3 The Intensity of a Spectral Line 38
- 2.2.4 The Absorption Coefficient 40

2.3 The Width and Shape of Spectral Lines 41
- 2.3.1 Line profiles 41
- 2.3.2 Doppler Broadening 42
- 2.3.3 Pressure Broadening 43
- 2.3.4 The Zeeman Effect 46
- 2.3.5 Self-Absorption Broadening 46

2.4 Fabry-Perot Interferometry 50
- 2.4.1 General Principles 50
- 2.4.2 Dispersion 53
- 2.4.3 Scanning 53
- 2.4.4 Free-Spectral Range 56
- 2.4.5 Intensity Distribution 56
- 2.4.6 Dielectric Plate Coatings 60
- 2.4.7 The Theoretical Finesse 61
- 2.4.8 Contrast of the Fringes 63
- 2.4.9 Resolving Limit and Resolving Power 63
- 2.4.10 Deviation from the Theoretical Finesse 65
- 2.4.11 Light-Gathering Power 66
- 2.4.12 Auxiliary Dispersion 67
- 2.4.13 The Effect of Stopping Down the Interferometer 68
- 2.4.14 Reduction of Measurements 68
- 2.4.15 The Advantages and Disadvantages of the Fabry-Perot Interferometer as an Instrument for High Resolution Spectroscopy 73

2.1 THE ORIGIN OF ATOMIC SPECTRAL LINES.

2.1.1 Summary of Electronic Structure and Nomenclature.

An electron in an atom is characterized by a set of four quantum numbers n,l,m_l,m_s, where n is the principal quantum number, l is the quantum number representing the orbital angular momentum, m_l is the quantum number for the component of the orbital angular momentum in a particular direction and m_s is the quantum number representing the spin in a particular direction. The Pauli Exclusion Principle forbids more than one electron in a particular atom to have the same set of quantum numbers. m_s is derived from the spin angular momentum quantum number, s, which always has the value $\frac{1}{2}$. In addition, spin-orbit interactions occur, resulting from magnetic interaction between the magnetic moment due to spin and the magnetic moment due to orbital angular momentum. The result of this interaction is that l and s are coupled to give a new inner quantum number, $j=l\pm s$. The properties of these quantum numbers are summarized in Table 2.1.

TABLE 2.1: Quantum numbers for a single electron.

QUANTUM NUMBER	SYMBOL	No. POSSIBLE VALUES	POSSIBLE VALUES	COMMENTS
PRINCIPAL	n		1,2,.....	
ORBITAL ANGULAR MOMENTUM	l	n	0,...,n-1	
MAGNETIC	m_l	2l+1	+1,...,0,...,-1	in z direction
SPIN ANGULAR MOMENTUM	s	1	$\frac{1}{2}$	
SPIN	m_s	2	$\pm\frac{1}{2}$	in z direction
INNER	j	2	$l+\frac{1}{2}$, $l-\frac{1}{2}$	spin-orbit

In a multi-electron atom the individual quantum numbers combine to give resultant quantum numbers. The resultant quantum numbers are summarized in Table 2.2.

TABLE 2.2: Quantum numbers in a multi-electron atom.

QUANTUM NUMBER	SYMBOL	POSSIBLE VALUES
RESULTANT ORBITAL ANGULAR MOMENTUM	L	$\|l_1\|+\|l_2\|+\|l_3\|+\ldots \to 0$
RESULTANT SPIN	S	$s_1 + s_2 + s_3 + \ldots$
RESULTANT INNER	J	L+S, L+S-1, ..., |L-S|. 2L+1 values.

Each possible combination of the quantum numbers results in a possible energy level or term, which is given a label reflecting the values of the quantum numbers involved. The label takes the form of a letter with superscripts and a subscript. The letter gives the value of L according to the conversion:

0	1	2	3	4	5	6	.....
S	P	D	F	G	H	I	.....

The left superscript is the value of the multiplicity, given by 2S+1. The right superscript indicates the parity of the term, odd parity being indicated by an o. The parity of a term is $(-1)^{\Sigma l}$, where Σl is the sum of the individual l values. The right subscript is the value of J for the term.

Spectral lines are the result of radiative transitions between terms and, in the simplest case, are governed by the Russell-Saunder's coupling scheme. In this scheme the

resultant quantum numbers L and S are obtained as previously described and then combined to form a resultant J. Transitions between terms are only permitted if certain selection rules are obeyed. These are

$$\Delta J = 0, \pm 1 \quad \text{with } J=0 \not\rightarrow J=0 \quad \text{forbidden,}$$

$$\Delta L = \pm 1$$

and $$\Delta S = 0.$$

Additionally, transitions can only take place between terms of opposite parity. The ΔJ rule is normally obeyed but the ΔL and ΔS rules are sometimes broken, particularly in the heavier elements where Russell-Saunder's coupling is not a good description.

For the higher terms of heavier elements the quantities L and S loose their significance because of spin-orbit interactions at the single electron level. In this case the values of s and l combine to form j and a resultant for the whole atom is obtained by summing all the j values. This is the basis for the j-j coupling scheme.

2.1.2 Hyperfine Structure and Isotope Shift.

There are two effects which may result in the differences observed when an atomic spectral line is viewed under high resolution rather than ordinary resolution. These are shifts which result from the different isotopes of an element present and hyperfine structures relating to nuclear spin effects.

Hyperfine structures are the result of interaction between the total angular momentum of the electrons and

the nuclear spin angular momentum. The nuclear spin angular momentum has an associated quantum number I. Coupling between J and I causes further splitting in the terms and, consequently, in the spectral lines. The quantum number I is a constant which is characteristic of any given isotope of an element. It has half-integral and integral values for nuclei of odd and even mass numbers respectively. Nuclei with an even number of neutrons and protons have always been observed[116] to have the value I=0. I is associated with the angular momentum, $\tilde{I}$, of the nucleus by

$$\tilde{I} = \hbar \sqrt{I(I+1)} \quad . \qquad (\hbar = h/2\pi) \qquad 2.1$$

The coupling of $\tilde{I}$ with $\tilde{J}$ may be demonstrated by the vector addition in Figure 2.1 to produce an overall total angular momentum, $\tilde{F}$, of the atom including the nucleus. With $\tilde{F}$ is associated the hyperfine structure

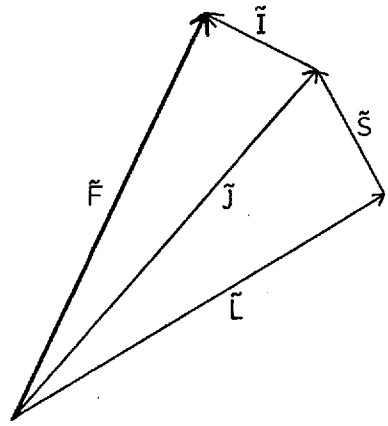


Figure 2.1: The relationship between the vectors $\tilde{L}, \tilde{S}, \tilde{J}, \tilde{I}$ & $\tilde{F}$.

quantum number,F,by the relation

$$\tilde{F} = \hbar \sqrt{F(F+1)}, \qquad 2.2$$

where F can have the values $J+I, J+I-1, \ldots, |J-I|$. Therefore,a particular multiplet level,of given J,splits into 2I+1 (for I<J) or 2J+1 (for I>J) levels. The selection rule for transitions between hyperfine levels is

$$\Delta F = 0,\pm 1 \quad \text{with } F=0 \nrightarrow F=0 \text{ forbidden.}$$

Isotope shifts are due to two different causes, the difference in the nuclear mass between different isotopes and the differences in the charge distribution in the nucleus. The mass shift is only appreciable for the lighter elements,a change in the mass number being insignificant for heavy nuclei. Conversely,the shift due to changes in the charge distribution is only important for heavy elements.

To a first approximation,the effect of isotopic mass differences upon a transition is given by[116]

$$\Delta\sigma/\sigma = \Delta\{1/(1+ m/M)\} \qquad 2.3$$

where, $\Delta\sigma$ is the shift in Kaysers about the wavenumber σ, m is the mass of the electron and M is the mass of the isotope. The line due to the heavier isotope has the greater wavenumber.

Therefore, as a result of the above effects,each isotope will have its own set of hyperfine structure components and these sets will be displaced relative to each other for different isotopes.

2.1.3 Multiplet Intensity Ratios.

The intensity ratio of multiplet transitions is given by the sum rule.[116]

"For the transition between two term multiplets, the two sums of intensities of all transitions from any one level and from any other level are in the ratio of the statistical weights of the two levels."

The statistical weight of a level is 2J+1 and of a hyperfine level is 2F+1. Within a hyperfine multiplet the ratios of the sums of the intensities of all transitions from two states with quantum numbers F and F' are in the ratio of their statistical weights: (2F+1)/(2F'+1). The hyperfine multiplets follow the sum rule very much more closely than ordinary multiplets.

2.2 THE EMISSION AND ABSORPTION OF LINE RADIATION.

2.2.1 The Boltzmann Distribution.

If a system is in thermal equilibrium at a temperature T, then the ratio of the number of atoms occupying two energy levels, E_2 and E_1, is given by

$$N_2/N_1 = (g_2/g_1)\ \exp\{-(E_2-E_1)/kT\}, \qquad 2.4$$

where, g_2 and g_1 are the statistical weights of the two levels. The values N_2 and N_1 are the number densities of the higher and lower energy levels respectively, so that the total number density, N, may be expressed in terms of the number densities of each energy level:

$$N = N_0 + N_1 + N_2 + N_3 + \ldots \qquad 2.5$$

In this expression, N_0 is the number density of the ground state. It is often more convenient to express the population of a particular state in terms of the total number density. This may be done by defining a partition function

$$U(T) = \sum_{j=0}^{\infty} g_j \exp\{-E_j/kT\} . \qquad 2.6$$

this gives the population of the jth. energy level to be

$$N_j = \frac{N}{U(T)} g_j \exp\{-E_j/kT\} . \qquad 2.7$$

At moderate temperatures the partition function, U(T), converges rapidly and only the first few terms need be included in Equation 2.6. Tables of the partition function have been published by Drawin and Felinboch.[117]

2.2.2 The Saha-Eggert Ionization Equilibrium.

The Boltzmann distribution may be extended to the ionization equilibrium, giving an equation known as the Saha equation. If the number densities of atoms in the zth. and (z+1)th. stages of ionization are N_z and N_{z+1}, respectively, and the electron density is N_e ,

$$\frac{N_e N_{z+1}}{N_z} = \frac{2(2\pi mkT)^{3/2}}{h^3} \frac{U_{z+1}}{U_z} \exp\{-\chi/kT\} . \qquad 2.8$$

In Equation 2.8 U_{z+1} and U_z are the appropriate partition functions, χ is the ionization energy for $M^{z+} \rightarrow M^{(z+1)+} + e$, and m is the rest mass of the electron; the other symbols having their usual meanings.

It is important to remember that the value N_{z+1}

refers to the total number density of ions of charge z+1 irrespective of their particular energy levels. The Boltzmann equation must be used to determine the population of a particular level.[6] In general, it is seldom necessary to consider more than two successive stages of ionization; by the time N_{Z+1} is appreciable N_{Z-1} is usually negligible.

2.2.3 The Intensity of a Spectral Line.

The specific intensity of a spectral line, I_ν, may be defined as the energy crossing unit area in unit time per unit solid angle per unit frequency interval.[6] The integral of I_ν with respect to frequency is the total intensity, I. The specific intensity is often referred to as the radiance. Another important quantity is the energy density per unit frequency interval, ρ, defined by Plank's law.[6] This is related to the specific intensity by

$$I_\nu = \frac{c}{4\pi} \rho_\nu \qquad 2.9$$

The energy density has units of joule/metre^3.

A radiative transition between two energy levels in an atom may take place by one of the intrinsic processes shown in Figure 2.2.

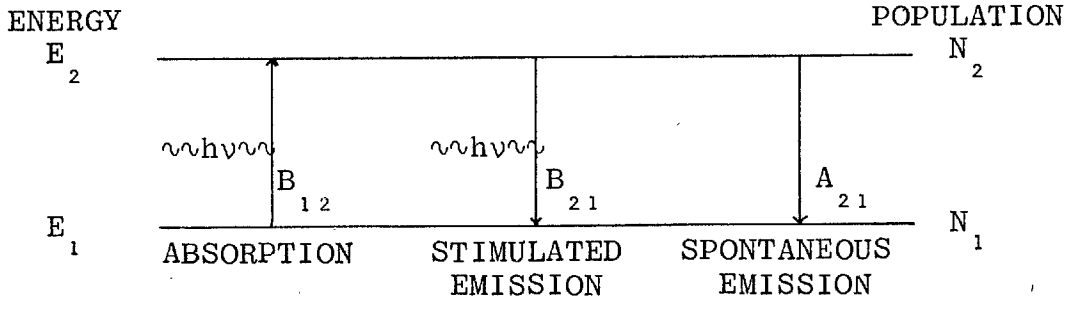


Figure 2.2: Radiative processes.

Spontaneous emission may take place between E_2 and E_1 with a probability A_{21}, being the number of transitions taking place in unit time. Therefore, the number of transitions per unit volume in unit time is $N_2 A_{21}$. Absorption may take place between E_1 and E_2 if radiation of frequency ν is incident, the number of transitions per unit volume in unit time being

$$\frac{8\pi h\nu^3}{c^3} \frac{B_{12} N_1}{(\exp\{h\nu/kT\}-1)} . \qquad 2.10$$

Sililarly, for stimulated emission the number of transition per unit volume in unit time is

$$\frac{8\pi h\nu^3}{c^3} \frac{B_{21} N_2}{(\exp\{h\nu/kT\}-1)} . \qquad 2.11$$

The Einstein coefficients, A_{21}, B_{21} and B_{12}, are intrinsic properties of the atom and may, in theory, be calculated from the appropriate wave equation. The following relations are useful:

$$A_{21} = 8\pi h\nu^3 B_{21}/c^3 \qquad 2.12$$

$$g_1 B_{12} = g_2 B_{21} . \qquad 2.13$$

These B values have been defined in terms of the energy density per unit frequency interval, ρ. Some authors define B in terms of the specific intensity, in which case a conversion may be made by using Equation 2.9.

The oscillator strength, f_{12}, is related to the Einstein coefficients by

$$f_{12} = -\frac{g_2}{g_1} f_{21} = \frac{4mh\varepsilon_0}{e^2} \nu_{12} B_{12}, \qquad 2.14$$

where, m is the rest mass and e the charge of the electron, and ε_0 is the permittivity of free-space.

The lifetime of an excited state is easily obtained from the Einstein coefficient for spontaneous emission. If an excited state combines with a number of lower energy levels, the lifetime, τ_2, of the excited state is given by

$$\tau_2 = 1 \Big/ \sum_j A_{2j} . \qquad 2.15$$

2.2.4 The Absorption Coefficient.

If radiation is emitted from a region within a source then on passing through to the outside the possibility of absorption or re-emission exists. The extent of the absorption of radiation is determined by the absorption coefficient of the medium through which the radiation passes. When radiation of intensity I_ν passes through an absorbing medium the amount of energy absorbed in a distance δx is given by[152]

$$-\delta I_\nu(x) = k_\nu I_\nu(x) \delta x . \qquad 2.16$$

Equation 2.16 defines the absorption coefficient, k_ν, as the fractional decrease in intensity per unit path length. If radiation of incident intensity I_0 passes through a thickness l, the emerging intensity (found by integrating Equation 2.16) is given by

$$I_\nu = I_0 \exp\{-\int_0^l k_\nu dx\} . \qquad 2.17$$

If the absorbing medium is homogeneous this equation simplifies to

$$I_\nu = I_0 \exp\{-k_\nu l\} . \qquad 2.18$$

The quantity $\int_0^l k_\nu dx$ ($k_\nu l$ for a homogeneous medium) is known as the optical depth. A environment may be described as optically thin if $k_\nu l << 1$ and optically thick if $k_\nu l >> 1$. If the radiation from a particular atom is to reach the spectrometer without significant absorption then the optical density must be low, i.e. $k_\nu l << 1$.

The above equations hold for all k_ν and l but if $k_\nu l << 1$ Equation 2.18 simplifies to

$$I_\nu = I_0(1-k_\nu l) , \qquad 2.19$$

giving

$$k_\nu = (1/l)(\{I_0 - I_\nu\}/I_0) . \qquad 2.20$$

2.3 THE WIDTH AND SHAPE OF SPECTRAL LINES.

2.3.1 Line Profiles.

In this section the factors affecting the frequency distribution of an atomic spectral line will be discussed assuming that the spectrometer used to view the line is ideal. The importance of any line broadening process is described in terms of its half-width, which is defined as the width of the line at half its peak intensity.

The emission of a spectral line is the result of a transition between two energy levels. These levels have

a finite spread because of the uncertainty principle, $\Delta E \Delta t \simeq \hbar$, where ΔE is the energy spread and Δt is the uncertainty in time associated with finding the atom in that particular state. Δt may be measured[116] by the mean lifetime, τ, of the state so that the spread, in wavenumbers, for a state j may be written

$$\delta\sigma_j \simeq \frac{1}{2\pi c\tau_j} \quad . \qquad 2.21$$

For a ground state or a metastable state τ is very large, making $\delta\sigma$ negligible. However, other states for which optical transition are allowed have mean lifetimes in the range 10^{-6} to 10^{-9}s. These values correspond to a $\delta\sigma$ in the range 10^{-2} to 10^{-5} cm^{-1}. A transition involves two energy levels, i and j, therefore the total spread

$$\delta\sigma_N = \delta\sigma_i + \delta\sigma_j \qquad 2.22$$

$\delta\sigma_N$ is known as the natural half-width of a line; this broadening being a consequence of classical or quantum mechanics. Apart from this intrinsic natural broadening a number of other broadening mechanisms exist.

2.3.2 Doppler Broadening.

If a monochromatic light source is moving with a velocity, whose component in the line of sight is v_x , the emitted frequency appears to be shifted by an amount $\nu_0 v_x/c$, where ν_0 is the frequency of the source at rest. The random motion of atoms in a gas causes spectral lines, emitted or absorbed by atoms in the gas, to be broadened

as a result of this Doppler effect. If the distribution of gas velocities follows Maxwell's law[7] then the broadening effect will be a Gaussian function. The half-width of a Doppler broadened profile is given by[116]

$$\delta\sigma_G = (2\sigma_0/c)\sqrt{\{(2RT\ln 2)/M\}} , \qquad 2.23$$

where, σ_0 is the wavenumber at the line centre, R is the gas constant, T is the absolute temperature and M is the relative atomic weight of the emitting atom.

It may be seen from Equation 2.23 that the Doppler half-width is directly proportional to the wavenumber (or the frequency). Therefore, the Doppler effect is more important for lines in the high frequency part of the spectrum. $\delta\sigma_G$ is also proportional to $\sqrt{T}$ which indicates that the half-width may be reduced by decreasing the temperature of the source.

2.3.3 Pressure Broadening.

The interaction of a radiating atom with other atoms, ions or electrons has a very complicated effect upon spectral lines. As yet there is not an exact theory available but two different approaches to the problem have been made![116]

Firstly, the effect of other atoms has been considered to be caused by collisions breaking the otherwise unperturbed wavetrains. In an analogous treatment to natural broadening, the line width is determined by the time between two collisions rather than the natural lifetime. According to the Lorentz theory[116] an optical

collision only requires a change in phase sufficient to cause incoherence of the light waves emitted before and after the collision. For such a model the collisional half-width, $\Delta\sigma_C$, may be expressed by

$$\Delta\sigma_C = \rho_0^2 \bar{v}N/c \ , \qquad 2.24$$

where, N is the number density of perturbing atoms, $\bar{v}$ is the average speed and ρ_0^2 is the optical collision cross-section. Using the kinetic theory of gases, Equation 2.24 becomes

$$\delta\sigma_C = \{\rho_0^2 N/c\}\sqrt{((8RT/\pi)(\{1/M_2\} + \{1/M_1\}))} \ , \qquad 2.25$$

where, M_1 and M_2 are the relative atomic or molecular weights of the colliding species. The quantity ρ_0^2 is difficult to evaluate theoretically and is usually given an empirical value.

The second approach, known as the quasi-static or statistical approximation, assumes that the interacting particles are at rest but distributed in space in a random fashion. Each atom may be regarded as emitting one definite frequency at any given instant but the effect of many radiating atoms leads to an intensity distribution, whose calculation is purely a statistical problem.

If the perturbation potential of a particular energy level is $\Delta V(r)$ then the transition between two levels is changed by

$$\delta\sigma = (1/hc)\left(\Delta V_1(r) - \Delta V_2(r)\right) \ , \qquad 2.26$$

where, ΔV_1 is for the upper state and ΔV_2 is for the lower state.

a)CHARGED PARTICLES.

A radiating atom at a distance r from an ion or electron is perturbed by an electric field $F = e/4\pi\varepsilon_0 r^2$. For hydrogen or hydrogen-like ions, ΔV is proportional to F resulting in the linear Stark effect, which splits lines symmetrically. For other atoms the quadratic Stark effect predominates, in which $\Delta V \propto F^2$. This effect splits energy levels asymmetrically and usually causes a shift towards the low wavenumber end of the spectrum.

b)RESONANCE INTERACTION.

This effect may occur between an atom in the upper energy level of a resonance transition and a like atom in the ground state. For this effect $\Delta V \propto 1/r^3$.

c)DISPERSION FORCES.

Dispersion forces act between any atoms in any state and are usually greatest for high energy levels and heavy atoms. The interaction is always an attraction between the two particles and $\Delta V \propto 1/r^6$.

d)REPULSIVE EFFECTS.

Repulsive potentials play a secondary role because of their short range except when other effects are very small. The repulsion may be considered to be caused by the mutual penetration of electron orbitals and it does not lend itself readily to simple theoretical evaluation. A potential of $\Delta V \propto -1/r^{12}$ has often been useful.

2.3.4 The Zeeman Effect.

The influence of an external magnetic field splits each energy level into 2J+1 sub-levels of equal separation. Each sub-level is specified by a quantum number M_J, whose value may be J, J-1, ..., 0, ..., 1-J, -J. The selection rule for electric dipole radiation is

$$\Delta M_J = 0, \pm 1 \ . \qquad 2.27$$

$\Delta M_J = 0$ produces π-components, which are polarized with the electric vector parallel to the magnetic field, whilst, $\Delta M_J = \pm 1$ gives σ-components, which are polarized with the electric vector perpendicular to the field when viewed at right-angles to the field. On viewing along the direction of the magnetic field the σ-components are circularly polarized and the π-components do not appear. The order of magnitude of the splitting is determined by the value of $\mu_B B$, where, B is the magnetic field strength and μ_B is the Bohr magneton. For a field strength of 0.1 Wb m^{-2} ($\equiv$ 1 kilogauss) the splitting is about 0.05 cm^{-1}, which is comparable with the Doppler half-width for a light element.

2.3.5 Self-Absorption Broadening.

An emission line of centre frequency ν_0 will have an intensity-frequency distribution, Figure 2.3, determined by the frequency dependence of the emission coefficient, j_ν. The frequency dependence of j_ν will be the result of all the broadening processes previously described. The emission coefficient is defined as the energy emitted

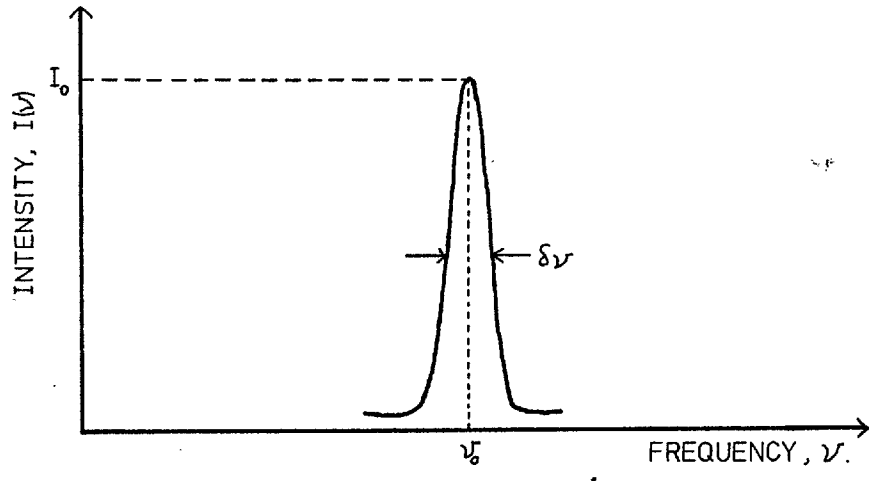


Figure 2.3: The Intensity-Frequency Distribution of a Spectral Line.

per second per unit volume per unit solid angle per unit frequency interval. The integral of the emission coefficient over the emission line is related to the total energy emitted per second per unit volume into unit solid angle, irrespective of the frequency distribution:

$$\int_{\text{line}} j_\nu d\nu = (h\nu_0/4\pi)\, N_2 A_{21} \quad \text{(ignoring stimulated emission).} \qquad 2.28$$

The peak emission intensity, I_0, can not be higher than the intensity emitted by a black body in equilibrium at that particular temperature and frequency. Therefore, once I_0 reaches saturation any increase in the total energy emitted must result in an increase in the effective half-width, Figure 2.4. This effect is known as the saturation of emission of radiation in a gas at constant temperature.

An absorption line viewed against a continuum, of intensity I_0, will have a frequency distribution, Figure 2.5, dependent upon the frequency distribution

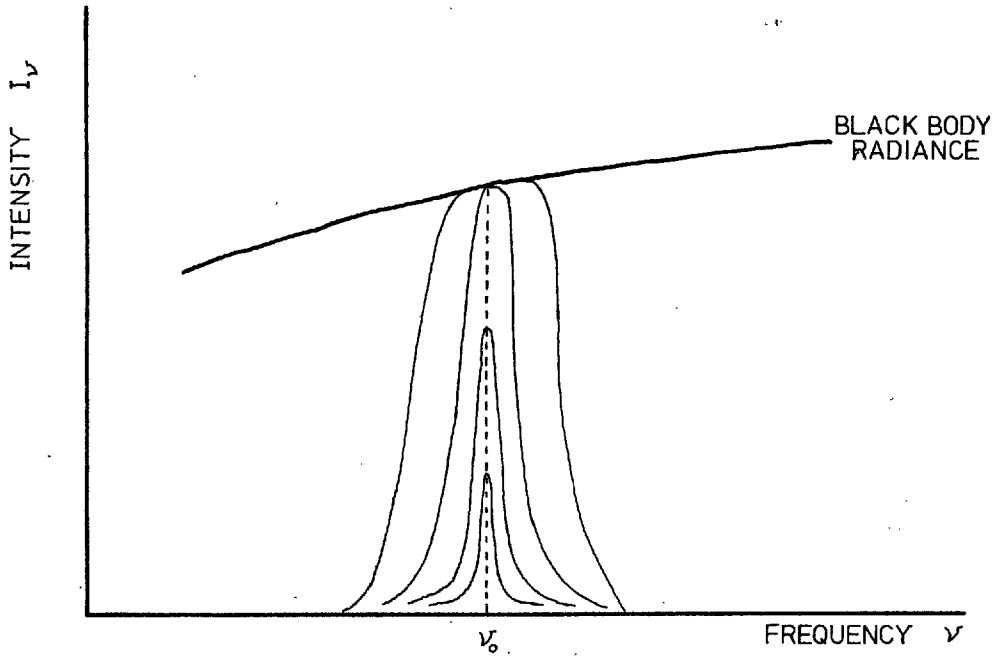


FIGURE 2.4 : An Emission Line Approaching Saturation.

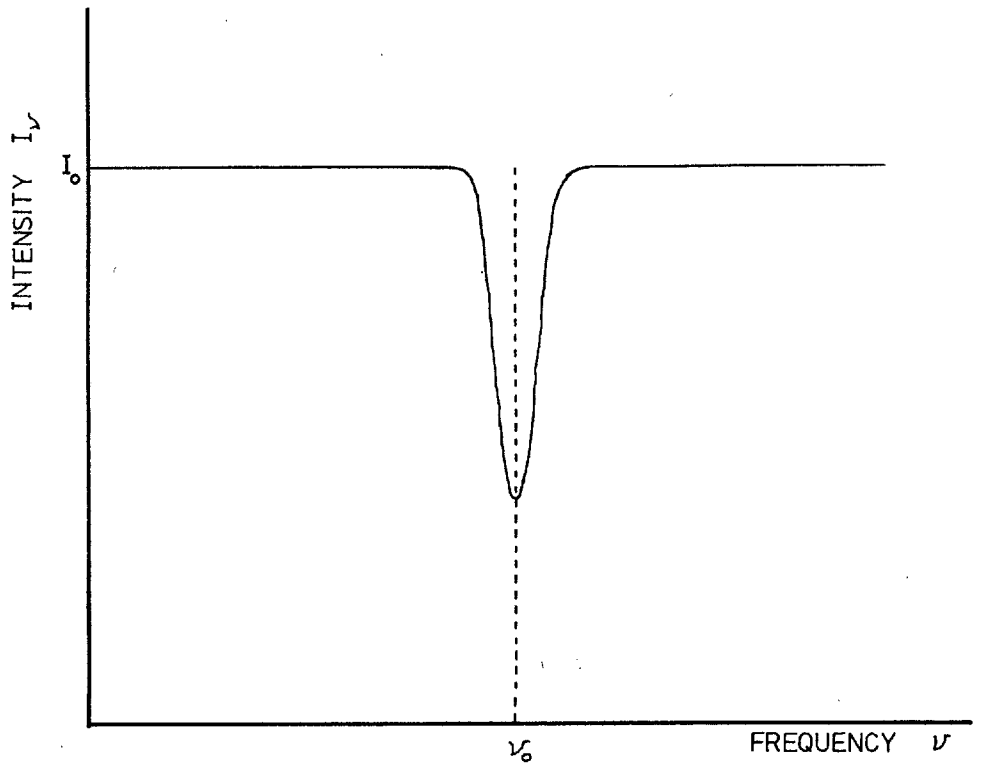


FIGURE 2.5 : An Absorption Line.

of the absorption coefficient.

If the source radiation passes through a layer, which is not optically thin,then partial absorption of the line will take place. The absorption coefficient is greatest at the centre frequency,ν_0,where the intensity is greatest. Therefore,an emission line will be absorbed preferentially in the centre rather than in the line wings. As the optical density increases the emission line peak approaches a saturation value,Figure 2.6. The effect is known as self-absorption and it results in the effective line width being much larger than would be expected in an optically thin source.

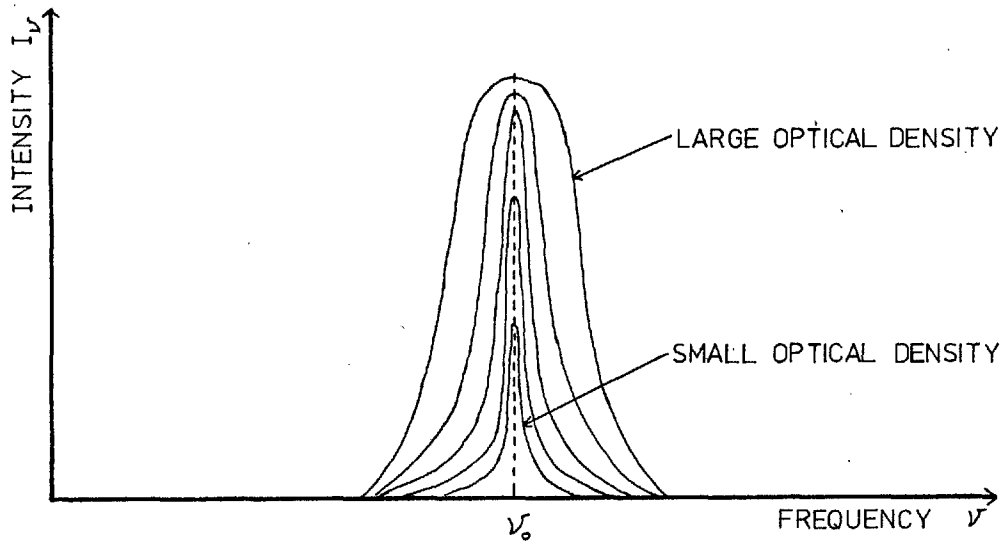


Figure 2.6: The effect upon an emission line of increasing the optical depth.

A special case occurs when radiation passes through a gas containing atoms at a significantly lower temperature than the emitting atoms. In this case the half-width of the profile of the absorption coefficient is much narrower than the half-width of the emitted line so that a dip is produced at the line centre. This is an effect known as self-reversal and it is characteristic of a temperature gradient in the source.

2.4 FABRY-PEROT INTERFEROMETRY.

2.4.1 General Principles.

The high resolution studies described in this work have been carried out using an interferometer based upon the instrument introduced in 1897 by C.Fabry and A.Perot.[118] The use of Fabry-Perot interferometers is well known, theoretical treatments being given by Tolansky,[119-120] Francon[121] and Jacquinot[122/3]. In view of the large volume of detailed theoretical material available in the literature only those aspects which are particularly pertinent to this work will be described here.

Fabry-Perot's interferometer consists of a pair of accurately flat silica or glass plates held parallel in a rigid but adjustable mount. The optical arrangement most frequently used is shown in Figure 2.7. The surfaces CD and C'D' are coated with a highly reflective, thin, metal or dielectric film. The reflectivity is usually greater than 90% and the absorption as low as possible. Light from a point A' in the source plane, S, is collimated by LENS1 and impinges on the plates at an angle θ. LENS2

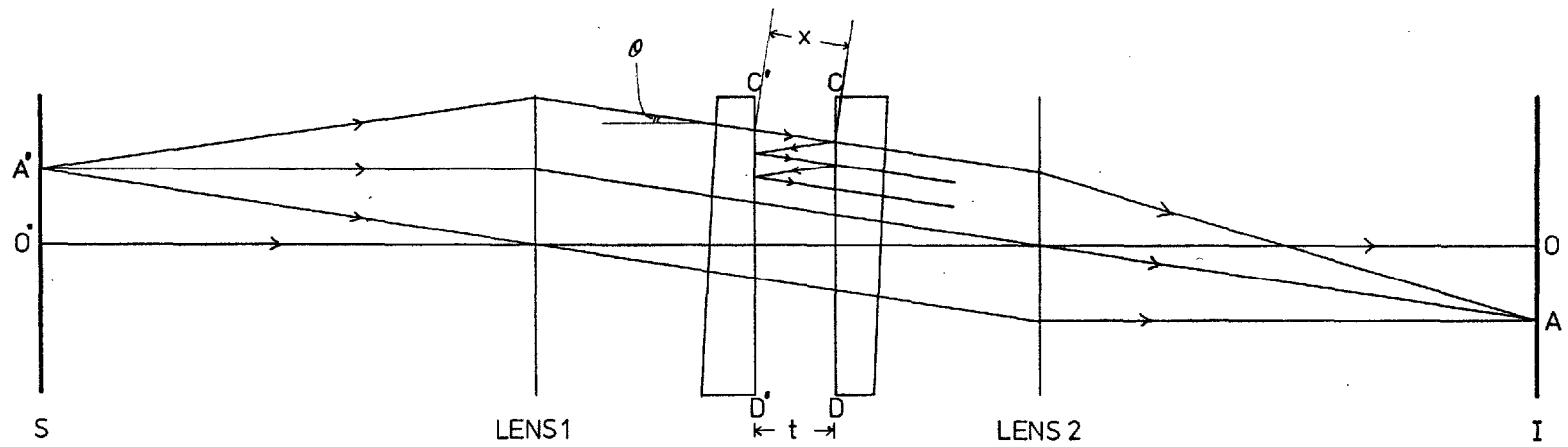


FIGURE 2.7: Fabry-Perot Interferometer — Optical Arrangement.

focuses the rays to a point A in the image plane,I. Radiation incident at an angle θ undergoes multiple reflections and,as shown in Figure 2.7,successively reflected rays emerge parallel with a constant path difference,l,between them. It is evident that $l = x+x\cos 2\theta$ and $x = t/\cos\theta$, giving

$$l = 2t\cos\theta. \qquad 2.29$$

The phase difference,ξ,between successive rays is given by

$$\xi = 2\pi l/\lambda = \frac{4\pi t\cos\theta}{\lambda} = 4\pi\sigma t\cos\theta . \qquad 2.30$$

Parallel rays meet at A in the image plane,I,at which point interference takes place. The condition for a maximum of intensity is $\xi=2\pi$,giving $l=n\lambda$, where n is a positive integer equal to the order of interference. Therefore,allowing for the refractive index,μ,of the medium between the plates, Equation 2.29 becomes

$$n\lambda = 2\mu t\cos\theta. \qquad 2.31$$

A series of concentric rings centred about the axis OO' is produced because of the cylindrical symmetry of the system. All rays incident at an angle θ are superimposed by LENS2 and,provided Equation 2.31 is satisfied,form an intensity maximum ring of radius OA. Such rings are known as fringes of equal inclination.

The plates in Figure 2.7 are made with slight wedge angles so that reflections from the front and back surfaces are thrown clear of the true ring pattern.

2.4.2 Dispersion

The angular dispersion of the Fabry-Perot interferometer may be obtained by differentiating Equation 2.31 with respect to θ :

$$n \frac{d\lambda}{d\theta} = 2\mu t \sin\theta . \qquad 2.32$$

In practice the angle of incidence, θ, is kept as small as possible so that $\sin\theta \simeq \theta$ and μ may be set equal to 1. Therefore, $n \simeq 2t/\lambda$ and Equation 2.32 becomes

$$\frac{d\theta}{d\lambda} = \frac{1}{\lambda\theta} . \qquad 2.33$$

It is of interest to note that the angular dispersion is independent of t and as $\theta \to 0$, $d\theta/d\lambda \to \infty$. Therefore, the dispersion at the centre of the ring system is infinite. If the focal length of LENS2 in Figure 2.7 is f then the reciprocal linear dispersion is

$$\frac{d\lambda}{dx} = \frac{1}{f} . \frac{d\lambda}{d\theta} = \frac{\lambda\theta}{f} . \qquad 2.34$$

2.4.3 Scanning.

The production of a circularly symmetrical ring pattern has been described. Originally the Fabry-Perot interferometer was used spectrographically, the ring pattern being incident upon the entrance slit of a prism spectrograph. The image produced on the photographic plate contains sufficient information for the reduction of measurements. In this case the intensity function is recorded as a function of θ.

In Equation 2.31, $(n\lambda)$ is a function of three

variables, μ, t and θ. Therefore, there are potentially three methods of achieving wavelength scanning:

$$\frac{d\lambda}{d\theta} = \frac{2\mu t}{n} \sin\theta \quad , \theta \text{ varies, } \mu \text{ and } t \text{ constant.} \qquad 2.35$$

$$\frac{d\lambda}{d\mu} = \frac{2t}{n} \cos\theta \quad , \mu \text{ varies, } \theta \text{ and } t \text{ constant.} \qquad 2.36$$

$$\frac{d\lambda}{dt} = \frac{2\mu}{n} \cos\theta \quad , t \text{ varies, } \theta \text{ and } \mu \text{ constant.} \qquad 2.37$$

Equation 2.35 is used in the photographic method but is unsuitable for use photoelectrically because a photomultiplier tube can only produce one channel of information.

The use of Equation 2.36, in which the refractive index of the medium between the plates is changed, is well known.[1 2 3] This is normally achieved by enclosing the interferometer assembly in a gas-tight box and varying the pressure of the enclosed gas linearly with time. If a photomultiplier tube is mounted behind a circular aperture monitoring the intensity at the centre of the ring pattern then Equation 2.36 reduces to

$$\frac{d\lambda}{d\mu} = \frac{2t}{n} , \qquad 2.38$$

and the output of the photomultiplier may be recorded as a function of time. This method of <u>pressure scanning</u> suffers from a number of difficulties in practice. High pressures or gases other than air may be needed to scan the required number of orders. It is difficult to change the pressure uniformly with time to produce a linear wavelength scale.

The windows in the gas-tight box reduce light throughput and adjustments to the plate parallelism can not readily be made while scanning. Scanning speeds are slow (usually less than one order per second) and continuous repetitive scanning is difficult to achieve,resulting in limitations to the degree of signal processing that may be carried out.

The alternative method,and the one adopted in the instrument used in this work, is to vary the plate separation,t,by a small amount as described by Equation 2.37. The arrangement is similar to that used for pressure scanning with the central spot of the ring pattern being viewed by a photomultiplier tube. The use of a piezoelectric transducer to control the plate separation will be described later but there are problems in maintaining plate parallelism. The major advantage of piezoelectric rapid scanning is that the line profiles may be observed on an oscilloscope and adjustments to the plate parallelism made in real time, i.e. the effect of any adjustment may be seen immediately. Another advantage of rapid scanning is that signal averaging may be used to improve signal-to-noise ratios within a reasonable measuring period. Of course,it may be argued that the reduction in the quality of plate parallelism during rapid scanning defeats any advantages of signal averaging. Whilst this is true for high scanning frequencies it is normally possible to improve signal quality by a judicious choice of operating parameters.

In Equation 2.33 it is shown that the angular dispersion is not constant with θ. The use of a circular

scanning aperture eliminates this problem by setting θ to be constant. Secondly, setting $\theta=0$ means that the light throughput of the plate assembly is high and there is virtually no lateral displacement, or walk-off, of the multiple reflections.

2.4.4 Free-Spectral Range.

In the piezoelectric scanning Fabry-Perot interferometer, in which the angle of incidence $\theta \simeq 0$, and setting $\mu=1$, the order number, n, is obtained from Equation 2.31,

$$n = \frac{2t}{\lambda} = 2t\sigma. \qquad 2.39$$

Therefore,

$$\frac{dn}{d\lambda} = \frac{-2t}{\lambda^2} \quad \text{and} \quad \frac{dn}{d\sigma} = 2t, \qquad 2.40$$

giving

$$\Delta n = \frac{-2t\Delta\lambda}{\lambda^2} = 2t\Delta\sigma. \qquad 2.41$$

The free-spectral-range, $\Delta\sigma$ or $\Delta\lambda$, is the maximum range which can be scanned before overlap with another order occurs. This is obtained by substituting $\Delta n=1$ into Equation 2.41 and neglecting signs:

$$\Delta\lambda = \frac{\lambda^2}{2t} \quad \text{or} \quad \Delta\sigma = \frac{1}{2t}. \qquad 2.42$$

It can be seen from these equations that it is generally more convenient to work in wavenumbers.

2.4.5 Intensity Distribution.

The reflectance, R, the transmittance, T, and the absorption, A, of a surface may be defined[121] such that

$$T + R + A = 1 . \qquad 2.43$$

The transmittance is defined as

$$T = \frac{\text{Transmitted energy}}{\text{Incident energy}} , \qquad 2.44$$

and R and A may be similarly defined in terms of the reflected energy and absorbed energy, respectively. If the reflected amplitude rather than the reflected intensity is considered, as is required in the discussion of interference phenomena, the coefficient of reflection, r, is composed of two parameters - ρ, the reflected fraction of the amplitude and ϕ, the phase change of reflection at a dielectric or metallic film. This may be expressed as

$$r = \rho \exp\{-i\phi\} . \qquad 2.45$$

The reflectance is related to the coefficient of reflectivity by

$$R = rr^* = \rho^2 . \qquad 2.46$$

Similar relationships exist for the transmittance, T, the transmission coefficient, t, and the transmitted fraction of the amplitude, τ :

$$T = \frac{\text{Transmitted energy}}{\text{incident energy}} = tt^* = \tau^2 , \qquad 2.47$$

where, $$t = \tau \exp -i\phi . \qquad 2.48$$

On considering the two partially reflecting surfaces, AA' and BB', of the Fabry-Perot etalon in Figure 2.8 ray SI_1 incident at an angle θ produces a series of reflected rays, I_1J_1, J_1I_2, I_2J_2, ... Each time a ray passes

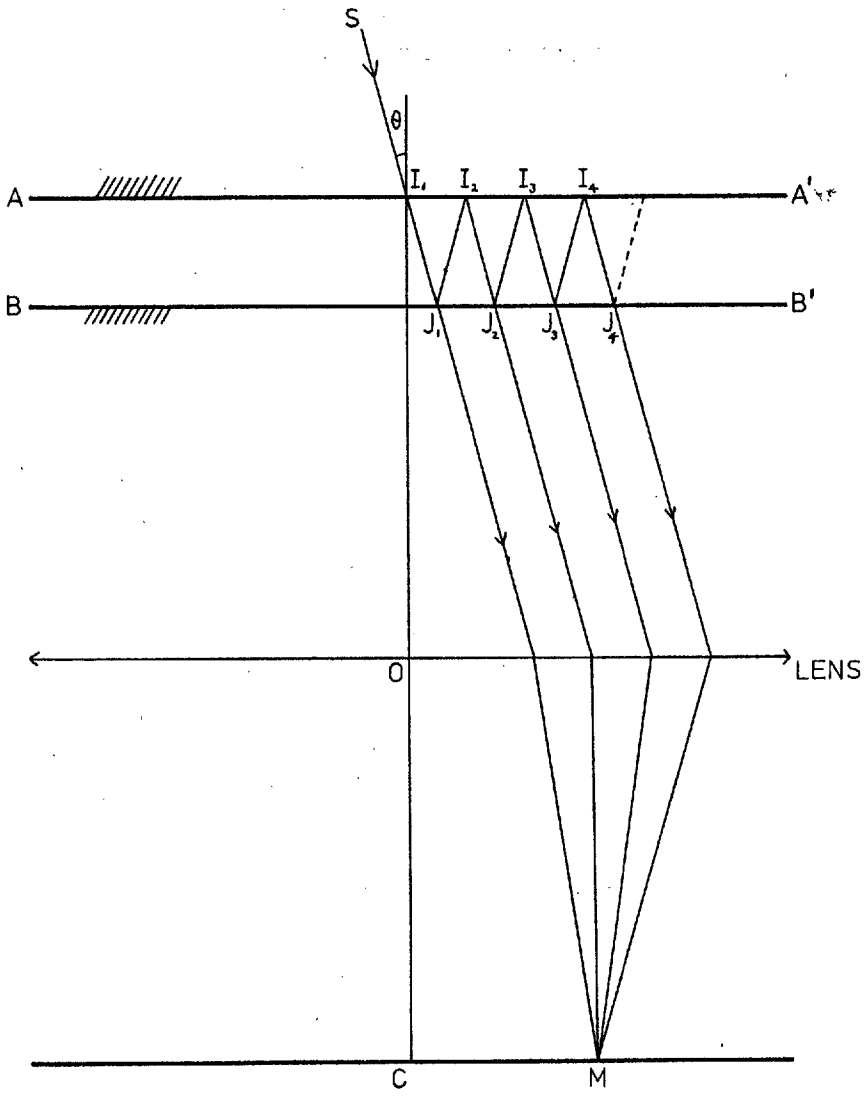


Figure 2.8: Multiple Reflections in a Fabry-Perot Etalon.

through the semi-reflecting coating it is multiplied by the transmission coefficient,t,and for each reflection by the reflection coefficient,r. The amplitude at a point M,where the rays interfere,is the sum of the amplitudes of the individual rays:

$$\Phi_M = \Phi_{J_1M} + \Phi_{J_2M} + \Phi_{J_3M} + \ldots.$$

$$= t^2 + t^2r^2\exp\{-i\xi\} + t^2r^4\exp\{-2i\xi\} + \ldots.. \qquad 2.49$$

where ξ was defined in Equation 2.30. The sum of this

infinite series may be shown[121] to be

$$\Phi_M = t^2/(1-r^2\exp\{-i\xi\}). \qquad 2.50$$

The intensity, $I = \Phi_M \Phi_M^*$, may be shown to be

$$I = I_{max}/(1+f'\sin^2\{\psi/2\}) , \qquad 2.51$$

where $f' \equiv 4R/(1-R)^2$ and $\psi = \phi + \xi$.

Equation 2.51 is known as an Airy distribution function and may be rearranged in a number of useful ways. From Equation 2.30 and approximating $\psi \simeq \xi$, Equation 2.51 may be written as a function of the path difference, l:

$$I = I_{max}/(1+f'\sin^2\{\pi\sigma/l\}). \qquad 2.52$$

From Equation 2.42, in terms of the free-spectral-range, $\Delta\sigma$,

$$I = I_{max}/(1+f'\sin^2\{\pi\sigma/\Delta\sigma\}). \qquad 2.53$$

The maximum of interference has an intensity I_{max} given[6] by

$$I_{max} = I_0(T/(1-R))^2 = I_0(1-\{A/(1-R)\})^2 , \qquad 2.54$$

where I_0 is the incident intensity.

The minima have an intensity

$$I_{min} = I_0(T/(1+R))^2 . \qquad 2.55$$

From Equation 2.55 I_{min} can never reach zero at any point in the fringe pattern but it will be small if $R \gg T$.

2.4.6 Dielectric Plate Coatings.

Equation 2.54 implies that the peak intensity, I_{max}, is high only if $A<<(1-R)$. Metallic coatings absorb a substantial proportion of the non-reflected radiation hence placing a restriction on the value of R that may be used in practice. This problem may be overcome by using dielectric coatings; the reflectance may be made as high as 0.98 without significant absorption taking place.

Two dielectric materials are required, one of high refractive index, μ_2, and one of low refractive index, μ_1. They are deposited on the interferometer plates in alternate layers $\lambda/4$, starting and finishing with the high index material. The optical thickness is $\mu_i s_i$, where s_i is the thickness of the ith. film, so

$$\mu_1 s_1 = \mu_2 s_2 = \lambda/4 . \qquad 2.56$$

Figure 2.9 shows the changes in phase which occur when a ray of phase ψ is incident upon a series of transparent thin films, remembering that an advance of π in the phase occurs when a ray travelling through a medium, of refractive index μ_1, is reflected at the interface with

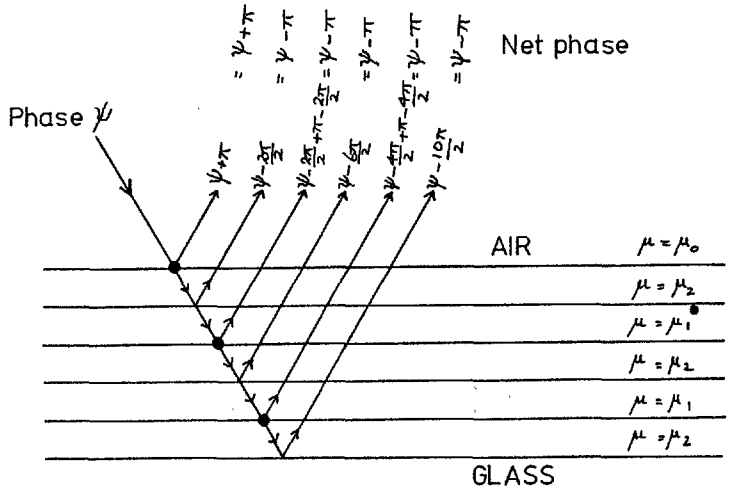


FIGURE 2.9: A Dielectric Coating.

a medium of refractive index μ_2, if $\mu_2 > \mu_1$. These occurrences are indicated by a • in Figure 2.9. Each pass through a layer of optical thickness $\lambda/4$ will result in a phase lag of π. The emerging rays are in phase resulting in an intensity maximum, provided $\mu_0 < \mu_1 < \mu_2$. The materials most frequently used[124] are cryolite (Na_3AlF_6), $\mu_1 \simeq 1.3$, and zinc sulphide (ZnS), $\mu_2 \simeq 2.3$. These multiple films are fabricated by vacuum deposition while maintaining strict control of the thickness of each film. Additionally, the multiple film has to be prepared in a single operation without breaking the vacuum in between each film. The major disadvantage of the dielectric coating is that the wavelength range is small, typically less than 30nm.

2.4.7 The Theoretical Finesse.

Figure 2.10 shows the Airy distribution as a function of wavenumber(Equation 2.53). As before, $\Delta\sigma$ is the free-spectral-range, I_{max} is the intensity maximum and $\delta\sigma$ is the width at half the maximum intensity. Moving out a distance $\delta\sigma/2$ from the maximum and setting $I_{max}/I(\delta\sigma/2) = 2$ in Equation 2.53:

$$1 + f' \sin^2\{\pi\delta\sigma/2\Delta\sigma\} = 2 . \qquad 2.57$$

For sharp fringes $\delta\sigma << \Delta\sigma$, therefore,

$$\sin\{\pi\delta\sigma/2\Delta\sigma\} \simeq \pi\delta\sigma/2\Delta\sigma = 1/\sqrt{f'} . \qquad 2.58$$

$$\text{Therefore, } \delta\sigma = \frac{2\Delta\sigma}{\pi\sqrt{f'}} = \frac{(1-R)}{\pi\sqrt{R}}\Delta\sigma. \qquad 2.59$$

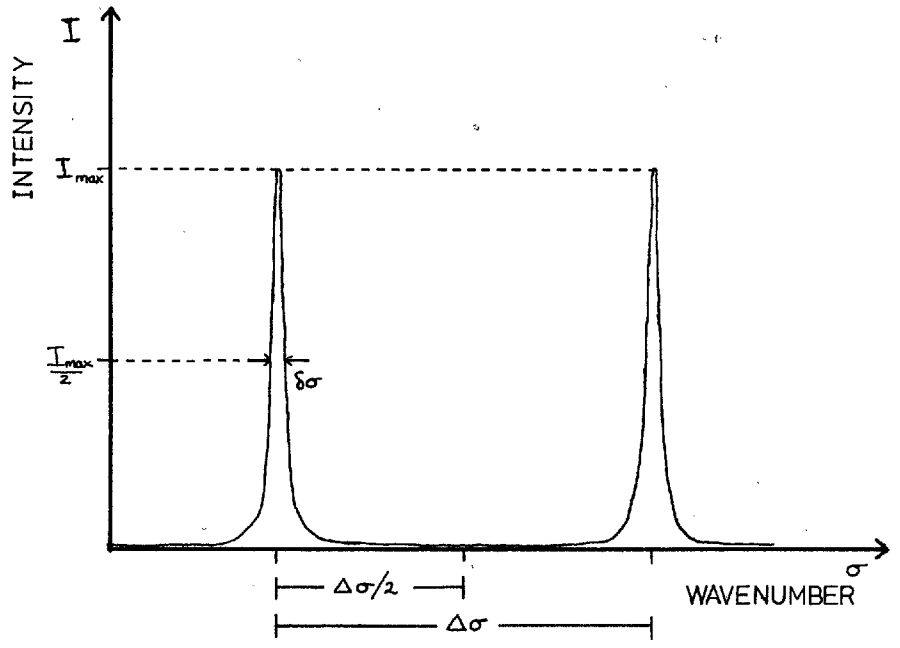


FIGURE 2.10: Airy Distribution as a Function of Wavenumber.

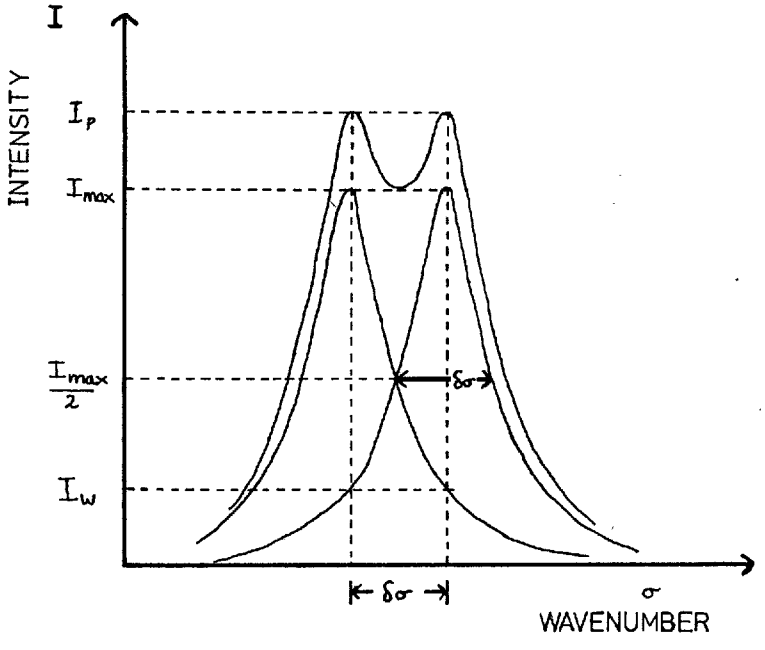


FIGURE 2.11: Rayleigh's Criterion Applied to Fabry-Perot Fringes.[6]

The finesse,F,is defined as the ratio of the free-spectral-range to the half-intensity width:

$$F = \frac{\Delta\sigma}{\delta\sigma} = \frac{\pi\sqrt{f'}}{2} = \frac{\pi\sqrt{R}}{1-R} . \qquad 2.60$$

This expression for the finesse is a theoretical one and,for the moment,does not take surface imperfections or scanning into account. Under such conditions the finesse is a function of the reflectance only. The finesse may also be considered to be the number of rays in Figure 2.8 that combine to cause interference at point M.

2.4.8 Contrast of the Fringes.

In order for the fringe pattern to be visible the contrast,C,must be greater than 1. The contrast is defined,using Equations 2.54 and 2.55,by

$$C = I_{max} / I_{min} = \left((1+R)/(1-R)\right)^2 \qquad 2.61$$

2.4.9 Resolving Limit and Resolving Power.

The modified form of the Rayleigh Criterion[6] requires that for two adjacent lines to be just resolved the intensity at their saddle point must be 80% of the peak intensity (Figure 2.11). The peak intensity,I_p,is the sum of the intensity maximum of one line,I_{max},and the intensity,I_w, of the other line at a distance $\delta\sigma$away from the line centre. The value of I_w is obtained by putting $\delta\sigma$ into Equation 2.53 and,by a method analogous to that used in deriving Equation 2.58,

$$\sin^2\{\pi\delta\sigma/\Delta\sigma\} \simeq \frac{\pi^2(\delta\sigma)^2}{(\Delta\sigma)^2} = \frac{4}{f'} . \qquad 2.62$$

Therefore,

$$I_w = \frac{I_{max}}{1+4} = \frac{I_{max}}{5} , \qquad 2.63$$

and

$$I_p = I_{max} + I_w = \frac{6}{5} I_{max} . \qquad 2.64$$

Therefore,when two equal lines are just resolved they are separated by their half-intensity width,$\delta\sigma$. This results in a saddle point of 5/6, or 83%,of the peak intensity which is sufficiently close to the 80% of the Rayleigh criterion.

Using Equation 2.60 the resolving limit,$\delta\sigma$,is

$$\delta\sigma = \frac{\Delta\sigma}{F} = \frac{1}{2tF} . \qquad 2.65$$

The resolving limit is independent of wavenumber and depends only upon the finesse and the plate separation.

The resolving power (using Equations 2.39 and 2.42) is given by

$$\Xi = \frac{\sigma}{\delta\sigma} = \frac{\sigma F}{\Delta\sigma} = nF. \qquad 2.66$$

From a theoretical point of view n,and hence Ξ ,may be made as high as required simply by increasing the plate separation. In practice, this may not be fully exploited if a small free-spectral-range results in spectral overlap. As the free-spectral-range is decreased the intensity throughput of the etalon decreases(Equation 2.53) and signal measurements become more difficult. The source having a finite width results in not all the

radiation passing through the plates being exactly normal. Consequently,if n is very large, i.e. t is large, some rays may be lost by the lateral displacement of successive reflections between the plates.

2.4.10 Deviation from the Theoretical Finesse.

In practice the surfaces of the Fabry-Perot plates can never be made perfectly flat and this departure from flatness limits the effective finesse that can be achieved. Additionally,there are effects caused by the scanning aperture and the bowing of the plates during the scanning process. The effective practical finesse,F_E,may be considered to be composed of the theoretical finesse,F, resulting from the reflectivity of the plate coatings, the surface defects finesse,F_D,and the scanning finesse, F_S.

Chabbal[125] has shown that an imperfect etalon may be regarded as a mosaic of small perfect etalons of slightly differing separations. A summary of this treatment has been given by Bousquet.[124] F_D is independent of the etalon spacing but depends upon the variations in the spacing resulting from surface imperfections and on errors in the adjustment of the plate parallelism. If an aperture is used to isolate the central spot of the interference pattern,while the fringe is expanding within the area of the aperture the flux passing through remains constant but falls suddenly to zero as the ring expands beyond the boundary of the aperture.

In practice,the effective finesse is determined by

the value of the defects finesse because the reflectivity of the coatings may be made very high without any significant absorption and the scanning finesse may be made as high as necessary. Values of the scanning finesse for different scanning apertures have been tabulated by Sargent.[126] Dynamic effects resulting from the inertial bowing of the plates during scanning have been described by Cooper and Greig[127] together with thermal effects on the plate assembly.

2.4.11 Light-Gathering Power.

The light-gathering power or entendue of a spectrometer may be defined by

$$\Upsilon = \frac{SA}{f^2} , \qquad 2.67$$

where, S is the area of the slit, A is the area of the limiting aperture and f is the focal length of the collimating lens.

In the case of the Fabry-Perot interferometer the slit is replaced by a circular aperture of radius a, which isolates the central spot in the fringe pattern. The admission angle, Ω, is, therefore,

$$\Omega = \frac{\pi a^2}{f^2} . \qquad 2.68$$

It can be shown[6] that the resolving power is

$$\Xi = 2\pi/\Omega . \qquad 2.69$$

Using Equation 2.66 the limit of resolution is

$$\delta\sigma = \frac{\sigma}{\Xi} = \frac{\sigma\Omega}{2\pi} = \frac{\sigma a^2}{2f^2} . \qquad 2.70$$

Therefore, for the Fabry-Perot interferometer the light-gathering power is given by

$$T = \frac{\pi a^2 A}{f^2} = \Omega A = \frac{2\pi A}{\Xi} \qquad 2.71$$

Using previous equations, notably Equation 2.66, T may be expressed in terms of a number of different parameters:

$$T = \frac{2\pi A \delta\sigma}{\sigma}$$, in terms of the resolution limit. 2.72

$$T = \frac{2\pi A \Delta\sigma}{\sigma F}$$, in terms of the finesse and free-spectral-range. 2.73

$$T = \frac{\pi A}{\sigma F t}$$, in terms of the finesse and the plate separation. 2.74

2.4.12 Auxiliary Dispersion.

The order number, n, in a Fabry-Perot interferometer may be several orders of magnitude greater than in a diffraction grating. Consequently, there is a problem of successive orders overlapping. For example, if the plate separation, t, is 10mm and the wavelength, λ, is 400nm then the order number, n, is given by Equation 2,39:

$$n = \frac{2t}{\lambda} = 50000.$$

The free-spectral-range, from Equation 2.42, is 0.008nm, therefore, the 50000th. order of 400nm will coincide with the 50001st. order of 399.992nm. Therefore, it is usually necessary to use some form of additional dispersion to separate the orders. Prism and grating instruments have been used for this purpose and a detailed description

has been given by Tolansky.[120] An alternative method is to concatenate a series of etalons of successively increasing free-spectral-range,[128] having the advantage of a greater light-gathering power than a grating or prism system.

2.4.13 The Effect of Stopping Down the Interferometer.

The introduction of a stop immediately before the plates normally results in an increase in the effective finesse. There are a number of possible reasons for this improvement. Firstly,it appears that plates may be made flat to a greater accuracy over their central area. Secondly,by restricting the incident radiation to the central region of the plates the effect of any mal-adjustment in the plate parallelism will be minimised. Of course,there is a reduction in the light-gathering power (see Equation 2.71) when a stop is inserted so a compromise has to be made between signal intensity and any improvement in the finesse.

2.4.14 Reduction of Measurements.

The net function,$Y(\sigma)$, detected by the photo-multiplier tube may be considered to be composed of three major system functions.[125] The source function, $B(\sigma)$,represents the line profile emitted by the source which enters the spectrometer. In the ideal case the function detected would be equal to the source function but,unfortunately, distortion takes place as a result of two main causes: the function of the plates,E,and the

function of the scanning aperture,X. Therefore,Y may be written as a convolution of B,E and X:

$$Y = B * E * X. \qquad 2.75$$

Some of these functions may be decomposed into a series of basic functions. These are the Lorentz function,

$$L(x) = \text{constant}/(1+ x^2/\beta_1^2), \qquad 2.76$$

the Gaussian function,

$$G(x) = \text{constant } \exp\{-x^2/\beta_2^2\} , \qquad 2.77$$

and the Airy function described previously. The source function,B,may be decomposed into a Gaussian contribution arising from Doppler broadening and a Lorentz contribution from the remaining broadening processes. The etalon function,E,is formed from the Airy function and a Gaussian function for the surface deformations caused by the random microstructure. In some cases it is necessary to include a rectangular function to account for spherical surfaces.[124] As a result of the convolutions being associative and commutative the individual Gaussian and Lorentz contributions may be combined separately to give total Lorentz and Gaussian contributions.[129,130] Therefore, the net function,Y,may be expressed as a convolution of the four functions,

$$Y = L * G * A * X . \qquad 2.78$$

A frequently used approximation is to assume that A * X is approximately a Lorentz function;[132] alternatively, it may be possible to calculate these functions from the

instrumental parameters.[129-131] In many applications the contribution of the instrumental function to the total observed function is assumed to be negligible.

It remains to discuss the separation of the Lorentz and Gaussian functions from their convolution, the Voigt function. The Voigt function is usually expressed in the form

$$H(x,a) = \frac{a}{\pi}\int_{-\infty}^{+\infty}\frac{\exp\{-t^2\}dt}{a^2+(x-t)^2} \quad , \qquad 2.79$$

where,

$$a = \frac{\delta\sigma_L}{\delta\sigma_G}\sqrt{\ln 2} \quad \text{,(ratio of Lorentz to Gaussian half-widths)} \qquad 2.80$$

$$x = \frac{\sigma-\sigma_0}{\delta\sigma_G}\sqrt{\ln 2} \quad \text{,(wavenumber scale in units of the Gaussian half-width)} \qquad 2.81$$

$\delta\sigma_L$ = Lorentz half-width,

$\delta\sigma_G$ = Gaussian half-width,

σ_0 = wavenumber at the line centre and

σ = wavenumber at which the value of the function is to be evaluated.

Therefore, it can be seen that the Voigt function gives the value of the intensity at a particular wavenumber, where the wavenumber has been converted into a displacement from the line centre in units of the Gaussian half-width; and for a particular value of the damping constant, a, being the ratio of the Lorentz to Gaussian half-widths. This integral can not be solved analytically but a number of tables have been prepared by numerical integration, the most detailed being by Posener.[133] The table consists of values of H(x,a) at different values of x and a, therefore, $\delta\sigma_G$ and/or $\delta\sigma_L$ may be obtained by a look-up procedure.

B.H.Armstrong[134] has published a review of the properties of the Voigt function and a computer program in included for the evaluation of H(x,a) at different values of x and a.

There does not appear to be a general method in the literature for the deconvolution of all the possibly contributing functions in Equation 2.78; approximations are usually made for some of the functions.

In many applications, including this work, the values of the half-widths are important rather than the complete functions. The first stage in separating the individual half-widths is to remove the instrumental half-width, $\delta\sigma_A$, from the observed half-width, $\delta\sigma_E$. A well known and simple method is by Minkowski and Bruck[135] in which a graph of $\delta\sigma_T/\delta\sigma_E$ against $\delta\sigma_A/\delta\sigma_E$ is used, where $\delta\sigma_T$ is the true half-width after removal of the instrumental half-width and $\delta\sigma_E$ is the observed half-width containing contributions from $\delta\sigma_A$ and $\delta\sigma_T$. Such a graph has been reproduced in Figure 2.12. In drawing the graph the instrumental function has been assumed to be purely Airy and the source function to be purely Gaussian. The use of the graph is straightforward: the value of $\delta\sigma_A$ is known from a finesse measurement and this is divided by $\delta\sigma_E$, the observed half-width, to obtain $\delta\sigma_A/\delta\sigma_E$. Using the graph a corresponding value of $\delta\sigma_T/\delta\sigma_E$ is obtained from which $\delta\sigma_T$ is calculated. A similar graph has been prepared by Chabbal[125] and a set of tables by Hernandez.[130] Another possibility is to approximate the instrumental function to a Lorentz function.[132]

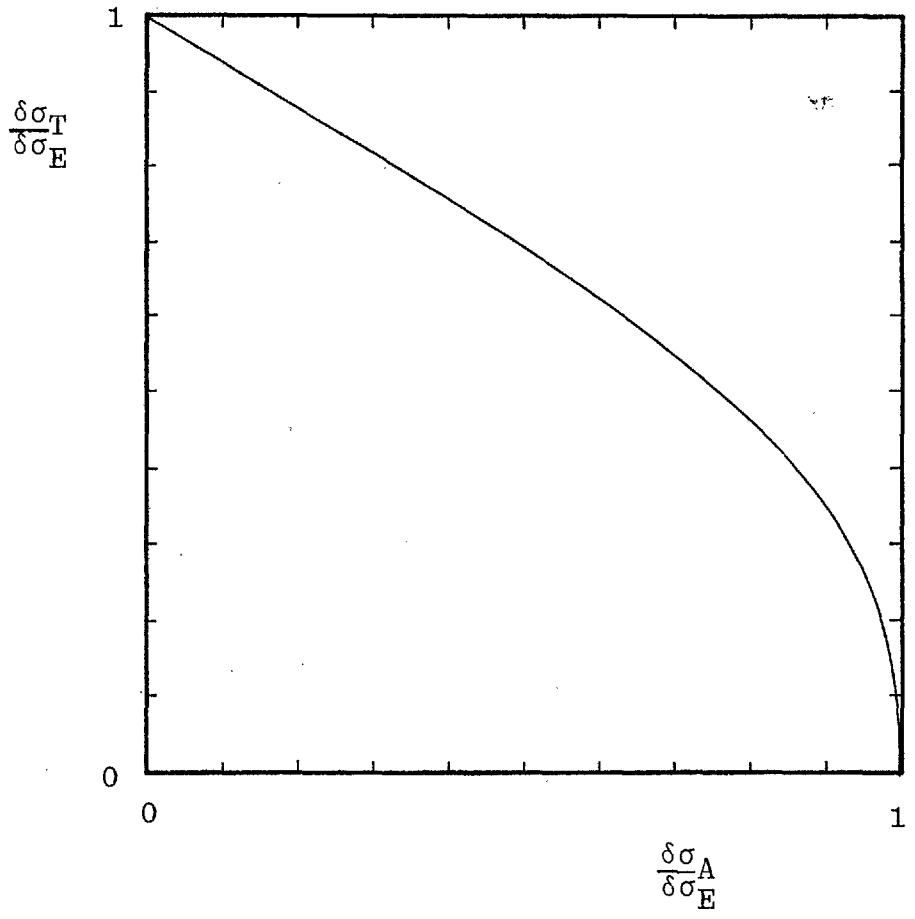


Figure 2.12: Graph Showing $\delta\sigma_T/\delta\sigma_E$ vs. $\delta\sigma_A/\delta\sigma_E$.[135]

On removing the instrumental function the Voigt half-width remains. In some cases either the Gaussian or the Lorentz contribution may be taken as negligible, in which case $\delta\sigma_T$ reduces to a single function. If these approximations are unsuitable a number of different methods exist for separating $\delta\sigma_G$ and $\delta\sigma_L$ from $\delta\sigma_T$. The most accurate method is to use successive approximations

and a table of Voigt profiles.[133] A useful approximation, adequate for most purposes, has been given by Danos and Geschwind,[136]

$$\delta\sigma_T \simeq \sqrt{(\delta\sigma_G^2 + \delta\sigma_L^2)}. \qquad 2.82$$

The usefulness of this approximation has been discussed by Posener.[133]

The ultimate method is to convolute Gaussian and Lorentz functions successively until the best possible fit is obtained to the experimental data. A simple version of this method has been used by Human and Scott[95] to evaluate their results but, unfortunately, the usefulness of such a technique is limited by any lack of precision in the data.

Two useful relationships are, for a series of combining Gaussian half-widths,

$$\delta\sigma_G = \sqrt{(\delta\sigma_{g_1}^2 + \delta\sigma_{g_2}^2 + \delta\sigma_{g_3}^2 + \ldots\ldots)}, \qquad 2.83$$

and, for a series of Lorentz half-widths,

$$\delta\sigma_L = \delta\sigma_{l_1} + \delta\sigma_{l_2} + \delta\sigma_{l_3} + \ldots\ldots \qquad 2.84$$

2.4.15 The Advantages and Disadvantages of the Fabry-Perot Interferometer as an Instrument for High Resolution Spectroscopy.

There are essentially three candidates for inclusion in this discussion: the diffraction grating (notably of the echelle type), the Michelson and the Fabry-Perot

interferometers. In addition, the wavelength range of interest is restricted to between 200nm and 1000nm.

When a grating spectrometer or a Fabry-Perot interferometer is used a spectral element is recorded during a time t. If there are N spectral elements then the time taken to record the spectrum is Nt. In Fourier transform spectrometry using the Michelson interferometer all N elements contribute to the signal at each setting. Therefore, the entire scan would take only time t if the number of sampling points were the same. In fact, 2N sampling points are required[6] so there is a time saving of N/2. This results in a signal-to-noise improvement of $\sqrt{N}$ compared with the Fabry-Perot and grating spectrometers, a result known as the Fellgett advantage. Although effective in the infra-red region of the spectrum it does not hold in the visible region under discussion where the principal source of noise is photon noise. Additionally, the number of sampling points required to obtain modest resolution becomes prohibitively high, thus eliminating the Michelson interferometer from the discussion.

The advantages of the Fabry-Perot interferometer over the diffraction grating may be summarised as:

* High light-gathering power - some two orders of magnitude better than a grating with the same effective area.
* A resolving power greater by an order of magnitude (at least) than a grating.
* The resolving power may be changed at will by changing the plate separation.

The disadvantages are:

* The need for additional dispersion to separate overlapping orders.
* The instrumental function is complicated.
* The Fabry-Perot interferometer is not suitable for scanning over a wide wavelength range because its resolving power is a function of its free-spectral-range, and vice-versa (Equation 2.66).

CHAPTER THREE

INSTRUMENTATION.

3.1 Optics 77

3.2 The Electronics 81
3.2.1 High Voltage Photomultiplier Tube Supply 81
3.2.2 Scan Generator 81
3.2.3 Signal Processing 82

3.3 Alignment of the Optical System 88

3.4 Operation 90

3.5 The Measurement of the Finesse 91

3.1 OPTICS.

The theory describing the operation of the Fabry-Perot interferometer used for the high resolution studies has been presented in Chapter two. A schematic diagram of the optical arrangement is shown in Figure 3.1. The instrument is an adaption of the Hilger and Watts model N250 interferometer, which was based upon the earlier prototype constructed by Cooper and Greig.[127,137]

The particular source under study was focused by LENS1 (Figure 3.1) to give an image in the plane of the secondary source aperture. The magnification of this image was adjusted by making a judicious choice of the source-LENS1 and the LENS1-aperture distances. In order to make measurements of the light from the whole of the source the image magnification was adjusted so that the secondary source aperture was filled. For making measurements at different lateral positions in the source an image magnification of ca. x10 was used.

According to the argument in Section 2.4.11 the diameter of the secondary source aperture was required to be the same as the scanning aperture for optimum light-gathering power. Therefore, for high light throughput the diameter of the aperture was required to be as large as possible but the aperture was required to be as small as possible to produce a large scanning finesse. As previously discussed in Chapter two, the scanning finesse is not usually the limiting parameter in the overall finesse. Using the table given by Sargent;[126] a scanning aperture of diameter 0.5mm was selected to produce a

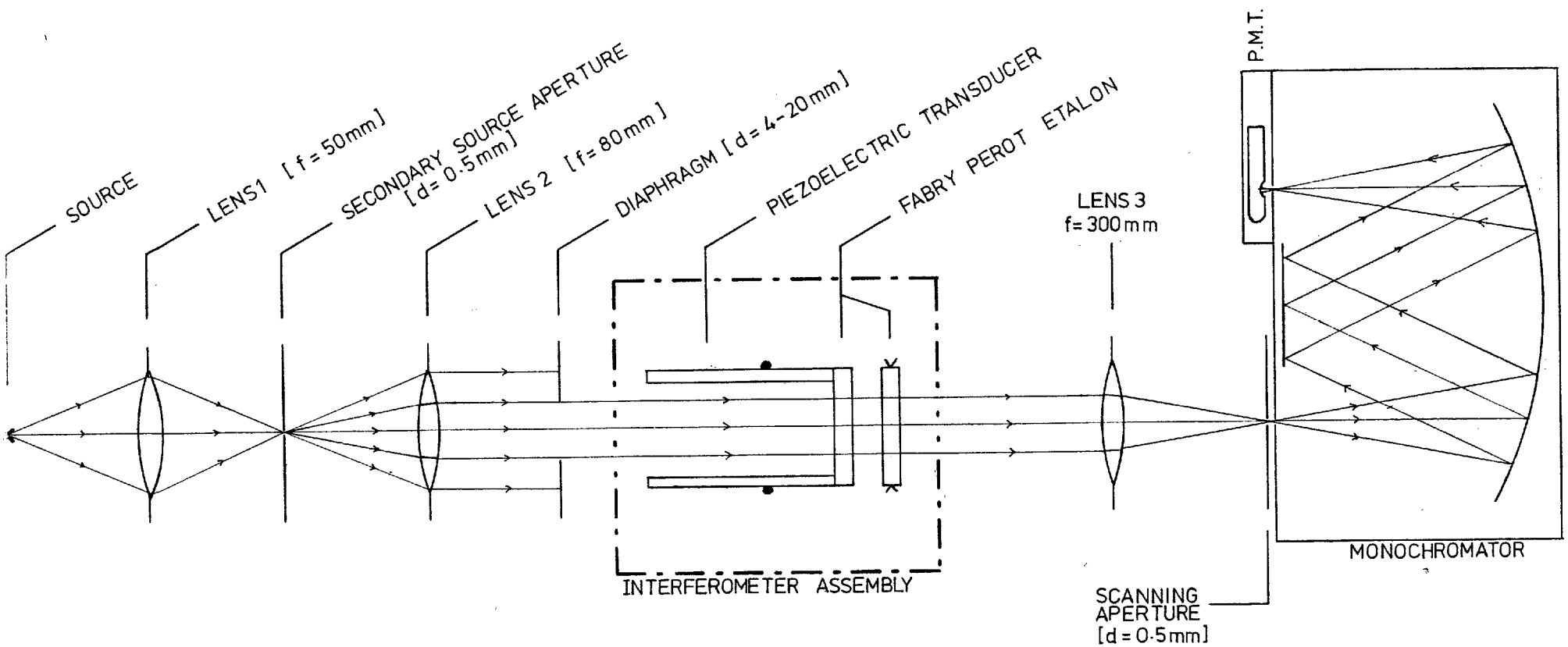


FIGURE 3.1: Schematic Diagram of the Optical System.

scanning finesse of ca. 150 . This value was considered to be sufficiently large in comparison with the overall expected finesse.

The radiation from the secondary source aperture was collimated by LENS2 (Figure 3.1) and passed through an adjustable diaphragm, the diameter of which was normally set at 10mm.

The base of the interferometer assembly was composed of two heavy steel bars held parallel by a clamp at each end. The clamps rested upon three adjustable screws, by which the assembly could be levelled. The interferometer plates and their mounts were supported in two frames, which could slide along the steel bars enabling the plate separation to be varied from 0 - 75mm. When in the desired position, the frames were clamped to the steel bars by two capstan screws. A tie-bar was also fitted between the tops of the frames in order to improve the rigidity of the assembly.

One frame was used to support the piezoelectric transducer and the oscillating plate. It was fitted with three screws to enable the plate to be made normal to the incident radiation. The other frame was used to support the fixed plate and was fitted with a similar set of three screws. In addition, three other screws were provided, adjustment of which changed the tension in the three springs holding the mirror mount to the frame. Very fine control of the plate parallelism was possible by using these three screws.

The Fabry-Perot plates used were made of vitreous

silica, flat to $\lambda/150$ at the mercury green line (546.1nm), with a dielectric coating giving 96% reflection and less than 1% absorption.

One of the plates was attached to a piezoelectric transducer using epoxy-resin cement. The piezoelectric transducer was a tube of barium titanate, capronic grade 3 (Plessey,Towcester),of internal diameter 19mm,external diameter 25mm and length 73mm. The inner and outer cylindrical surfaces were coated with silver to form electrodes for connection to the high voltage scan generator. The piezoelectric transducer and its plate were mounted in the frame using a rubber O-ring located at their centroid. Scanning was achieved by applying a varying voltage waveform to the piezoelectric transducer causing its longitudinal dimension,and hence the plate separation, to change by a very small amount.

The radiation passing through the etalon was focused on to the scanning aperture by LENS3 (Figure 3.1) to form an image of the secondary source aperture superimposed upon the interference fringe pattern. The centre of the fringe pattern was isolated by the scanning aperture and allowed to pass into a grating monochromator (Techtron Si-Ro-Spec),having a reciprocal linear dispersion of 3.3nm mm^{-1} and an aperture of f/10, to separate the different orders of interference. A Hamamatsu type R213 side-window nine stage photomultiplier tube was placed at the exit slit of the monochromator.

The use of the instrument for spectroscopic studies at low resolution was possible by removing the interferometer

assembly (Figure 3.1).

3.2 THE ELECTRONICS.

3.2.1 High Voltage Photomultiplier Tube Supply.

The E.H.T. unit used was an Hilger and Watts type FA.187 capable of supplying 350-1050V d.c. at up to 2mA. It was connected to the photomultiplier tube by co-axial cable.

3.2.2 Scan Generator.

Two different generators were used to supply the scanning waveforms,one for slow scanning the other for rapid scanning.

An Aim Electronics SSG212 slow scan generator was used to produce a triangular waveform with a continuously variable amplitude from 0-20V. The scanning period was variable in two ranges from 5-55s and from 50-550s. The corresponding frequencies were 0.2-0.018Hz and 0.02-0.0018Hz,respectively. A useful feature was a sample and hold switch which enabled the output to be held at a particular value.

A Chelsea Instruments TWG10 rapid scan generator was used to provide scanning frequencies in two switched ranges of 0.2-16.5Hz and 6.25-500Hz. The amplitude of the triangular waveform was adjustable between 0 and 10V. An additional output was available which supplied a fixed amplitude square wave in synchronism with the triangular waveform. This output was used for gating purposes,which will be described later.

The triangular output from the selected generator was taken via a switch into a Chelsea Instruments HVA10 amplifier. This device had a gain of 100 with a maximum rated output of ±400V. The output of the amplifier was taken via a voltmeter,which was only used in the slow scanning mode, to the piezoelectric transducer. The amplifier was only capable of following frequencies of up to ca. 50Hz without distorting the waveform.

3.2.3 Signal Processing.

When the instrument was used for slow scanning or as a spectrometer with low resolution, the output from the photomultiplier tube was taken across a 22kΩ load into a Servoscribe RE 511.20 chart recorder.

In rapid scanning mode,the signal from the photomultiplier tube was required to be taken to an oscilloscope,for display purposes,and into a signal averager for accumulating the data. The signal from the photomultiplier tube was not capable of driving both inputs and,in any case,this signal was incompatible with the input requirements of the signal averager. It was not desirable to view the signals generated during the positive-going and negative-going parts of the scanning waveform because of their lack of registration. A previous attempt had been made to z-modulate the oscilloscope display using the synchronization output of the scan generator,thus cutting out the display during one half of the scanning cycle. This method was not satisfactory because of the large time constant on the input to the

oscilloscope. In view of the requirements outlined above a gating/amplifier unit was constructed,capable of providing two outputs,suitably amplified, and gating out the signal during the return section in the scanning cycle.

Figure 3.2 is a schematic diagram of the electronics used in making interferometric measurements. The signal from the photomultiplier tube was taken,via the amplifier/gating control unit,to the inputs of the oscilloscope and the signal averager. The display outputs from the averager were also taken to the second input channel of the oscilloscope. The signal averager (Data Laboratories, Model DL102) was capable of accumulating a preset number of scans and was triggered by the synchronization output of the scan generator. Controls were available to vary the sweep time and the delay between the receipt of the trigger pulse and the start of the sweep,thus enabling the required portion of the scan to be recorded.

Two outputs were available from the signal averager. The two hundred data points were stored in the averager as 16BIT words and these were available sequentially at the digital output. This digital output was taken,via an interface,to a high speed paper tape punch (Data Dynamics, Model 1133). X and Y analogue outputs from internal digital-to-analogue converters were taken to an X-Y plotter (Bryans,Model 2000).

In addition to the specification mentioned above, the amplifier/gating control unit was also required to insert a reference level pulse into the signal going into the

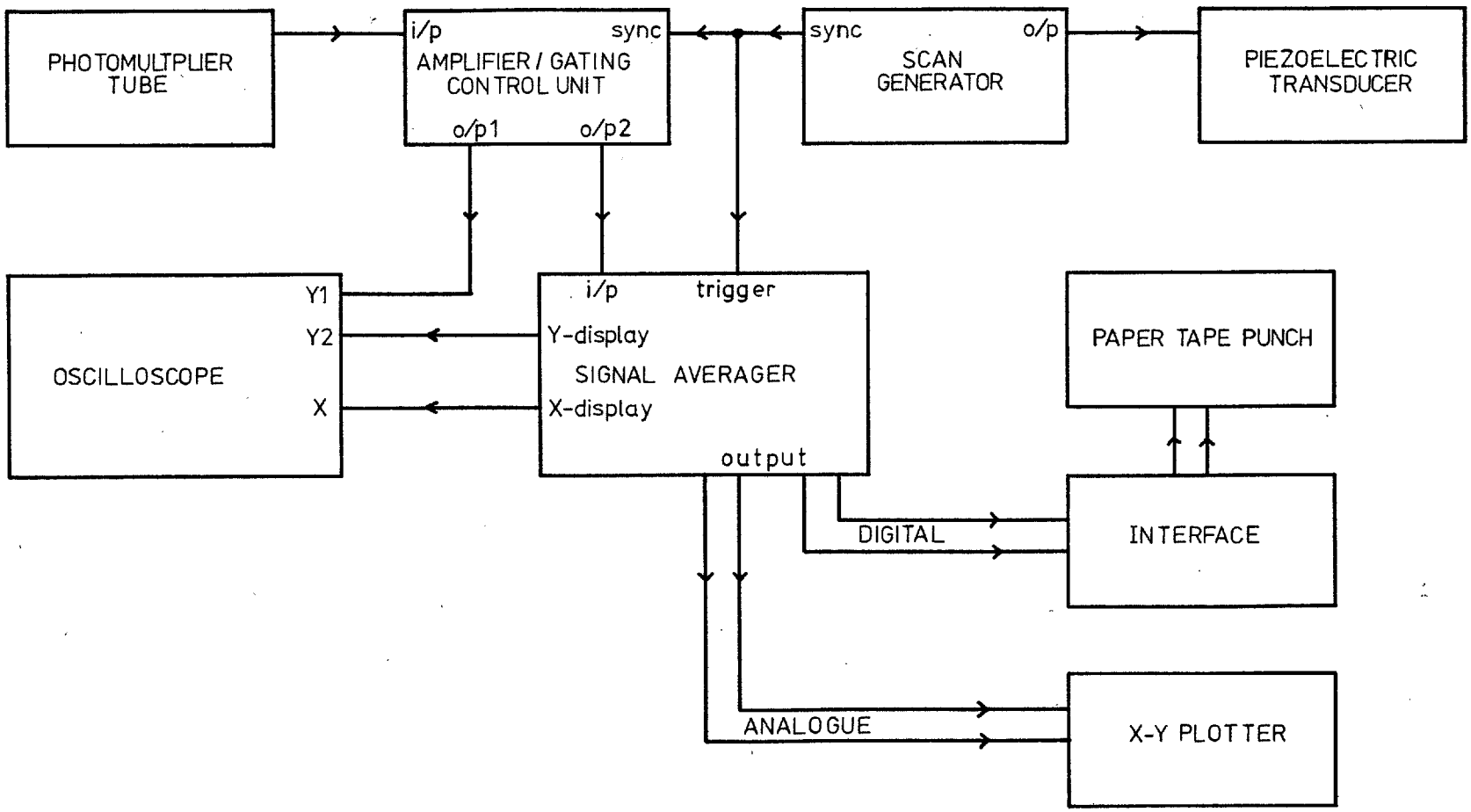


FIGURE 3.2: Interferometer Electronics.

signal averager. This need arose from the circulating nature of the store in the signal averager and the requirement to measure the background emission. Without a reference pulse it would have been impossible to match up the signal trace with its background trace.

The circuit of the amplifier/gating control unit employed is shown in Figure 3.3. The input from the photomultiplier tube was taken across the load,C1 and R1, and via R2 into the inverting input of the amplifier IC1a. The gain of this amplifier was set by the ratio R4/R2 and the amplifier was provided with an offset control,VR1, in addition to the usual offset-null potentiometer,VR2. The output of IC1a was then divided and taken to two identical circuits. The signal via R5 was controlled by an analogue gate,IC6a, and taken to the inverting input of the amplifier IC7b. The gain of this amplifier was variable from 1-23 by means of VR4, and again an offset control,VR3,was provided. The inverting input of IC7b was also capable of being grounded by the analogue gate IC6d. By use of the complementary control signals GS1 and GS2 the input to the amplifier(IC7b) was either the signal or at ground potential.

The gating control signals, GS1 and GS2,were derived from the synchronization output of the scan generator by means of the following circuit. The signal from the scan generator square wave output had a voltage swing of +7.5 to -7.5V. This signal was taken,via R20,to the inverting input of amplifier IC1b. The amplifier had a variable negative gain set by R20,R18 and VR10, and an

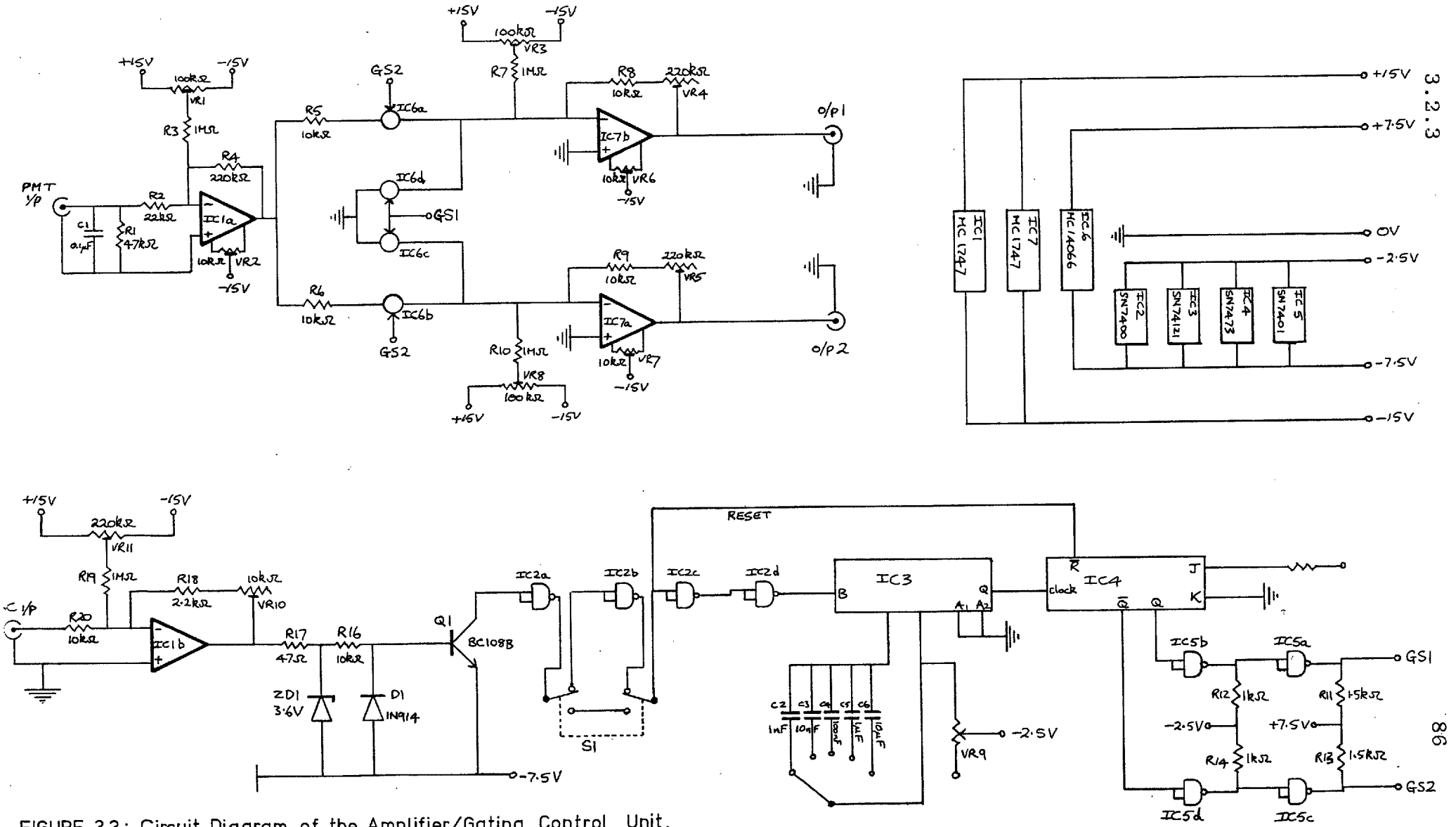


FIGURE 3.3: Circuit Diagram of the Amplifier/Gating Control Unit.

offset control,VR11. The output of the amplifier IC1b was taken via R17 and a voltage limiter,zener diode ZD1,to a buffer amplifier,Q1. At this point the voltage swing had been converted to be in the range -7.5 to -4V,suitable for the TTL in the next stage. The signal was taken via the inverter,IC2a,and the optional inverter,IC2b,to the reset input,$\overline{R}$,of the JKflip-flop,IC4. The optional inverter could be switched in or out of circuit by switch S1. This was to enable either the positive-going or the negative-going ramp from the scan generator to be selected. The output from IC2b was also taken via IC2c and IC2d to the input,B, of the monostable multivibrator,IC3. The output,Q,from IC3 was taken to the clock input of IC4. The inclusion of IC2c and IC2d was to delay the signal via the monostable so that signals from IC2b and IC3 did not reach IC4 at exactly the same time. The complementary outputs,Q and $\overline{Q}$, of IC4 were taken via IC5 for level conversion giving an output voltage swing of ca. -7.5 to +7.5V. This was the required input level for the CMOS gates in IC6.

The operation of the circuit was as follows. While the synchronization pulse was at LOGIC 0 the output of the JKflip-flop was held low by the reset line. During the positive-going edge of the synchronization pulse the JKflip-flop was enabled by the reset line going to LOGIC 1. The same positive-going edge,slightly delayed, also caused the monostable to trigger and its output to go to LOGIC 1 for a time set by VR9 and S2. After this time the output from the monostable went to LOGIC 0,

causing the clock input to the JKflip-flop to be triggered and the output,Q, from the JKflip-flop to go to LOGIC 1. The output,Q, from the JKflip-flop then remained at LOGIC 1 until reset by the synchronization pulse going to LOGIC 0. In this way the signal from the photomultiplier tube could be gated-out during the return sweep period in the scan and a reference pulse inserted into the signal of duration set by VR9 and S2.

3.3 ALIGNMENT OF THE OPTICAL SYSTEM.

It was found that great care and attention to detail was required to produce a reasonable working finesse. The first stage of the alignment procedure was carried out using a 0.5mW He-Ne LASER. All the components were removed from the optical bar,except for the secondary source aperture,and the LASER was mounted in the source position at the end of the bar. Having set the secondary source pinhole to be at the correct height, the LASER was levelled and centred until the LASER beam would pass through the pinhole,when it was placed at any position along the optical bar. When this had been carried out the secondary source aperture was fixed in its final position and the monochromator position was adjusted until the LASER beam entered via the pinhole and emerged from the centre of the exit slit. In order to assist with this stage in the alignment procedure the photomultiplier tube was removed, because it would have been damaged by the high radiance of the LASER beam, and a simple photoresistor (ORP12) was used to monitor the intensity of the throughput.

The next stage involved the alignment of the lenses on the optical bar. It was found necessary to modify the Barfit stands so that they could be exactly centred on the optical bar by using three allen screws and locking nuts. The lenses were aligned by requiring the transmitted beam to enter the monochromator and all the beams reflected from lens surfaces to return along the incident path of the LASER beam. The adjustable diaphragm was also centred in its final position on the optical bar. The interferometer assembly was then mounted on the optical bar but with only the left plate (attached to the transducer) fitted. By using the three positioning screws on the frame, the plate was adjusted to be normal to the incident LASER beam. The base of the interferometer was levelled by ensuring that the plate on its mount and frame maintained its normality to the LASER beam when the frame was moved to any position along the steel bars. The second interferometer plate was then mounted in position and approximate parallelism was attained by the use of the coarse adjustment screws until a concentric interference ring pattern formed on the entrance pinhole to the monochromator.

When this stage in the alignment procedure had been completed the LASER was removed from the optical bar and a Hilger and Watts N306 fringe viewer was mounted in the space between the interferometer assembly and LENS3 (Figure 3.1). The fringe viewer consisted simply of a highly corrected achromatic telescope, focused at infinity, fitted with a beam splitter and an eyepiece. A neon-filled

hollow cathode lamp was mounted on the optical bar in the source position and focused using LENS1 to give an image which filled the secondary source pinehole. The position of LENS2 was then adjusted until the image of the pinhole was in focus when viewed through the telescope. The position of LENS3 was adjusted, having removed the telescope, so that the fringe pattern was focused on the entrance pinhole of the monochromator. Final adjustment of the position of LENS3 was made by making finesse measurements.

3.4 OPERATION.

The routine adjustment of the plate parallelism was made in the rapid scan mode at a scanning frequency of ca. 10Hz. A neon-filled calcium hollow cathode lamp was normally used as the source during this procedure. The first stage was to look back along the optical axis of the interferometer towards the source and the coarse screws on the fixed plate were adjusted until a concentric ring pattern was observed. In order to see the fringes it was necessary to operate the hollow cathode lamp at a very low current, ca. 3mA. After obtaining the fringe pattern visually and increasing the hollow cathode lamp current to ca. 20mA it was usually possible to observe some form of signal on the oscilloscope. Fine tuning of the parallelism was carried out using the fine controls while viewing the trace on the oscilloscope. The adjustment was carried out so that peaks on the oscilloscope were as narrow, tall and

symmetrical as possible. The voltage of the scanning waveform was adjusted,if necessary,so that three orders were scanned. The sweep time control on the signal averager was normally set at 0.1s. The delay before control on the signal averager and the scan frequency control were adjusted so that the averager measured two orders and that these were centred in the sweep period.

3.5 THE MEASUREMENT OF THE FINESSE.

Finesse measurements were made using a calcium hollow cathode lamp and a very small plate separation of 0.7mm. Using Equation 2.42 the free-spectral-range was 7.14 cm^{-1} or 0.128nm at this plate separation. Under these experimental conditions the half-width of the calcium 422.67nm line was found to be 0.0012nm[32] The half-width of the calcium line was,therefore,expected to be small in comparison with the free-spectral-range, the ratio between the two values being 107. Therefore, the major contribution to the observed line width under these conditions would be due to the instrumental function.

Measurements of the finesse were made using the slow scan and the rapid scan modes of operation. The level of the scan generator was adjusted to allow two successive orders to be observed. The separation between the maxima,$\Delta\sigma$,was measured and the half-width,$\delta\sigma$.The experimental finesse was calculated as the ratio $\Delta\sigma/\delta\sigma$. Typical experimental values obtained for the finesse were 28 in slow scan mode and 25 in rapid scan mode (10Hz).

These results correspond to instrumental half-widths of 0.255 cm^{-1} and 0.286 cm^{-1}, respectively, using Equation 2.60.

The finesse values measured were not independent of the wavelength because of the properties of the dielectric coatings. The strong lines of mercury (404.67nm) and calcium (422.67nm) were at the two ends of the useful working wavelength range. Measurements of the finesse at the indium 451.13nm line and at the strontium 396.93nm line gave values of only 4 and 5.5, respectively.

CHAPTER FOUR

THE PREPARATION AND OPERATION OF ELECTRODELESS DISCHARGE LAMPS.

4.1 The Preparation of Electrodeless Discharge Lamps 94
4.1.1 General 94
4.1.2 The Lamp Blank 94
4.1.3 The Vacuum Apparatus 96
4.1.4 Degassing Procedure 97
4.1.5 Fill Material 98

4.2 The Operation of Electrodeless Discharge Lamps 101
4.2.1 Microwave Supply 101
4.2.2 Resonance Cavities 102
4.2.3 Temperature Regulation 104

4.1 THE PREPARATION OF ELECTRODELESS DISCHARGE LAMPS.

4.1.1 General.

A large number of papers have been published describing the preparation and properties of the electrodeless discharge lamp(EDL). These have originated mainly from J.D.Winefordner *et al.* at the University of Florida,U.S.A., and from T.S.West and co-workers at the Imperial College,London. A review has been published by Haarsma *et al.*[50]

4.1.2 The Lamp Blank.

Lamp blanks were prepared from transparent fused silica tubing of nominal internal diameter 8mm with a wall thickness of *ca.* 1mm. The lengths of silica tubing were first washed with detergent solution and then with 50%v/v nitric acid. After several rinses with distilled water they were dried over a Bunsen flame. The blanks were made from the silica tubing using the method described by Dagnall *et al.*[41] The dimensions of the blanks used are shown in Figure 4.1. The bulb length has not been found to be critical in the range 25-50mm[138] and most workers have used tubes of length within this range.[50] After sealing-off the internal length of the bulb was *ca.* 40mm. The internal diameter of the lamp, *ca.* 8mm, is the most frequently mentioned size used in the literature. Mansfield *et al.*[139] found an internal diameter in the range 5-9mm to be the optimum value.

The lamp blanks were not treated chemically in any

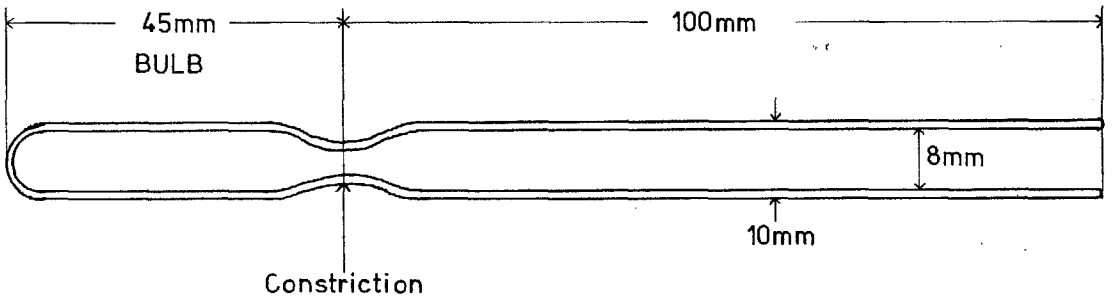


FIGURE 4.1: The EDL Blank.

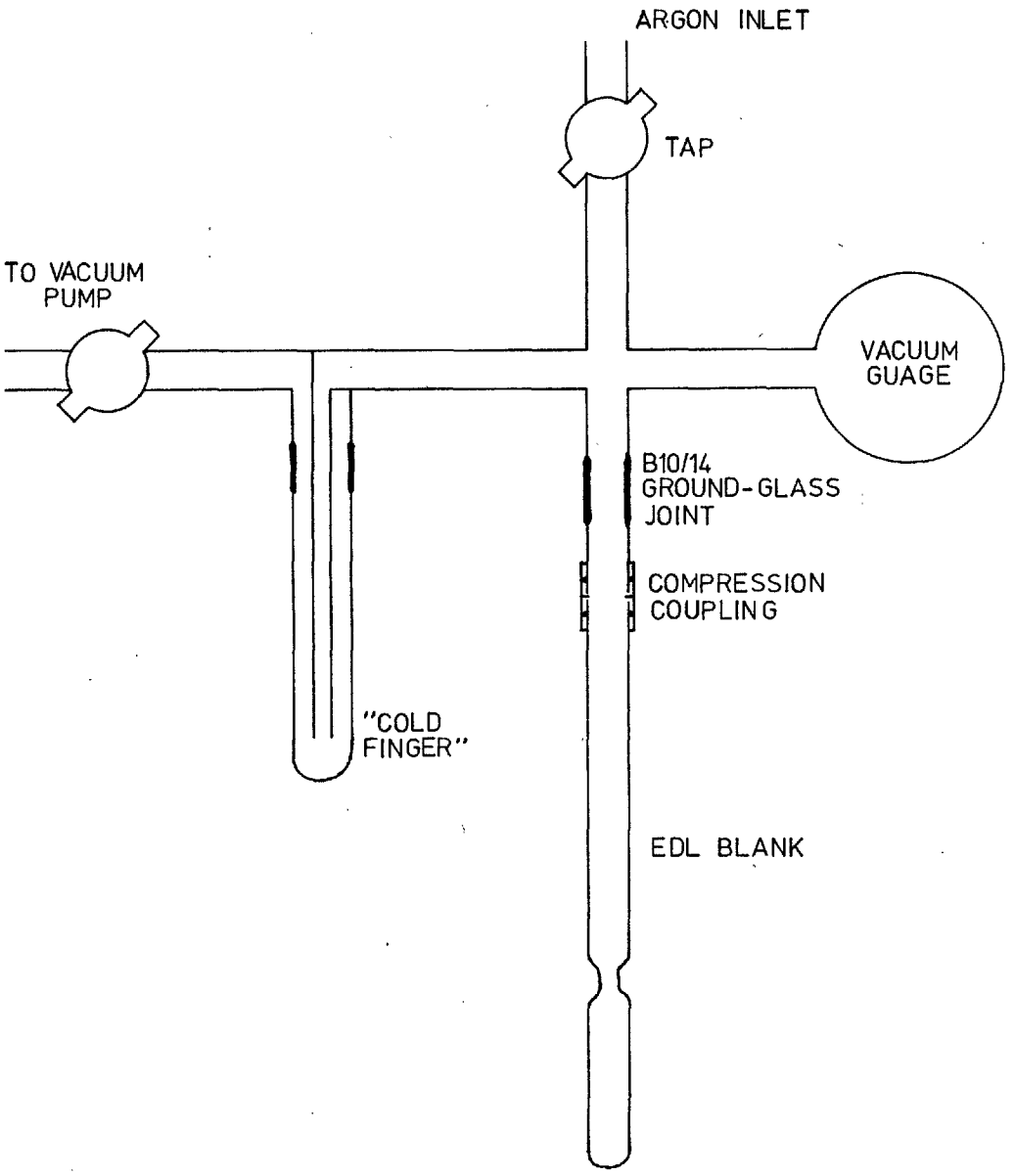


FIGURE 4.2: Vacuum Line for the Preparation of an EDL.

way before being used. The method used by Aldous et al.;[140] by which boric acid was used to form a protective layer of borate glass on the inner surface of the EDL, was not considered necessary as very reactive metals were not used.

4.1.3 The Vacuum Apparatus.

The vacuum line used in the preparation of the EDL's was a very simple arrangement based upon the previous designs by West et al. [141] A schematic diagram of the vacuum line used is shown in Figure 4.2. The McCloud mercury manometer used in some previous designs was replaced by a Speedivac barometric pressure guage, having a range of 0-20 torr in divisions of 1torr. Mercury contamination has been shown previously to be a problem when McCloud guages are used.[138] The Speedivac type of guage also had the advantage of giving a continuous reading of the pressure in the line. The vacuum line was connected to a two-stage rotary vacuum pump via a high vacuum ground-glass tap. A liquid nitrogen cold trap was used to prevent oil vapour from the pump diffusing into the line. Although the boiling point of argon is higher than the boiling point of nitrogen only a small amount of liquid argon was collected in this trap. The line was connected to a cylinder of argon by a rotaflo tap and a conventional cylinder head pressure regulator. Ordinary commercial grade argon was used at a line pressure of 15p.s.i.

A B14 socket was provided for the connection of an

EDL blank to the line. The EDL blank was connected to a B14 cone by a compression coupling containing rubber olives. This method of connection was found to be vastly superior to using rubber or plastics tubing because it prevented the lamp from inclining out of the vertical while being heated. The problem of foreign matter finding its way into the lamp from the tubing was also eliminated.[142]

4.1.4 Degassing Procedure.

The EDL blank was connected to the vacuum pump and the bulb was heated to just below its softening point for ca. 10 minutes using an oxy-propane hand torch. Occasionally the bulb was flushed with argon and then the heating was resumed. The merits of degassing have been subject to some controversy in the literature. Some authors[141,38] have restricted degassing to heating the EDL bulb for five minutes with a hand torch, whilst on other occasions heating for several hours at high temperatures has been recommended.[143] Other authors have questioned the usefulness of degassing if the lamp blank is to be re-opened to the atmosphere during the introduction of the fill material.[138,142] Whilst the latter point has some validity, there appears to be considerable evidence in favour of some form of degassing procedure. Perhaps it is necessary to distinguish between material that is adsorbed onto the surface of the quartz and material that is loosely bound in the quartz lattice just below the surface. Presumably, heating to a high temperature under vacuum removes all adsorbed

species,such as water,oxygen etcetera,and some species from below the surface of the quartz. By flushing with argon during the degassing procedure and allowing the lamp to cool under an argon atmosphere,it appears reasonable that vacant sites below the surface of the quartz which previously contained undesirable impurities will now contain argon. During the re-exposure to the atmosphere for the introduction of the fill material it does not seem likely that very much diffusion into the walls of the silica would occur,especially in view of the relatively short time of exposure and the absence of any heating. Such care in degassing would appear to be rewarded during the operation of the lamp when any heating of the silica walls by the discharge would tend to liberate trapped argon rather than quenching species such as oxygen or water.

Following the heating procedure an argon plasma was induced in the lamp,while it was still attached to the vacuum line,using a ¼-wave microwave resonance cavity. Occasionally the blank was flushed with argon. Dagnall et al.[143]recommend this technique. It seems reasonable to allow any interaction that would occur between the plasma and the silica walls,resulting in the release of species from the wall,to take place as much as possible before the lamp is sealed.

4.1.5 Fill Materials.

Bartley[138]has stressed the importance of avoiding the introduction of oxides into the EDL. Their presence

has been noticed to cause premature lamp failure, failure of the discharge to fill the bulb or the inability of the lamp to ignite at all.

The type of material used in the EDL depends upon its vapour pressure. For example, in the case of cadmium or mercury the elements have a sufficient vapour pressure for sufficient atoms to be present in the vapour phase and, hence, be excited in the plasma. Other elements are much less volatile and so a compound more volatile than the element alone must normally be used. The most frequently used compounds are the iodides although chlorides and bromides have been used. One problem is that the metal tends to react with the quartz in some cases so that an excess of iodine remains in the lamp resulting in an iodine spectrum or the quenching of the discharge. For this reason it is common to prepare the iodide *in situ* with excess metal being present.[38] Iodine has advantages over chlorine and bromine because it is much easier to handle in a vacuum line.

The technique used to prepare the iodides *in situ* was as follows: A small amount of the metal was selected and a piece with freshly cut surfaces obtained using a scalpel in order to remove thick oxide coatings. A small piece of the metal, *ca.* 1-5mg, was then introduced into the bulb of the EDL blank and the blank was returned to the vacuum line and evacuated as quickly as possible. After flushing with argon several times the metal was sublimed carefully a small distance up the wall of the bulb. At this point there was the opportunity to volatilize some

of the metal out of the bulb if this was judged necessary. After allowing the blank to cool it was removed from the vacuum line and a small piece of resublimed iodine was added, *ca.* 1-5mg. The blank was returned to the vacuum line and flushed with argon several times. The iodine remaining at the bottom of the bulb was then warmed very gently until it had completely evaporated. The blank was flushed several times with argon and then the solid on the side of the bulb was sublimed a further short distance up the wall. In most cases the iodine had only reacted with the surface of the metal layer;this could be observed during the sublimation procedure. The lamp was filled with argon to a pressure of *ca.* 2torr and then sealed-off.

In the case of an EDL containing the element alone the first part of the above procedure was adopted with subsequent sealing-off under argon.

Problems were encountered in preparing a manganese EDL by making the iodide *in situ*. These were attributed to the difficulty in introducing oxide-free manganese. Therefore,anhydrous manganese chloride was used which had been prepared by recrystallizing *Analar* grade manganese (II)chloride and then by heating in a furnace at *ca.* 500°C to remove the water of crystallization.

The preparation of the mercury-199 isotope EDL caused considerable problems because the mercury had been supplied as the oxide,the least suitable form. Simple heating of the oxide *in situ* was not found to be satisfactory because of incomplete decomposition and loss of mercury

by volatilization. Other procedures have been described in the literature[144,145] but a simple and reasonably effective method was found to be reduction in situ using alkaline hydrogen peroxide solution. A few milligrams of the single isotope-enriched mercury(II)oxide was introduced into the EDL blank and then a few microlitres of 20 volume hydrogen peroxide solution was added and made alkaline with freshly prepared ammonia solution. This reduction,

$$HgO + H_2O_2 \rightarrow Hg + H_2O + O_2,$$

has the useful property that all the starting reagents and the unwanted products are easily volatilized out of the lamp by connection to the vacuum pump.

Argon was used as the fill gas for all the electrodeless discharge lamps prepared in this work; this gas has also been the choice of almost all other workers. However, Silvester and McCarthy[146] reported that under certain conditions helium gave optimum results. The usual fill gas pressures quoted in the literature are in the range 1-5torr. In this study fill pressures of either 2 or 3torr were used. EDL's were prepared for each of the elements shown in Table 4.1.

4.2 THE OPERATION OF ELECTRODELESS DISCHARGE LAMPS.

4.2.1 Microwave Supply.

Microwave power was supplied by a Microtron 200 (Electro-Medical Supplies Limited, Wantage, Berkshire), capable of generating up to 200W at a frequency of

TABLE 4.1: Materials Used to Prepare EDL's.

ELEMENT	MATERIAL	FILL PRESSURE OF ARGON (torr)
Antimony	Iodide prepared *in situ*.	2
Arsenic	Element	2
Cadmium	Element	3
Gallium	Iodide prepared *in situ*.	2
Germanium	Iodide prepared *in situ*.	2
Indium	Iodide prepared *in situ*.	2
Lead-207	Iodide prepared *in situ*.	3
Manganese	Anhydrous $MnCl_2$	2
Mercury-199	Reduction of ^{199}HgO	2
Selenium	Element	2
Zinc	Iodide prepared *in situ*.	2

2450MHz. This was connected by coaxial cable *via* a reflected power meter to the particular resonance cavity being used.

4.2.2 Resonance Cavities.

The bulk of this work was carried out using a Broida-type 3/4-wave resonance cavity,model 210L (E.M.S. Ltd.),although,for the purpose of making a comparison, the Evensen-type ¼-wave cavity,model 214L,was also used. The 3/4-wave cavity is shown in Figure 4.3. A major advantage of the 3/4-wave cavity is that it tends to protect the EDL from drafts and gives good thermal

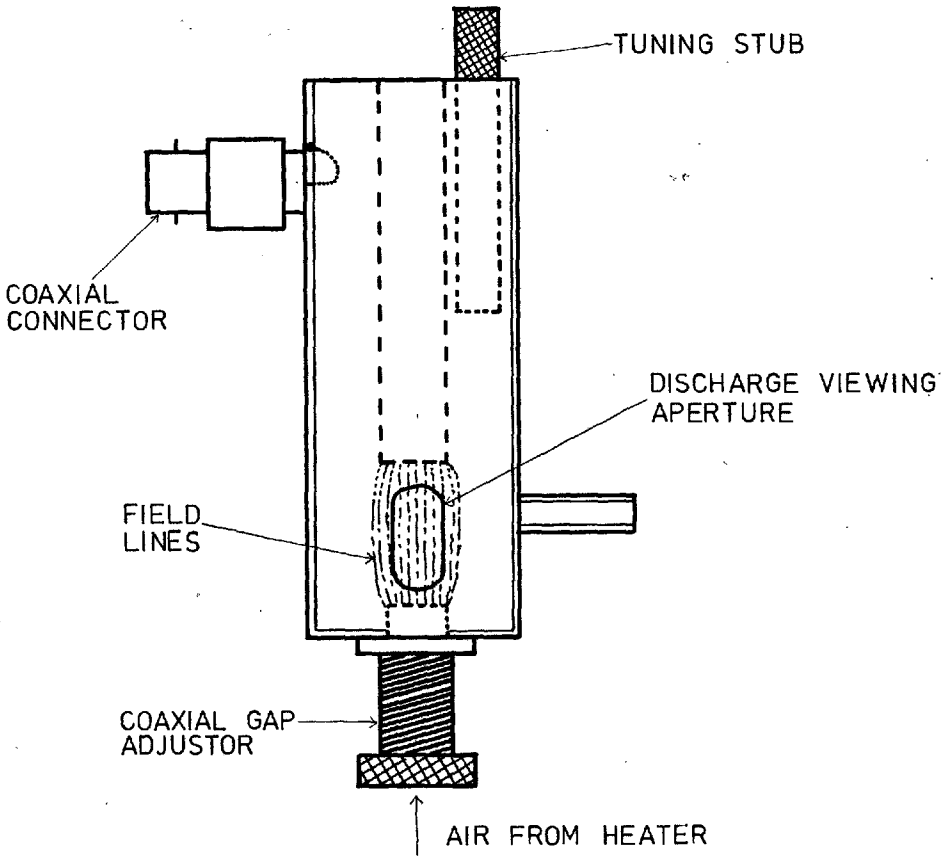


FIGURE 4.3: Broida-Type 3/4-Wave Resonance Cavity.

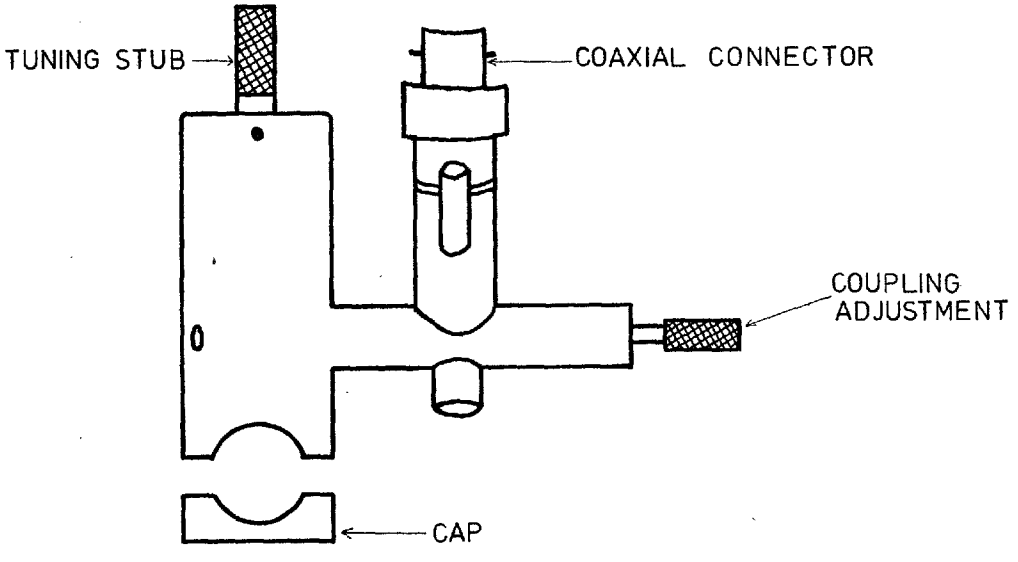


FIGURE 4.4: Evensen-Type 1/4-Wave Resonance Cavity.

stability because of its enclosed design. The coupling of the microwave power to the EDL in this type of cavity is not very efficient and varying the position of the tuning stub makes very little difference to the magnitude of the reflected power. However, the electric field in this type of cavity is probably more uniform in the vicinity of the EDL than in the ¼-wave type of cavity.[147]

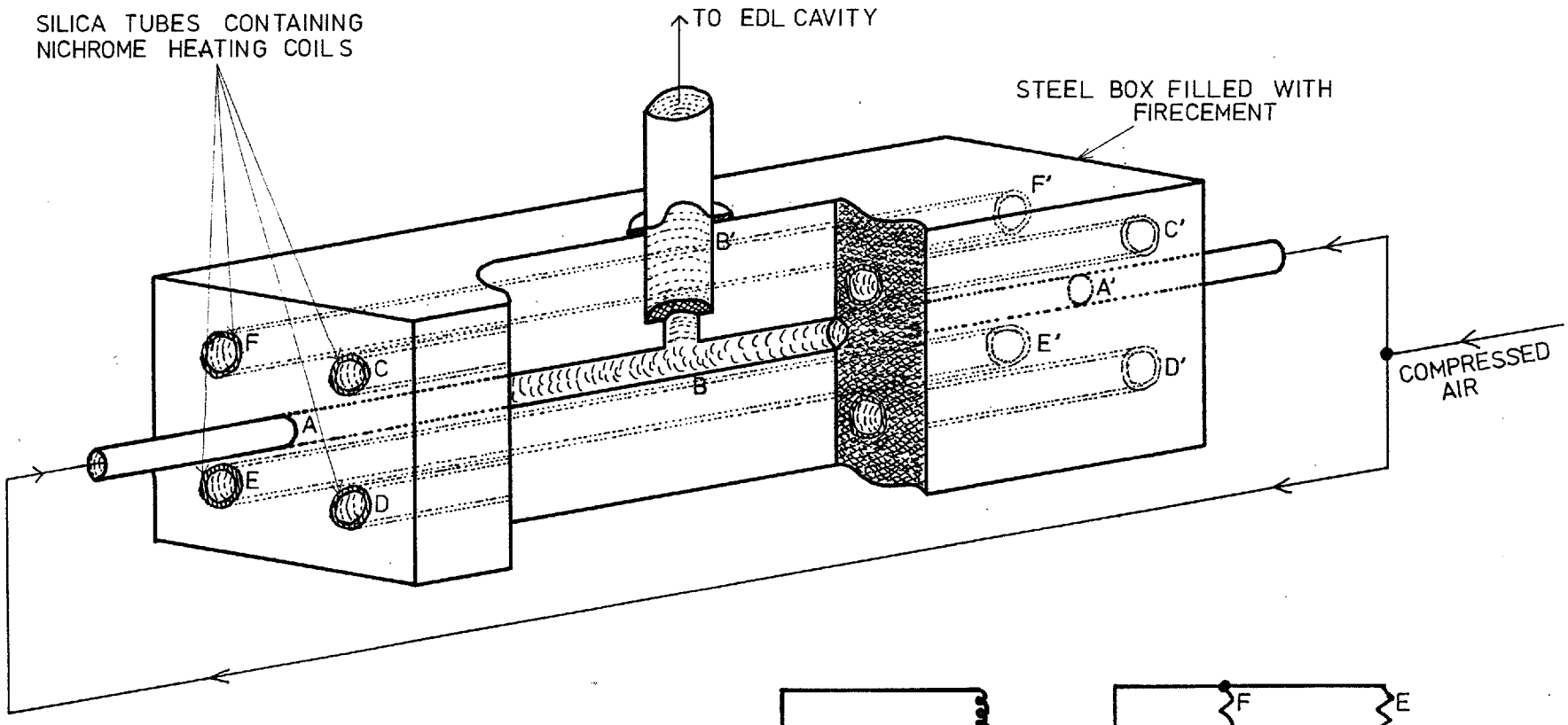
The ¼-wave cavity is shown in Figure 4.4. The ¼-wave cavity produces a more intense microwave field than the 3/4-wave cavity and very efficient coupling is usually possible by the careful adjustment of the tuning stubs. The magnitude of the reflected power may be reduced almost to zero in this type of cavity. However, disadvantages include a tendency to overheat discharge tubes and the lack of draft shielding. The relatively open design of the cavity makes it less easy to use than the 3/4-wave type for temperature-controlled operation. The localized nature of the field can also result in material plating out in certain parts of the lamp.

4.2.3 Temperature Regulation.

Early research workers examining the properties of EDL's relied upon the microwave field to provide energy for excitation as well as the heat necessary to maintain the vapour pressure of the material within the lamp at the required level. Browner and Winefordner[47] have shown that the control of the temperature of the lamp has an important effect upon the radiance and stability of the discharge. It has also been pointed out that with the

vapour pressure of the material inside the lamp being controlled by the temperature the quantity of material introduced into the lamp during its preparation should become less critical. Human and Butler[148] suggested that a vapour pressure of 1-2torr of the material inside the lamp was necessary for optimum operation. Other authors have suggested values of 5torr[149] and 0.005torr[47] as more suitable vapour pressures.

Previous methods for the temperature control of EDL sources have involved passing heated air through the resonance cavity and over the surface of the lamp. These heaters have used either a compressed air supply or an impeller fan to pass air over a resistively heated coil.[138, 149, 48] This technique was found to suffer from a number of problems. The heater coil tended to become corroded by the passage of air and become very brittle through rapid heating and cooling. These problems resulted in a high incidence of heater failure. The heater coil had a very small heat capacity so that any slight variation in the supply voltage was quickly repeated in the temperature of the air stream. In some designs[149] the heater coil was wound on a solid steel core, insulated with asbestos tape, and coated with alumina cement. The expansion and contraction of the metal core quickly resulted in cracks appearing in the cement and this resulted in the fracture of the heater coil. Therefore, a new type of EDL heater was designed which would allow operation up to 500°C. A schematic diagram of the heater design is shown in Figure 4.5.



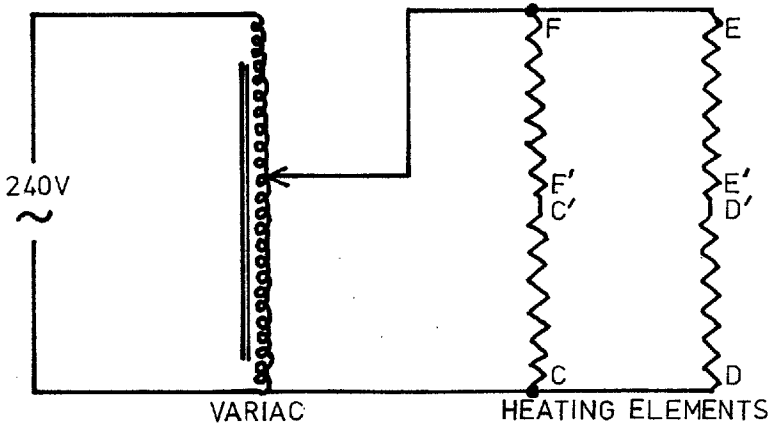
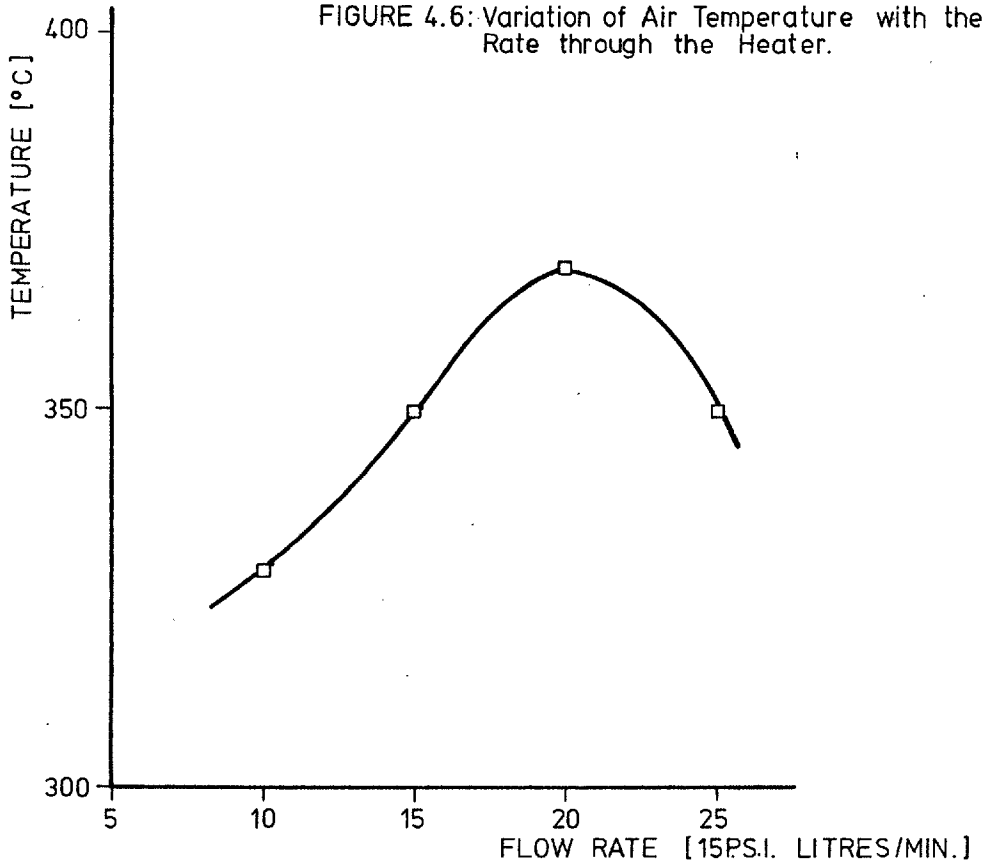


FIGURE 4.5: Air Heater for Thermostatting EDL's.

The heater was moulded from firecement set in a steel box. A stainless steel tube with flange was screwed onto the top of the box for the purpose of mounting the cavity. During the moulding process a central channel AA' and a perpendicular channel BB' were made for the passage of air. Four silica tubes (i.d. 8mm) CC',DD',EE' and FF' were also set into the firecement for the location of the heating coils. 5cm pieces of ¼inch o.d. stainless steel tubing were fixed into the central channel at A and A', using firecement, for the introduction of compressed air. Compressed air was supplied via ¼inch copper tubing to both stainless steel inlet tubes. Two spiral heating elements (Type SE6,1000W,250V,Wellco Electric Limited) were required, being wired in parallel and connected to a Variac transformer. One heating element was connected to follow the path FF'C'C and the other followed EE'D'D in Figure 4.5.

This design of heater was found to have a number of advantages. The heating coils are not in direct contact with the air stream making them less liable to brittle fracture resulting from rapid heating and cooling. The relatively large heat capacity of the firecement produced a stable air stream temperature although the time taken for the air stream to reach the set temperature could be up to an hour. However,the latter point was not a problem in practice,being more than compensated for by the temperature stability. The compressed air was supplied by a compressor at 15p.s.i. via a filter and pressure regulator unit. A flow meter was used to control the flow

FIGURE 4.6: Variation of Air Temperature with the Flow Rate through the Heater.



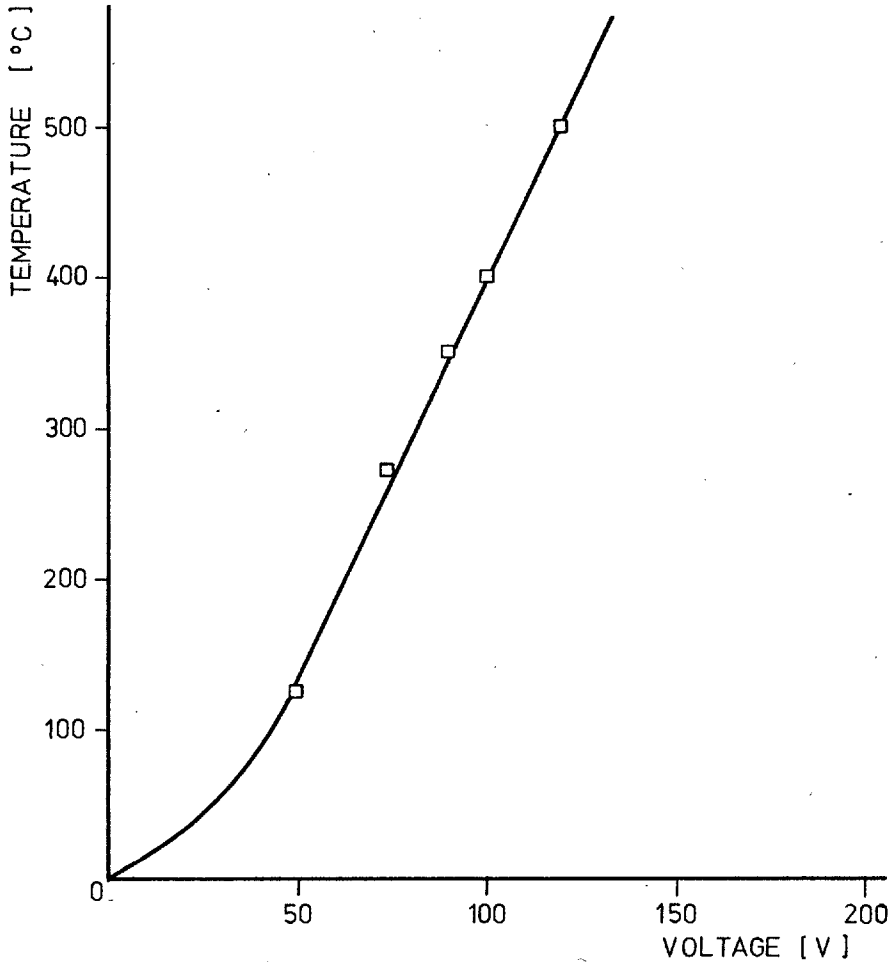


FIGURE 4.7: Air Temperature vs. Variac Voltage.

rate of air through the heater and cavity. The optimum flow rate at a Variac setting of 90V was found to be $20dm^3\ min^{-1}$. The variation of the air stream temperature with the flow rate is shown in Figure 4.6 and a calibration curve of temperature against the Variac voltage is shown in Figure 4.7. The variation of the temperature with the applied voltage was found to be linear over a working range of 150-500°C.

The temperature was measured inside an EDL blank using an alumel-chromel thermocouple. The EDL blank was placed in the cavity in the normal position for EDL operation and silicone grease was used to maintain good thermal contact between the thermocouple and the inner wall of the blank. The reference thermocouple was immersed in an ice/water mixture contained in a Dewar vessel.

A curve showing the time taken for the air temperature to rise to the set temperature is shown in Figure 4.8.

The 3/4-wave cavity fitted directly onto the outlet tube on the top of the heater, the hot air passing through the coaxial gap adjuster and over the surface of the lamp. This form of direct connection was not possible with the ¼-wave cavity because of its open design. Instead, the EDL was operated in a silica tube (i.d. 12mm, o.d. 14mm) connected to the top of the heater, the outer silica tube being a close fit in the ¼-wave cavity.

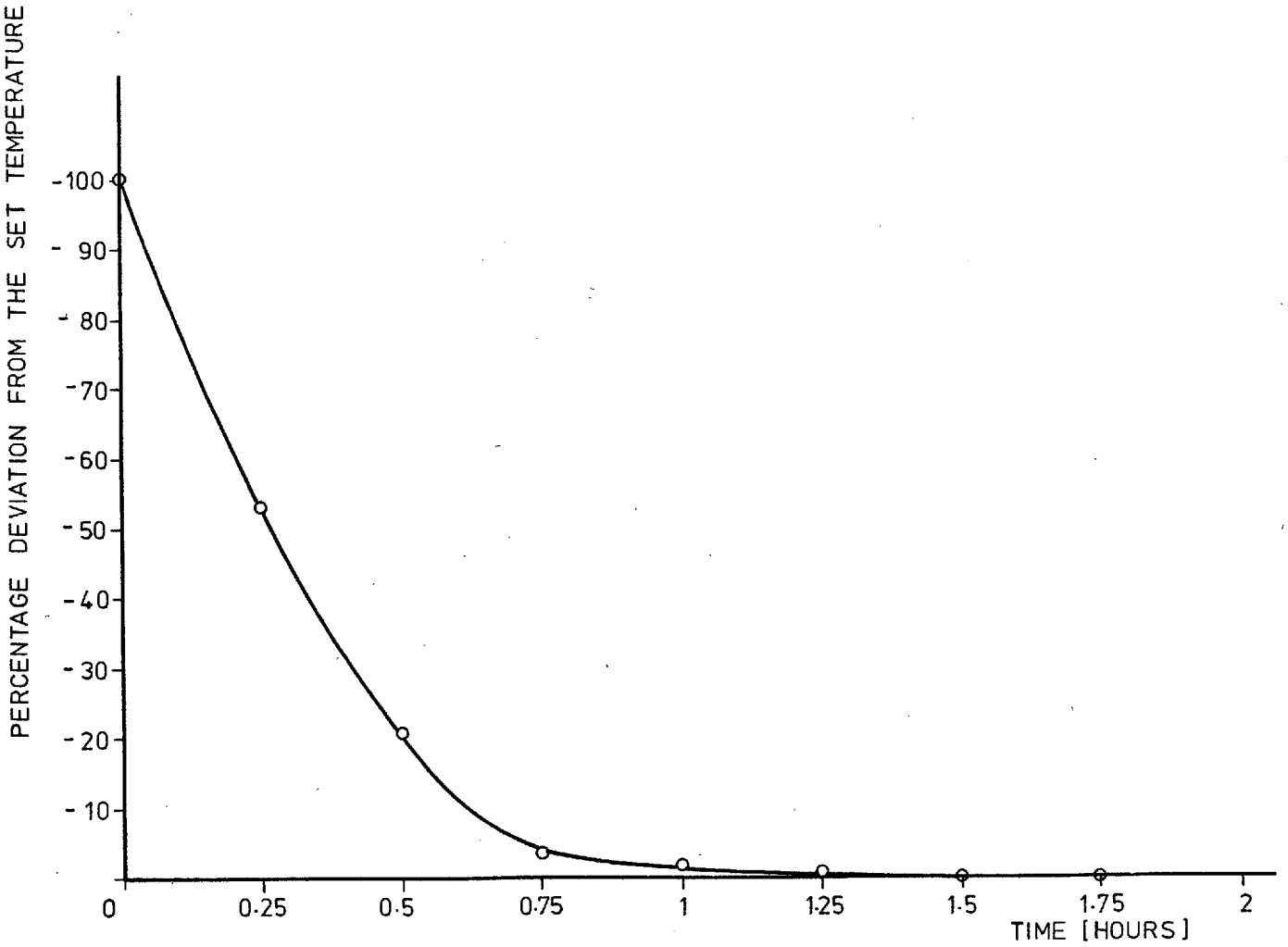


FIGURE 4.8: Time Taken for the Air to Attain the Set Temperature.

CHAPTER FIVE

SOME OBSERVATIONS OF ELECTRODELESS DISCHARGE LAMPS.

5.1 Introduction 112

5.2 Studies Made Without Spatial Resolution 112

5.3 The Radial Distribution of Intensity from EDL Sources 116
- 5.3.1 Experimental 116
- 5.3.2 Processing of Results 116
- 5.3.3 General Observations 117
- 5.3.4 The Effect of the Operating Power upon EDL Operation 123
- 5.3.5 Different Resonance Cavities 125
- 5.3.6 The Effect of the Operating Temperature 127
- 5.3.7 Measurements Made at Different Wavelengths 132

5.4 Measurements Made of the Intensities of Hyperfine Components 139
- 5.4.1 Introduction 139
- 5.4.2 Lead 140
- 5.4.3 Indium 146
- 5.4.4 Mercury 149

5.5 The Measurement of Excitation Temperatures in an Indium EDL 151
- 5.5.1 Theoretical 151
- 5.5.2 Procedure 154
- 5.5.3 Results 154

5.6 Discussion 160
- 5.6.1 Sputtering 160
- 5.6.2 The Electrical Skin Depth 161
- 5.6.3 Self-Absorption in the Centre of the Lamp 163
- 5.6.4 The Possible Reason for the Existence of the TYPE B Discharge 165
- 5.6.5 The TYPE A Discharge 171

5.1 INTRODUCTION.

A summary of the recent studies made of electrodeless discharge lamps was presented in Chapter 1 and their preparation and operation was described in Chapter 4.

The majority of papers reporting on the properties of EDL's have concentrated,firstly,on the source being operated without any form of temperature regulation and, secondly,on the intensity integrated over the whole of the source. More recently,[47] some studies have been reported in which the EDL temperature has been regulated. The results of these studies have shown that the operation of an EDL in a temperature controlled environment has distinct advantages over the conventional mode of operation with regard to the improved stability and spectral radiance of the source. Browner and Winefordner[47] reported that certain EDL's do not show the form of spatial distribution of radiance that would be expected for homogeneous emission. In this study the spatial distribution of emitters in a series of EDL's has been investigated further.

5.2 STUDIES MADE WITHOUT SPATIAL RESOLUTION.

A number of studies have been made of the total radiation emitted by EDL's,operated with temperature regulation.[47,138,149] In the literature several parameters have been monitored in an attempt to evaluate the performance of an EDL source. In general, the values of

the source operating parameters which result in a maximum of radiant output do not concur with the optimum values for making measurements either in atomic fluorescence spectrometry or in atomic absorption spectrometry. Browner and Winefordner[47] have produced a series of graphs for a number of different EDL sources in which absorbance, fluorescence and source radiance signals have been plotted as functions of the EDL wall temperature and the microwave power. Their results for a typical EDL, zinc, have been reproduced in Figure 5.1 showing the effect of varying the wall temperature of the EDL.

The following general conclusions have been made. At relatively low temperatures, for all the elements studied, the absorbance signal was found to be nearly constant with temperature until a certain temperature was reached. This temperature appeared to be a particular value for an EDL containing a given element but was different for other elements. After this value of the temperature had been reached the absorbance decreased very rapidly with further increases in the temperature. The magnitudes of the source radiance and the fluorescence radiance normally passed through a maximum as the thermostat temperature was increased. However, the maximum of fluorescence radiance sometimes occurred at a lower value of the temperature than for the maximum of source radiance.

The decrease in the absorbance signal when the temperature was raised above a certain value was presumably caused by the onset of self-absorption. Self-absorption

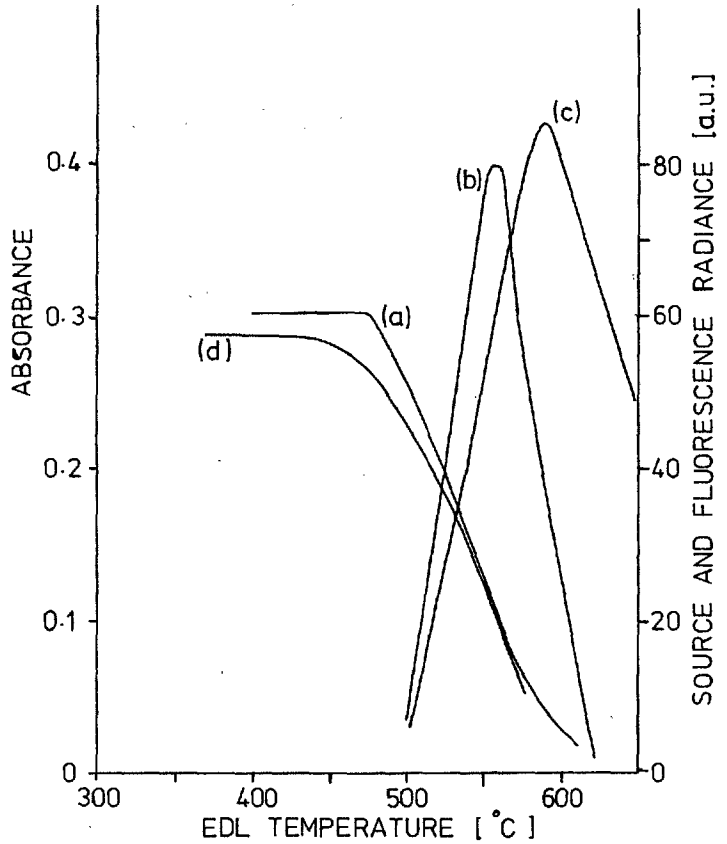


FIGURE 5.1: Zinc Absorbance, Source and Fluorescence Radiance vs. Thermostat Temperature.[47] Wavelength = 213.8nm. Power = 40W. Solution Concentration = 10μg cm^{-3}. (a)-Absorbance, Ar 1torr (b)-Fluorescence, Ar 1torr (c)-Source Radiance, Ar 1torr (d)-Absorbance, He 1torr.

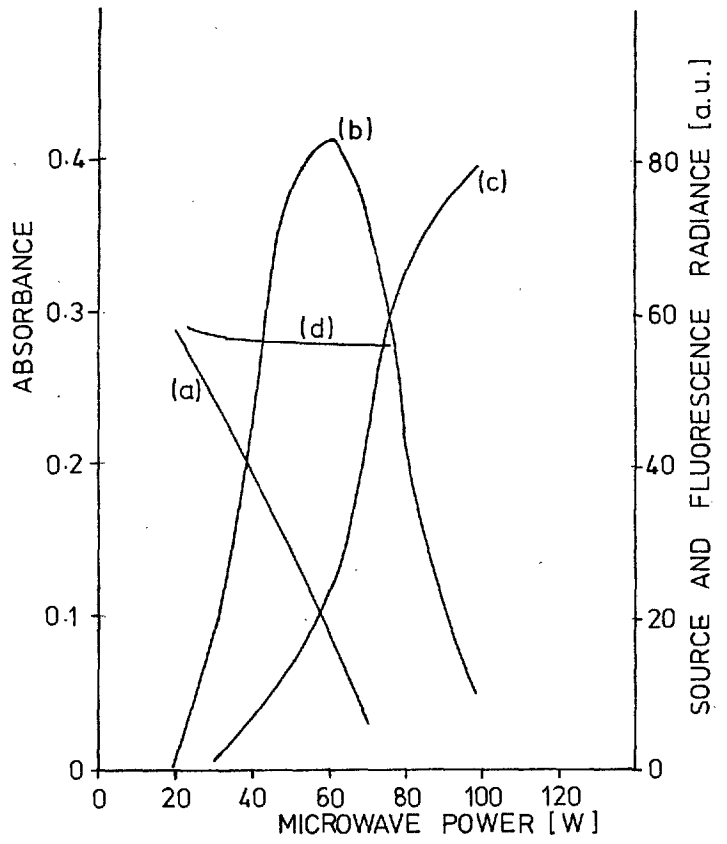


FIGURE 5.2: Zinc Absorbance (a), Source (c) and Fluorescence (b) Radiance vs. Microwave Power.[47] Wavelength = 213.8nm, Argon Pressure = 1 torr, Solution Concentration = 10μg/cm^3. Curves (a), (b) & (c) - Unthermostatted, Curve (d) = Source Absorption Measurements - Lamp Thermostatted at 450K.

would decrease the effective emission at the centre line frequency so that the line would become less sensitive to absorption by ground state atoms. The radiant output of the source was very low, compared with its potential maximum of emission, when the absorbance measurements were optimised. These results suggest that the fluorescence signal is more dependent upon the source radiance than upon the line profile of the source as expected theoretically.

The most noteworthy feature in Figure 5.2 is the difference between curves (a) and (d). In the thermostatted mode of operation (curve (d)) the absorbance signal is virtually unaffected by changes in the microwave power compared with the curve (a), showing the microwave power dependence of the absorbance signal using an EDL without temperature control. Comparison of curve (a) in Figure 5.2 with curve (a) in Figure 5.1 indicates similarities relating to the heating effect of the microwave power when the EDL is operated without temperature control.

When EDL sources were operated without any form of temperature regulation it was normally necessary to use relatively high values of the microwave power to achieve a maximum of fluorescence radiance and in many cases it was not possible to increase the microwave power sufficiently to reach the maximum of fluorescence and source radiance. The relatively large rate of change of intensity with microwave power when the source is not thermostatted results in small, and usually unavoidable, changes in the microwave power having a large effect upon the analytical signal. The control of the source

operating temperature is also easier to achieve than the stabilization of microwave power generators.

The above results indicate the distinct advantages which may be observed when an EDL source is operated with temperature regulation.

5.3 THE RADIAL DISTRIBUTION OF INTENSITY FROM EDL SOURCES.

5.3.1 Experimental.

The optical arrangement used has been described in Chapter 3.

The appropriate resonance cavity was mounted on the heater,as described in Chapter 4, and the whole assembly was mounted on a micropositioning device,which allowed movement of the source in three mutually perpendicular directions. LENS1 (Figure 3.1) was positioned close to the source so that an approximately ten-fold enlargement of the source was focused in the plane of the secondary source aperture. Lateral scanning of the source was achieved by moving the source horizontally and perpendicular to the optical axis in prescribed increments. The measurements of the source radiance were made with the interferometer assembly removed and with the signal from the photomultiplier tube taken directly to the chart recorder.

5.3.2 Processing of Results.

On performing a lateral intensity scan of a cylindrically symmetrical source there is a variation

in the optical depth viewed depending upon the distance of the viewing position from the centre of the source. Effectively,the lateral intensity observed at a particular position is the result of integrating through the source in the direction of observation, the 'so-called' Abel integral. The lateral scans of intensity have been converted into radial scans by using the inverse Abel transform technique described in Chapter 7.

5.3.3 General Observations.

Lateral intensity scans were made for a number of different EDL sources,operated in the 3/4-wave resonance cavity. The initial operating conditions were those that resulted in a source suitable for use in atomic fluorescence spectrometry as previously described. The resultant radial intensity distributions are shown in Figures 5.3-5.8 for argon,arsenic,germanium,indium,tin and mercury EDL sources.

The observed radial intensity distributions may be divided easily into two distinct types,which will be described as type A and type B for ease of reference.

Examples of the type A discharge are shown in Figures 5.3 (mercury),5.4 (arsenic) and 5.5 (argon). The common feature observed in these distributions of intensity is the presence of a maximum of intensity in the centre of the lamp with the intensity reducing to zero as the edge of the discharge is approached. On traversing from the centre of the lamp to the edge the radial intensity remains relatively constant for a

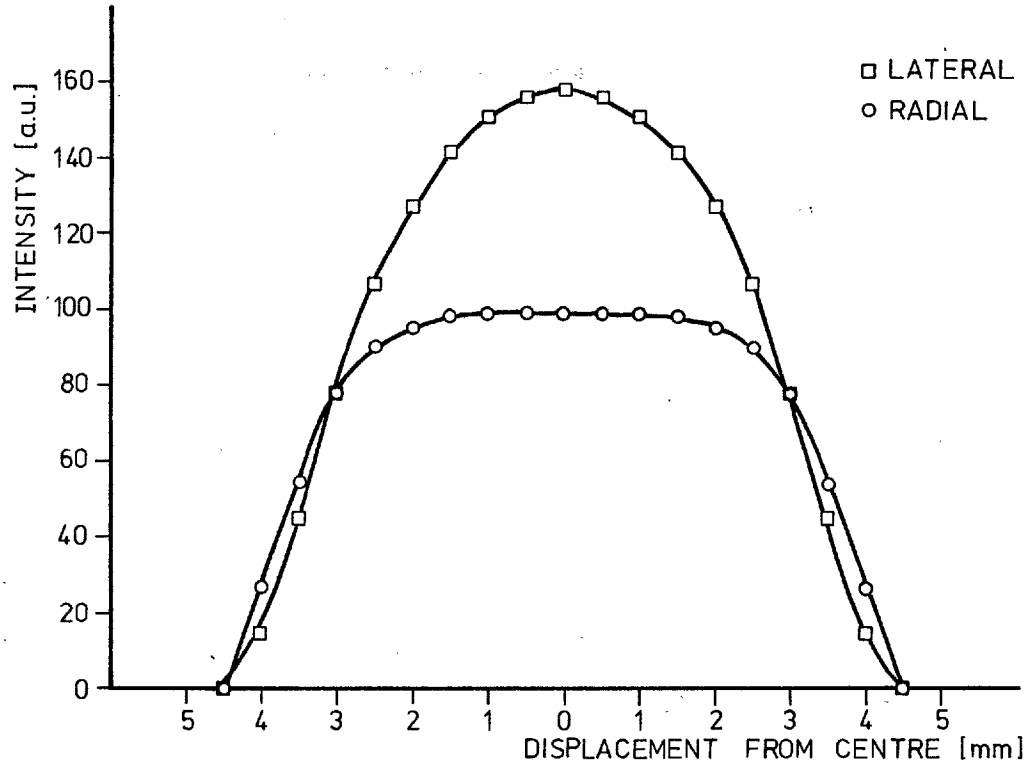


FIGURE 5.3: Radial and Lateral Intensity Distributions for a Mercury EDL. T = 150°C, Power = 15W, Wavelength = 404.66nm.

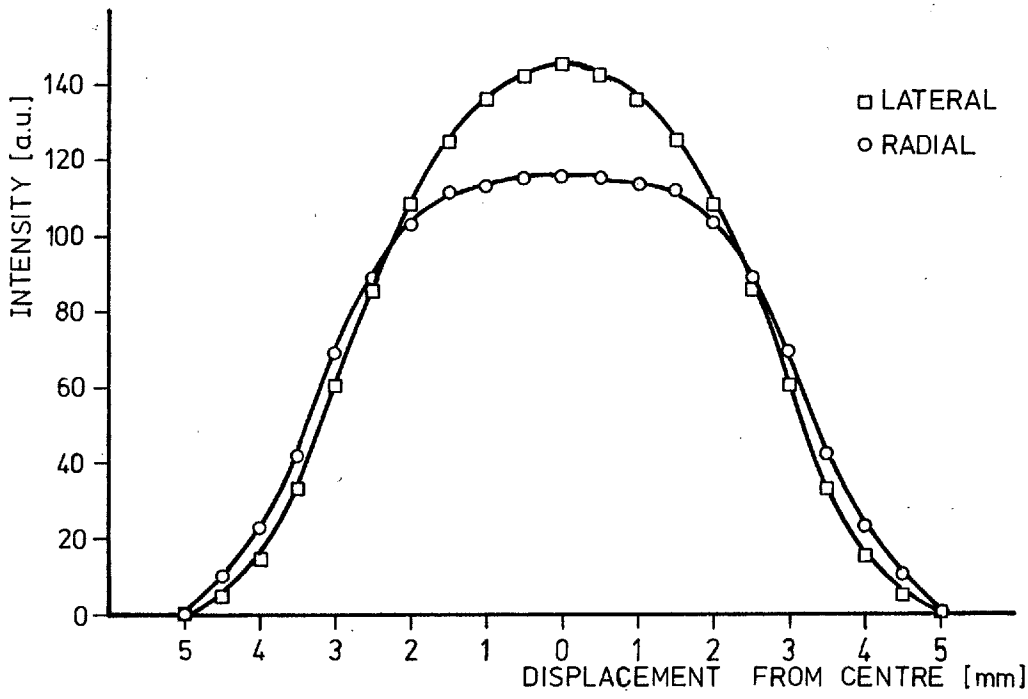


FIGURE 5.4: Radial and Lateral Intensity Distributions for an Arsenic EDL. Air cooled at 10dm³/min, Power = 45W, Wavelength = 234.98nm.

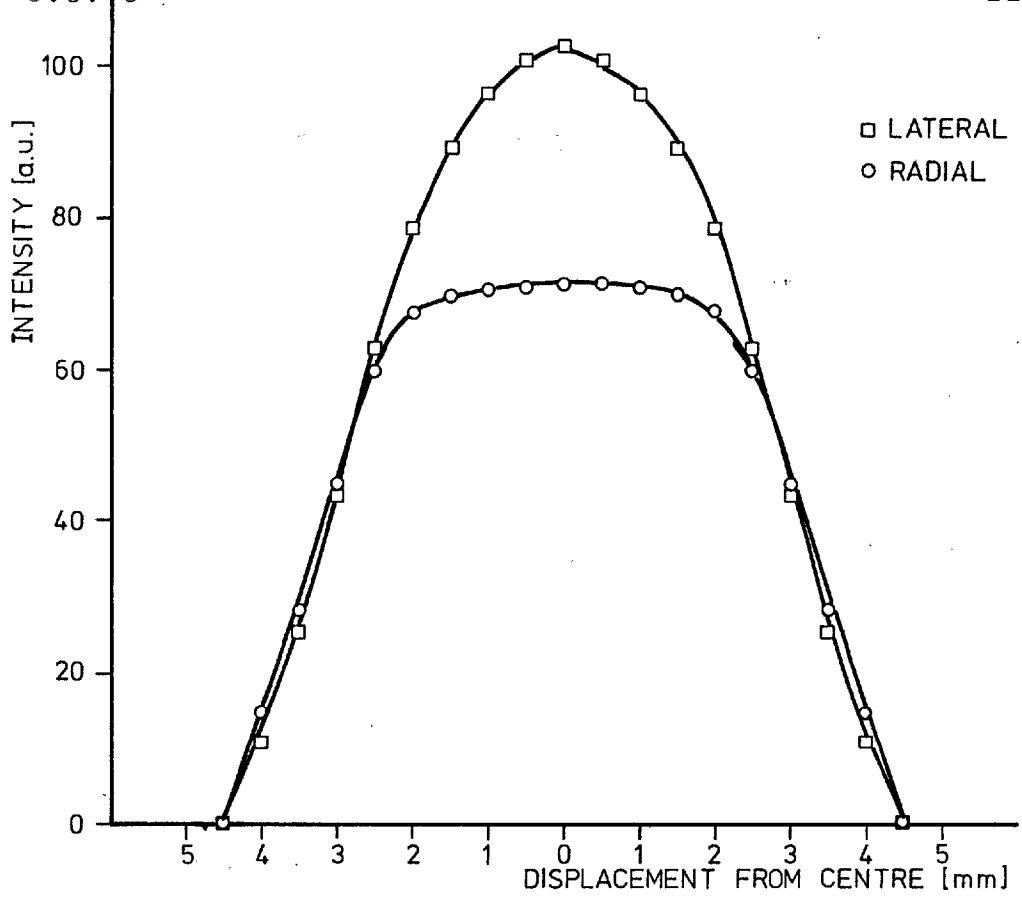


FIGURE 5.5 : Radial and Lateral Intensity Distributions for an Argon EDL. T = 200°C, Power = 45W, Wavelength = 418.19nm.

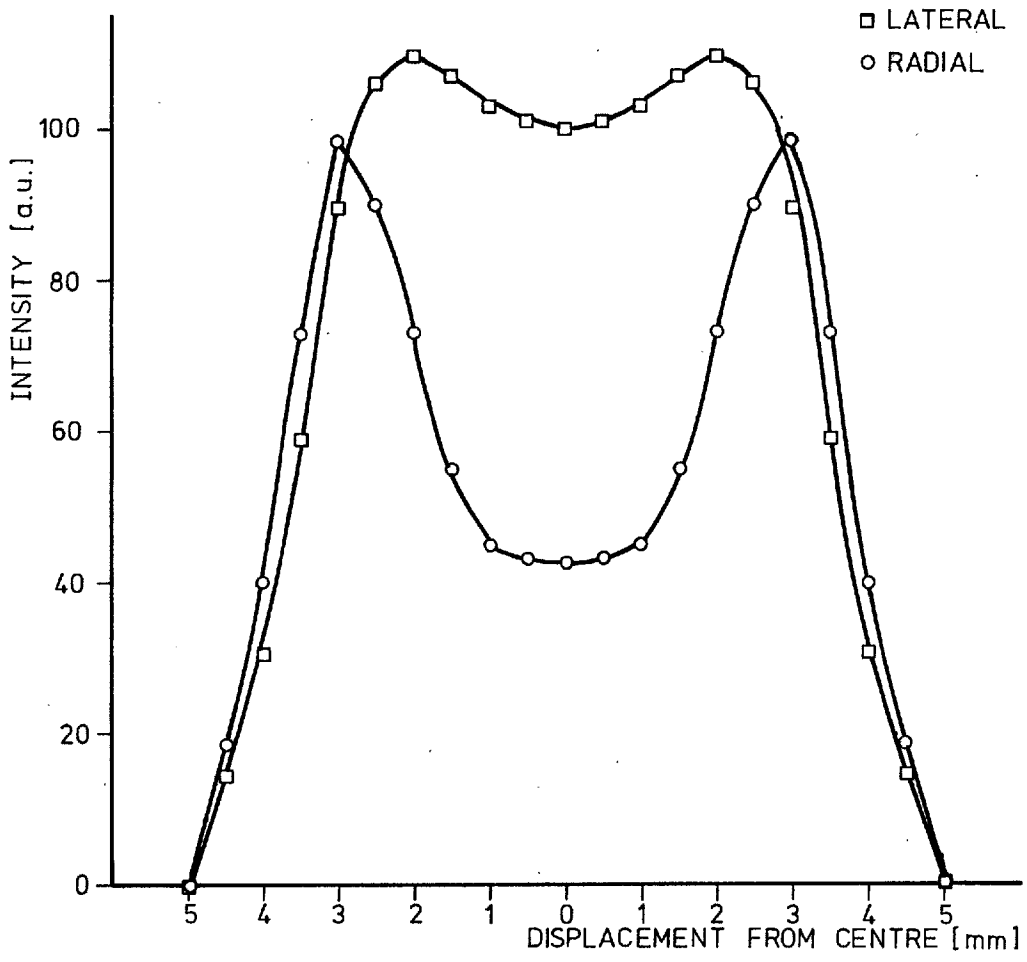


FIGURE 5.6 : Radial and Lateral Intensity Distributions for a Germanium EDL. Air Cooled at 25dm³/min, Power = 40W, Wavelength = 303.9nm.

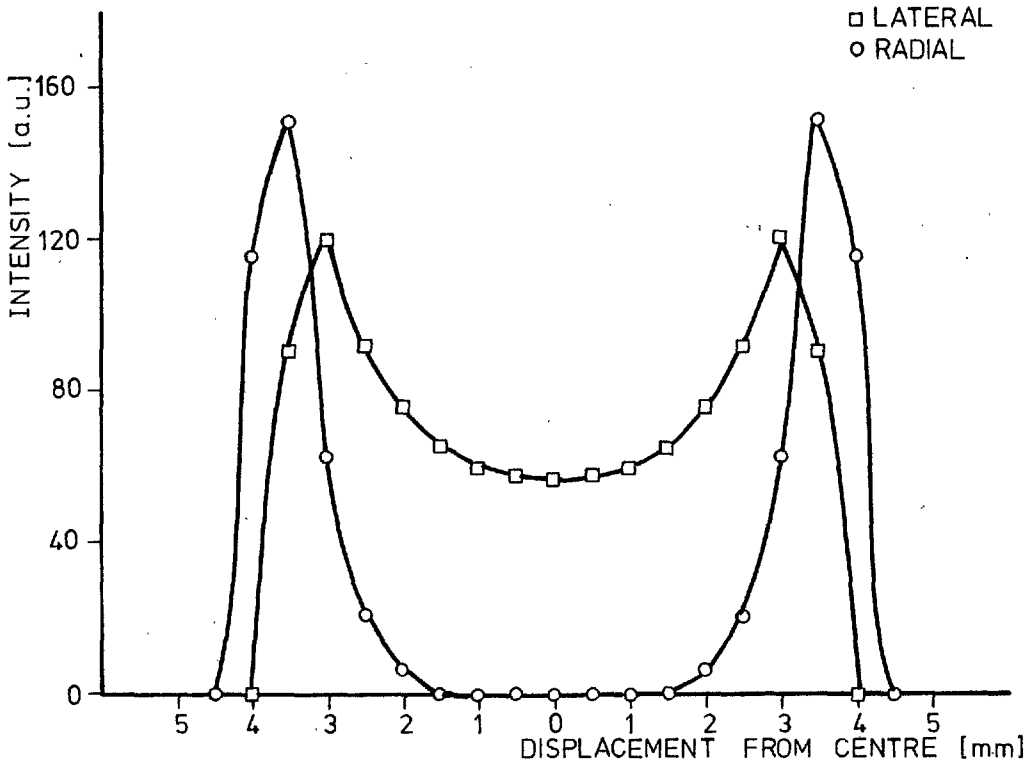


FIGURE 5.7: Lateral and Radial Intensity Distributions for an Indium EDL. T = 300°C, Power = 40W, Wavelength = 451·13nm.

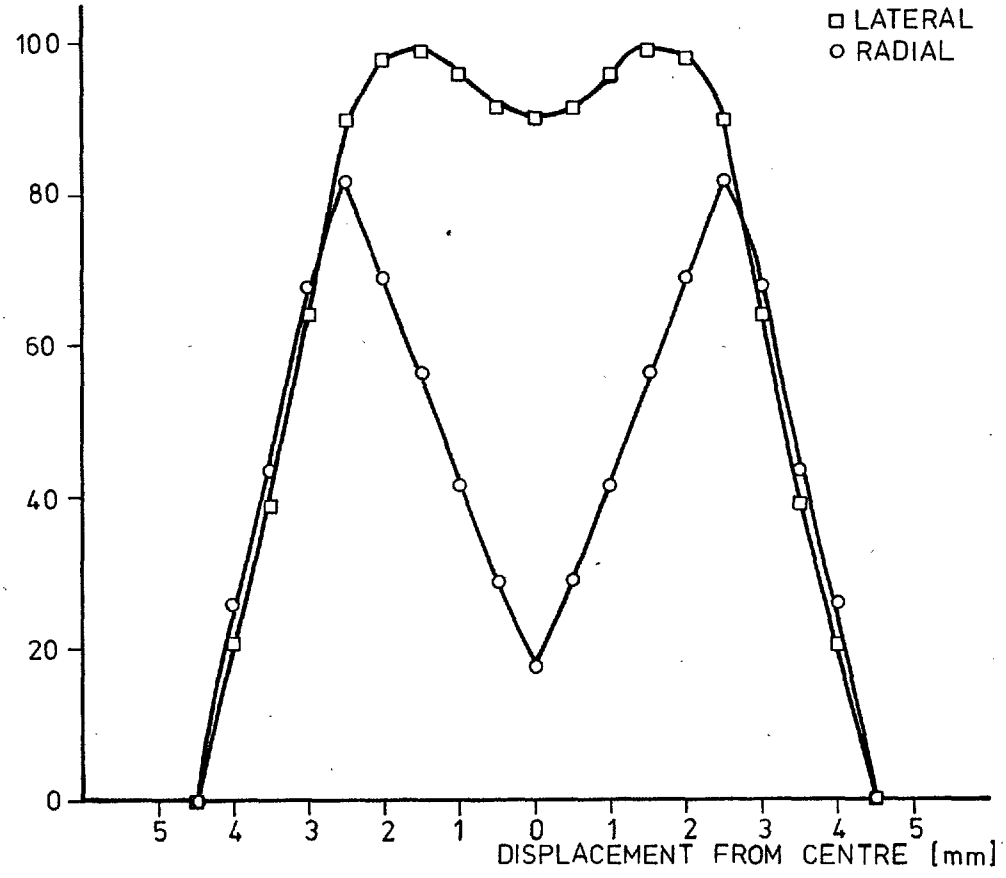


FIGURE 5·8: Lateral and Radial Intensity Distributions for a Tin EDL. T = 250°C, Power = 40W, Wavelength = 283·6nm.

distance,dependant upon the particular element and the operating conditions,before the decrease of the intensity to zero takes place. This effect is particularly noticeable for the mercury (Figure 5.3) and argon (Figure 5.5) radial distributions of intensity and has been attributed to the presence of a homogeneous discharge.[47] Obviously,the discharge can only be partially homogeneous because of collisional effects occurring at the walls of the lamp.

Examples of the type B radial distribution of intensity are shown in Figures 5.6 (germanium),5.7 (indium) and 5.8 (tin). The characteristic feature of the type B distribution is the minimum of radial intensity at the centre of the lamp with a maximum of emission just inside the lamp envelope. This effect is clear in Figure 5.7 for the indium EDL where the intensity at the centre of the lamp is essentially zero. It is also noteworthy that the maximum of radial intensity occurs nearer to the wall of the lamp than does the maximum of the laterally observed intensity. The latter effect is characteristic of the result of carrying out an inverse Abel transform upon a type B lateral distribution of intensity.

The observation of the two types of intensity distributions was quite reproducible for EDL's prepared for each element and can not be ascribed to trivial optical artifacts or the behavior of particular EDL's.

Under the normal operating condition,described previously,EDL's prepared for the elements mercury,

arsenic and selenium displayed the type A distribution of intensity,whilst EDL's prepared for gallium,manganese, and lead showed the type B distribution of intensity,in addition to the elements mentioned above. These observations are summarized in Table 5.1.

TABLE 5.1: EDL Sources Showing the Type A and Type B Distributions of Intensity.

ELEMENT	OPERATING CONDITIONS†	WAVELENGTH (nm)	TYPE
Antimony	150°C,40W	259.8	B
Argon	200°C,45W	418.19	A
Arsenic	air cooled at 10dm³/min 45W	234.98	A
Cadmium	150°C,30W	228.8	B
Gallium	air cooled at 20dm³/min 35W	417.21	B
Germanium	air cooled at 25dm³/min 40W	303.9	B
Indium	300°C,40W	451.13	B
Lead	400°C,40W	405.78	B
Manganese	300°C,70W	403.0	B
Mercury	150°C,15W	404.66	A
Selenium	150°C,50W	203.98	A
Thallium	200C,40W	377.57	B
Tin	250°C,40W	286.3	B
Zinc	200°C,45W	213.86	B

† Power values refer to absorbed microwave power and temperatures refer to the air stream temperatures.

5.3.4 The Effect of the Operating Power upon EDL Operation.

The effect of different values of the microwave operating power upon the radial distribution of intensity for a mercury EDL is shown in Figure 5.9. The observations made at the 253.6nm mercury line for the EDL operated at microwave powers of 40W and 20W indicate that there is not a change in the shape of the radial distribution of intensity curves when this change is made in the microwave power. As expected, the intensity of the 253.6nm mercury line increases with the absorbed microwave power although the percentage increase in intensity at the centre of the discharge is not commensurate with the percentage increase in the microwave power. In Figure 5.9 a 100% increase in the absorbed microwave power has resulted in a 42% increase in the intensity at the centre of the lamp.

Figure 5.10 shows the radial distribution of the intensity of the 410.18nm line emitted by an indium EDL operated at 300°C and at operating powers of 30,40 and 50W. The intensity at a particular position in the EDL increases with the absorbed microwave power without an appreciable change in the shape of the radial distribution of intensity. The change in the overall intensity when the absorbed microwave power is increased from 40W to 50W is observed to be relatively small in comparison with the intensity changes observed for changes in the microwave power from 30W to 40W.

Observations made when the EDL was operated at the higher temperature of 350°C indicated that an increase in the absorbed microwave power from 40W to 50W had very

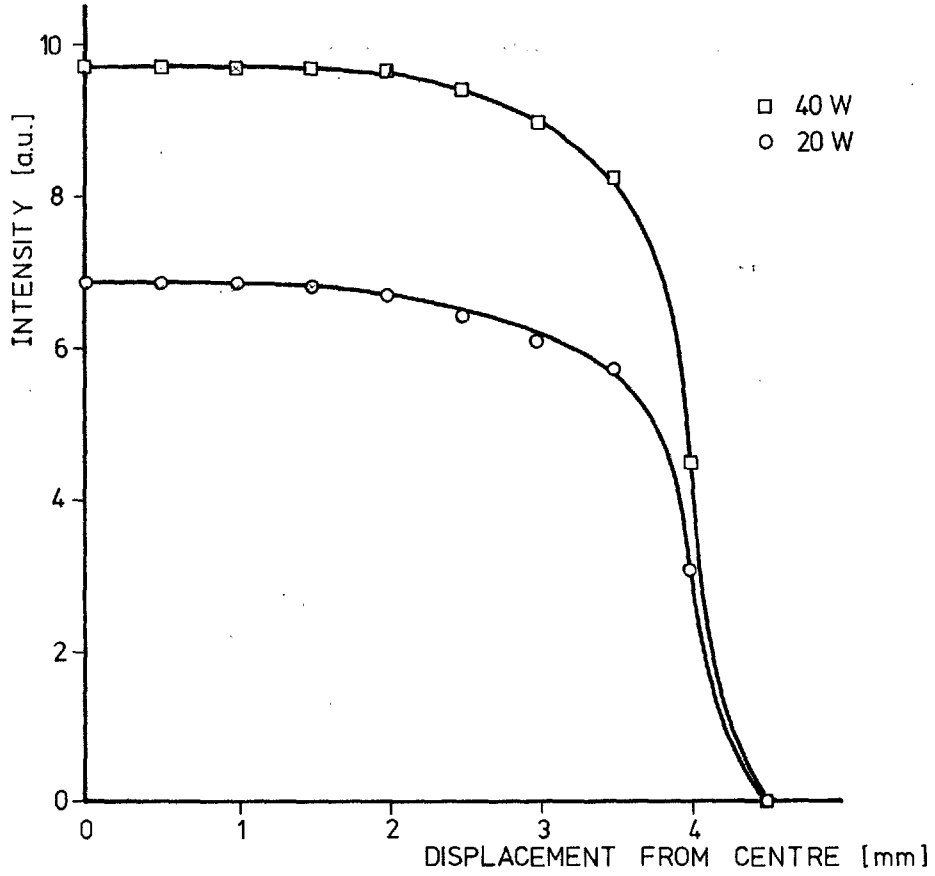


FIGURE 5·9 : The Effect of the Microwave Power upon the Radial Intensity Distribution of a Mercury EDL.
T = 150°C, Wavelength = 253·6nm.

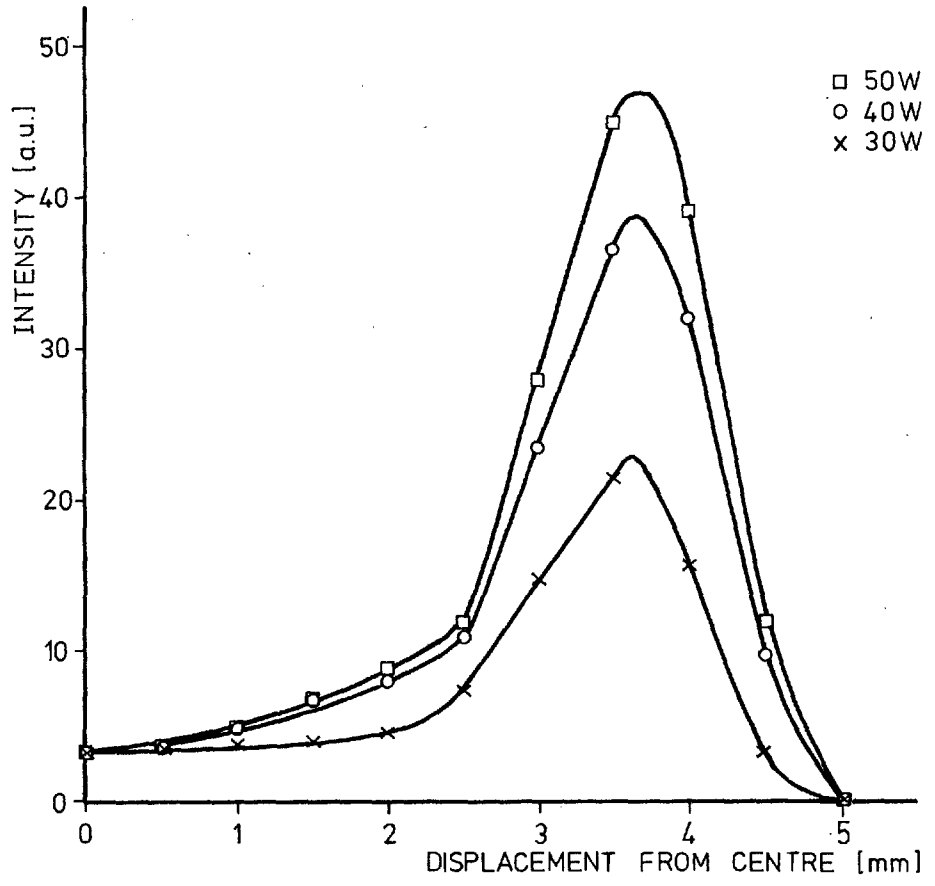


FIGURE 5·10 : The Effect of the Microwave Power upon the Radial Intensity Distribution of an Indium EDL.
T = 300°C, Wavelength = 410·18nm.

little effect upon the overall intensity. This effect is shown in Figure 5.11. The latter observation indicates that the attainment of the plateau region in the power vs. radiance curve, discussed in Section 5.2, has been achieved.

Observations made with a number of different EDL sources indicated that variations in the absorbed microwave power did not alter substantially the shape of the radial distribution of intensity.

5.3.5 Different Resonance Cavities.

Measurements of the radial distribution of intensity were made using both ¼-wave and 3/4-wave resonance cavities. The type of intensity distribution observed was not affected by the choice of cavity although the overall intensity observed was slightly greater for the source operated in the ¼-wave cavity at identical values of the absorbed microwave power. This difference may be attributed to more efficient coupling of the microwave power into the EDL using the ¼-wave cavity than may be obtained with the 3/4-wave cavity.

Although the difference between the incident power and the reflected power represents the absorbed power, the latter quantity is the power absorbed by the cavity plus its contents. The design of the 3/4-wave resonance cavity results in the coupling being inherently less efficient than in a ¼-wave cavity.

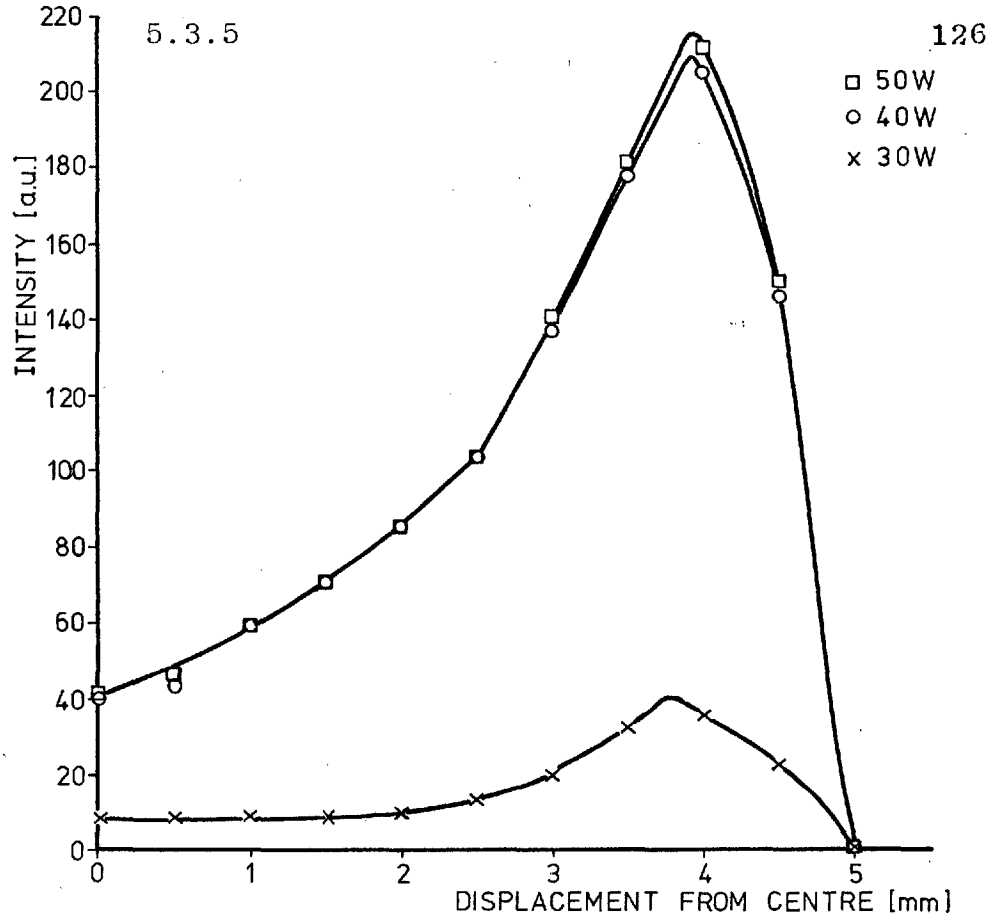


FIGURE 5·11 : The Effect of the Microwave Power upon the Radial Intensity Distribution for an Indium EDL. T=350°C, Wavelength = 410·18nm.

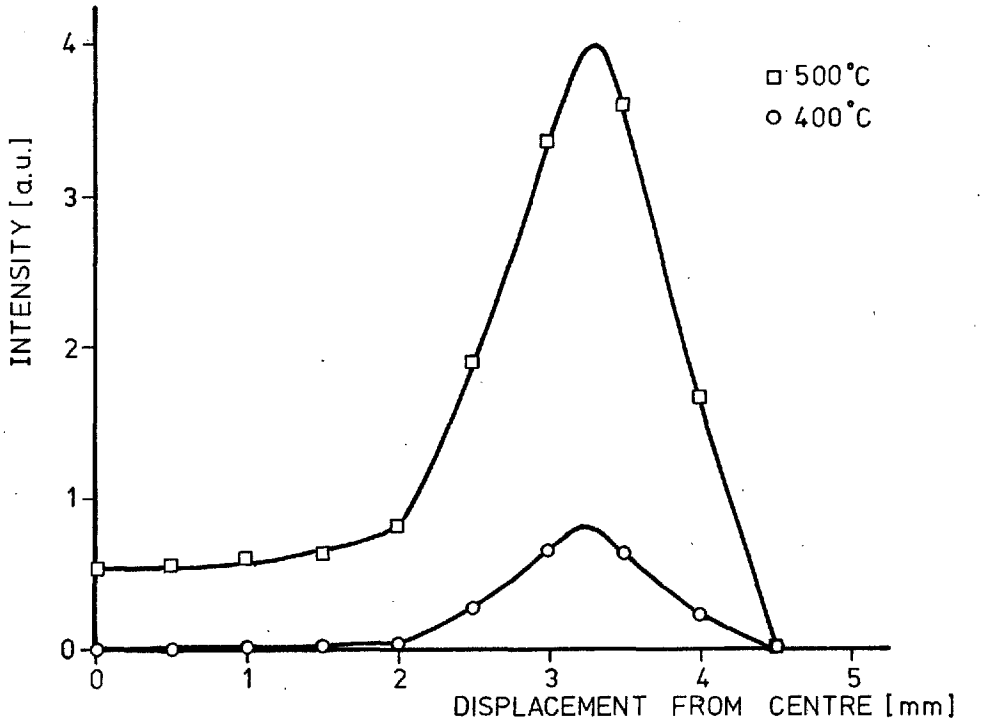


FIGURE 5·12 : The Effect of the Thermostat Temperature upon the Radial Intensity Distribution of a Lead EDL.
Power = 30 W, Wavelength = 405·78nm.

5.3.6 The Effect of the Operating Temperature.

The radial distributions of intensity for the lead 405.78nm line emitted by an EDL operated at a constant microwave power of 30W (absorbed) at temperatures of 500°C and 400°C are shown in Figure 5.12. It may be observed that the intensity of the maximum of emission is a strong function of the temperature; the intensity increase is about five-fold for an increase in the absolute temperature of about 15%. At an operating temperature of 400°C the intensity at the centre position is virtually zero but at 500°C this value has increased by a much greater factor than have the maxima of intensity; at 500°C the intensity at the centre may no longer be considered as negligible.

The effect of the value of the operating temperature upon the radial distribution of intensity of the 404.6nm mercury line from an EDL is shown in Figure 5.13. On cooling the mercury EDL with an air flow of 20dm^3/min the radial distribution of intensity conforms approximately to the distribution that would be expected for a homogeneous discharge: the intensity of the 404.6nm line remains virtually constant with distance away from the centre of the lamp until the wall of the lamp is approached. As the operating temperature is increased the distribution of intensity appears to become less homogeneous.

On operating the EDL at temperatures higher than ca. 200°C the discharge became unstable and eventually extinguished. In some instances an unstable pinch discharge was formed in which the emission was concentrated in a

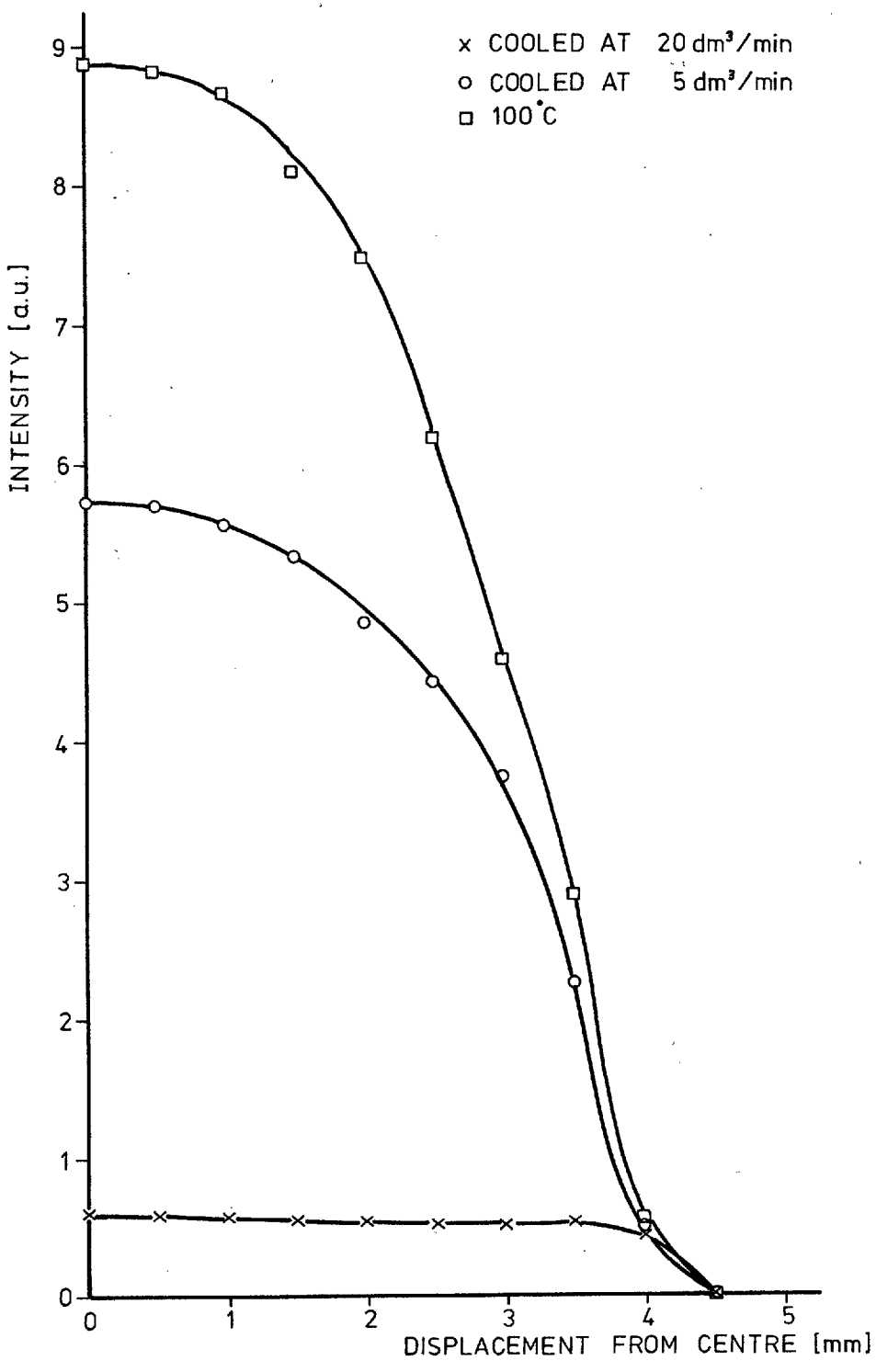


FIGURE 5-13: The Effect of the Thermostat Temperature upon the Radial Intensity Distribution of a Mercury EDL.
Power = 30W, Wavelength = 404·6nm.

filament in the centre of the lamp.

The effect of different operating temperatures upon the radial distribution of intensity of the 410.18nm indium line is shown in Figure 5.14. On operating an indium EDL at 250°C or at 350°C,with a constant absorbed microwave power of 40W, the type B discharge was observed. A interesting effect was observed when the EDL was heated to 400°C. Under these conditions the nature of the discharge changed and a maximum of emitted intensity occurred in the centre of the lamp. This change from a type B distribution to a type A distribution was found to be quite reproducible.

The intensity at the centre of an indium EDL operated at 250°C is negligible in comparison with the intensity maximum. This observation no longer applies when the EDL is operated at 350°C. This phenomena is similar to the effects observed with a lead EDL.

A change in the type of discharge was also observed when the operating temperature of a tin EDL was increased from 250°C to 400°C. The effect of the operating temperature upon the radial distribution of intensity of the 286.33nm tin line is shown in Figure 5.15. At 400°C and 40W absorbed microwave power the maximum of intensity occurs at the centre of the lamp in contrast with the type B distributions of intensity observed at operating temperatures of 250°C and 100°C. It is noticeable that in the type A distribution observed at an operating temperature of 400°C the intensity decreases very rapidly on moving the viewing position away from the centre of the lamp.

The effect of the operating temperature upon the

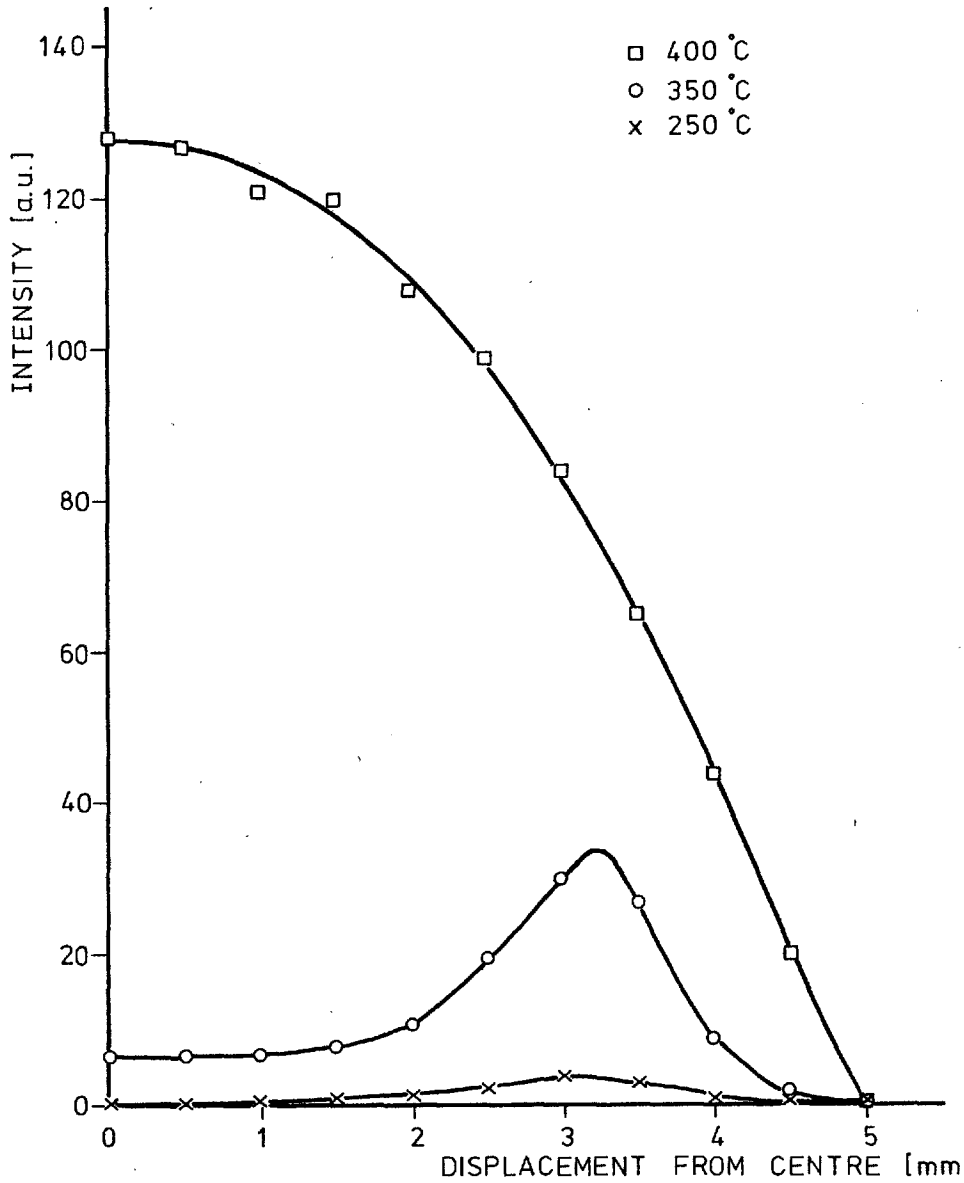


FIGURE 5·14: The Effect of the Thermostat Temperature upon the Radial Intensity Distribution of an Indium EDL.
Power = 40W, Wavelength = 410·18nm.

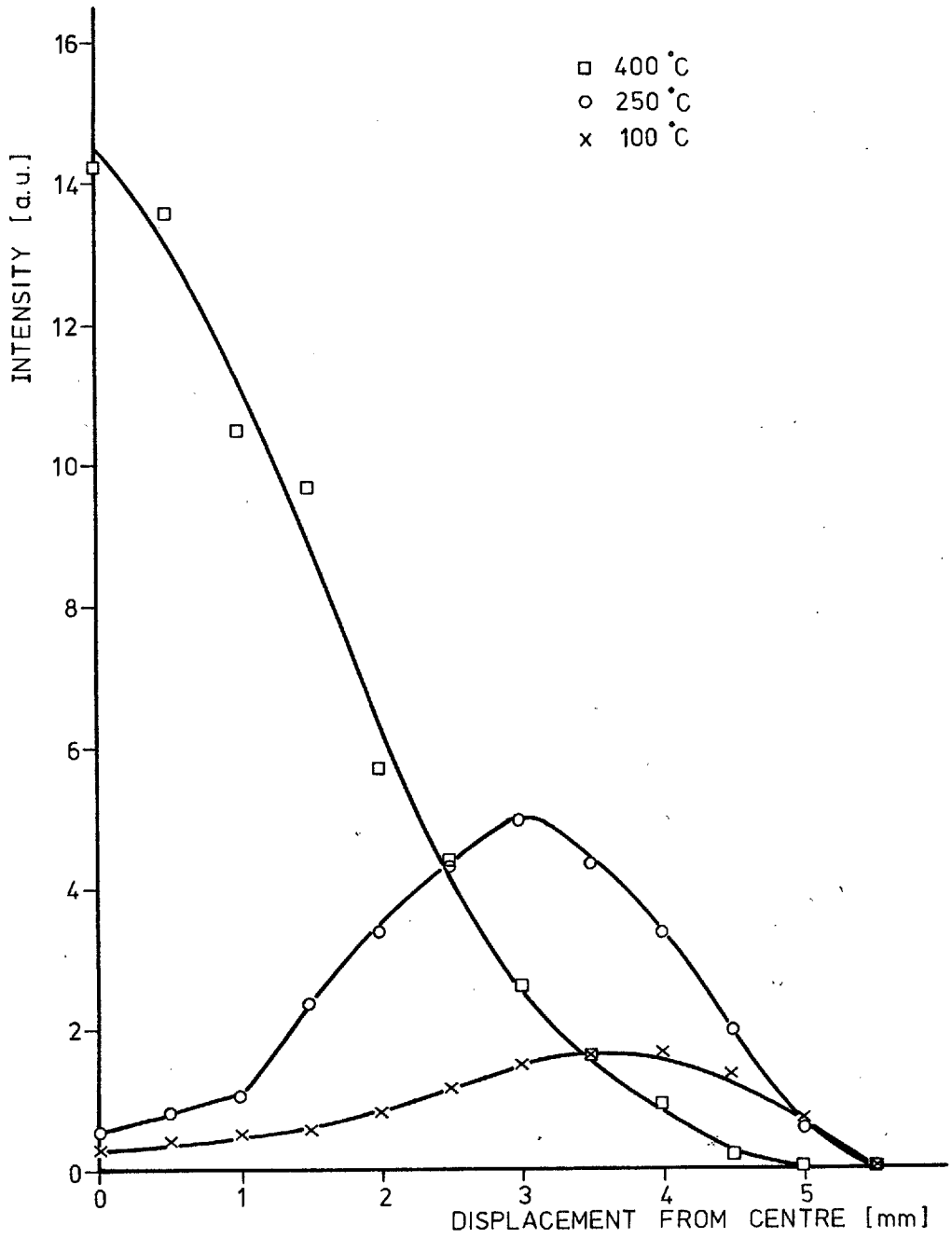


FIGURE 5.15: The Effect of the Thermostat Temperature upon the Radial Intensity Distribution of a Tin EDL.
Power = 40 W, Wavelength = 286·33nm.

radial distribution of intensity of the 228.8nm cadmium line is shown in Figures 5.16 and 5.17. For these measurements the absorbed microwave power was constant at 35W. The cadmium EDL was observed to have the type B discharge at all the experimental values of the temperature from 500°C to 200°C and with air cooling at $20dm^3\ min^{-1}$. When the air cooling was increased from $5dm^3\ min^{-1}$ to $20dm^3\ min^{-1}$ the value of the intensity at the centre of the lamp became a smaller fraction of the maximum intensity.

The lateral intensity distributions (before the application of the inverse Abel transform) were interesting in that they did not show a dip in the intensity at the central viewing position until cooling was applied at the rate of $20dm^3\ min^{-1}$. This indicated the necessity of using the Abel inversion procedure to obtain the radial intensity information.

5.3.7 Measurements Made at Different Wavelengths.

The radial distributions of intensity for a series of lines emitted by mercury, indium and manganese EDL's are shown in Figures 5.18, 5.19 and 5.20, respectively. The radial distributions of intensity of the mercury lines are all type A, whilst those of the indium lines are all type B. The distributions shown by the manganese EDL are also all type B, but it is noticeable that the maxima of intensity of the two Mn II lines studied, 257.6nm and 294.9nm, are closer to the centre of the lamp than the maxima for the Mn I lines.

The energies of the various transitions in Figures

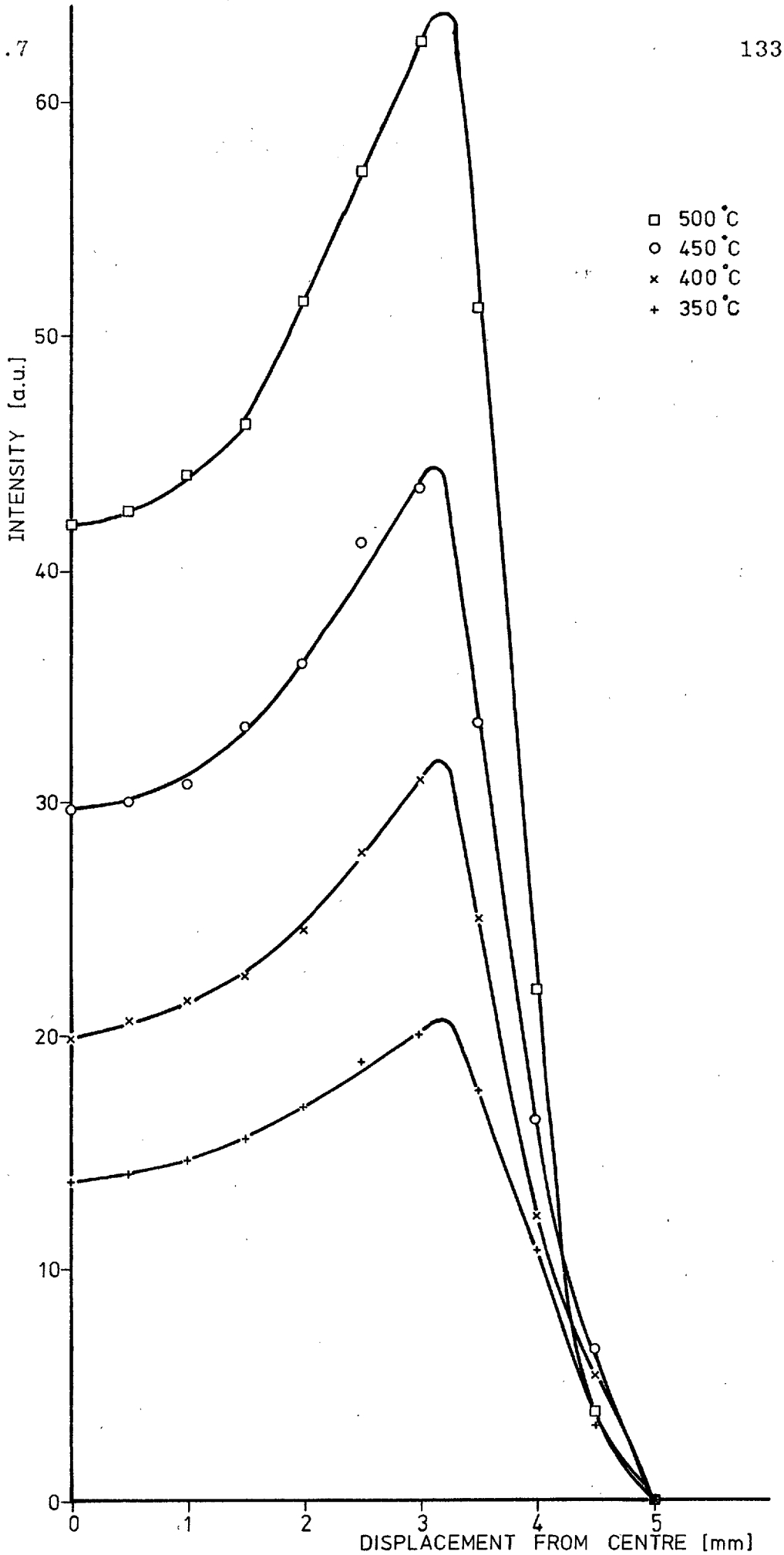


FIGURE 5·16: The Effect of the Thermostat Temperature upon the Radial Intensity Distribution of a Cadmium EDL.
Power = 35W, Wavelength = 228·8nm.

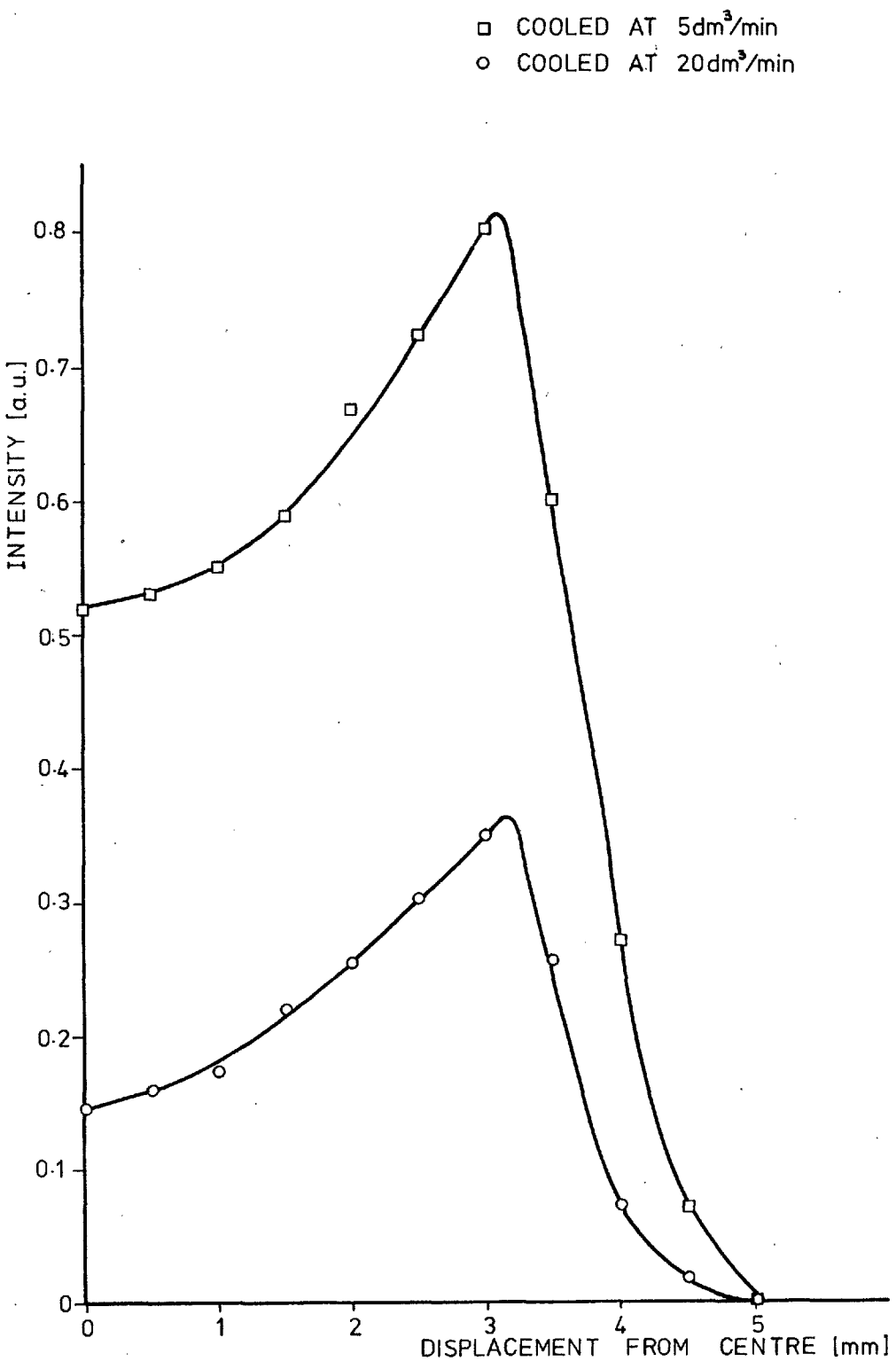


FIGURE 5·17 : The Effect of the Cooling-Air Flow Rate upon the Radial Intensity Distribution of a Cadmium EDL.
Power = 35W, Wavelength = 228·8nm.

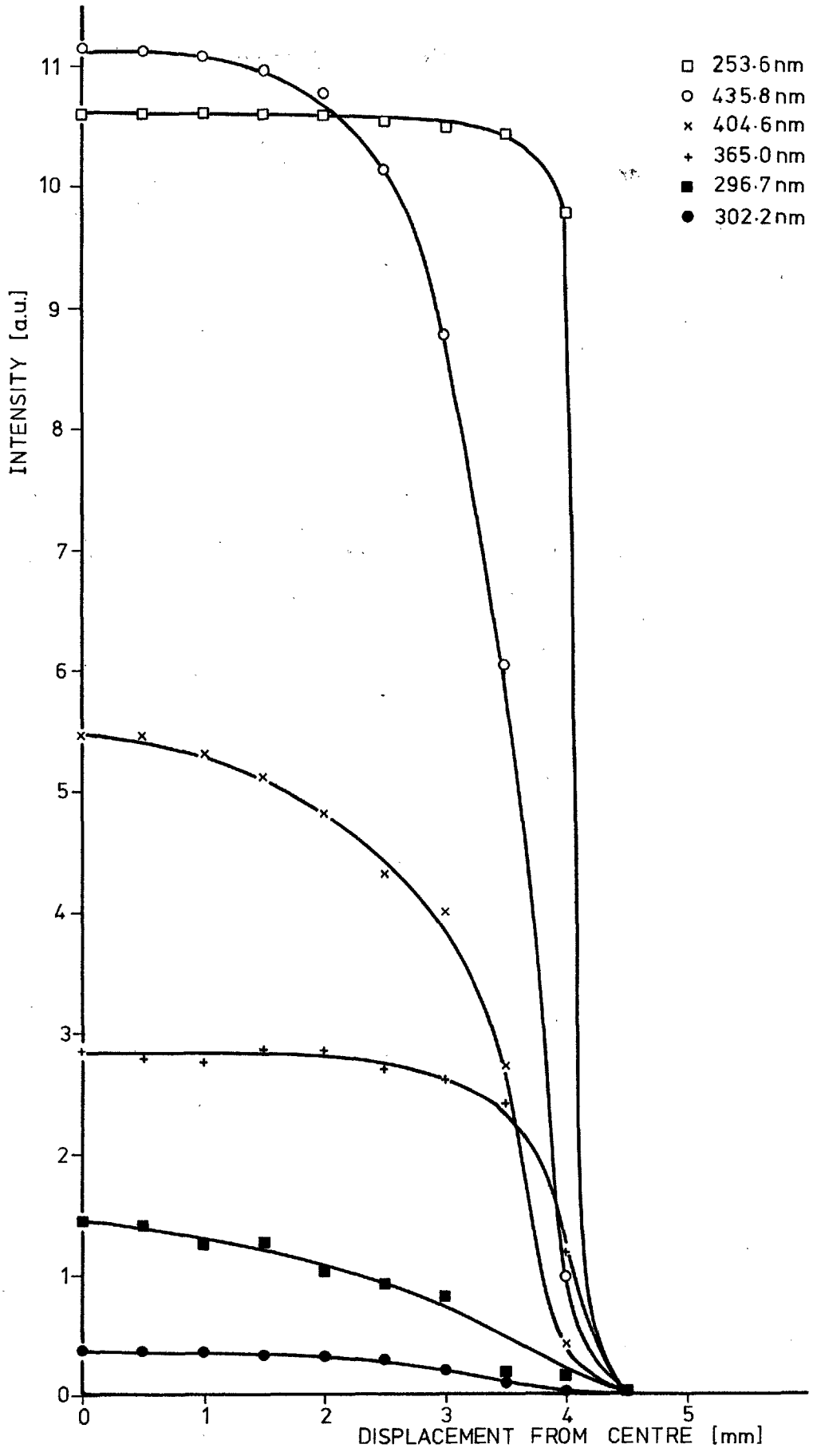


FIGURE 5·18: The Radial Intensity Distribution of a Mercury EDL at Different Wavelengths. T = 150°C, Power = 30W.

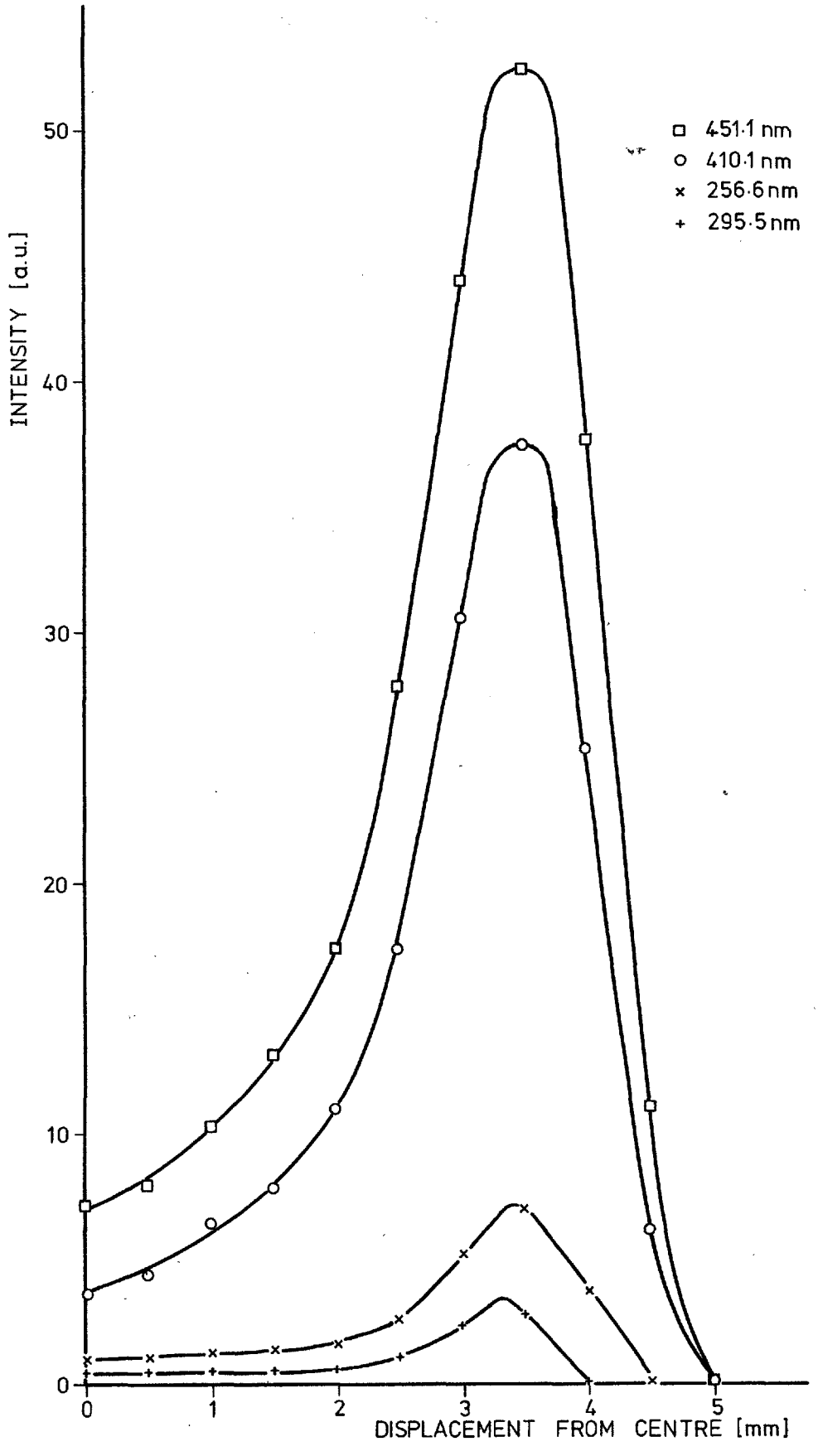


FIGURE 5·19: The Radial Intensity Distribution of an Indium EDL at Different Wavelengths. T = 300 °C, Power = 40 W.

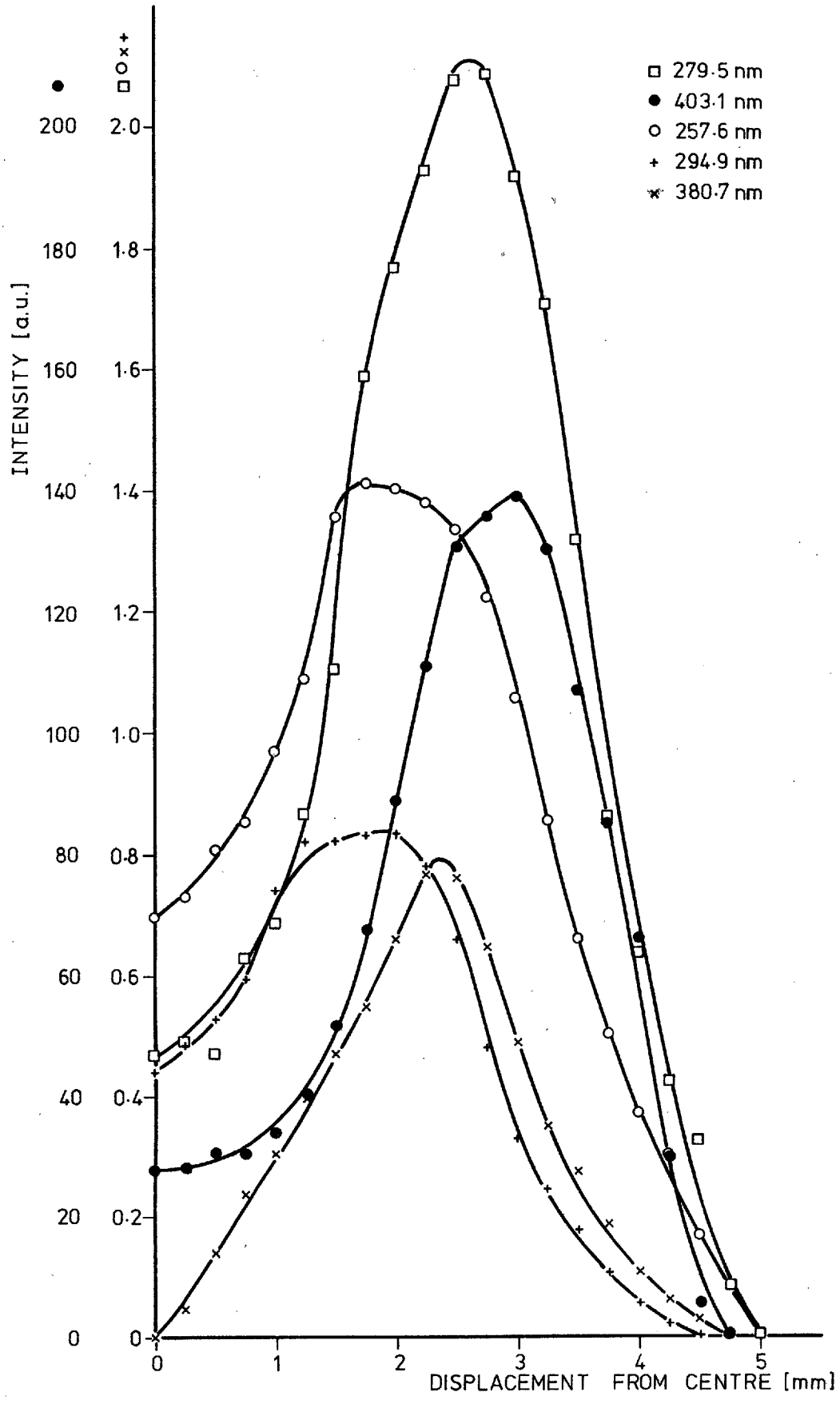


FIGURE 5.20 : The Radial Intensity Distribution of a Manganese EDL at Different Wavelengths. T = 350°C, Power = 60W.

5.18 to 5.20 are given in Table 5.2.[150] The wavelengths were selected to give a range of excitation energies for each element and,where possible,to give transitions finishing in ground states and in non-ground states.

TABLE 5.2: Transition energies for the lines measured in Figures 5.19-5.21.

ELEMENT	SPECTRUM	TRANSITION (cm^{-1})	TRANSITION ENERGY (eV)	WAVELENGTH (nm)
Hg	I	0-39412	4.886	253.65
Hg	I	37645-71336	4.177	296.73
Hg	I	44043-77129	4.102	302.15
Hg	I	44043-71431	3.730	365.01
Hg	I	37645-62350	3.063	404.66
Hg	I	39412-62350	2.844	435.84
In	I	0-39048	4.841	256.01
In	I	2213-36302	4.226	293.26
In	I	0-24373	3.022	410.18
In	I	2213-24373	2.747	451.13
Mn	II	0-38807	4.811	257.61
Mn	I	0-35770	4.435	279.48
Mn	II	9473-43370	4.203	294.92
Mn	I	17052-43314	3.256	380.67
Mn	I	0-24802	3.075	403.08

Suitable indium lines were not available which finished in energy levels greater than $2213cm^{-1}$,a ground state multiplet.

5.4 MEASUREMENTS MADE OF THE INTENSITIES OF HYPERFINE COMPONENTS.

5.4.1 Introduction.

The origin and theory of hyperfine structure components in atomic lines were presented in Chapter 2; the close agreement between the intensities predicted by the sum rule and the observed intensities of hyperfine components has been mentioned. Those components which have the greatest intensity in emission will also have the greatest absorption coefficient when compared with other members of the hyperfine multiplet. By measuring the relative intensities of two hyperfine components, with different theoretical intensities, and taking their ratio, the extent of self-absorption of the emitted source radiation may be monitored.[151]

The Fabry-Perot interferometer was used to make measurements of the relative intensities of the hyperfine components. However, there were some limitations to the range of elements which could be studied. The emitted wavelength was required to be in the range acceptable to the interferometer plates and the hyperfine structure had to be relatively simple. The presence of only one isotope was also important in order to avoid spectral overlap. The most suitable element for study was indium, having only one naturally occurring isotope (^{115}In) and a set of only four well spaced nuclear hyperfine components at the 410.18nm line. Naturally occurring lead was not suitable for these measurements because of its multi-isotope composition. However, the ^{207}Pb isotope

was used,having three nuclear hyperfine components at the 405.78nm line. The third element chosen was the ^{199}Hg isotope,having only two hyperfine components at the 404.6nm line.

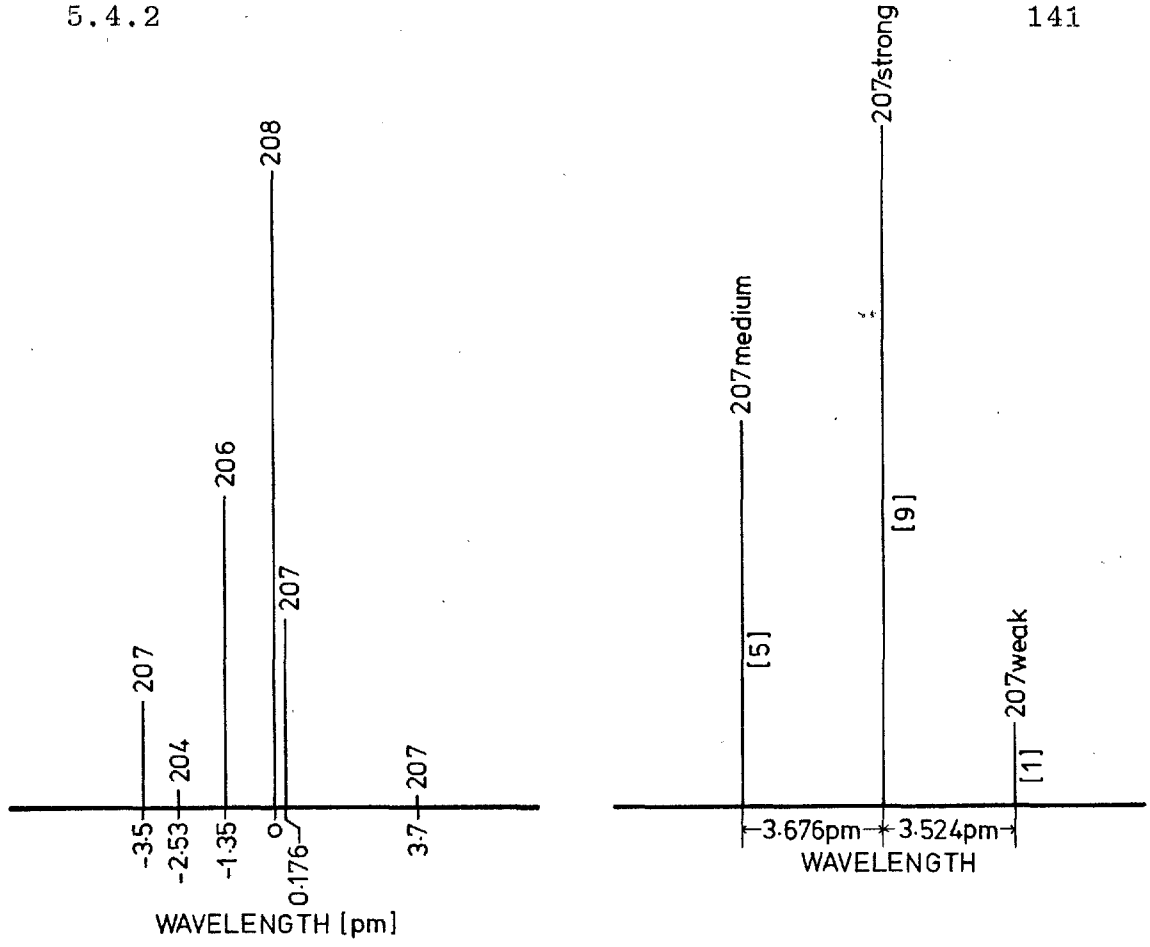
5.4.2 Lead.

The hyperfine structure of the 405.78nm lead line is shown in Figure 5.21 together with the theoretical relative intensities of the components due to ^{207}Pb. These components have been designated strong,medium and weak with respect to their relative intensities. The theoretical ratios were derived by the method described in Chapter 2.

The lead 405.78nm transition is between the terms $^3P_2$ and $^3P_1$,and the nuclear spin quantum number of ^{207}Pb is $\frac{1}{2}$. Therefore,for the $^3P_2$ term F may take the values 5/2 and 3/2,for the $^3P_1$ term F has the values 3/2 and 1/2. An energy level diagram is shown in Figure 5.22. There are three allowed transitions with relative theoretical intensities of 9,5 and 1.

The ratio of the strong line to the medium line was used to monitor the extent of self-absorption at different positions in the lead EDL,operated at a number of different microwave powers and temperatures. Although,theoretically, the ratio of the strong line to the weak line should have given greater sensitivity,the signal-to-noise ratio for the weak line was not satisfactory at some positions in the lamp. The free-spectral-range of the interferometer was adjusted to give minimum overlap of the components.

The hyperfine intensity ratio for the 405.78nm lead



Displacement of Components due to the Isotopic Composition from the Central ^{208}Pb Wavelength.

Nuclear Hyperfine Structure of ^{207}Pb. [ ] = Relative theoretical intensities.

FIGURE 5·21:- Lead - Hyperfine Structure of the 405·78nm Line.

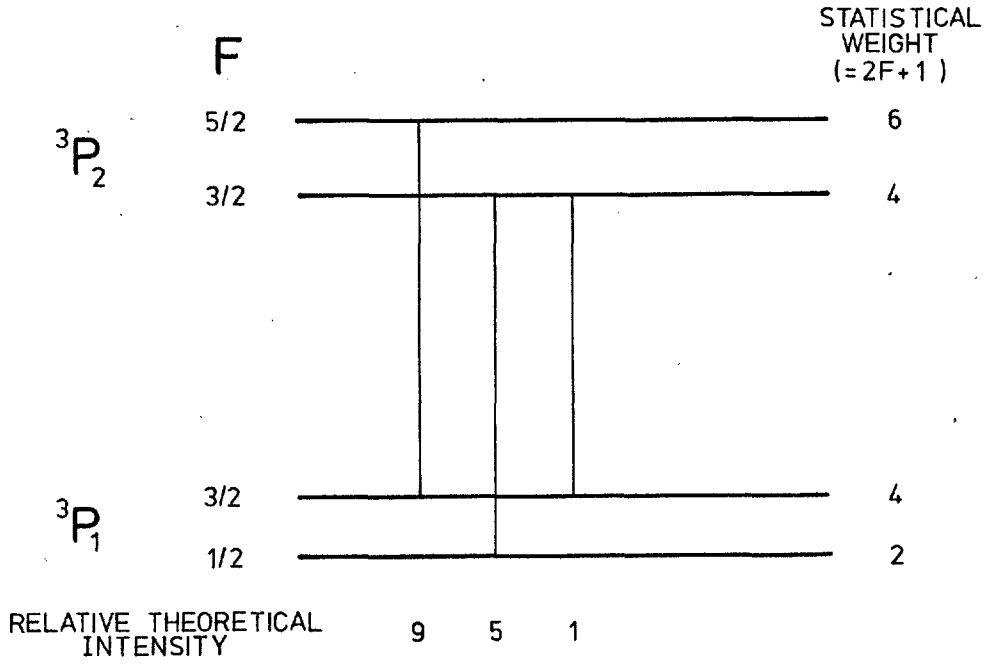


FIGURE 5·22: Nuclear Hyperfine Structure Energy Levels for Lead-207 at the 405·78nm Line.

line is shown in Figure 5.23 at different displacements from the centre of the lamp. For comparitive purposes the lateral distribution of the total intensity is also included,having been measured under the same operating conditions of 30W absorbed microwave power and an air stream temperature of 400^{0}C. The theoretical value of the hyperfine intensity ratio (9) is approached at the centre of the lamp. This ratio is a minimum just inside the edge of the discharge,where an approximate correspondence is made with the maximum of the lateral intensity. The minimum of the hyperfine intensity ratio indicates a maximum of self-absorption in the radiation. Right at the edge of the lamp the hyperfine intensity ratio increases and,hence,the extent of self-absorption decreases as might be expected for radiation originating and escaping from the edge of the discharge.

The effect of the absorbed microwave power,at a constant operating temperature of 400^{0}C,upon the hyperfine intensity ratio is shown in Figure 5.24.

The general pattern is that the overall extent of self-absorption increases with the absorbed microwave power.

The effect of the value of the operating temperature upon the hyperfine intensity ratio is shown in Figure 5.25. At 300^{0}C the lateral variation in the extent of self-absorption is less than at higher temperatures. The hyperfine intensity ratio is severely reduced when the EDL is operated at 500^{0}C.

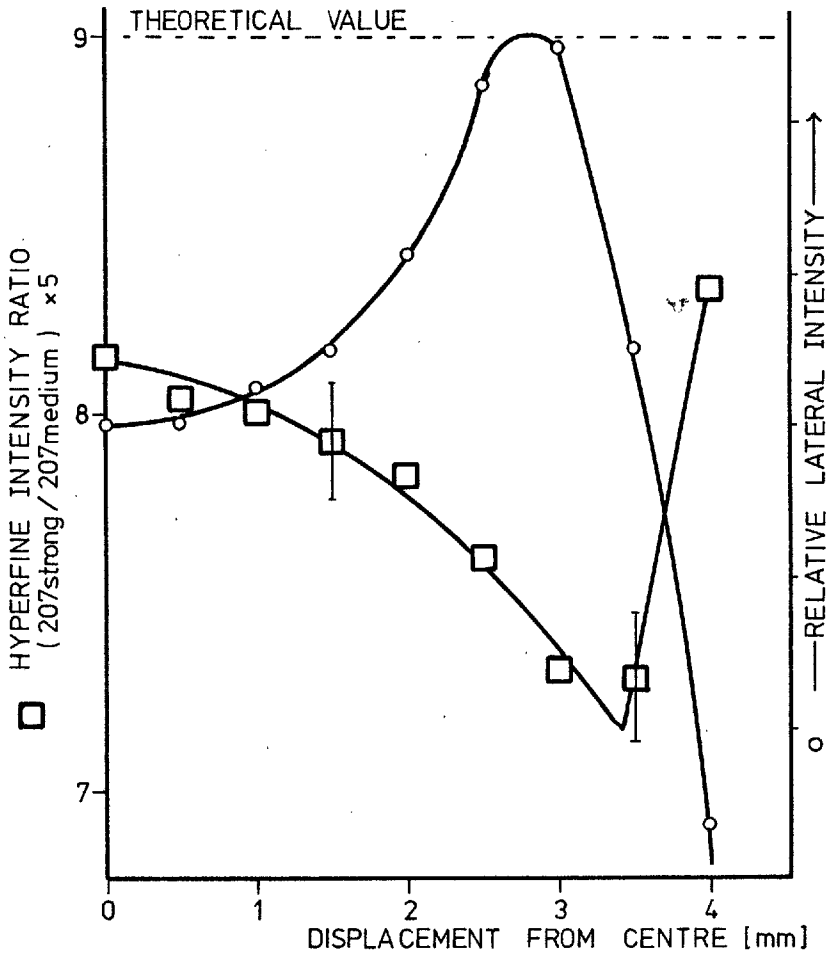


FIGURE 5·23: The Hyperfine Intensity Ratio of the 207strong and 207medium Lines in a Lead EDL.
T = 400 °C, Power = 30 W, Wavelength = 405·78nm.

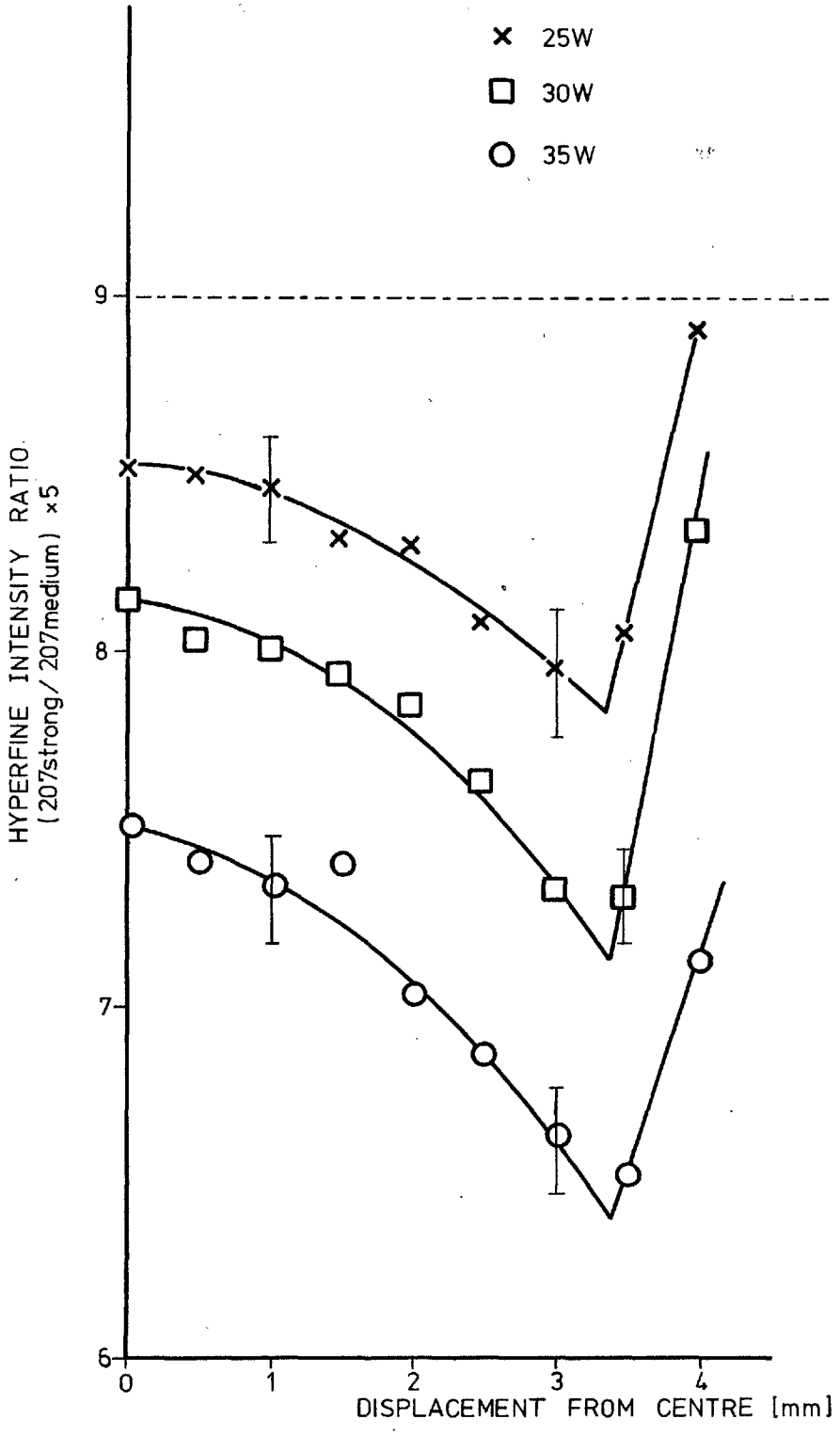


FIGURE 5.24: The Hyperfine Intensity Ratio in a Lead EDL at Different Absorbed Microwave Powers.
T = 400 °C, Wavelength = 405.78nm.

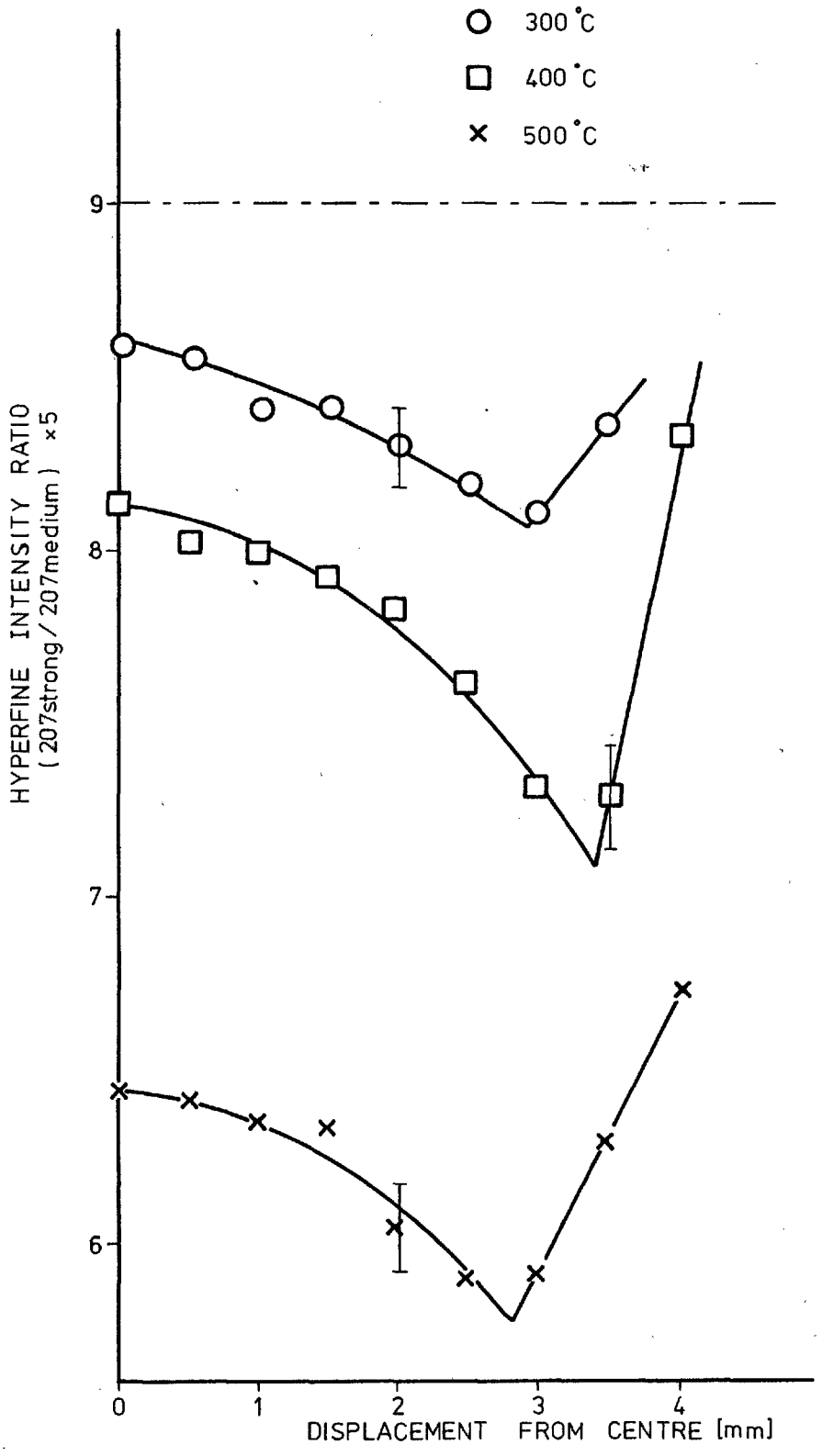


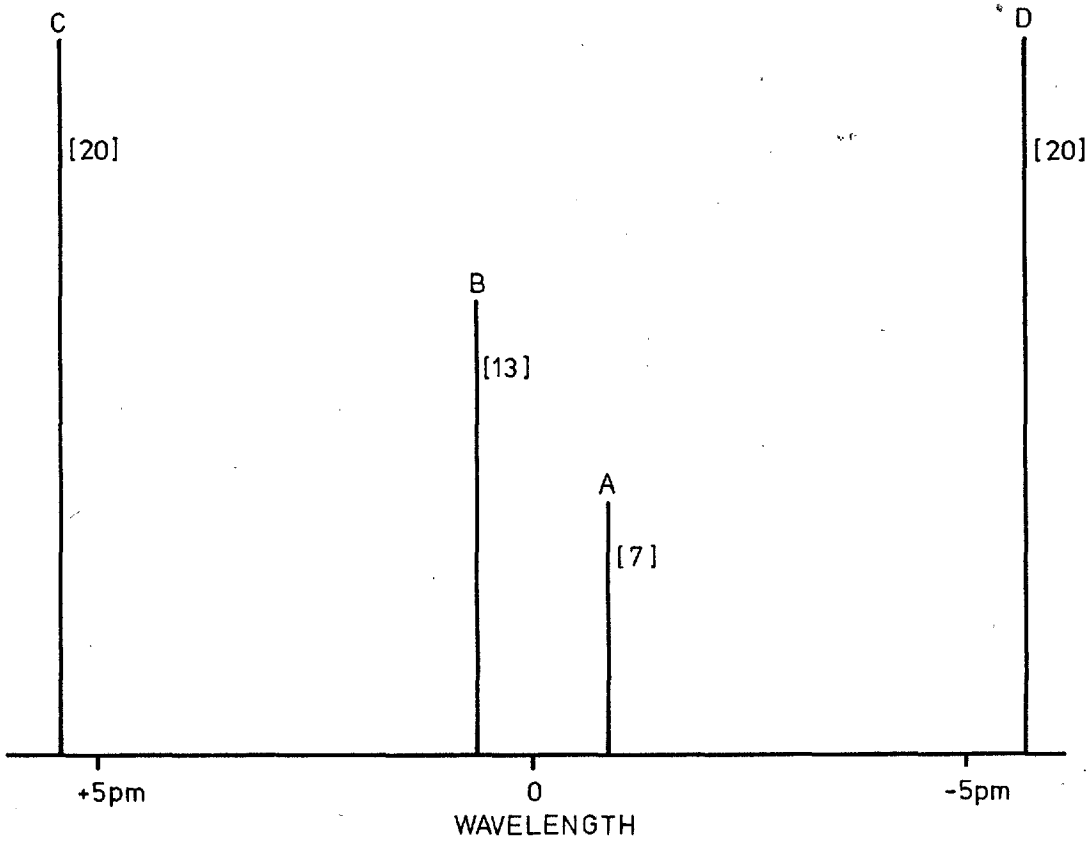
FIGURE 5·25 : The Hyperfine Structure Intensity Ratio in a Lead EDL at Different Thermostat Temperatures.
Power = 30W , Wavelength = 405·78nm.

5.4.3 Indium.

The nuclear hyperfine structure of the 410.18nm indium line is shown in Figure 5.26. The line consists of four components labelled A,B,C and D with relative theoretical intensities of 7,13,20 and 20,respectively. The transition is $^2S_{\frac{1}{2}} - {}^2P_{\frac{1}{2}}$ and the nuclear spin quantum number is 9/2. For both terms F may take the values 5 and 4. A diagram of the hyperfine energy levels is shown in Figure 5.27. In order to determine the extent of self-absorption in the emitted radiation the ratio of the D and B components was measured.

The results for an indium EDL operated at 300°C and at an absorbed microwave power of 30W are shown in Figure 5.28,together with the lateral distribution of the total line intensity at 410.18nm. The results concur with those obtained with the lead EDL with regard to the maximum of self-absorption occurring where the total line intensity is greatest. In this case the hyperfine intensity ratio reached almost the theoretical value of 20 at the central position,corresponding to almost zero self-absorption taking place.

Measurements made of the hyperfine intensity ratio at an operating temperature of 350°C (Figure 5.29) revealed an insignificant difference between the results obtained at absorbed microwave powers of 30W and 40W. At 400°C the hyperfine intensity ratio was virtually constant with displacement from the central position, it being only 20% of the theoretical value. The latter condition corresponded with the formation of the type A



[ ] = RELATIVE THEORETICAL INTENSITY.

FIGURE 5·26: The Hyperfine Structure of the Indium 410·18nm Line.

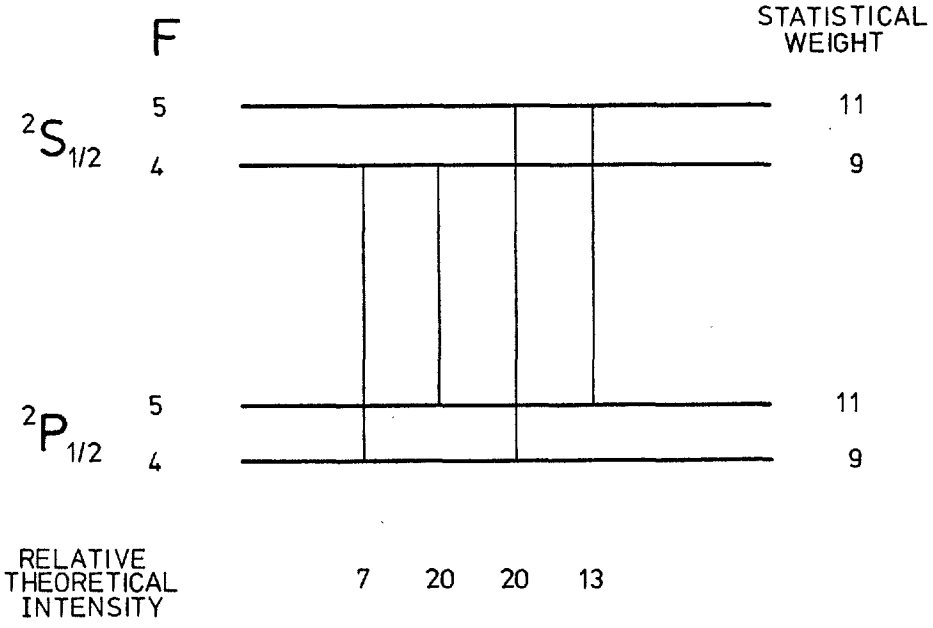


FIGURE 5·27: Hyperfine Energy Level Diagram for the Indium 410·18nm Line.

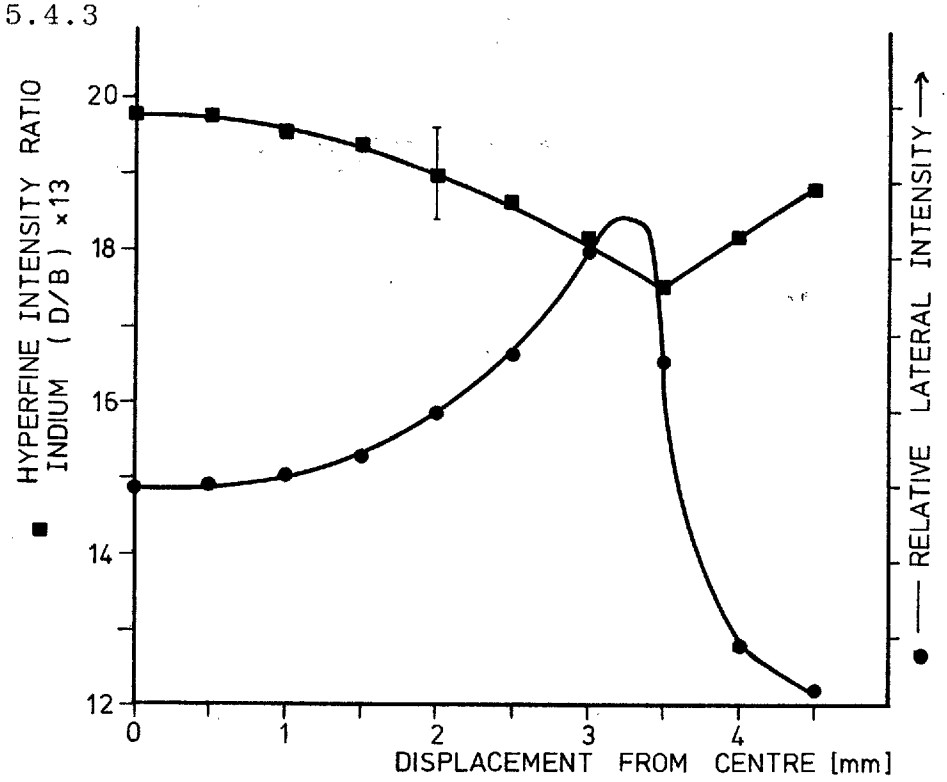


FIGURE 5·28: Distributions of the Total Intensity and the Hyperfine Structure Intensity Ratio in an Indium EDL. T =300°C, Power = 30W, Wavelength = 410·18nm.

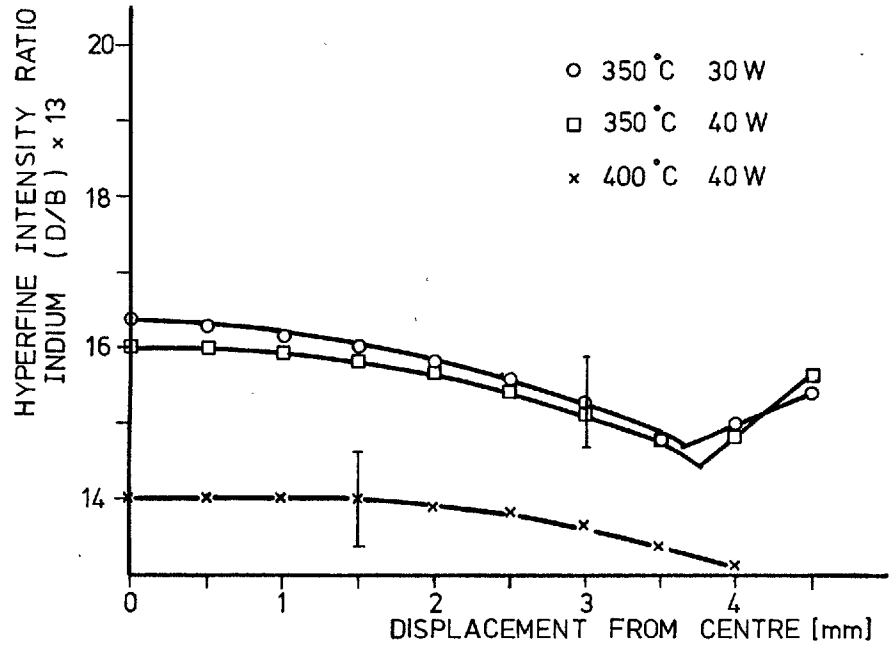


FIGURE 5·29: The Variation of the Distribution of the Hyperfine Intensity Ratio in an Indium EDL with the Absorbed Microwave Power and the Thermostat Temperature. Wavelength = 410·18nm.

intensity distribution in the EDL (Figure 5.14).

5.4.4 Mercury.

The nuclear spin quantum number of mercury (^{199}Hg) is ½ and the transition at 404.6nm is between the terms ^3P_o and $^3S_1$. The F values for the $^3S_1$ term are 3/2 and 1/2,whilst for the ^3P_o term only F=½ is possible. The possible transitions are shown in Figure 5.30.

The value of the hyperfine intensity ratio at different displacements from the central viewing position is shown in Figure 5.31 for a mercury EDL operated at 100°C and 20W. The choice of the 404.6nm line is not the most pertinent from the point of view of making measurements of the extent of self-absorption; the lower level of the transition is at 4.667eV above the ground state. Therefore,it is interesting that the hyperfine intensity ratio is much lower than its theoretical value (2) in the centre of the lamp.

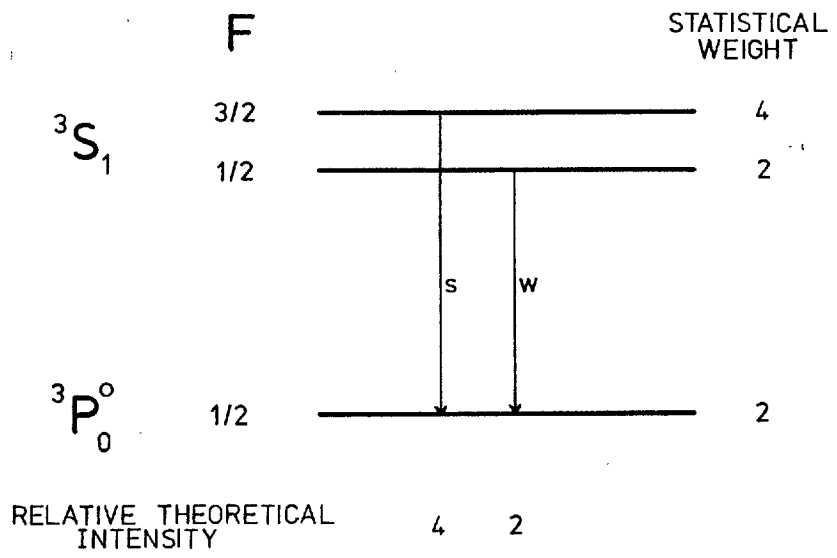


FIGURE 5·30: Hyperfine Energy Level Diagram for the 404·6nm Mercury-199 Line.

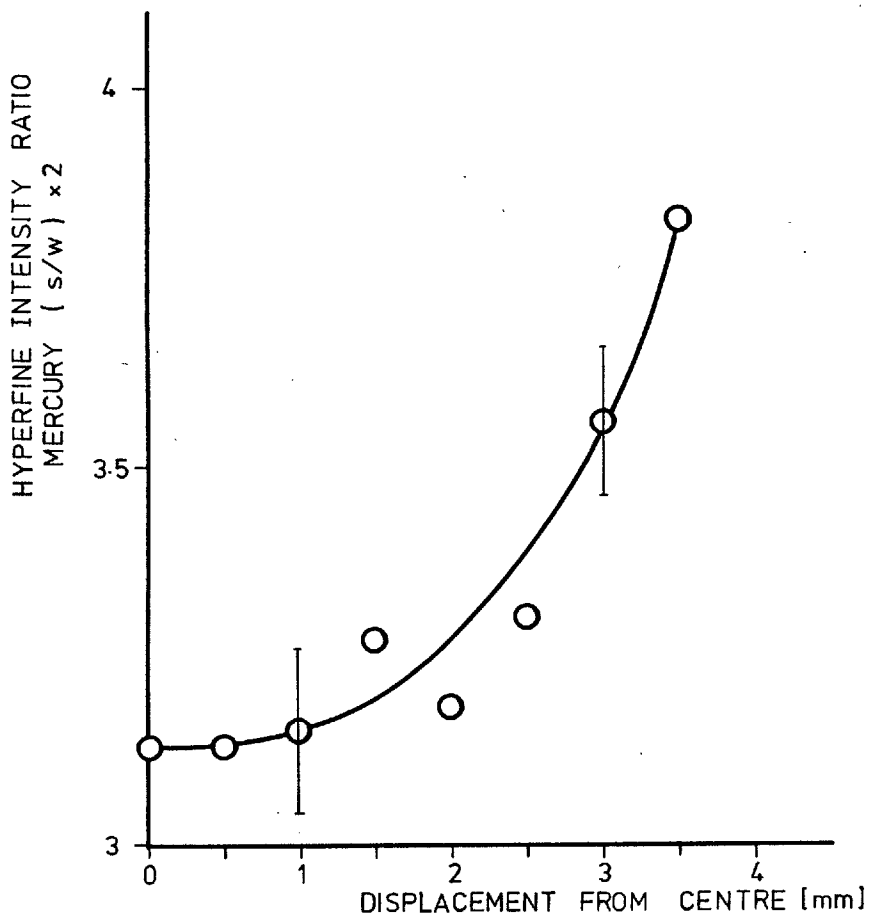


FIGURE 5·31: The Distribution of the Hyperfine Structure Intensity Ratio in a Mercury EDL.
T = 100 °C, Power = 20W, Wavelength = 404·6nm.

5.5 THE MEASUREMENT OF EXCITATION TEMPERATURES IN AN INDIUM EDL.

5.5.1 Theoretical.

The intensity of an atomic spectral line was given by Equation 2.9 and is reproduced here as Equation 5.1:

$$I_\nu = \frac{c}{4\pi} \rho_\nu . \qquad 5.1$$

The energy density, ρ_ν, is $N_2 A_{21} h\nu$, where, N_2 is the number density in the upper energy level, A_{21} and ν are the Einstein transition probability and the frequency of the transition, respectively. Therefore Equation 5.1 becomes

$$I_\nu = \frac{c}{4\pi} N_2 A_{21} h\nu . \qquad 5.2$$

It is useful to consider two transitions originating from different upper levels but terminating in the same lower energy level. This is shown diagrammatically in Figure 5.32.

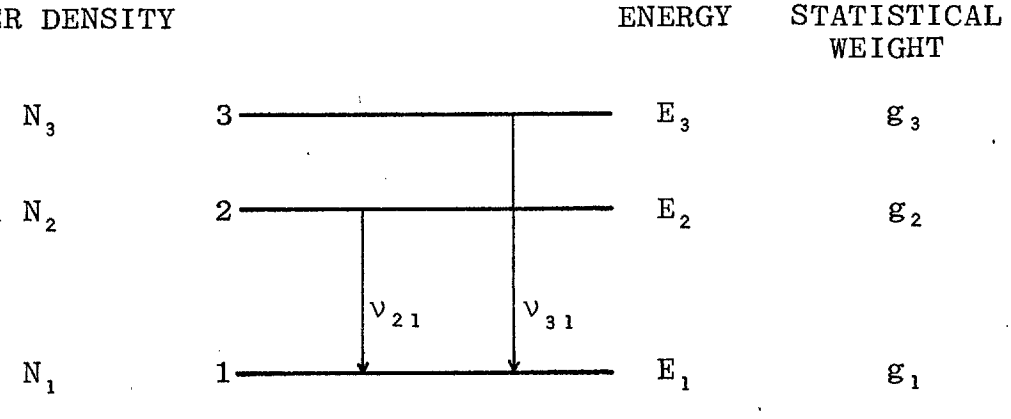


Figure 5.32: Energy Level Diagram for a System with Transitions from Energy Levels E_3 & E_2 to E_1.

The intensity of the transition from E_2 to E_1 is given by combining Equations 5.2 and 2.7,

$$I_{21} = \frac{c}{4\pi} A_{21} h\nu_{21} \frac{N}{U(T)} g_2 \exp\{-E_2/kT\}. \qquad 5.3$$

Similarly, for the transition from E_3 to E_1,

$$I_{31} = \frac{c}{4\pi} A_{31} h\nu_{31} \frac{N}{U(T)} g_3 \exp\{-E_3/kT\}. \qquad 5.4$$

Combining Equations 5.3 and 5.4 gives,

$$\frac{I_{21}}{I_{31}} = \frac{A_{21}\nu_{21}g_2}{A_{31}\nu_{31}g_3} \exp\{(E_3-E_2)/kT\}. \qquad 5.5$$

Equation 5.5 relates the Boltzmann excitation temperature, T, to the intensity ratio of two atomic spectral lines.

In order to obtain accurate values of the excitation temperature it is necessary that the observed intensities have not been reduced by self-absorption. The ratio of the integrated absorption coefficients for the two transitions is given by[152]

$$\frac{K_{12}}{K_{13}} = \frac{g_2 f_{21}}{g_3 f_{31}} \exp\{(E_1-E_1)/kT\}, \qquad 5.6$$

which, obviously, simplifies to

$$K_{12}/K_{13} = g_2 f_{21}/g_3 f_{31}, \qquad 5.7$$

because the lower energy level is the same for both transitions. Equation 5.7 implies that K_{12}/K_{13} will be unity if the gf-values are the same for both transitions. The following pair of transitions conform to the latter requirement and both have the same lower energy level.

Wavelength	Transition	gf
410.176nm	0-24373cm^{-1}	0.47
256.015nm	0-39048cm^{-1}	0.46

The emitted intensity, I_{em}, is reduced by self-absorption and the observed intensity, I_{obs}, is given by

$$I_{obs} = \frac{\alpha}{K} I_{em} (1-\exp\{-Kl\}), \qquad 5.8$$

where, K is the integrated absorption coefficient for the transition, l is the path length and α is a constant. Therefore, the intensity ratio, given by Equation 5.5, becomes

$$\frac{I_{obs_{21}}}{I_{obs_{31}}} = \frac{I_{em_{21}} K_{13}(1-\exp\{-K_{12}l\})}{I_{em_{31}} K_{12}(1-\exp\{-K_{13}l\})} . \qquad 5.9$$

As K_{13}/K_{12} is equal to unity then Equation 5.9 reduces to

$$I_{obs_{21}}/I_{obs_{31}} = I_{em_{21}}/I_{em_{31}}, \qquad 5.10$$

correction for self-absorption becomes unnecessary and Equation 5.5 may be used directly.

5.5.2 Procedure.

Measurements of the intensities of the indium 410.18nm and 256.0nm lines were made at different lateral positions in an indium EDL, operated at a number of different temperatures and microwave powers. An inverse Abel transform was carried out upon the data to convert the lateral distributions into radial distributions.

A standard calibrated tungsten source was not available to measure the response of the monochromator and photomultiplier tubes to different wavelengths. However, a comparison was made between the equipment used and another system, which had been calibrated previously. It was found to be necessary to multiply the intensity measurements made at 256.0nm by a factor of 1.5834 in order to correct for the spectral response of the system.

The numerical values used in the calculation of the excitation temperatures are given in Table 5.3.

TABLE 5.3: Data Used for the Calculation of Excitation Temperatures.[155]

λ_{21}	= 410.176nm	λ_{31}	= 256.015nm
ν_{21}	= 7.30887×10^{14}Hz	ν_{31}	= 1.17100×10^{15}Hz
g_2A_{21}	= $1.9\times10^{8}s^{-1}$	g_3A_{31}	= $4.7\times10^{8}s^{-1}$
E_1 = 0	E_2 = 4.84123×10^{-19}J		
E_3 = 7.75609×10^{-19}J			
k = 1.38054×10^{-23}JK ^{1}.			

5.5.3 Results.

The variation of the measured excitation temperature

with the distance from the centre of the EDL is shown in Figures 5.33-5.36. Figures 5.33,5.34 and 5.35 show the effect of variations in the absorbed microwave power at the different operating temperatures of 300°C, 350°C and 400°C, respectively. In general, the differencies between the measurements made at different powers are relatively small and probably insignificant.

The most interesting results are shown in Figure 5.36, in which the radial distribution of excitation temperature is plotted for different values of the operating temperature at a constant absorbed microwave power of 50W. At the edge of the discharge there is relatively little difference between the measurements of the excitation temperature at different operating temperatures. There is not a significant difference between the measurements made at 300°C and 350°C, and these values are only ca. 250K greater than the measurement made at an operating temperature of 400°C. The curves in Figure 5.36, however, diverge rapidly towards the central position in the EDL where there is a difference of ca. 650K between the excitation temperatures for the lamps operated at 300°C and 350°C. There is a difference of ca. 1100K between the excitation temperatures for the lamps operated at 350°C and 400°C.

The measurements made at an operating temperature of 300°C indicate that there is an approximately 2200K difference in the excitation temperature between the centre of the lamp and the edge. This gradient decreases when the operating temperature is increased; at an

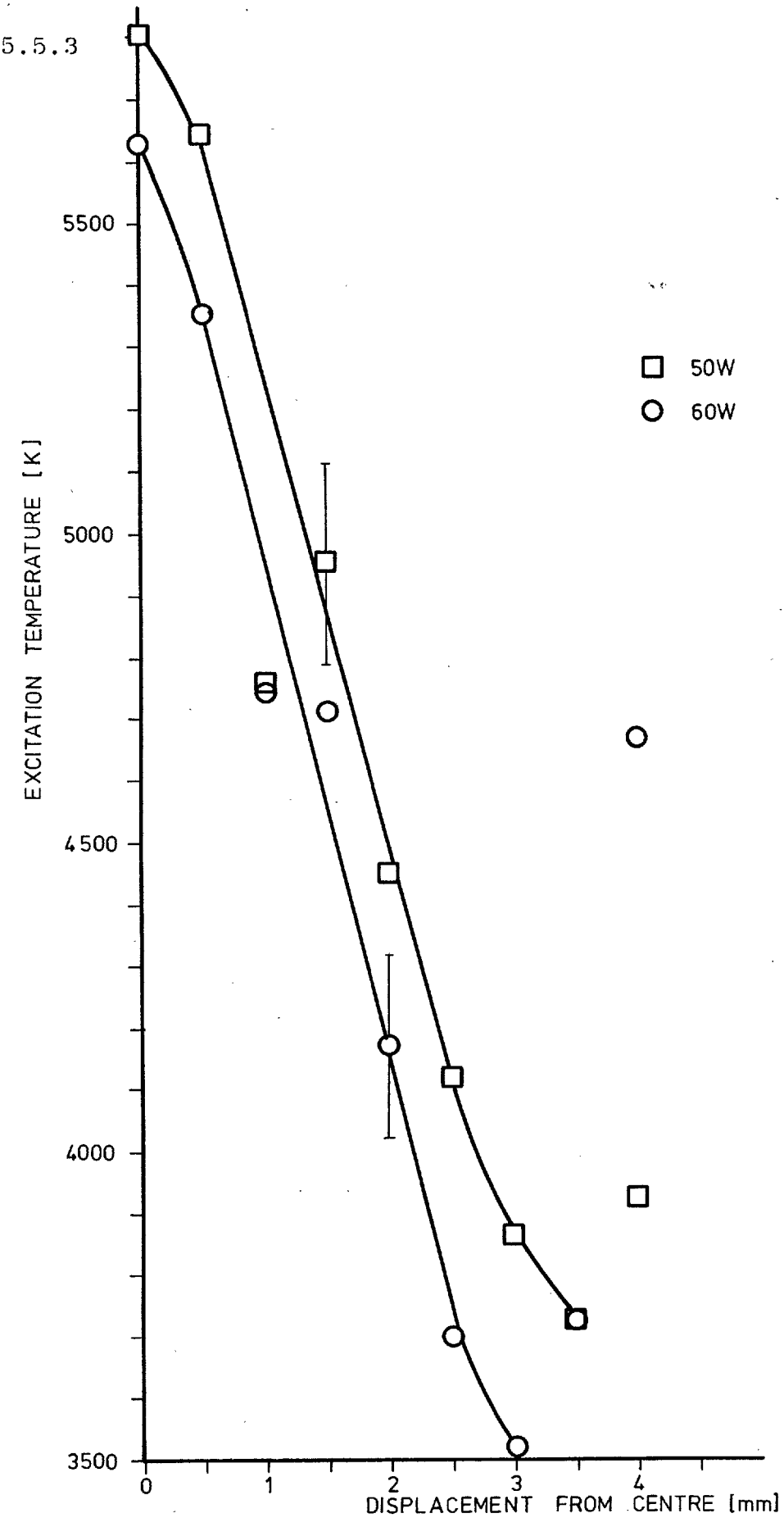


FIGURE 5.33: The Radial Distribution of the Excitation Temperature in an Indium EDL Operated at 300°C.

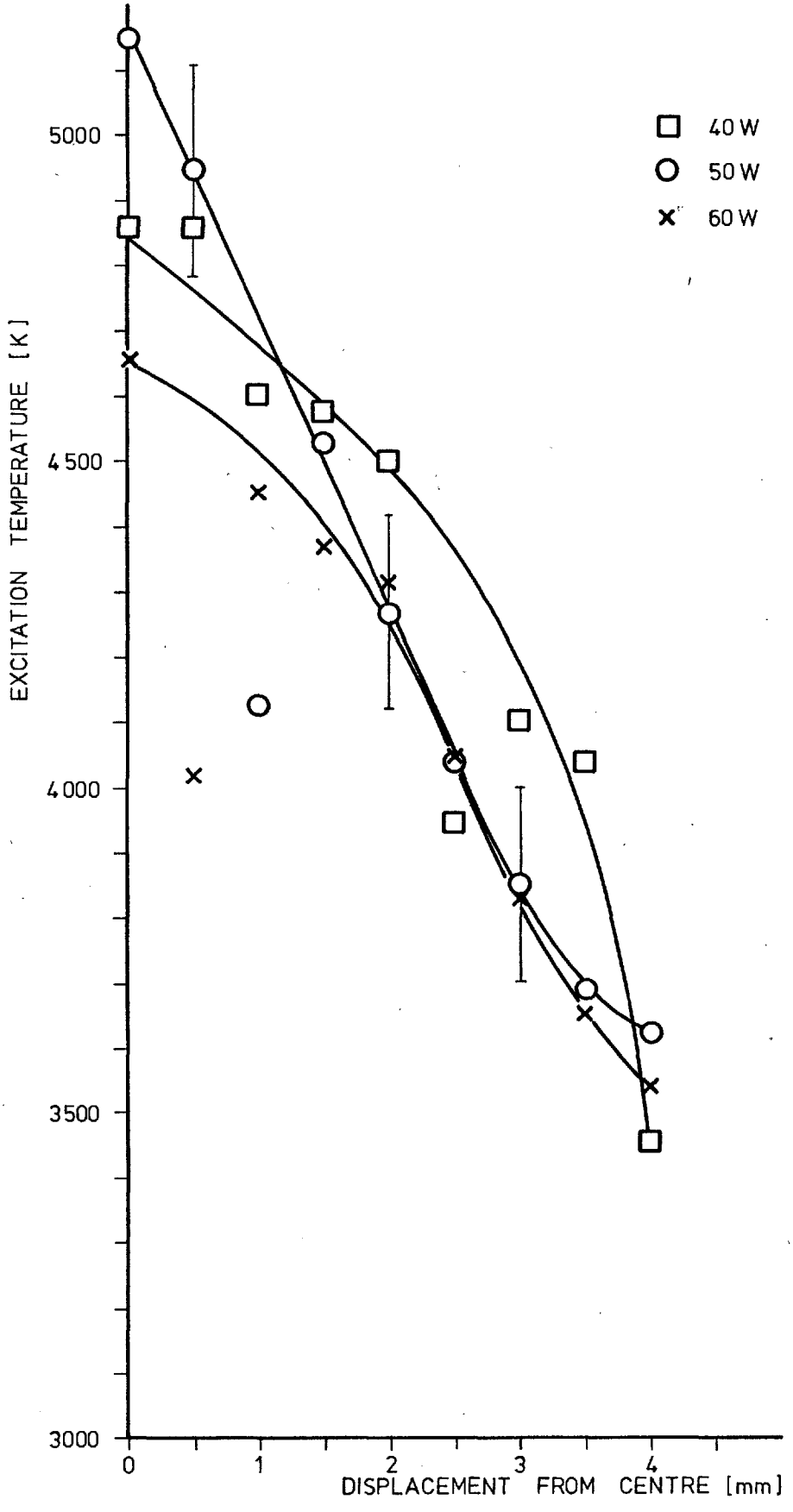


FIGURE 5.34: The Radial Distribution of the Excitation Temperature in an Indium EDL Operated at 350 °C.

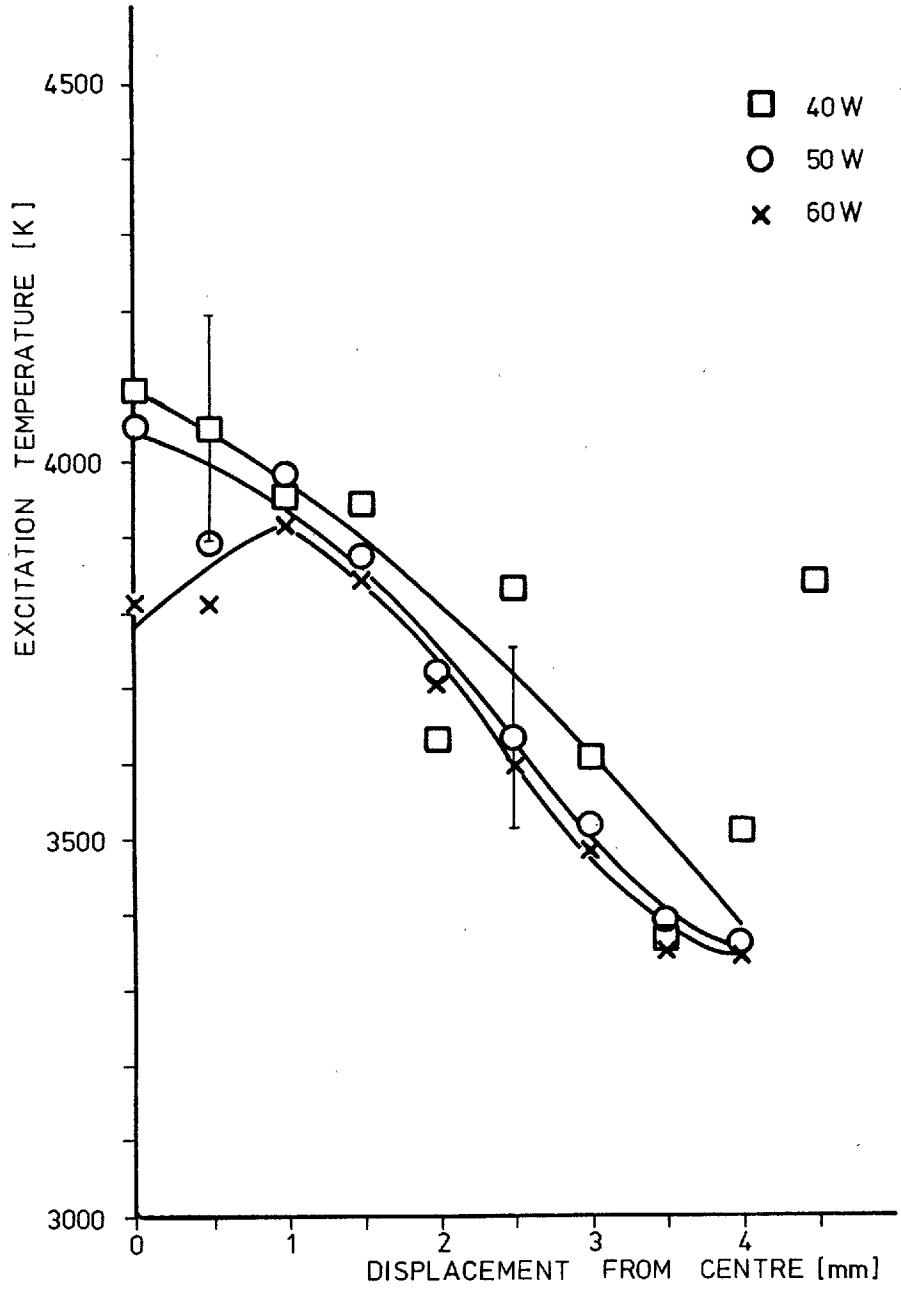


FIGURE 5·35 : The Radial Distribution of the Excitation Temperature in an Indium EDL Operated at 400 °C.

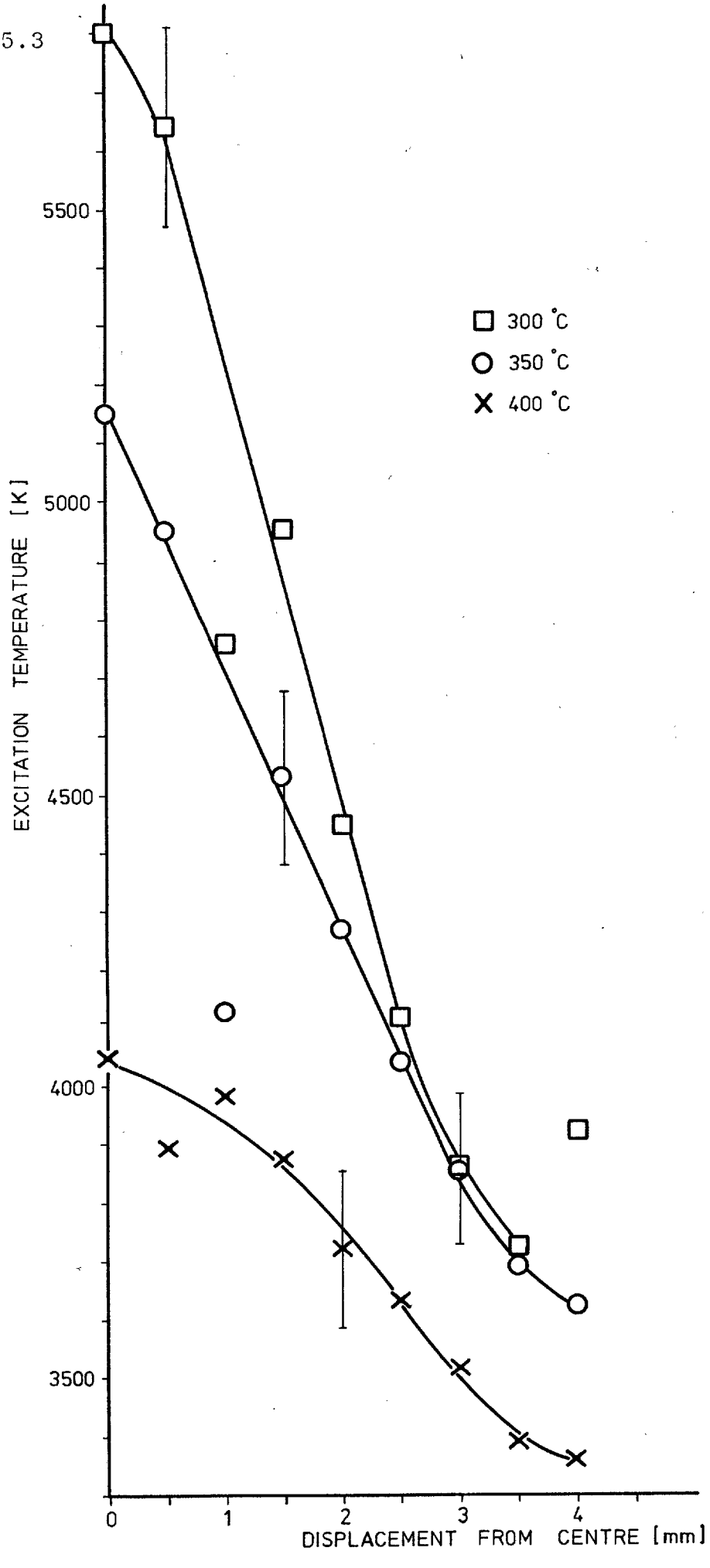


FIGURE 5-36: The Radial Distribution of the Excitation Temperature in an Indium EDL Operated at 50W.

operating temperature of 400^{0}C the difference in the excitation temperature is only 700K between the centre and the edge of the EDL.

The errors in the measurements of the excitation temperature have been indicated by error bars in the figures. However, in general, an excitation temperature of 4500K is ±150K. Although this error is relatively large there is still a significant variation in the excitation temperature with radial position in the EDL.

5.6 DISCUSSION.

5.6.1 Sputtering.

If the gas temperature inside the EDL source is greater than the temperature of the air stream used to thermostat the lamp then the only means by which energy may be dissipated thermally is through the walls of the lamp. This being the case,there must be a temperature gradient between the centre of the EDL and the wall.The wall being the coolest part of the EDL makes it probable that material inside the EDL will tend to condense on the wall if the material is unable to remain in the vapour phase. Because the plating of material onto the wall must be a dynamic process,as the relatively low pressure inside the lamp makes collisions with the wall highly probable,it is useful to consider the possible processes by which material from the inner surface of the lamp might return to the vapour phase.

A possible mechanism by which atoms may be ejected

from the surface of the wall is by sputtering,the process involved in the operation of a hollow cathode lamp. In such a process collisions of argon ions with the walls would result in the formation of a cloud of atoms just inside the wall which might account for the observed maximum of emission intensity at a position close to the wall of the EDL. However,this idea is difficult to justify when consideration is taken of the electrodynamics involved. The argon ion,being a charged species,would be expected to follow the oscillations of the incident electric field at 2450MHz. However,the relatively high inertial mass of argon means that it is highly unlikely that an argon ion would be able to follow the motion of the electric field. Therefore,it appears that an argon ion can not gain a substantial amount of energy directly from the electric field and so sputtering is unlikely to occur.

5.6.2 The Electrical Skin Depth.

The existence of constricted (arc-like) discharges within EDL's is well known,particularly when the lamp contains a large amount of material and/or it is operated at high temperatures and high microwave powers. Such constrictions may be interpreted[153,154] as the result of linear current pinching taking place when two or more conductors are placed close together. In the plasma,as a result of the interaction of their induced magnetic fields, each filament of current moves close to the other filaments resulting in a compact linear cluster. Discharges

which are constricted in such a manner are unsuitable for use as sources because of their instability and noise.

At high frequencies the current density is not constant at all positions across the conductor;the current is concentrated in a region close to the surface of the conductor. In a conductor with cylindrical symmetry,the depth at which the current has decreased to 1/e th. of its value at the surface is known as the electrical skin depth,s. In Chapter 1 it was mentioned that Scott et al.[80] used the following equation for the calculation of the skin depth.

$$s(cm) = 5.03/\sqrt{\mu\sigma\nu} \quad , \qquad 5.11$$

where, μ= relative permeability,ν= frequency (MHz) and σ= specific electrical conductivity ($\Omega^{-1}cm^{-1}$).

Boumans and De Boer[78] calculated the electrical skin depth in an argon plasma,operated at 52MHz and at atmospheric pressure,to be about 2.7mm. The major problem involved in applying this calculation procedure to the discharge in an EDL source is in obtaining a value for the specific electrical conductivity. If the parameters in Equation 5.11 are kept constant except for the frequency, which is increased to 2450MHz, then the value of s that is obtained becomes 0.4mm. In their calculation for the argon plasma at atmospheric pressure Boumans and De Boer used a value of 7875K for the electron temperature. For the 2450MHz electrodeless discharge at low pressure values

in the order of 30000K have been quoted for the electron temperature.[53,54] As the specific electrical conductivity would be expected to increase with the electron temperature the skin depth would be expected to decrease correspondingly. However, the electron temperature is not the only parameter involved in the calculation. The electron density has been found[53] to be much lower in the EDL source than in an ICP source; the electron density in an EDL is probably about $10^{11}cm^{-3}$. The lower value of the electron density would be expected to lower the specific electrical conductivity and increase the skin depth.

The specific electrical conductivity was measured by Avni and Winefordner[53] to have an average value of ca. $20\times10^{4}\Omega^{-1}cm^{-1}$. On putting this value into Equation 5.11 and using the values

$$\sigma = 20\times10^{4}\Omega^{-1}cm^{-1},$$

$$\mu = 1,$$

$$\nu = 2450MHz,$$

a value of 2.3μm for the skin depth is obtained.

Whilst the electrical skin depth is an important parameter in the coupling of energy from the microwave field into the plasma it is not apparent that it is the sole explanation for the existence of the type B form of intensity distribution. The actual existence of the type A distribution amplifies this argument.

5.6.3 Self-Absorption in the Centre of the Lamp.

It is useful to consider that the possible reason for the existence of the type B discharge is that the

radiation emitted by atoms in the centre of the lamp has been self-absorbed and,hence, only radiation emitted near the edge of the discharge escapes.

Measurements made of the hyperfine intensity ratio in an EDL exhibiting the type B discharge have shown that there is an effective maximum of self-absorption taking place just inside the wall of the EDL with a minimum of self-absorption taking place at the very edge of the discharge. The measurements show that the self-absorption is at a minimum in the centre of the discharge. The only way in which the interpretation of the hyperfine intensity data could be incorrect is if the self-absorption occurring in the centre of the discharge was so severe as to prevent any of the radiation emitted by atoms in the centre of the lamp from escaping. If any radiation escapes from the central region of the lamp then any self-absorption which had occurred along the path to the edge of the lamp would be expected to be revealed in the hyperfine intensity measurements.

The mean-free-path of electrons in an EDL has been measured[53] to be ca. 1cm. This implies that an electron has a higher probability of colliding with the wall of the lamp than with any other species inside the lamp because the internal diameter of the EDL bulb is only 0.8cm. Therefore,it appears unlikely that the number density inside the EDL source is sufficiently large to permit the total absorption of any radiation from the centre of the discharge. Therefore,it must be deduced that the measurements made of the extent of self-absorption are valid.

5.6.4 The Possible Reason for the Existence of the Type B Discharge.

It has been mentioned already that sputtering is an unlikely cause of atoms leaving the wall of the EDL and entering the vapour phase. It appears most likely that material leaves the wall by thermal means and there are a number of pieces of information which suggest that this process is taking place. Firstly,when the temperature of the air stream flowing over the surface of the EDL is increased the intensity of the emitted radiation is observed to increase. This agrees with the idea that more material is being evaporated from the wall at the higher temperature resulting in an increase in the atom population in the discharge.

Secondly,measurements of the extent of self-absorption taking place at different operating temperatures have shown that the extent of self-absorption increases with the temperature at any radial position in the discharge. Obviously, an increase in the self-absorption is symptomatic of an increase in the number density of ground state atoms. Browner and Winefordner[47] showed that the gas temperature inside the EDL must be the same as the temperature of the air stream flowing over the EDL. This is not necessarily the case. Their calculation involving the thermal conductivity of silica simply results in the conclusion that the inside surface of the wall of the EDL is at approximately the same temperature as the outer surface. Because the discharge in the EDL is not in thermal equilibrium or in

LTE there is no reason to suppose that the wall temperature reflects the gas temperature in other parts of the EDL.

Once material has vaporized from the surface of the wall it is next useful to consider whether,or not, the material will distribute itself homogeneously throughout the EDL. By the term homogeneous distribution it is intended here to describe a distribution,which is homogeneous with respect to the element rather than the state of the element,be it neutral or charged.

The pressure inside the EDL is obviously an important parameter in its operation. Experiments with a flow-through microwave plasma system have indicated that when the pressure is an order of magnitude greater than 10torr a constricted discharge tends to occur. As a constricted discharge did not occur in EDL's,when operated normally, it is reasonable to suppose that a vapour pressure of 10torr is a good estimate of the order of magnitude of the greatest pressure in an EDL. The variation of the vapour pressure with the temperature of a number of materials used in EDL manufacture is shown in Figure 5.37. For lead iodide a vapour pressure of 10torr corresponds with a temperature of ca. 570^{0}C. Therefore,approximating that a lead EDL at 800K has a vapour pressure of ca. 10torr, the number density of lead atoms may be estimated. Using the ideal gas equation, PV=nRT, the volume of the EDL is ca. $1.5\times10^{-6}m^{3}$, so that $n\simeq3\times10^{-7}$moles. This volume corresponds with a number density,N,of $1.2\times10^{23}m^{-3}$. The mean-free-path,l,

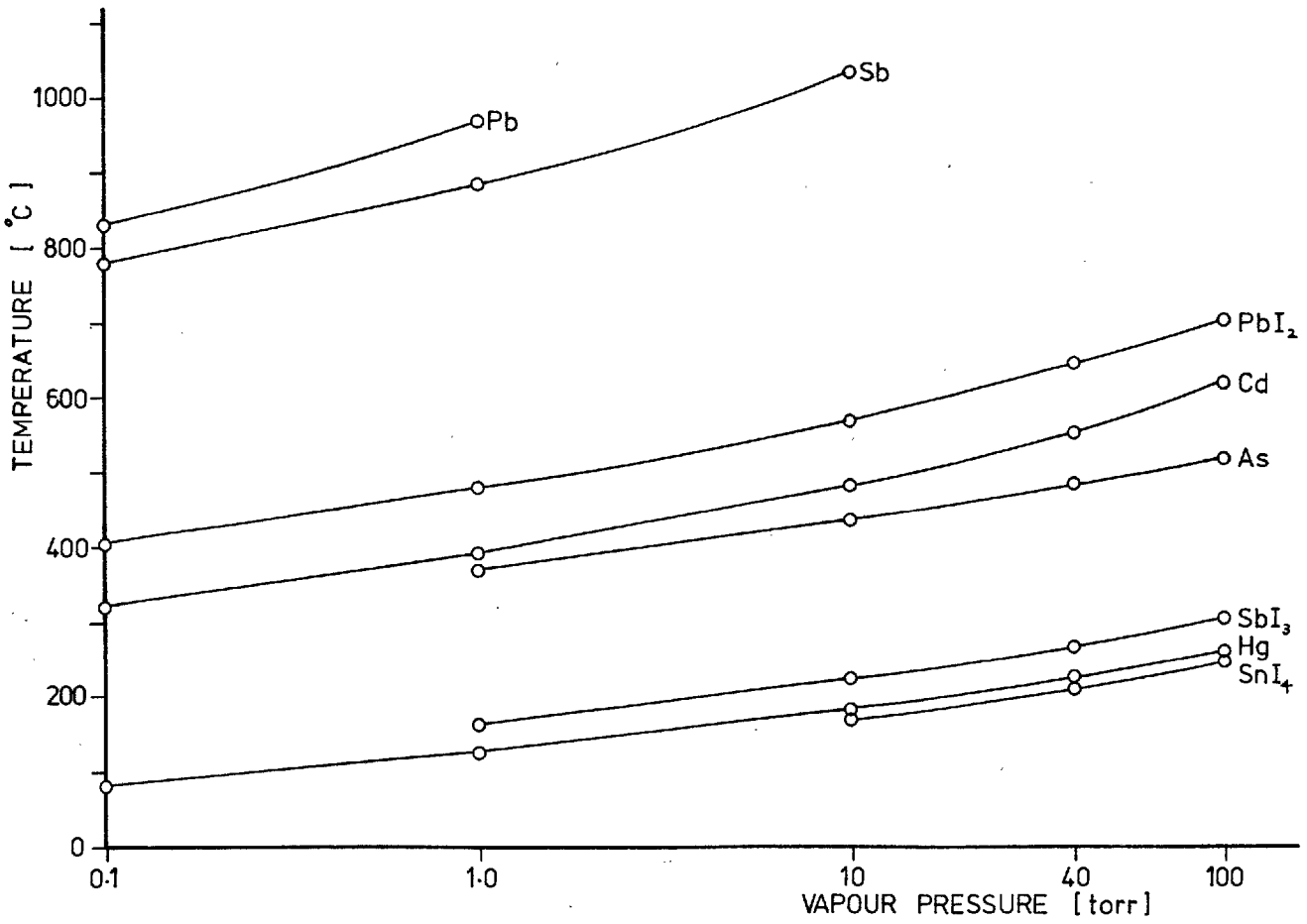


FIGURE 5·37: The Temperature - Vapour Pressure Curves for a Number of Materials used in the Manufacture of EDL's.

is given by[7]

$$l = 1/(\pi N \sigma^2 \sqrt{2}), \qquad 5.12$$

where σ is the diameter of the colliding species. For lead, $\sigma = 0.35$nm so that $l \simeq 15\mu$m. This figure represents probably the lowest value of the mean-free-path because the vapour pressure is almost certainly less than 10torr. For the purpose of comparison, the mean-free-path of argon atoms at atmospheric pressure and at 800K has been calculated to be ca. 0.11μm. It may be observed that the latter value is approximately two orders of magnitude smaller than the value estimated for lead in an EDL. Because the distribution of argon in an EDL at atmospheric pressure would be expected to be homogeneous it is also reasonable to suppose that the distribution of lead atoms in the vapour phase in a lead EDL would be homogeneous by comparison of the values of the mean-free-paths.

The results suggest that the vapour pressure of the material in the vapour phase inside the EDL is a function of the temperature of the air stream flowing over the EDL, and that the material vapourized distributes itself homogeneously inside the discharge. The problem remains of explaining the maximum of intensity emitted from near the edge of the discharge.

As the results suggest that the extent of self-absorption is low in the centre of the EDL the most probable reason for the lack of emission from the central region is that atoms in excited states are being ionized,

thus reducing the effective population of neutrals. Such a situation would be characterized by a gradient in the excitation temperature,with a high value in the centre and a relatively low value near the edge of the lamp. The excitation temperatures measured at operating temperatures of 300°C and 350°C (Figures 5.33 and 5.34) exhibit this effect. At these two temperatures there is a reduction in the excitation temperature of between 1000K and 2000K in moving from the centre of the EDL to the edge.

There is other evidence to suggest that the upper energy levels,from which the observed radiative transitions occur,have been depopulated in the central region of the EDL by ionization. Measurements made of the radial distribution of intensity of manganese I lines and manganese II lines in a manganese EDL have indicated (Figure 5.20) that the maximum of intensity for the manganese II lines occurs between 0.5mm and 1mm closer to the centre of the EDL than the maximum of intensity of the manganese I lines. The energy levels for some of the manganese transitions are given in Table 5.4.

The excitation energies of the ion lines are interspersed with those of the atom lines which may account for the relatively small difference in the radial position at which the two maxima of intensity occur. The ion lines of manganese also show the skin effect and it is not easy to account for the reduction in the intensity of the ion lines in the centre of the lamp. The ionization energy of the process $Mn^{+} \rightarrow Mn^{2+}$

is 15.64eV,which is comparable with the first ionization energy of argon. Whilst this relatively high ionization energy does not mean that depopulation of Mn^{+} by the formation of Mn^{2+} is ruled out, significant depopulation by this means is unlikely because a skin discharge is not obtained with mercury,which has a first ionization energy of 10.43eV. A more plausible explanation is that depopulation occurs by excitation to higher energy levels rather than by ionization. It is noticeable in Figure 5.20 that the intensity emitted in the centre of the EDL is not such a small fraction of the maximum intensity for the ion lines compared with the atom lines. This indicates that the depopulation occurring is less severe for the ion lines than for the atom lines.

TABLE 5.4: The Transition Energies for the Manganese Lines Given in Figure 5.20.

WAVELENGTH (nm)	SPECTRUM	TRANSITION (cm^{-1})	ENERGY OF TRANSITION (eV)
257.610	II	0-38807	4.811
279.842	I	0-35770	4.435
294.920	II	9473-43370	4.203
380.672	I	17052-43314	3.256
403.076	I	0-24802	3.075

Mn I ionization energy = 7.432eV ≡ 59960cm

Mn II ionization energy =15.64eV ≡ 126147cm

Further evidence for depopulation occurring in the centre of the EDL by excitation and/or ionization is the comparison of the first ionization energies for those elements which do,and for those elements which do not show the type B discharge. A list of the elements studied is given in Table 5.5,together with their first ionization energies. It is clear that,of all the elements studied, all those showing the type B discharge have a first ionization energy less than ca. 9.4eV,whereas,all those showing a type A discharge have a first ionization energy greater than or equal to 9.75eV. The logical conclusion is that there is insufficient energy available to ionize and cause significant depopulation of atom levels of elements having an ionization energy greater than or equal to 9.75eV.

5.6.5 The Type A discharge.

The type A distributions of intensity show a maximum of intensity in the centre of the EDL which decreases towards the edge of the lamp. This information is characteristic of a gradient in the amount of energy available for excitation as previously described for the type B discharge. Presumably, the energy available in the centre of the lamp is not enough to depopulate the upper levels of the observed transitions sufficiently to have an appreciable effect upon the intensity.

The results of the hyperfine intensity ratio measurements for mercury,shown in Figure 5.31,are worthy of some mention here. These measurements were made on the

TABLE 5.5: The Relationship Between the Type of Discharge and the First Ionization Energy for the Elements Studied.

ELEMENT	TYPE OF DISCHARGE	1st. IONIZATION ENERGY (eV)
Argon	A	15.755
Mercury	A	10.43
Arsenic	A	9.81
Selenium	A	9.75
Zinc	B	9.391
Cadmium	B	8.99
Antimony	B	8.64
Germanium	B	7.88
Manganese	B	7.43
Lead	B	7.42
Tin	B	7.34
Thallium	B	6.106
Gallium	B	6.0
Indium	B	5.785

404.6nm line,which is not a ground state transition, because this was the only wavelength suitable for making measurements using the interferometer. A partial Grotrian diagram for Hg I is given in Figure 5.38. The 404.656nm transition ($^3P_0$-$^3S_1$) ends in the $^3P_0$ term, which is metastable. The $^3P_0$ term is also populated radiatively by transitions from the $^3D_1$ and $^3S_1$ terms so a substantial population of the $^3P_0$ term would be expected. The hyperfine intensity ratio measurements show essentially

the relative population of the $^3P_0$ term at different radial positions. The measurements show that there is a substantial population of species excited at 4.667eV.

It is important to realize that the hyperfine intensity measurements do not show that there is a substantial population of ground state atoms in the centre of the discharge,a theory which would have been in conflict with the model of a gradient in the excitation temperature.

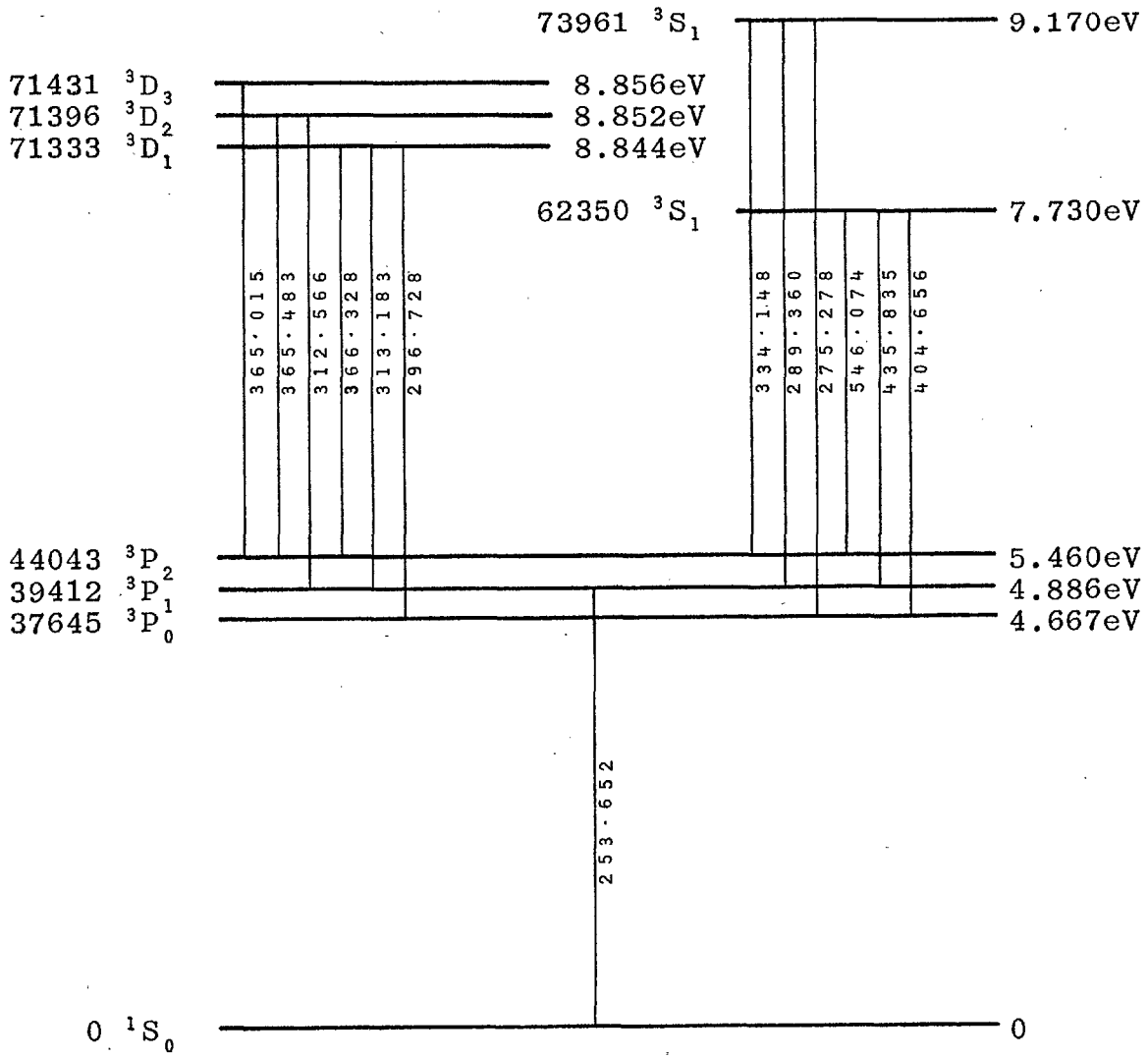


Figure 5.38: Partial Grotrian Diagram for Hg I.[150]
(The numbers beside the transitions are wavelengths in nm)

The transition between the type B distribution of intensity for the indium EDL operated at 300°C and 350°C, and the type A distribution when the EDL was operated at 400°C requires some explanation. Although measurements of the hyperfine intensity ratios were not possible at 400°C because of self-absorption, the trend observed is that the extent of self-absorption taking place increases with the air stream temperature. Also, because of the dependence of the vapour pressure on the temperature, the vapour pressure inside the EDL at 400°C would be expected to be greater than at lower temperatures, provided there is still excess material remaining on the walls of the lamp. Additionally, the variation of the excitation temperature with radial position is very much less at 400°C than at lower operating temperatures.

This evidence leads to the conclusion that some form of collisional process is causing less energy to be available for excitation and/or ionization in the centre of the discharge, thus reducing the previous depletion of of population of the high energy levels of observed transitions.

CHAPTER SIX

THE MEASUREMENT OF THE STRONTIUM LINE HALF-WIDTH IN THE RADIO-FREQUENCY PLASMA.

6.1 Introduction 176

6.2 Apparatus 177
6.2.1 Plasma Instrumentation 177
6.2.2 The Optical Arrangement 179

6.3 The Hyperfine Structure of the 407.771nm Sr II Line 181

6.4 Results 183
6.4.1 Calibration Curves for Strontium 183
6.4.2 Line Profile Measurements Made with Lateral Resolution 184
6.4.3 Line Profile Measurements Made with Vertical Resolution 188
6.4.4 Measurement of the Doppler Temperature at Different Viewing Heights 189

6.5 Discussion 195

6.1 INTRODUCTION.

The inductively coupled plasma (ICP) has become increasingly popular recently as a source for optical emission spectroscopy. Its use as a source has many advantages over other sources,such as DC-arcs,AC-sparks and flames. In particular,the ICP source has a high temperature,gives good limits of detection and above average precision compared with alternative optical emission sources. Many of the chemical interferences encountered in flames are not found in the ICP,where free-radicals and other chemically reactive species are not present. Calibration curves are normally linear over several orders of magnitude above the limit of detection making the ICP source particularly useful in simultaneous multi-element analysis,where many elements in widely differing concentrations are encountered.

There are two major reasons for the study of atomic line profiles being important. Firstly,the analytical chemist is interested in establishing the operating conditions which are most beneficial in obtaining good limits of detection,accuracy and precision. Secondly, line profiles may be used to characterize phenomena taking place in the ICP source with the intention of obtaining information about the excitation processes occurring.

In this Chapter the studies made of the profile of the 407.771nm strontium II line,emitted by an ICP source,are described.

6.2 APPARATUS.

6.2.1 Plasma Instrumentation.

The torch used to support the plasma was of a demountable design described previously,[156,160] and it is shown schematically in Figure 6.1. The torch consisted of three concentric fused silica tubes,18mm i.d., 16mm o.d., and 6mm o.d., mounted in a brass base using epoxy resin. Argon gas was supplied to a tangential coolant inlet at 12.8$dm^3min^{-1}$and to the injector tube at 0.86dm^3min^{-1}. The so-called plasma gas inlet was not used except for flushing air from the torch before initiating the plasma. The torch was mounted in a work coil of internal diameter 26mm, consisting of 1½ turns of 6mm o.d. copper tubing. The work coil was fitted with water cooling and was connected directly to a capacitor matching network. Radio-frequency power was supplied to the matching network by a 2kW crystal-controlled radio-frequency generator,operating at 27.12MHz.(International Plasma Corp. Model 120-27.) The output power was continuously variable up to 2kW. In these studies a net RF power of 1.2kW was used.

A concentric glass pneumatic nebulizer (Meinhard type T230A2) and spray chamber was used for sample introduction with an argon flow rate of 0.86dm^3min^{-1} at 30p.s.i. This resulted in a sample uptake rate of 0.94 cm^3min^{-1}using an 8cm head. The nebulization efficiency was 2.2%(±0.1).

A high frequency Tesla coil was used to initiate

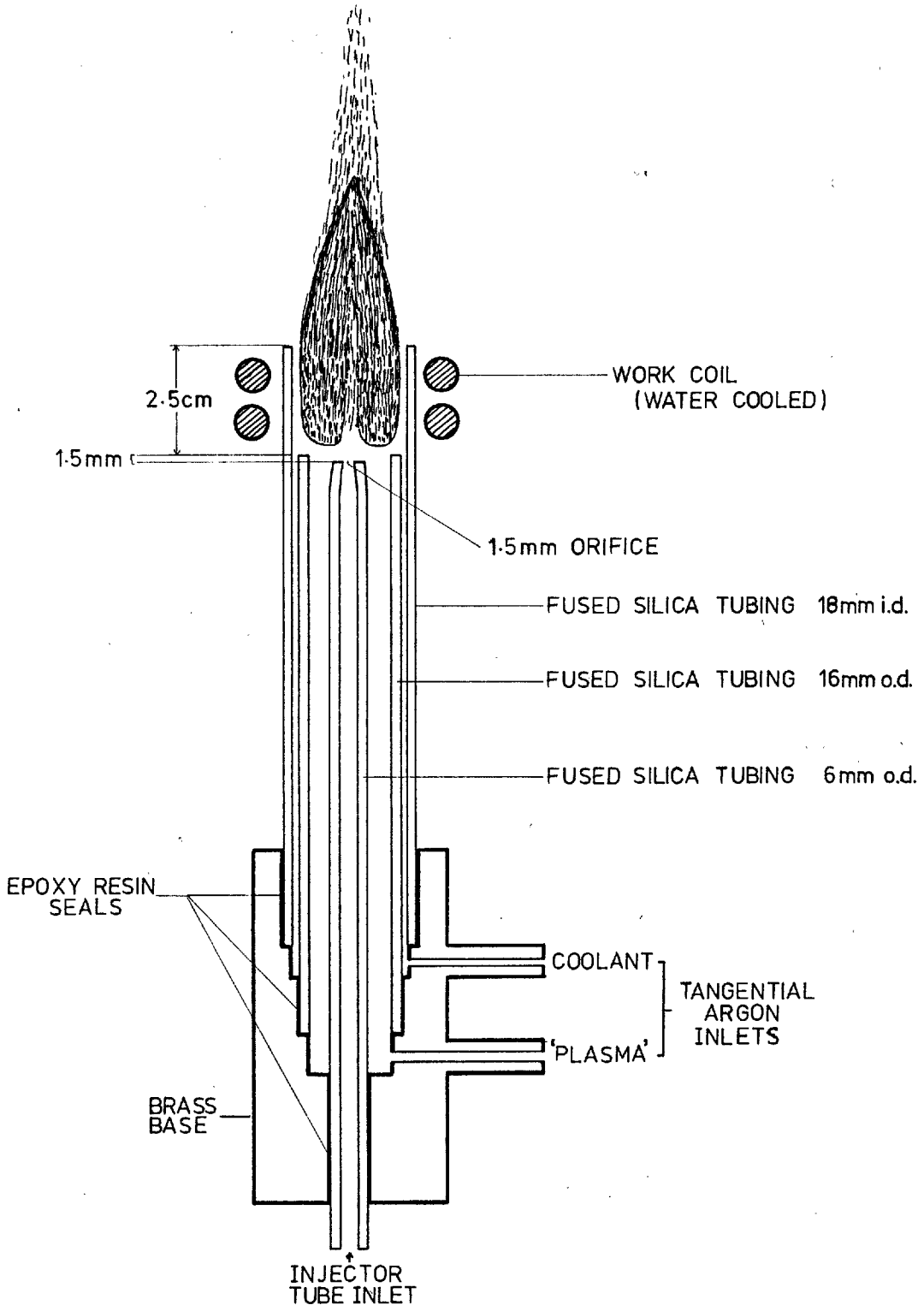


FIGURE 6·1: The Demountable Plasma Torch.

the plasma discharge.

6.2.2 The Optical Arrangement.

As a result of the limited space available it was not possible to mount the plasma torch at the source end of the optical bar of the interferometer assembly. A series of mirrors was used to collect the radiation emitted by the ICP and focus the radiation onto the secondary source aperture in the interferometer assembly. A diagram of the optical arrangement is shown in Figure 6.2. Radiation from the ICP was collected by a concave mirror,M1,having a diameter of 15.24cm and a focal length of 106.68cm. The concave mirror was used in a Newtonian reflecting telescope configuration with a plane mirror,M2. Light from mirror M2 was reflected by an additional mirror,M3,to a focal plane,F. A 5cm focal length lens was used to focus the image in the focal plane,F,onto the plane of the secondary source pinhole. The mirror positions were chosen so that the focal plane,F,of the concave mirror was just infront of M3 in order to avoid the effects of dust on mirror surfaces. In order to allow for the alignment of the interferometer it was possible to move lens L1 to the position A in Figure 6.2. A removable mirror,M4, was placed on the optical bar to reflect the light emitted by a hollow cathode lamp during the alignment procedure.

The optical system produced an approximately 1:1 image of the plasma in the plane of the secondary source aperture.

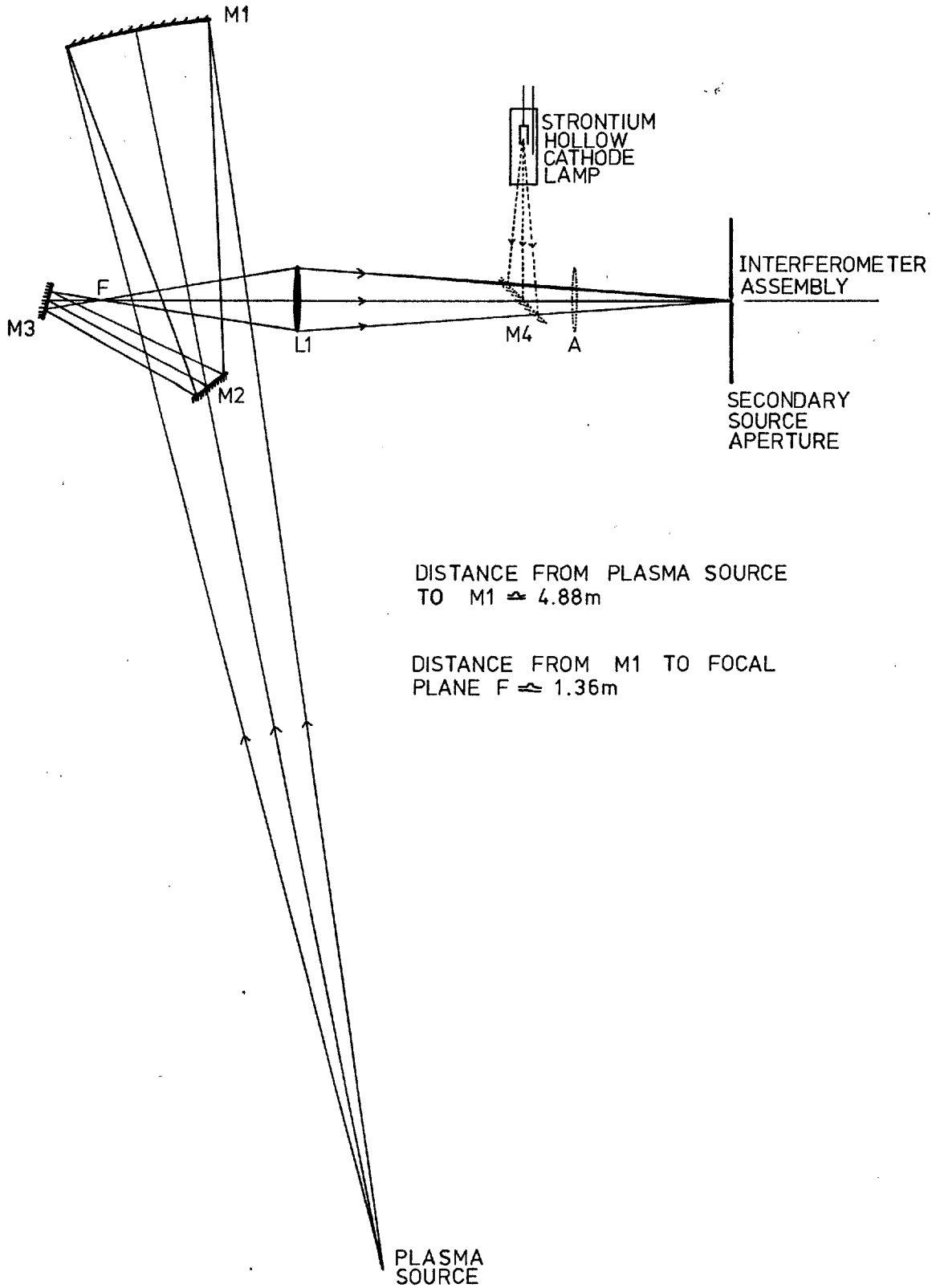


FIGURE 6.2 : The Optical Arrangement used to Interface the Plasma Source to the Interferometer.

The mirror M3 was mounted on a rotating stage so that the position of the image of the plasma could be moved horizontally in the plane of the secondary source aperture in order to facilitate lateral scanning of the source. The scanning arrangement is shown schematically in Figure 6.3. A micrometer screw was used to control the rotation of mirror M3.

The viewing height in the plasma was adjusted by means of the adjustable mount,upon which the capacitive coupling network and torch were mounted. The viewing height was specified by measuring the distance between the point in the plasma coincident with the secondary source aperture and the top of the load coil.

6.3 THE HYPERFINE STRUCTURE OF THE 407.771nm Sr II LINE.

Naturally occurring strontium contains four major isotopes with abundancies: ^{84}Sr 0.56%, ^{86}Sr 9.9%, ^{87}Sr 7.0% and ^{88}Sr 82.6%. Being isotopes with even mass numbers, ^{84}Sr, ^{86}Sr and ^{88}Sr do not show any nuclear hyperfine structure. The hyperfine structure and isotopic shifts for the 407.771nm Sr II line have been studied by Zhiglinskii and Kund.[157] There is a negligible shift in wavelength between the ^{84}Sr, ^{86}Sr and ^{88}Sr components but the ^{87}Sr isotope has two hyperfine components,shown in Figure 6.4 It is the lower level of the transition ($^2S_{\frac{1}{2}}$) which is split by the nuclear spin effect of the ^{87}Sr isotope (I=9/2). Although the $^2P_{\frac{3}{2}}$ term is also split,the magnitude of this splitting is negligible.

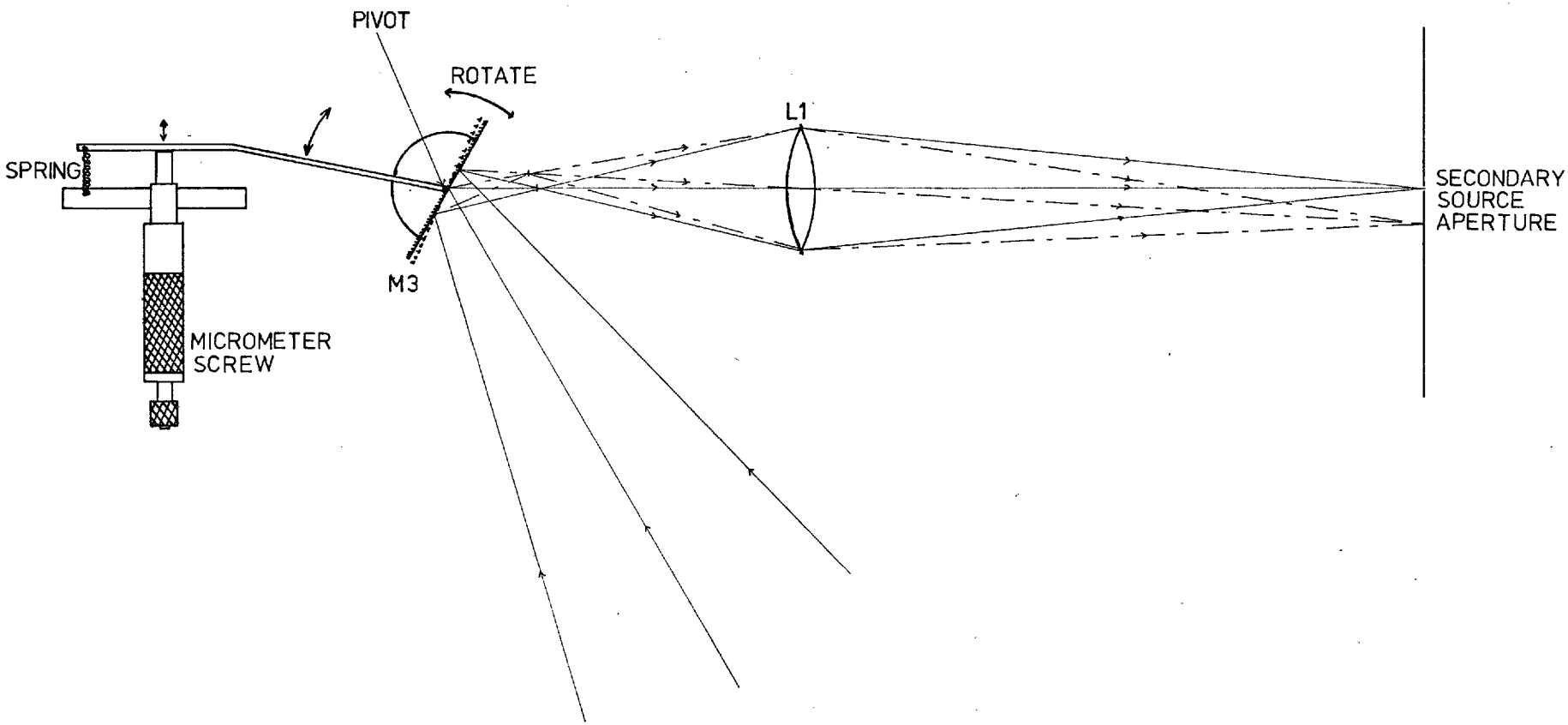


FIGURE 6.3: Details of the System used to Perform Lateral Scanning of the Plasma Source.

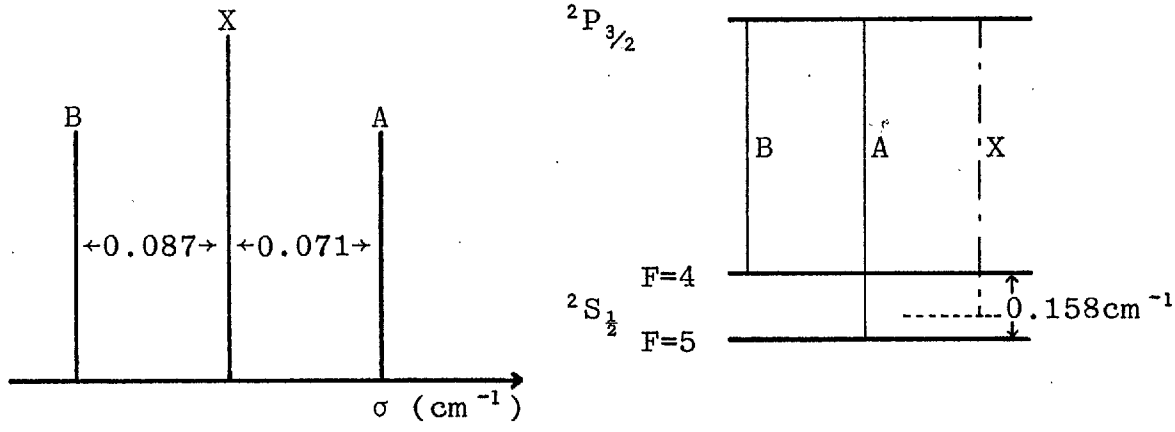


Figure 6.4: The Hyperfine Structure of the 407.771nm Sr II Line.[157,158]

Strontium was chosen as the element to study, firstly, because it has a strong emission line at 407.771nm, inside the working spectral range of the interferometer, and, secondly, because the natural abundance of ^{88}Sr was found to be sufficiently large to make the spectral contributions from the other strontium isotopes negligible. The absence of any hyperfine structure in the ^{88}Sr emission was also necessary in order to make line profile measurements.

6.4 RESULTS.

6.4.1 Calibration Curves for Strontium.

Calibration curves for strontium were constructed by making measurements of the intensity of the 407.771nm Sr II line for solution concentrations of 1,5,10,50,100, 500 and 1000μgcm^{-3}. These measurements were made at a

number of different viewing heights in the plasma,measured in mm above the top of the load coil. The results of these measurements are plotted as log(intensity) against concentration in Figure 6.5.

It was observed that the calibration curves began to be non-linear at all viewing heights for solution concentrations greater than 50μgcm^{-3} strontium.

A similar procedure was adopted for the measurements made at the 460.7nm Sr I line and these results are shown in Figure 6.6.

The intensity measurements shown in Figures 6.5 and 6.6 were made by focusing a 1:1 image of the plasma onto the entrance slit of a Monospek one metre monochromator, fitted with an EMI 6256B photomultiplier tube. These measurements were made without lateral resolution.

6.4.2 Line Profile Measurements Made With Lateral Resolution.

Line profile measurements of the 407.771nm Sr II line were made at various lateral positions and at a number of viewing heights in the plasma. The following operating parameters were employed:

Interferometer plate separation	= 7.747nm
Free-spectral-range	= 0.6454cm^{-1}
RF power	= 1200W
Signal Averager sweep time	= 0.1s.

The remaining parameters were given in Section 6.2.

The results of the measurements made at a viewing height of 10mm above the top of the load coil are shown in Figure 6.7. The points plotted in Figure 6.7 are the

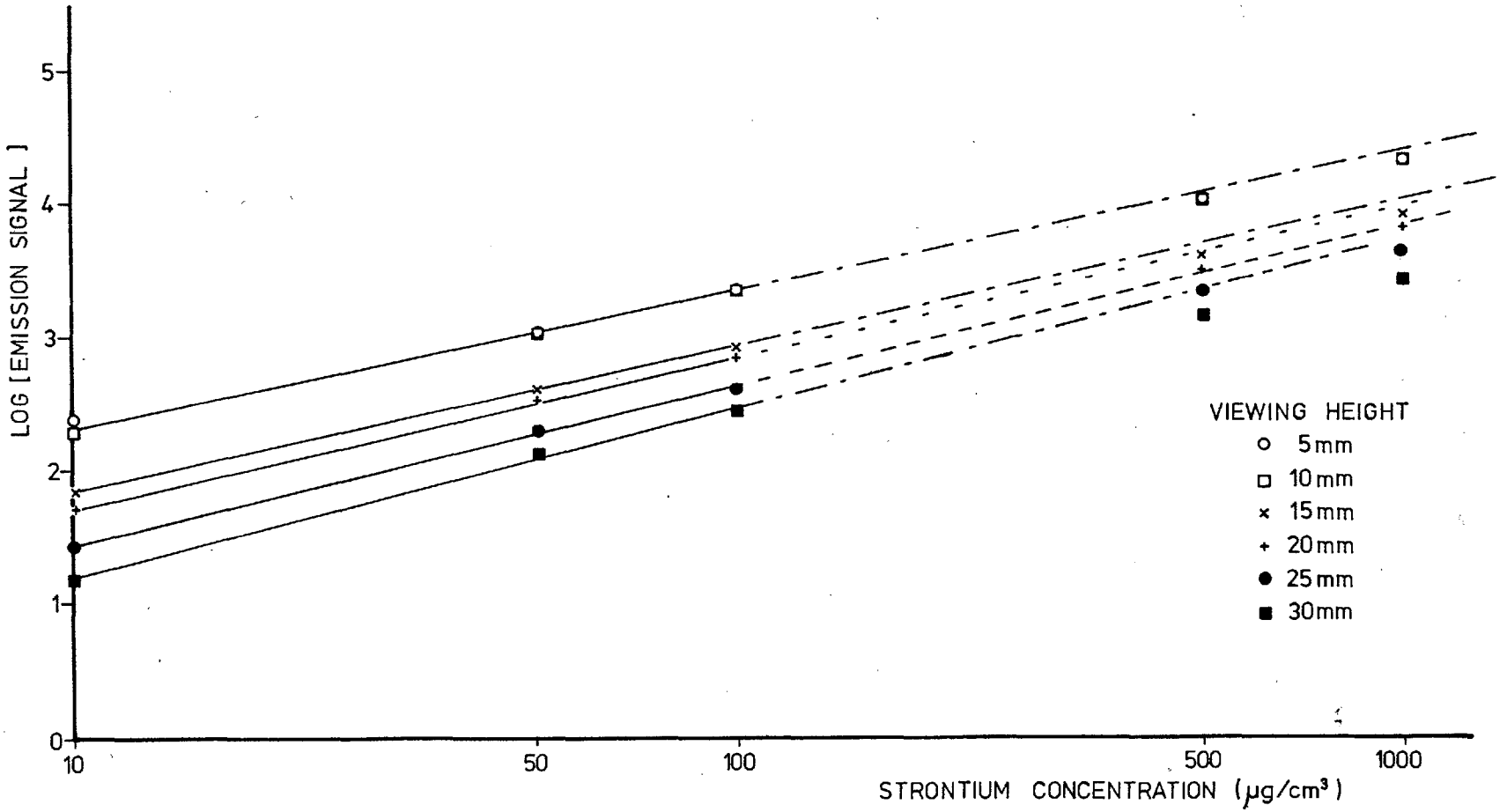


FIGURE 6-5: Calibration Graphs for Strontium Measured at Different Viewing Heights in the Plasma. Wavelength = Sr II 407·771nm.

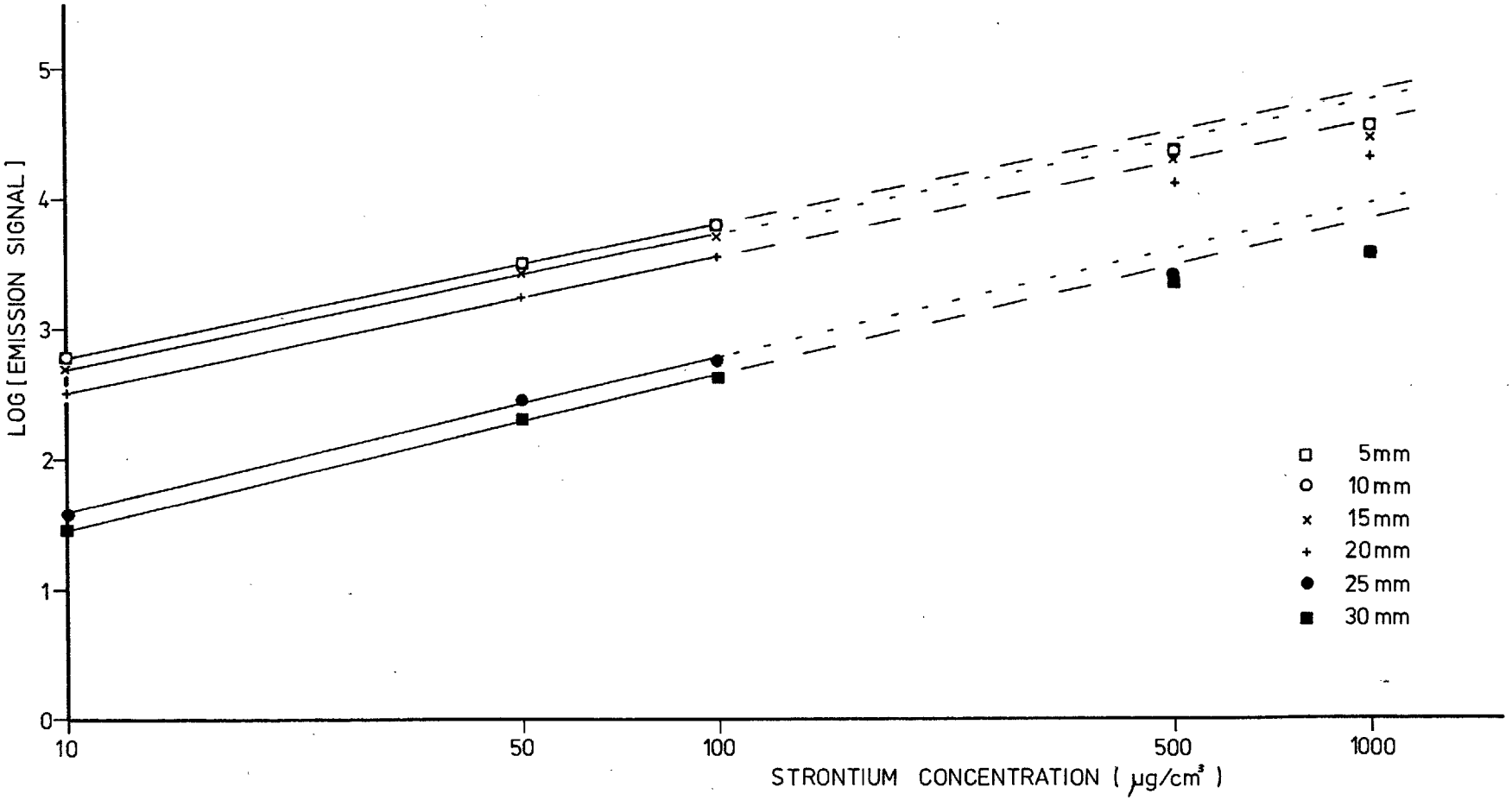


FIGURE 6·6: Calibration Graphs for Strontium Measured at Different Viewing Heights in the Plasma. Wavelength = Sr I 460·7nm.

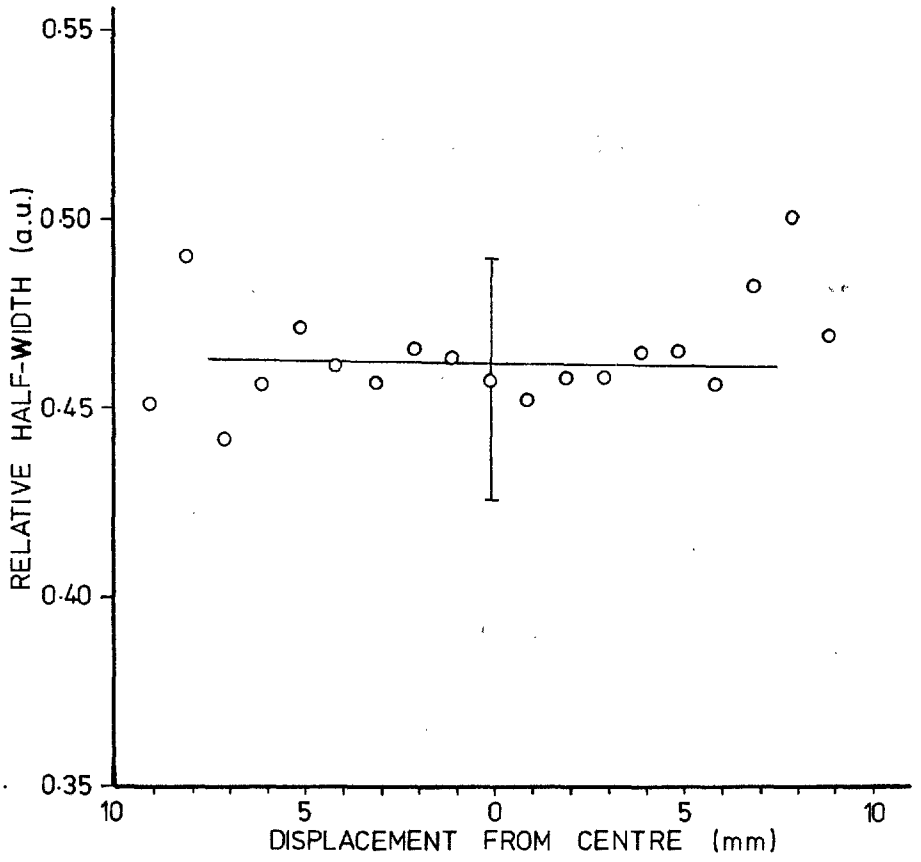


FIGURE 6·7: Line Profile Measurements Made at Different Lateral Positions in the Plasma. Viewing Height = 10mm ,Wavelength = Sr II 407·771nm. Solution Concentration = 100μg/cm^3.

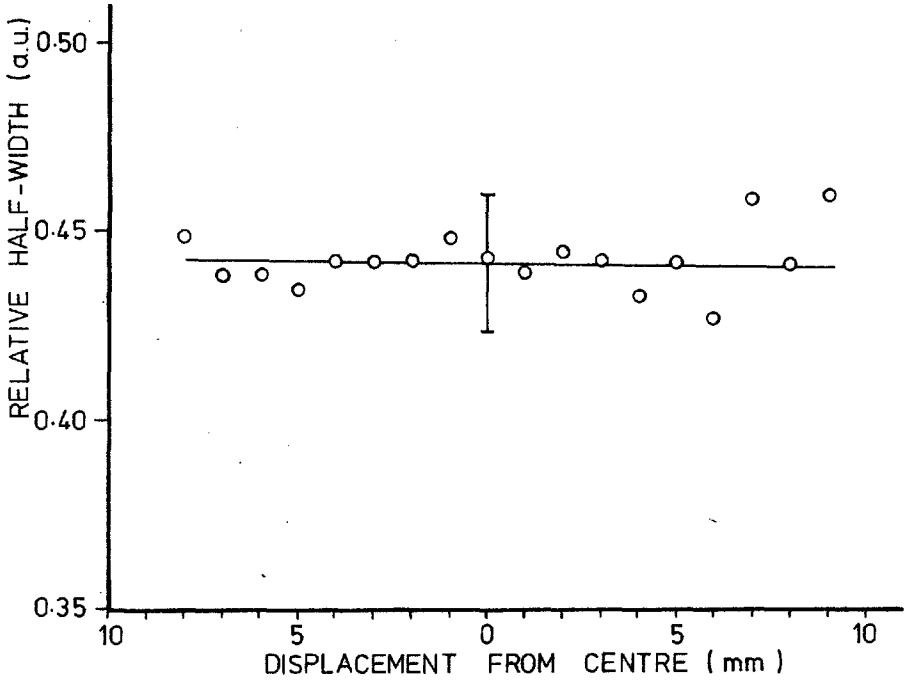


FIGURE 6·8: Line Profile Measurements Made at Different Lateral Positions in the Plasma. Viewing Height = 15mm ,Wavelength = Sr II 407·771nm. Solution Concentration = 100μg/cm^3.

average of six measurements.

Measurements were also made at viewing heights of 15mm and 25mm. The results of the measurements made at 15mm are given in Figure 6.8.

It may be observed in Figures 6.7 and 6.8 that it was not possible to measure any significant change in the line profile with the lateral position in the plasma.

The values of the half-width in Figures 6.7 and 6.8 represent the measured half-widths without correction for the instrumental function being made. As the instrumental half-width is a constant for all the measurements made, it was not necessary to correct for the instrumental function before the possibility of making measurements with lateral resolution was assessed. Measurement of the finesse at 25.5 gave an instrumental half-width of $(1/25.5)\times 0.6454 = 0.025 cm^{-1}$.

The errors in the measurements made at a viewing height of 15mm were found to be smaller than at viewing heights of 10mm and 25mm. The relatively large standard deviations in the data appeared to be due to noise originating in the plasma source itself. The measurements made at a viewing height of 10mm were noisy largely as the result of the high background emission present in the plasma. At greater viewing heights the noise appeared to be caused by the slight random motion in the positional stability of the plasma.

6.4.3 Line Profile Measurements Made With Vertical Resolution.

Measurements of the half-width of the 407.771nm Sr II

line were made at various viewing heights in the central position in the plasma. These measurements were made while nebulizing 10,50,100,500 and 1000μgcm^{-3} solutions of strontium. An interferometer plate separation of 8.1915mm was used, giving a free-spectral-range of 0.6104cm^{-1}. The instrumental half-width was calculated to be (1/25.5)×0.6104 =0.024cm^{-1}. The results of the measurements are shown in Figures 6.9 and 6.10 as line half-width plotted against concentration.

In the case of the introduction of the 1000μgcm^{-3} strontium solution, with the exception of the anomalous behaviour at a viewing height of 25mm, the greatest half-width is observed at 5mm above the load coil and the smallest half-width is observed at 35mm above the load coil, their being a decrease in line half-width with an increase in the viewing height.

When a 10μgcm^{-3} strontium solution was introduced into the plasma the effect of varying the viewing height was different to the case described previously. With the exception of the measurements made at 30mm above the load coil, the observed half-width of the strontium 407.771nm line was observed to increase with the viewing height, in the range 5mm to 25mm.

6.4.4 Measurement of the Doppler Temperature at Different Viewing Heights.

In Chapter 2 the relationship between the Doppler broadened line profile and the gas temperature was given by Equation 2.23. Other processes resulting in the

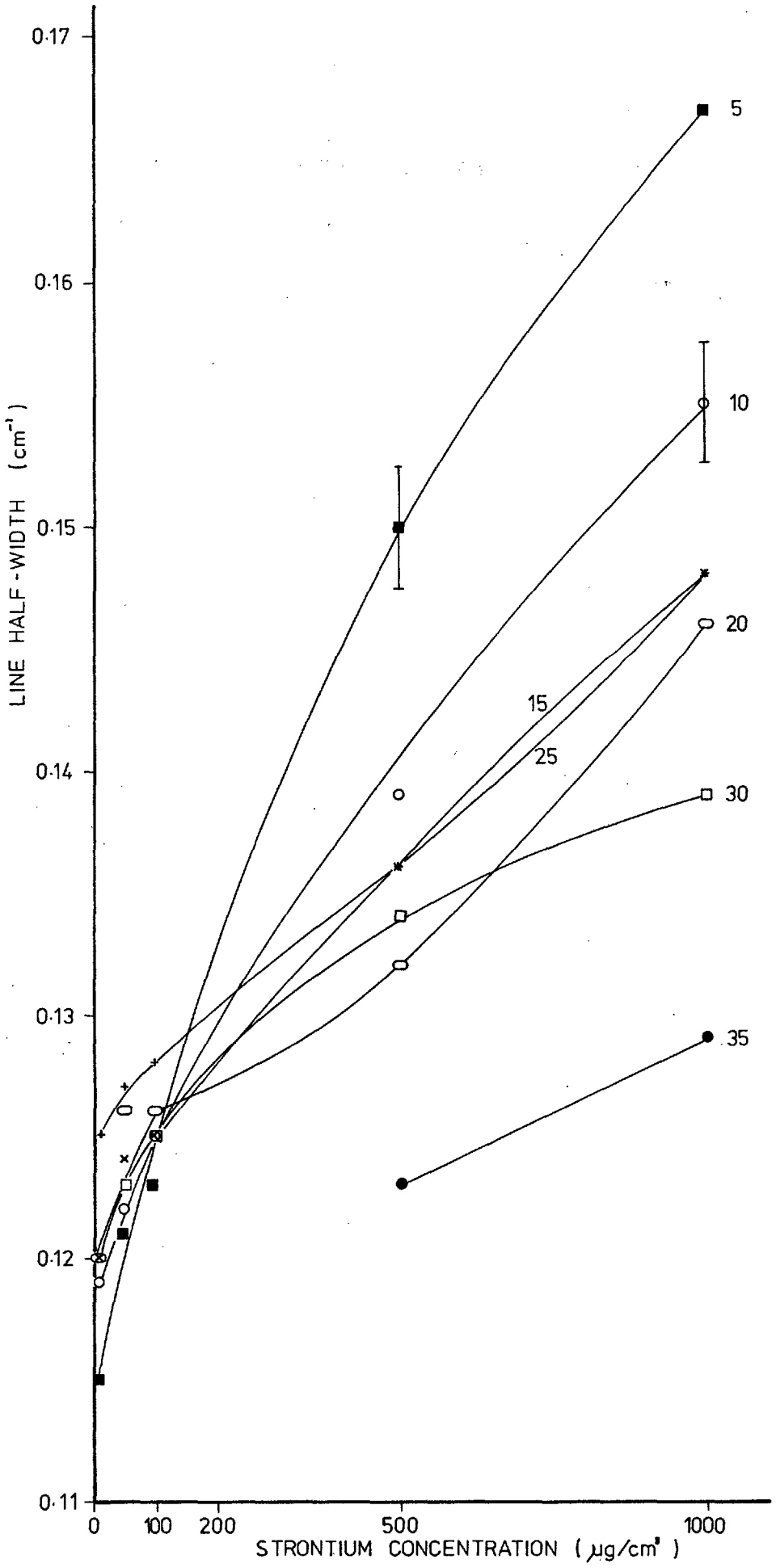


FIGURE 6·9: Height Variation of Line Half-Width vs. Sample Concentration in the Plasma. Wavelength = Sr II 407·771nm. (The numeric values are viewing heights in mm.)

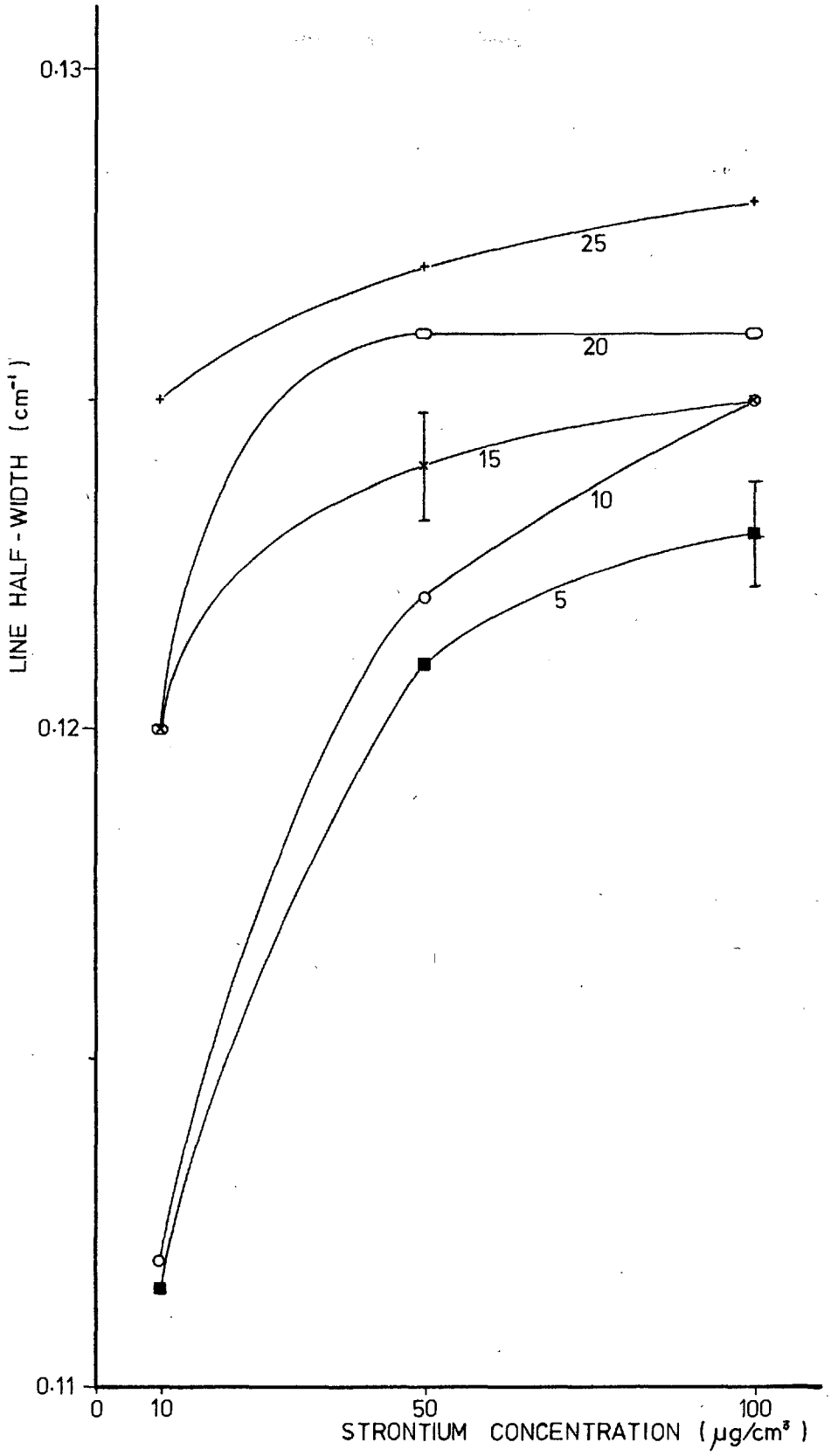


FIGURE 6·10: Enlargement of Figure 6·9 in the Concentration Range 10 - 100 μg/cm³.

broadening of an atomic line were also discussed, together with the techniques for performing deconvolution. The natural half-width of atomic spectral lines has already been shown to be negligible in comparison with measurements of the total line half-width made in the plasma.

The collisional half-width, $\delta\sigma_c$, may be calculated by using Equation 2.25, which has been reproduced here as Equation 6.1:

$$\delta\sigma_c = \rho_0^2 \frac{N}{c} \times \left((8RT/\pi) \times \{1/M_1 + 1/M_2\}\right)^{\frac{1}{2}}. \qquad 6.1$$

A literature value[159] of $50\times10^{-18}cm^2$ has been used for ρ_0^2. N, the number density of colliding species may be calculated to be

$$N = \frac{LP}{RT} \text{ (ideal gas equation)} = \frac{6.023\times10^{23}\times101325}{8.3143\times5000} = 1.47\times10^{24}m^{-3}.$$

This calculation has been performed assuming a temperature of ca. 5000K and the argon to be at atmospheric pressure ($101325Nm^{-2}$.) The values of M_1 and M_2 used in Equation 6.1 are worthy of some mention. If S.I. units are used, M_1 and M_2 are the masses of one mole of atoms in kilograms. Using the following values in Equation 6.1 the collisional half-width has been calculated.

Number density	N	$1.47\times10^{24}m^{-3}$
Squared cross-section	ρ_0^2	$50\times10^{-22}m^2$
Velocity of light	c	$2.998\times10^{8}ms^{-1}$
Gas constant	R	$8.3143JK^{-1}mol^{-1}$
Temperature	T	5000K
Atomic weight Ar	M_1	$39.948\times10^{-3}Kgmol^{-1}$
Atomic weight Sr	M_2	$87.62\times10^{-3}Kgmol^{-1}$

$$\delta\sigma_c = 4.8\times10^{-2}m^{-1} = 4.8\times10^{-4}cm^{-1}.$$

According to this calculation the collisional half-width contribution to the total half-width was found to be negligible. The free-spectral-range of the interferometer was $0.6454cm^{-1}$, with a measured finesse of 25, the instrumental half-width was calculated to be $0.026cm^{-1}$. The instrumental half-width was removed from the measured half-width by using the Lorentzian approximation in Equation 2.82.

The results obtained at a number of different viewing heights in the plasma and for a series of solution concentrations are given in Table 6.1.

The calibration curves in Figure 6.6 are linear for concentrations below $50\mu gcm^{-3}$ and significant deviation from linearity does not occur until concentrations greater than $100\mu gcm^{-3}$ are reached. It is reasonable to suppose that the extent of self-absorption is relatively small in magnitude at concentrations of $50\mu gcm^{-3}$ and below. The effect of self-absorption broadening upon the calculated Doppler temperatures is clear for solutions of high concentration, for which large values of Doppler temperature are obtained. The most realistic values of the Doppler temperature are those measured at strontium solution concentrations of $50\mu gcm^{-3}$ and $10\mu gcm^{-3}$.

The errors involved in making these measurements are high for a number of reasons. Firstly, there are significant errors introduced during the measurement of the line profile arising from noise in the source, electronic noise and variations in the parallelism of the interferometer

TABLE 6.1: Doppler Temperatures.

Viewing† Height (mm)	Solution Concentration ($\mu g cm^{-3}$)	Measured Half-Width (cm^{-1})	Corrected§ Half-width (cm^{-1})	Doppler Temperature (K)
5	1000	0.169	0.167	7900 (±450)
5	500	0.152	0.150	6400 (±400)
5	100	0.126	0.123	4300 (±300)
5	50	0.123	0.121	4100 (±300)
5	10	0.118	0.115	3700 (±300)
10	1000	0.157	0.155	6800 (±400)
10	500	0.141	0.139	5500 (±350)
10	100	0.128	0.125	4500 (±300)
10	50	0.125	0.122	4200 (±300)
10	10	0.122	0.119	4000 (±300)
15	1000	0.151	0.148	6300 (±400)
15	500	0.138	0.136	5300 (±350)
15	100	0.128	0.125	4500 (±300)
15	50	0.126	0.124	4300 (±300)
15	10	0.123	0.120	4100 (±300)
20	1000	0.148	0.146	6100 (±400)
20	500	0.135	0.132	5000 (±300)
20	100	0.129	0.126	4500 (±300)
20	50	0.128	0.126	4500 (±300)
20	10	0.122	0.120	4100 (±300)
25	1000	0.150	0.148	6200 (±400)
25	500	0.138	0.136	5300 (±350)
25	100	0.130	0.128	4600 (±300)
25	50	0.130	0.127	4600 (±300)
25	10	0.128	0.125	4500 (±300)
30	1000	0.141	0.139	5500 (±350)
30	500	0.136	0.134	5100 (±350)
30	100	0.128	0.125	4500 (±300)
30	50	0.125	0.123	4300 (±300)
35	1000	0.131	0.129	4700 (±300)
35	500	0.125	0.123	4300 (±300)

§ Corrected half-widths are the observed half-widths corrected for the instrumental contribution.
† The viewing height is measured above the top of the load coil.

plates. Secondly,an error is introduced in performing the deconvolution of the Doppler half-width from the measured half-width of the emission line. The latter error is relatively small in comparison with the other errors

involved. Six measurements were averaged together to produce each value in Table 6.1. It is not valid to consider six points to be an infinitely large population and,therefore,a rigorous statistical analysis of the errors in the data is not realistic. The errors in the results given in Table 6.1 have been estimated.

The results obtained in this work agree to within 400K of the measurements made by Human and Scott[95] at the 421.5nm Sr II line.

6.5 DISCUSSION.

The calibration curves measured at the 407.771nm Sr II line were found to be linear and to have approximately unity slope up to a solution concentration value of 50μgcm^{-3}. However,the divergence from linearity was found to be small until a solution concentration of 100μgcm^{-3}. It is useful to consider the possible reasons for this deviation from linearity in the calibration curves. Nebulization interferences from changes in the solution concentration over the range studied are not likely to be significant. The most likely reason for the onset of non-linearity is the increasing severity of self-absorption taking place as the solution concentration is increased. It is noticeable that the calibration curves measured at the 460.7nm Sr I line show much less deviation from linearity than do the measurements made at the 407.771nm Sr II line. The first ionization energy of strontium is a relatively low value of 5.68eV. Therefore, it might be expected that

the majority of the emitted strontium radiation is from strontium in the first ionized state. Using Equation 2.8, the ratio of the number density of the singly charged ions to that of the neutrals, N_{z+1}/N_z, may be calculated. Using a value of the electron density of $10^{21}m^{-3}$, [110] the value of N_{z+1}/N_z for strontium is ca. 0.12 at an ionization temperature of 4000K, and ca. 3.2 at 5000K. As the majority of the measurements of the excitation and ionization temperatures in the literature[160] have been greater than or equal to 5000K, it is reasonable to suppose that there is a substantial population of Sr^+ and that the population of Sr I levels is relatively small. This condition could account for the smaller extent of self-absorption observed for the Sr I line than for the Sr II line when the same sample concentration was introduced.

Human and Scott[95] made similar calibration curves but for calcium ion and atom lines. The calibration curves for the calcium 422.67nm atom line were observed to be linear until sample concentrations greater than ca. 5000 μgcm^{-3} were introduced. The calibration curves for the calcium 393.37nm ion line were observed to become non-linear when sample concentrations greater than 500μgcm^{-3} were introduced into the plasma. Additionally, measurements made at the calcium 442.5nm atom line, with a lower energy level of 1.6eV, resulted in calibration graphs curving away from the concentration axis at concentrations greater than ca. 1000μgcm^{-3}. It has been postulated that this curvature is caused by changes in the electron

temperature and electron density brought about as the result of the introduction of relatively easily ionized species into the plasma. The above authors[95] suggested that the relative linearity of the calibration curves measured at the 422.67nm Ca I line was the result of the combination of the opposing effects of ionization interference,tending to bend curves away from the concentration axis, and self-absorption,tending to bend curves towards the concentration axis.It is possibly more realistic to postulate that the 422.67nm Ca I line is less sensitive than the 442.5nm Ca I line at the temperatures involved in the plasma. Consequently,the concentration value at which self-absorption begins to cause bending of the calibration curve would be expected to be lower for the 442.5nm line compared with the 422.67nm line. This is because the 442.5nm line has a lower energy level which is 1.6eV above the lower energy level (ground state) of the 422.67nm line. Therefore, at a high temperature,the ground state might be expected to be depopulated to the greatest extent.

The noise encountered while making line profile measurements in different lateral positions appeared to be caused by movement of the plasma in the plasma torch resulting in an effect similar to flicker. Whilst such an effect is less noticeable when a relatively large portion of the plasma is being viewed, the signal-to-noise ratio becomes degraded severely when a small viewing window is used. Kornblum and de Galan[81] commented upon

the observed asymmetry in lateral distributions of intensity. They found that the asymmetry in the distribution of intensity could be attributed to asymmetry in the torch, and that symmetrical distributions could be re-established by the use of adjustment screws in a demountable torch assembly. The same authors have also suggested that it is advisable to grind the inner surface of the coolant tube in order to form as perfect a cylinder as possible.

The results of the line profile measurements given in Figure 6.10 show the occurrence of a maximum line half-width at a viewing height of 25mm and a minimum line half-width at a viewing height of 5mm above the load coil. The extent of self-absorption taking place when sample concentrations of 50$\mu g cm^{-3}$ and below were introduced has been shown to be small. Therefore, it is reasonable to suppose that the major contribution to the line width is the result of Doppler broadening taking place.

The introduction of the sample into the plasma by means of the injector gas flow and the consequent formation of the annulus shaped plasma has been discussed already in Chapter 1.

Where the injector gas,containing the sample aerosol, enters the centre of the plasma annulus there has been shown to exist a considerable gradient in the excitation temperature between the argon in the annulus and the injector gas stream.[160] As the sample passes up through

the plasma mixing of the relatively cool injector gas and the outer stream of argon takes place. The measurements shown in Figure 6.10 fit in with this idea, the strontium 407.771nm line having a relatively small half-width, consequently a low Doppler temperature, at a viewing height of 5mm, rising to a maximum half-width at a viewing height of 25mm. Above 25mm in the plasma the cooling effect of the surroundings would be expected to reduce the half-width as the viewing height is increased.

The reason for the change at high sample concentrations to the maximum line half-width being observed at 5mm and the minimum line half-width being observed at 35mm is not entirely clear. From Figure 6.6, the maximum of emitted intensity occurs at ca. 10mm above the load coil, but the intensity at 5mm is not very different from the value observed at 10mm. The most probable reason for the large value of the line half-width observed at 5mm for large sample concentrations is a large amount of self-absorption taking place. A large radial temperature gradient existing at 5mm would explain the formation of a large number of excited strontium ions, resulting in a high line intensity, and the formation of a large number of ground state strontium ions, resulting in a large amount of self-absorption taking place. It is not clear, however, how much of the self-absorption might be caused by some of the sample aerosol failing to penetrate the plasma and passing along the inner surface of the coolant tube.

Human and Scott[95] suggested that two different models could be used to explain the effects taking place in the plasma. At observation heights lower than 15mm they used a three-layer model, consisting of a central core, being a predominantly absorbing region, with emission originating from an annulus around the core. Above 20mm in the plasma they used a two-layer model with a central emitting region, surrounded by a layer of absorbing species.

It is notable that despite the postulated temperature gradients self-reversal of the line profiles was not observed at any position in the plasma for the solution concentration range studied.

Clearly, if there is a central channel at a viewing height of 5mm which disappears by the time 30mm is reached, there must be a transition zone. In Figure 6.11, which is a plot of line half-width against viewing height for a 1000μgcm^{-3} strontium solution, there is an inflexion between the viewing heights of 15mm and 25mm which may be indicative of the transition taking place.

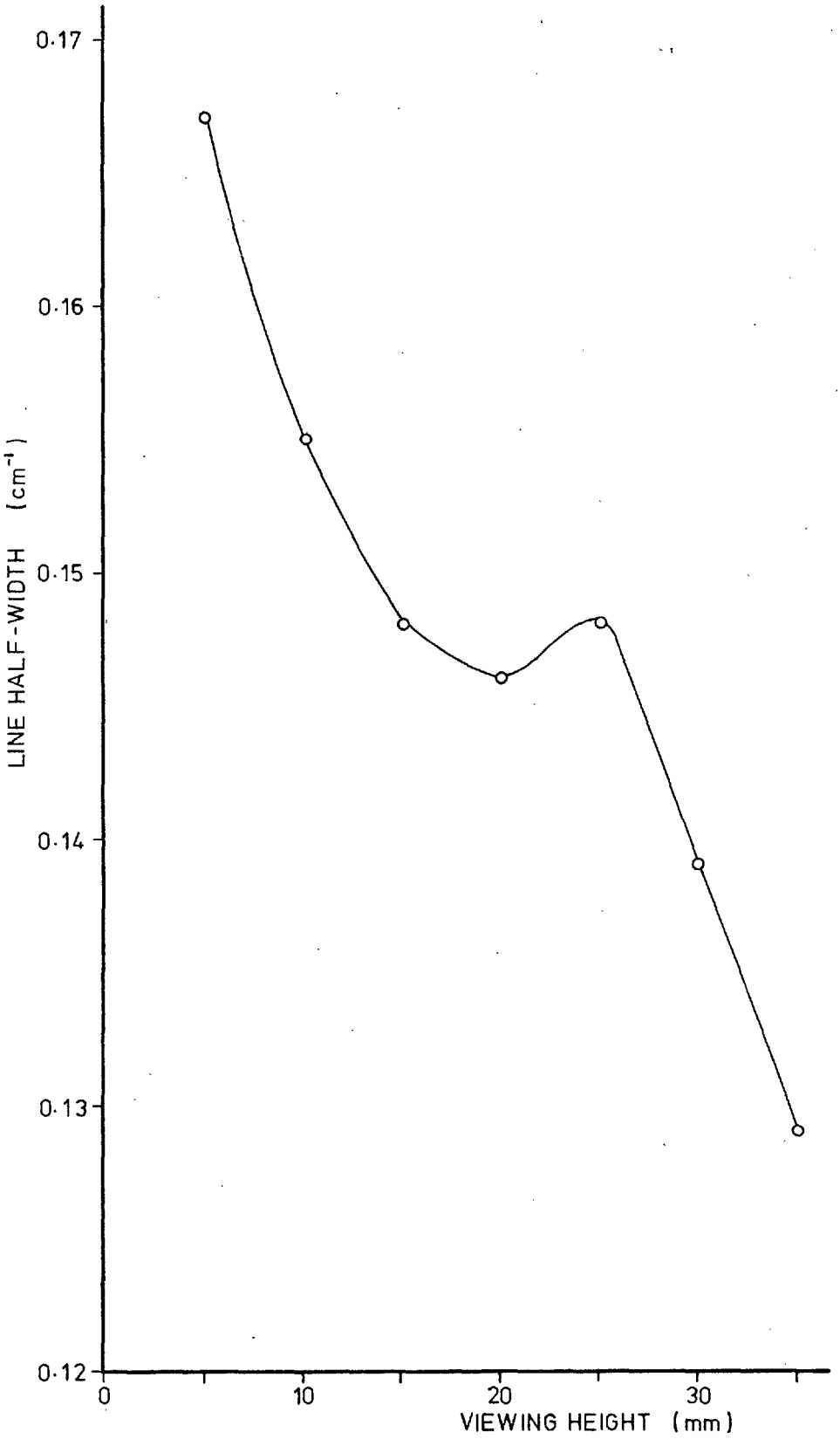


FIGURE 6·11: The Variation of Line Half-Width with Viewing Height for a Sample Concentration of 1000 $\mu g/cm^3$. Wavelength = Sr II 407·771nm.

CHAPTER SEVEN

THE TRANSFORMATION OF LATERAL TO RADIAL DISTRIBUTIONS OF INTENSITY.

7.1 Introduction 203

7.2 The Abel Integral 204

7.3 Curve Fitting Techniques 207

7.4 The Integration Procedure 212

7.5 A Computer Program to Perform the Inverse Abel Transform 213

7.6 Obtaining Radial Information in the Absence of Symmetry 215

7.1 INTRODUCTION.

On viewing a spectroscopic source using a spectrometer the source appears to be purely two-dimensional. It is possible to alter the position viewed by moving the source relative to the spectrometer, as indicated schematically in Figure 7.1, in a manner which will subsequently be referred to as lateral motion. The lateral motion effectively scans the entrance slit of the spectrometer over the plane of the source. The information produced by the scanning motion simply gives the variation of the source intensity over the plane. If the source is not a two-dimensional plane then the information acquired by the spectrometer must be modified or decoded in terms of the mathematical model of the source.

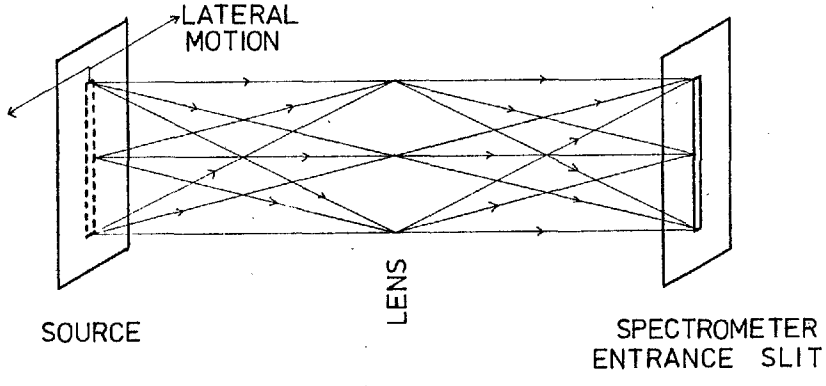


FIGURE 7.1: Lateral Scanning.

In the general case it is necessary to make a number of lateral scans viewing the source from different directions in order to obtain enough information about

the spatial distribution of intensity from within the source. A useful approximation,which is applicable to the majority of laboratory spectroscopic sources, is that the source has circular symmetry. For the case of circular symmetry of the source the lateral distribution of intensity observed by the spectrometer is described by an Abel integral expression in terms of the radial distribution of intensity.

7.2 THE ABEL INTEGRAL.

Consider a spectrometer which only accepts energy emanating from a narrow slice through the source as shown in Figure 7.2. If the slice is of width δx then it may be considered to be formed by sweeping a small volume element, $\delta x \delta y \delta z$,at a constant value of x. If the radiance at a point x is given as J(x) then the total radiance emitted from the observed slice is

$$I(x) = 2\delta x \delta z \int_{y=0}^{y=\infty} J(x)dy. \qquad 7.1$$

On changing to polar coordinates, $x^2+y^2 = r^2$ and R is defined as the radius,beyond which the radiance has decreased to zero. Equation 7.1 becomes

$$I(x) = 2 \int_{r=x}^{r=R} J(r)rdr/(r^2-x^2)^{\frac{1}{2}}. \qquad 7.2$$

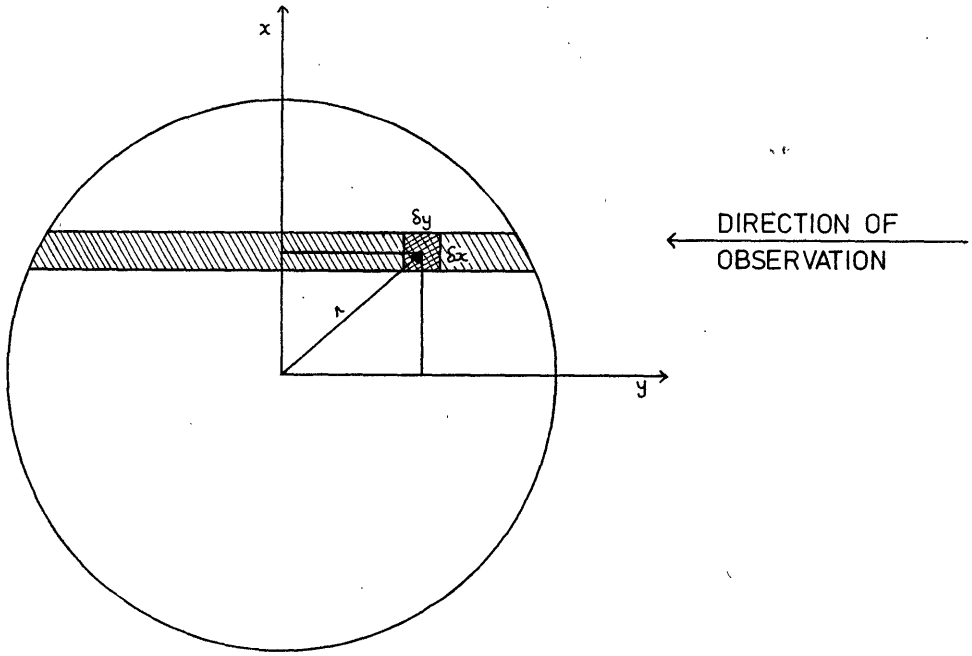


FIGURE 7.2: Sweeping a small volume to form a slice.

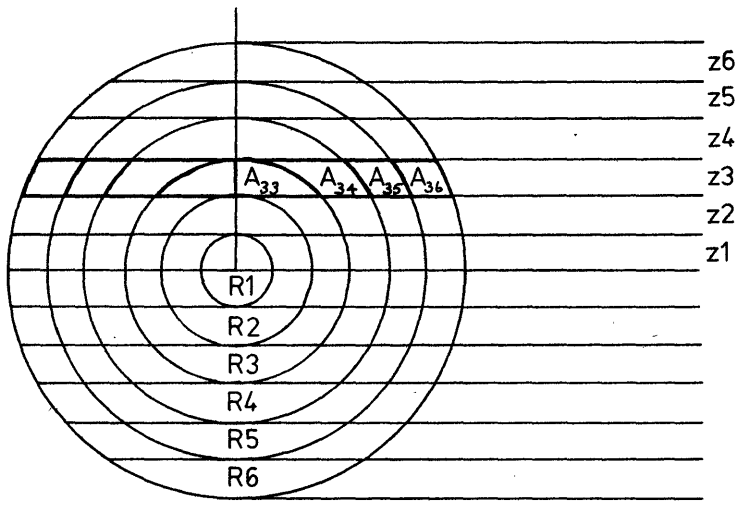


FIGURE 7.3: Lateral Zones and Radial Rings for the Hand Calculation of the Inverse Abel Transform.

Equation 7.2 is known as the Abel integral equation and it may be inverted analytically to give

$$J(r) = -(1/\pi) \int_{x=r}^{x=R} I'(x)dx/(x^2-r^2)^{\frac{1}{2}}. \quad 7.3$$

Equation 7.3 describes the inverse Abel transform,which translates the lateral intensity function,I(x), into the radial intensity function,J(r).

There are essentially two different methods by which this inverse Abel transform may be carried out.[161] The first method,which dates from the time when computers were not widely available,relies upon hand calculation and involves dividing the source into lateral viewing zones, z1-z6 (see Figure 7.3) and radial rings,R1-R6, of equal width. The overlap between the i^{th} lateral zone and the j^{th} radial ring will be termed A_{ij}. It is assumed that the intensity emitted throughout the width of a particular lateral zone or a radial ring is constant. For any known geometry, A_{ij} may be computed.[162] The intensity,I_i,viewed at a lateral zone,i,may be expressed as the sum of the A_{ij} terms for the slice:

$$I_i = 2 \sum_{j=1}^{jmax} A_{ij} J_j, \quad 7.4$$

where, j_{max} is the maximum value of j and J_j is the intensity emitted by the j^{th} ring. Because it is I_i which is observed and J_j which is required,it is necessary to invert Equation 7.4 to give

$$J_j = \tfrac{1}{2} \sum_{i=1}^{i_{max}} B_{ji} I_i \,, \qquad 7.5$$

where, i_{max} is the maximum value of i, and B is the inverse of matrix A. Various authors have discussed the use of the above procedure and tabulated values of the coefficients.[161-166]

The second method for the solution of the inverse Abel integral equation is to fit a curve to the data, I(x), observed experimentally, to calculate the first derivative of the curve and integrate numerically. This procedure was used in the computer program developed for this work.

A number of workers have used the inverse Abel transform to analyse results obtained with an ICP source.[81, 87, 94] Scheeline and Walters have described techniques for the correction of radial information for the presence of self-absorption and a continuum background. However, their method requires measurements of the lateral distribution of absorbers in the source to be made.

7.3 CURVE FITTING TECHNIQUES.

Currently, there are two well-known techniques for fitting curves to a series of data points. The relatively straightforward approach, used by Mermet[110] and de Galan,[106] amongst others, is to use a least-squares

fit of a polynomial or series of polynomials in a procedure which is simply an extension of the familiar linear least-squares technique. The choice of the order of the polynomial is an important decision; a high order will result in an accurate fit to the data points but the smoothing properties of a low order polynomial will be lost. A technique used frequently is to divide the data function into several regions, e.g. 3 or 4,[110] and fit an individual polynomial to each,while ensuring that the necessary conditions for continuity between the successive polynomials are fulfilled. Such an arrangement is known as a piecewise polynomial function.

An alternative technique makes use of spline functions. Spline functions were based upon a mathematical model of the procedure in which a draftsman uses a flexible metal strip,or spline,to join a series of points forming a curve. The spline fitting technique has superior smoothing properties compared with the least-squares technique.

A simple version of a spline fitting procedure[168] is to fit a polynomial of order k between each consecutive pair of base points so that the first and second differentials of the functions to the left and right of a given base point are equal at that base point. In such a simple arrangement it is straightforward to set up a matrix of coefficients,which can be solved by using one of the standard matrix inversion procedures. In this case it is necessary to specify the boundary conditions for the fitted spline functions such that the first and second

differentials are zero at both ends of the data function. This simple form of spline function is known as a natural spline and after some experimentation it was considered to be unsuitable for the purpose intended in this work because of the restriction in the boundary conditions.

A more general approach to spline functions was introduced by Schoenberg[169] in which the term B-spline was used to describe the function between two breakpoints in the data function. Recently, de Boor[170] published a series of FORTRAN sub-routines for use in calculating B-splines. A brief summary of the procedure adopted now follows.

The domain of the data function is to be divided so that each section is represented by an individual spline function. The joints between the spline functions are known as knots and their projections on to the abscissa are break points. If the order of the splines is chosen to be K and if there are N data points available then there is sufficient information available to construct N-K splines. Therefore, there will be N-K+1 knots or break points, ξ. The B-spline representation of the data will consist of,[170]

T(1)†....,T(N+K)	: the knot sequence,
A(1),....,A(N)	: the B-spline coefficients for the function represented on T(K) to T(N+1),
N	: the number of data points, and
K	: the order of the B-splines.

† The computer programming form of subscript notation has been adopted for ease of reference to the computer program.

The knot sequence, T(1) → T(N+K), is generated from the break points, $\xi_1 \rightarrow \xi_{N-K+1}$, by the addition of the end-knots, T(1) → T(K-1) and T(N+2) → T(N+K), which are included in order to ensure continuity at the boundaries. The knot sequence is constructed as follows (for N=10 and K=4),

	T(1)	=	ξ_1	=	0
	T(2)	=	ξ_1	=	0
	T(3)	=	ξ_1	=	0
T(K)	T(4)	=	ξ_1	=	0
	T(5)	=	ξ_1	=	1/7
	T(6)	=	ξ_2	=	2/7
	T(7)	=	ξ_3	=	3/7
	T(8)	=	ξ_4	=	4/7
	T(9)	=	ξ_5	=	5/7
	T(10)	=	ξ_6	=	6/7
T(N+1)	T(11)	=	ξ_7	=	1
	T(12)	=	ξ_8	=	1
	T(13)	=	ξ_8	=	1
T(N+K)	T(14)	=	ξ_8	=	1

for a normalized data domain.

The values of N and K are clear and the B-spline coefficients, A(1) → A(N), are calculated from the experimental data. Suppose a lateral scan of a source has been made at N positions, $\tau_1 \rightarrow \tau_N$, from the centre to the edge. At each τ we will have a measured intensity of $g(\tau)$.

If the set of B-spline functions of order K is

$$\{M_{iK}\}_{i=1}^{N},$$

then an element, f, of the set of spline functions which agrees with the data function, g, at the points $\tau_1 \rightarrow \tau_N$ may be expressed as

$$f = \sum_{i=1}^{N} A_i M_{iK},$$

involving the B-spline coefficients A(1) → A(N). These

coefficients can,therefore,be found as the solution to

$$\sum_{j=1}^{N} A_j M_{jK}(\tau_i) = g(\tau_i), \quad i = 1,\ldots,N.$$

This may be expressed in matrix form:

$$\begin{pmatrix} M_{1K}(\tau_1) & M_{2K}(\tau_1) & \ldots\ldots\ldots & M_{10K}(\tau_1) \\ M_{1K}(\tau_2) & M_{2K}(\tau_2) & \ldots\ldots\ldots & M_{10K}(\tau_2) \\ . & & & . \\ . & & & . \\ . & & & . \\ . & & & . \\ . & & & . \\ . & & & . \\ M_{1K}(\tau_9) & M_{2K}(\tau_9) & \ldots\ldots\ldots & M_{10K}(\tau_9) \\ M_{1K}(\tau_{10}) & M_{2K}(\tau_{10}) & \ldots\ldots\ldots & M_{10K}(\tau_{10}) \end{pmatrix} \cdot \begin{pmatrix} A_1 \\ A_2 \\ A_3 \\ A_4 \\ A_5 \\ A_6 \\ A_7 \\ A_8 \\ A_9 \\ A_{10} \end{pmatrix} = \begin{pmatrix} g(\tau_1) \\ g(\tau_2) \\ g(\tau_3) \\ g(\tau_4) \\ g(\tau_5) \\ g(\tau_6) \\ g(\tau_7) \\ g(\tau_8) \\ g(\tau_9) \\ g(\tau_{10}) \end{pmatrix}$$

Therefore, in the curve fitting procedure the sub-routine BSPLVN[170] is used to generate the M values and on solving the matrix equation, the values of the B-spline coefficients are obtained. The B-spline representation of the data function is obtained thus in the form of the parameters N and K, with the arrays T and A. Once this B-spline representation of the data function has been stored the value of the i^{th} derivative of the function may be obtained at any base point,within the range of the data, by a call to the function sub-program BVALUE.[170]

7.4 THE INTEGRATION PROCEDURE.

Simpson's rule for numerical integration is well known. The area under the curve,which is to be integrated, is divided up into an even number of uniform strips,a quadratic equation is used to approximate the function in a pair of strips and the area of the strip pair is calculated. The procedure is then repeated for the remaining pairs of strips.

In the application of the curve fitting procedure to the inverse Abel transform the spline order used was 4 (degree = 3). As it is the area under the differential of the data curve that is required, the order of the differential function is 3 (degree = 2 *i.e.* quadratic.) Therefore, in theory, the application of Simpson's rule should give a result which is exact whatever value of the strip width used. However,this is not quite the case because a *piecewise* polynomial function has been fitted to the data.

The direct application of Simpson's rule to solve the inverse Abel integral equation is not possible because the denominator becomes zero when x is put equal to r (Equation 7.3). This problem was solved by using an initial value of $x = r + \delta$,where δ is a very small number. In the computer program a value of 1×10^{-12} for δ was used.

For each value of r required (determined by the user) the differential of the data function divided by $\sqrt{(x^2 - r^2)}$ was integrated numerically from $x=r+10^{-12}$ to x=R. The

values of the ordinates required for each strip were obtained by making a call to BVALUE.[170]

7.5 A COMPUTER PROGRAM TO PERFORM THE INVERSE ABEL TRANSFORM.

The FORTRAN computer program written to perform the inverse Abel transform is included in Appendix A and was run on the Imperial College CDC6500/CYBER174 system. The program is divided into a number of sub-programs, three of which are by de Boor.[170] A brief description of the function of each sub-program now follows.

ABELTSP is the main sub-program used to control the flow of the whole program. The whole program has been designed to run interactively with the user or with batch processing. The user is invited to enter instructions for control of the procedure by using keys at a terminal or on cards. The following instructions are allowed;

*DATA.	Indicates that data is about to be entered.The first card after *DATA must be an identification card in the format: /dataname.
*SET,NBP=xx.	Specifies the number of output points required.
*SET,ISD=yy.	Specifies the density of integration strips to be used. yy is the number of strips the data will be divided.
*GO	Initiates the curve fitting and integration.

FREEFOR allows data points to be input as ordered pairs,separated by commas or spaces. The data is

checked for valid characters and normalized.

PINTA calculates the parameters required for the integration procedure.

PINTB performs the integration and outputs the results.

BANNA controls the printing of the output text.

POLYFT performs a B-spline curve fit to the data by making calls to BSPLVN, INTERV and F04ATF.

BSPLVN§ is used to generate the M_{jK} values.

INTERV§ is used by BSPLVN and BVALUE.

BVALUE§ is used to obtain the value of the first differential of the fitted spline function at the required base points.

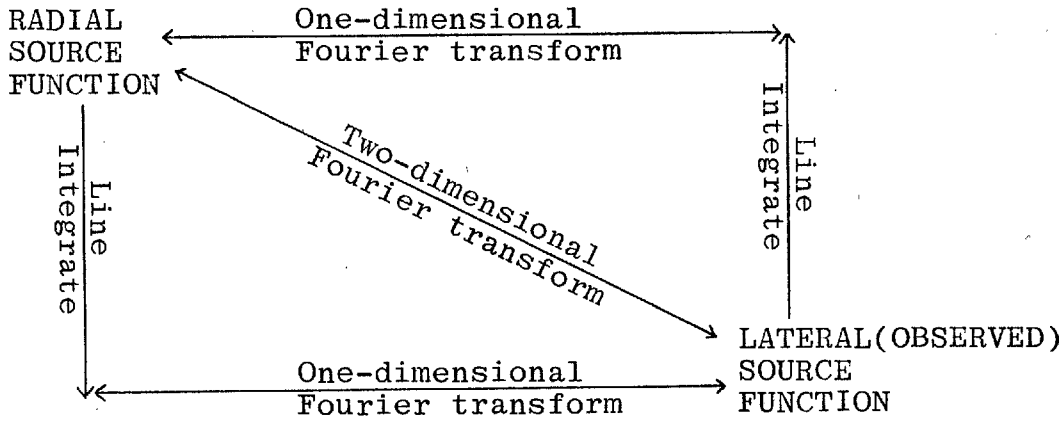
OPUTM is used to output an appropriate error message if required.

Calls are also made to the sub-programs JORIGIN and F04ATF. JORIGIN obtains the origin of the job and formats the output to be appropriate for a line printer or a terminal. F04ATF is a standard matrix inversion program available in the NAG¶ package.

§ These routines are supplied by de Boor.
¶ NAG is the Numerical Algorithms Group program library.

7.6 OBTAINING RADIAL INFORMATION IN THE ABSENCE OF SYMMETRY.

In order to obtain radial information about a source, which does not have circular symmetry,it is necessary to perform lateral scanning at every angle around the source. Bracewell[163] has considered the observed function to be the result of carrying out a two-dimensional Fourier transform upon the radial function. The conversion of the lateral data to the radial function may be carried out by line integration and taking one-dimensional Fourier transforms.Alternatively,one may take one-dimensional



Fourier transforms followed by the inverse process to line integration. The latter procedure,however,is potentially more difficult to achieve because information is lost in performing line integration.

CHAPTER EIGHT

CONCLUSIONS AND SUGGESTIONS FOR FURTHER WORK.

A substantial amount of the work described in this thesis has involved the preparation of electrodeless discharge lamp sources. Despite the recent paper by Winefordner et al.,[171] in which an optimization algorithm was used to optimize the preparation procedure for a cadmium EDL, considerable work remains to be undertaken before it will be possible to manufacture EDL's entirely reproducibly. The effect of impurities upon the operation of an EDL has been discussed in Chapter 4 and the conclusion remains that further work is required with regard to the preparation of EDL's using high-purity materials and high-vacuum equipment.

The improved stability of EDL sources when operated with temperature regulation has been confirmed and an improved design of heater has been used successfully for this purpose.

Measurements have indicated that a radial gradient in the excitation temperature occurs in an indium EDL with a maximum value in the centre and a minimum value at the edge. The value of the absorbed microwave power has been observed to have relatively less effect than the temperature of the air stream upon the gradient of the excitation temperature. On increasing the temperature of the air stream flowing over the EDL the gradient in the excitation temperature decreases and an overall reduction in the value of the excitation temperature is observed.

Two distinct types of radial distribution of intensity have been observed in EDL's operated with temperature regulation. These types have been classified

as type A, in which there is a maximum of emission intensity at the centre of the EDL, and type B, in which there is a maximum of emission intensity just inside the wall of the EDL and an intensity minimum at the centre.

The possibility of the type B distribution of intensity being merely the manifestation of an electrical skin depth has been considered to be unlikely. It has also been concluded that this form of discharge is unlikely to be the result of sputtering effects at the wall of the EDL or self-absorption in the centre of the EDL. Those elements having a first ionization energy less than ca. 9.5eV have been observed to show the type B distribution of intensity and it appears that there is sufficient energy available in the centre of the discharge to depopulate substantially the upper energy levels of observed transitions by excitation and/or ionization. For those elements with first ionization energies greater than ca. 9.5eV there appears to be insufficient energy available to cause substantial depopulation in the centre of the EDL and, consequently, the type A distribution of intensity is observed.

Measurements made of the strontium lines emitted by an ICP source have indicated that calibration graphs for strontium II lines become non-linear at lower sample concentrations than those observed for strontium I lines. It has been concluded that this effect is the result of the atom ground states being depopulated by excitation and ionization resulting in the self-absorption being less

severe for atom lines than for ion lines at a particular sample concentration.

Measurements made of the line half-width of the Sr II 407.771nm line in the plasma at various viewing heights,with a sample concentration of 50µg cm^{-3},showed the presence of a minimum in the Doppler temperature at 5mm and a maximum at 25mm above the load coil. These results were attributed to the progressive mixing of the relatively cool injector gas with the remainder of the plasma. The observed decrease in the Doppler temperature at viewing heights greater than 25mm has been attributed to the mixing of the tail-flame gases with the relatively cool surroundings.

The necessity of using the inverse Abel transform to obtain the radial intensity distribution from the corresponding lateral intensity distribution has been demonstrated. Although in many cases the type B lateral distribution showed a minimum of intensity in the centre of the discharge,in some instancies the presence of a central intensity minimum was not revealed until the inverse Abel transform of the data had been obtained. The curve-fitting procedure remains the most difficult aspect of the inverse Abel transform,however;spline functions have been shown to be useful in this application.

A possible area for future work includes the measurement of the Doppler temperature at different radial positions in an EDL. The extent of self-absorption has been shown in this work not to be negligible in most instancies and so it would be necessary to make

measurements of the absorption coefficient at different positions in the EDL. Additionally,it would be necessary to use the inverse Abel transform to obtain the radial information;it is doubtful whether a satisfactory signal-to-noise ratio would be observed using the existing instrumentation.

The measurement of the line profiles in carbon furnace atomizers,similar to those used in atomic absorption spectrometry,would be of interest. However, as discrete sample introduction is necessary and the atomization process is complete in a relatively short period of time scanning frequencies in the order of 10kHz would be required.

A substantial improvement in the interferometer instrumentation is required before either of the above suggestions could be achieved satisfactorily. The largest problem in the existing arrangement is the system of springs and screws used to adjust plate parallelism. These should be replaced with rigidly mounted piezoelectrically controlled spacers. A further improvement could be made in which the finesse of the system was automatically optimized and kept constant. Presently,half of the scanning waveform is not used for making measurements. During this period of time it would be possible to pass a low power laser beam through the optical system,using reflecting rotating sectors driven in synchronism by stepping motors,and collect the radiation using the photodiode. The whole system would be under microprocessor control - the finesse would be calculated

and correction applied to the parallelism of the plates.

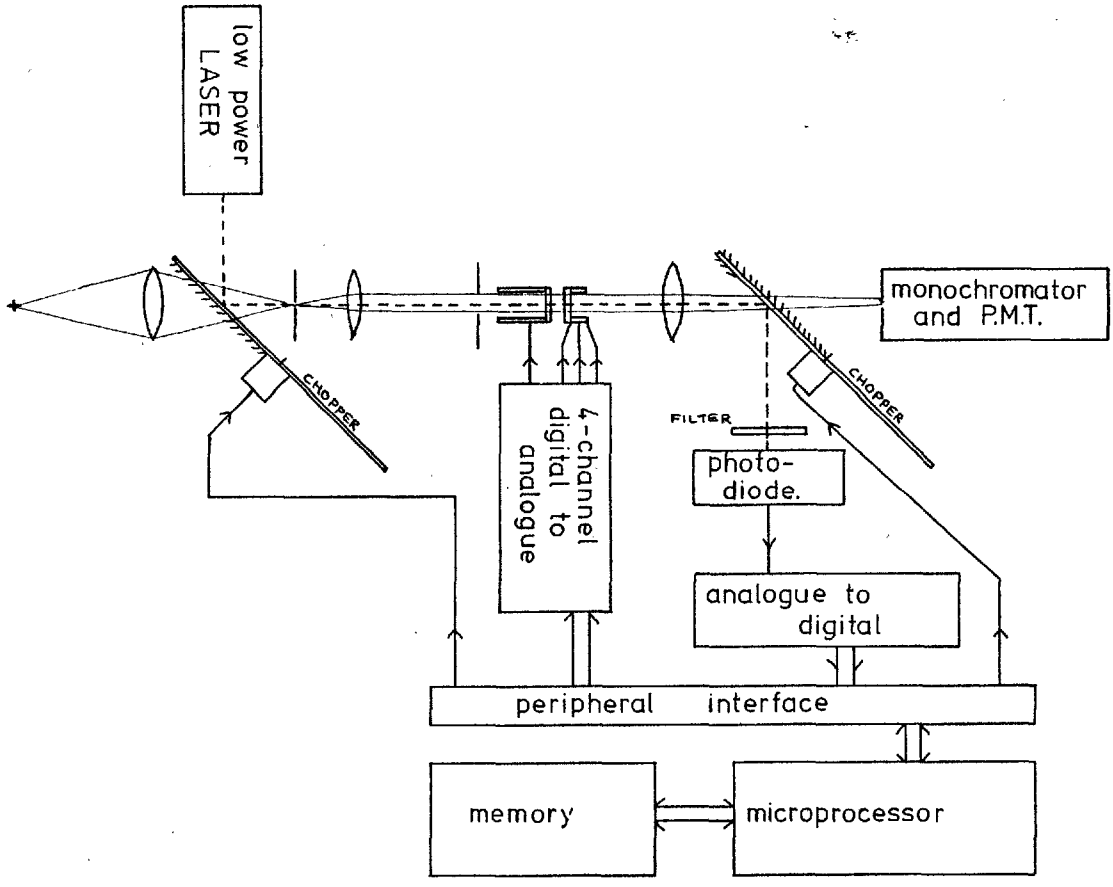


FIGURE 8.1: A Possible Configuration for Upgrading the Performance of the Interferometer.

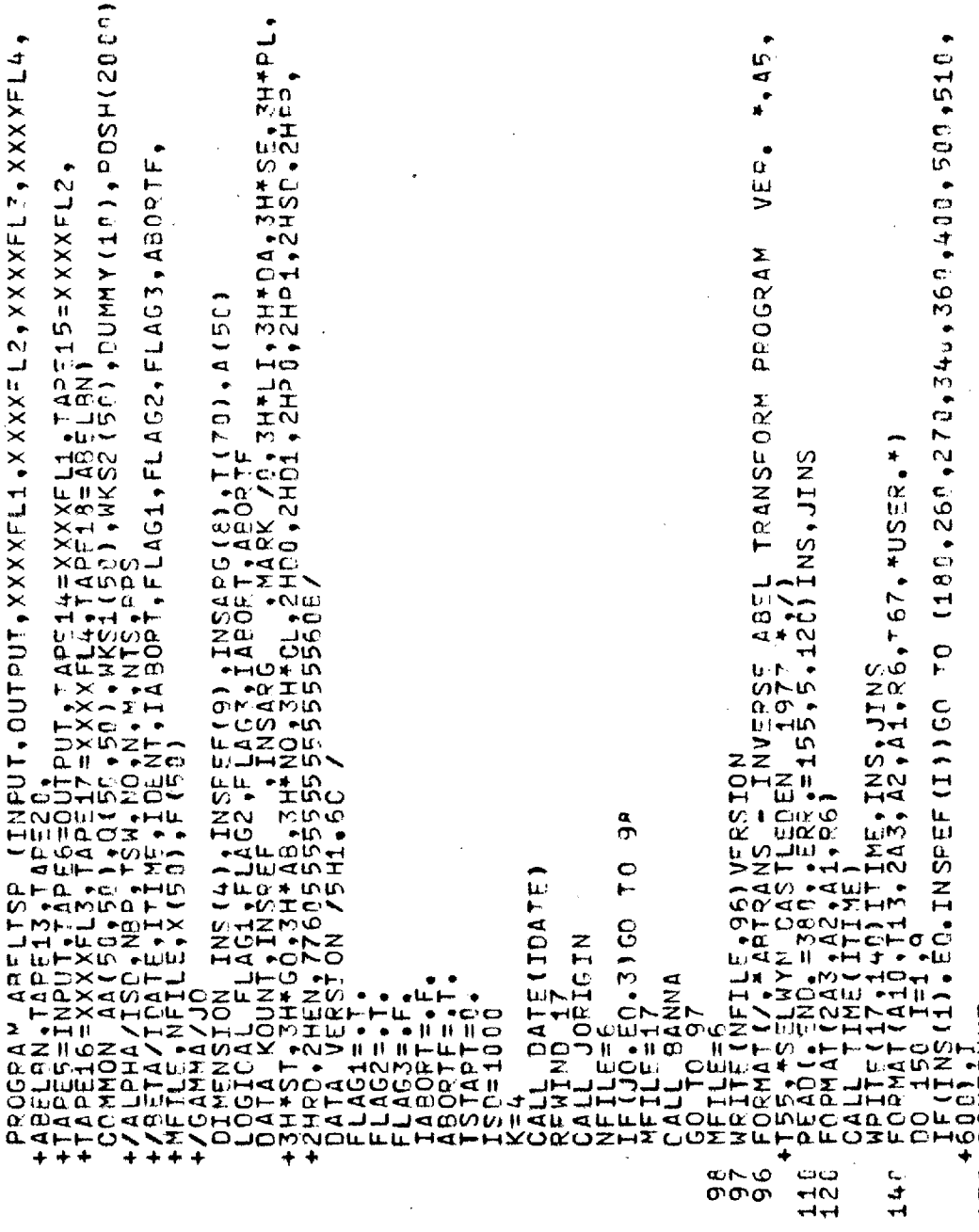
The application of a method of successive approximation to the solution of the inverse Abel transform might be useful. In such a technique, along the lines suggested by Bracewell;[163] a first approximation to the radial function corresponding to the lateral data function would be made. The estimated radial function would then be strip integrated to give a new lateral function. A correction would then be made to the radial function by comparing

the true and calculated lateral functions. This process would be repeated until the required level of accuracy had been achieved.

The Appendix which follows is a copy of the FORTRAN computer program used to obtain the Abel inverted data.

APPENDIX

A computer program for the inverse Abel transform.



```
      PROGRAM ABELTSP (INPUT,OUTPUT,XXXXFL1,XXXXFL2,XXXXFL3,XXXXFL4,
     +ABELRAN,TAPE13,TAPE20,
     +TAPE5=INPUT,TAPE6=OUTPUT,TAPE14=XXXXFL1,TAPE15=XXXXFL2,
     +TAPE16=XXXXFL3,TAPE17=XXXXFL4,TAPE18=ABELRAN)
       COMMON AA(50,50),Q(50,50),WKS1(50),WKS2(50),DUMMY(10),POSH(2000)
      +/ALPHA/ISC,NBP,ISW,NO,N,M,NTS,PPS
      +/BETA/IDATE,ITIME,IDENT,IABORT,FLAG1,FLAG2,FLAG3,ABORTF,
      +/GAMMA/JOB,NFILE,X(50),F(50)
      +/DELTA/INSREF(9),INSARG(8),T(70),A(50)
       DIMENSION IAG(4),IFLAG1,IFLAG2,IFLAG3,IABORT,ABORTF
       LOGICAL FLAG1,FLAG2,FLAG3,ABORTF
       DATA KOUNT,INSREF,INSARG,MARK /0,3H*LI,3H*DA,3H*SE,3H*PL,
      +3H*ST,3H*GO,3H*AB,3H*NO,3H*CL,2HD0,2HD1,2HP0,2HP1,2HSC,2HES,
      +2HRD,2HEN,77605555555555555560E/
       DATA VERSION /5H1.6C /
            FLAG1=.T.
            FLAG2=.T.
            FLAG3=.F.
            IABORT=.F.
            ABORTF=.T.
            ISTAPT=0
            ISC=1000
            K=4
            CALL DATE(IDATE)
            REWIND 17
            CALL JORIGIN
            NFILE=6
            IF(JO.EQ.3)GO TO 98
            MFILE=17
            CALL BANNA
            GO TO 97
        98  NFILE=6
        97  WRITE(NFILE,96)VERSION
        96  FORMAT(/,*ABTRANS - INVERSE ABEL TRANSFORM PROGRAM  VER. *,A5,
           +*,SELWYN CASTLEDEN 1977 *,/)
       110  READ(*,*END=380,*ERR=155,5,120)INS,JINS
       120  CALL FORMAT(2A3,A2,A1,R6)
            CALL TIME(ITIME)
            WRITE(17,140)ITIME,INS,JINS
       140  FORMAT(A10,T13,2A3,A2,A1,R6,T67,*USER.*)
            DO 150 I=1,9
            IF(INS(1).EQ.INSREF(I))GO TO (180,260,270,340,360,400,500,510,
           +600),I
       150  CONTINUE
       155  KOUNT=KOUNT+1
            IF(KOUNT.GT.5) GO TO 560
            GO TO 540
```

```
180  DO 190 I=1,4
     IF(INS(3).EQ.INSARG(I)) GO TO (210,220,230,240),I
190  CONTINUE
195  CALL OPUTM(2)
     GO TO 540
210  FLAG1=.F.
     GO TO 110
220  FLAG1=.T.
     GO TO 110
230  FLAG2=.F.
     GO TO 110
240  FLAG2=.T.
     GO TO 110
260  CALL FREFFOR(XSHIFT,XEXPAND,YSHIFT,YEXPAND)
     IF(IABORT) GO TO 520
     GO TO 110
270  I=0
     IF(INS(3).EQ.INSARG(8)) GO TO 800
275  MINS=0
     J=0
280  JJNS=JINS/64
     KINS=JJNS*64
     LINS=JINS-KINS
     I=I+1
     JINS=JJNS
     IF((LINS.GT.36).OR.(LINS.LT.27))GO TO 275
     MINS=MINS+((LINS-27)*(10**J))
     J=J+1
     IF(I.LT.6)GO TO 280
     IF(INS(3).EQ.INSARG(5)) GO TO 290
     IF(INS(3).EQ.INSARG(6))GO TO 310
     IF(INS(3).EQ.INSARG(7)) GO TO 304
     GO TO 195
290  IF(MINS.GT.2000)GO TO 470
     ISD=MINS
     CALL TIME(ITIME)
     WRITE(17,300) ITIME,ISD
300  FORMAT(A10,T15,*INTEGRATION STRIP DENSITY =*,I6,T67,*ATSP.*)
     GO TO 110
304  IF((MINS*2).GT.N)GO TO 470
     K=MINS
     CALL TIME(ITIME)
     WRITE(17,306)ITIME,K
306  FORMAT(A10,T15,*SPLINE ORDER =*,I2,T67,*ATSP.*)
     GO TO 110
310  IF(MINS.GT.200)GO TO 470
     NPP=MINS
     CALL TIME(ITIME)
```

```
      WRITE(17,320) ITIME,NBP
320   FORMAT(A10,T15,*NUMBER OF BASE POINTS =*,I6,T67,*ATSP.*)
      GO TO 110
800   IF(JO.NE.3)GO TO 820
      WRITE(6,810)
810   FORMAT(*ENTER CENTRE X-COORDINATE.*)
820   READ(5,830)TSTART
830   FORMAT(E12.6)
      CALL TIME(ITIME)
      WRITE(17,450)ITIME,TSTART
450   FORMAT(A10,T15,*CENTRE POSITION IN DATA =*,F10.6,T67,*ATSP.*)
      TSTART=(TSTART+XSHIFT)*XEXPAND
      IF(TSTART.LT.0.)CALL OPUTM(1)
      IF(TSTART.GE.1.)CALL OPUTM(4)
      GO TO 110
262   CALL OPUTM(3)
      GO TO 520
470   CALL OPUTM(4)
      GO TO 540
340   CALL OPUTM(5)
      GO TO 110
360   CALL OPUTM(6)
      GO TO 610
380   CALL OPUTM(7)
      GO TO 610
400   IF(FLAG3) GO TO 420
      CALL OPUTM(8)
      GO TO 520
420   IF(N.GT.50) STOP 2
      REWIND 15
      DO 422 I=1,N
      READ(15) X(I),F(I)
422   CONTINUE
      CALL PINTA
      M=N-1
      MESSN=0
      NPK=N+K
      CALL SECOND(SECB)
      CALL POLYFT(T,A,N,K,F,X,NPK,MESSN)
      CALL SECOND(SECA)
      SECE=SECA-SECB
      IF(MESSN.EQ.0) GO TO 425
      CALL OPUTM(12)
      GO TO 520
425   CALL SECOND(SECB)
      TBPS=(1.-TSTART)/FLOAT(NBP-1)
      TTSW=TBPS/FLOAT(NTS)
      USTART=(1.-TSTART)
```

```
      VAL=TSTART
      DO 423 J=1,NO
      IF(J.EQ.NO) VAL=X(N)
      POSH(J)= BVALUE(T,A,N,K,VAL,1,NPK)
      POSH(J)=POSH(J)*USTART
  423 VAL=VAL+TTSW
      CALL SECOND(SECA)
      SECF=SECA-SECB
      CALL SECOND(SECB)
      CALL PLOTB(TSTART,XSHIFT,YSHIFT,XEXPAND,YEXPAND)
      CALL SECOND(SECA)
      IF(IABORT) GO TO 560
      SECD=SECA-SECB
      WRITE(NFILE,428)SECE,SECF,SECD
  428 FORMAT(1H ,*FIT *,F7.3,2X,*LOK*,F7.3,2X,*INT *,F7.3,
     +2X,*CP SECONDS.*)
      GO TO 110
  500 ABORTF=.T.
      GO TO 110
  510 ABORTF=.F.
      GO TO 110
  520 IF(.NOT.ABORTF) GO TO 560
      FLAG3= .F.
      CALL OPUTM(9)
  540 IF(.NOT.ABORTF) GO TO 560
      CALL OPUTM(10)
      GO TO 110
  560 CALL OPUTM(11)
  610 IF(JO.EQ.3)STOP
      CALL BANNR
      STOP
  600 FLAG3=.F.
      GO TO 110
      END
      SUBROUTINE FREEFOR(XSHIFT,XEXPAND,YSHIFT,YEXPAND)
      COMMON /ALPHA/ISD,NBP,ISW,NO,N,M,NTS,BPS
     +/BETA/IDATE,ITIME,IDENT,IABORT,FLAG1,FLAG2,FLAG3,ABORTF,
     +NFILE,NFILE,X(50),F(50)
     +/GAMMA/JO
    60 FORMAT(80A1)
    68 FORMAT(1H ,I4,1X,I1,1X,I1,1X,15A1,2X,15A1)
      LOGICAL FLAG1,FLAG3,IABORT
      DIMENSION MBUFFX(15),MBUFFY(15)
      INTEGER BUFFX(15),BUFFY(15),XYTOG,POINTNO,DCHAR(13),COMMA,BLANK,
     +CHAR(80),CEE
      DATA BLANK,DCHAR,COMMA,CEE/1H ,1H0,1H1,1H2,1H3,1H4,1H5,1H6,1H7,
     +1H8,1H9,1H.,1H-,1HE,1H,,1HC/
      DATA ISLASH /1H//
```

```
      DATA ITEF/1HT/
      REWIND 13
      REWIND 15
      REWIND 16
      POINTNO=0
      K=80
      XYTOG=-1
      MWDA=0
      XBUFF1=0.
      XBUFF2=0.
      XBUFF3=0.
      READ(,END.=49,.ERR.=49,5,65)BUFFX(1),IDENT
      IF(BUFFX(1).NE.ISLASH) GO TO 49
      CALL TIME(ITIME)
      WRITE(17,66) ITIME,IDENT
      IF(JO.EQ.3)GO TO 5
      WRITE(NFILE,8)IDATE,ITIME,IDENT
      GO TO 10
    5 WRITE(NFILE,9)IDATE,ITIME,IDENT
    9 FORMAT(/,2A10,T30,*DATA IDENTIFICATION =*,A10)
   10 DO 12 I=1,15
      BUFFX(I)= BLANK
   12 CONTINUE
      IBXTOG = 0
      IDXTOG = 0
   14 DO 16 I=1,15
      BUFFY(I) = BLANK
   16 CONTINUE
      IBYTOG = 0
      IDYTOG = 0
   18 L=1
   20 K=K+1
      IF(K.LE.80) GO TO 24
      READ(5,60) (CHAR(I),I=1,80)
      IF(EOF(5)) 50,22
   22 K=1
   24 IF(CHAR(K).EQ.BLANK) GO TO 20
      DO 26 I=1,13
      IF(CHAR(K).EQ.DCHAR(I)) GO TO 32
   26 CONTINUE
      IF(CHAR(K).EQ.COMMA) GO TO 38
      IF(CHAR(K).EQ.ITEF) GO TO 50
      IF(CHAR(K).NE.DEF) GO TO 44
      IF((XYTOG.LT.0).AND.(L.EQ.1)) GO TO 28
      IF(XYTOG.LT.0) GO TO 10
      IF((XYTOG.GT.0).AND.(L.EQ.1)) GO TO 30
      GO TO 14
   28 POINTNO=POINTNO-1
```

```
      MWDA=0
      GO TO 10
   30 XYTOG = (-1)
      GO TO 10
   32 IF(L.GT.14) GO TO 46
      IF(XYTOG.GT.0) GO TO 34
      IBXTOG =1
      IF(CHAR(K).EQ.DCHAR(11)) IDXTOG=1
      BUFFX(L)=CHAR(K)
      GO TO 36
   34 IBYTOG =1
      IF(CHAR(K).EQ.DCHAR(11)) IDYTOG=1
      BUFFY(L) = CHAR(K)
   36 L=L+1
      GO TO 20
   38 XYTOG=-XYTOG
      IF(XYTOG.GT.0) GO TO 48
      IF(IDYTOG.LT.1) BUFFY(L)= DCHAR(11)
      IF(IBXTOG.GT.0) GO TO 40
      BUFFX(1)=DCHAR(1)
      BUFFX(2) =DCHAR(11)
   40 IF(IBYTOG.GT.0) GO TO 41
      BUFFY(1)=DCHAR(1)
      BUFFY(2)=DCHAR(11)
   41 POINTNO = POINTNO+1
      IF(MWDA.EQ.0) GO TO 42
      WRITE(15,68) MBUFPN,MBUFBX,MBUFBY,MBUFFX,MBUFFY
   42 MBUFPN=POINTNO
      MBUFBX=IBXTOG
      MBUFBY=IBYTOG
      MWDA=1
      DO 43 I=1,15
      MBUFFX(I)=BUFFX(I)
      MBUFFY(I)=BUFFY(I)
   43 CONTINUE
      GO TO 10
   44 CALL TIME(ITIME)
      WRITE(17,63) ITIME,CHAR(K)
      IABORT =.T.
      RETURN
   46 CALL TIME(ITIME)
      WRITE(17,64)ITIME,ITIME,BUFFX,ITIME,BUFFY
      IABORT=.T.
      RETURN
   48 IF(IDXTOG.LT.1) BUFFX(L)=DCHAR(11)
      GO TO 18
   49 CALLTIME(ITIME)
      WRITE(17,67)ITIME
```

```
      IABORT=.T.
      RETURN
   50 WRITE(15,68) MBUFPN,MBUFBX,MBUFBY,MBUFFX,MBUFFY
      REWIND 15
      POINTNO = 0
  100 XBUFF3=XBUFF2
      XBUFF2=XBUFF1
      N=POINTNO
      READ(15,70)POINTNO,IBXTOG,IBYTOG,XBUFF1,YBUFF1
      IF(EOF(15)) 106,102
   70 FORMAT(1H ,I4,1X,I1,1X,I1,1X,E15.8,2X,E15.8)
  102 IF(POINTNO.GT.1) GO TO 104
      XMIN=XBUFF1
      XMAX=XBUFF1
      YMIN=YBUFF1
      YMAX=YBUFF1
  104 IF(IBXTOG.EQ.0) XBUFF1=XBUFF2+(XBUFF2-XBUFF3)
      IF((POINTNO.LT.3).AND.(IBXTOG.EQ.0)) GO TO 112
      IF(IBYTOG.EQ.0) GO TO 114
      IF(XBUFF1.LT.XMIN) XMIN=XBUFF1
      IF(XBUFF1.GT.XMAX) XMAX=XBUFF1
      IF(YBUFF1.LT.YMIN) YMIN=YBUFF1
      IF(YBUFF1.GT.YMAX) YMAX=YBUFF1
      WRITE(16)XBUFF1,YBUFF1
      GO TO 100
  106 REWIND 15
      REWIND 16
      XSHIFT=-XMIN
      YSHIFT=-YMIN
      XEXPAND=1./(XMAX+XSHIFT)
      YEXPAND=1./(YMAX+YSHIFT)
  108 READ(16) XBUFF1,YBUFF1
      IF(EOF(16)) 110,109
  109 XBUFF1=(XBUFF1+XSHIFT)*XEXPAND
      YBUFF1=(YBUFF1+YSHIFT)*YEXPAND
      WRITE(15)XBUFF1,YBUFF1
      GO TO 108
  110 IF(.NOT.FLAG1) GO TO 210
      IF(JO.NE.3)GO TO 111
      WRITE(NFILE,151)
  151 FORMAT(*INPUT:*,T11,*ABSCISSA*,T28,*ORDINATE*,T42,
     +*NORM:*,T50,*ABSCISSA*,T61,*ORDINATE*)
      GO TO 113
  111 WRITE(6,150)
  113 REWIND 15
      REWIND 16
      DO 200 I=1,N
      READ(15)XBUFF1,YBUFF1
```

```
      READ(16)XBUFF2,YBUFF2
      IF(JO.NE.3)GO TO 118
      WRITE(NFILE,186)XBUFF2,YBUFF2,XBUFF1,YBUFF1
  186 FORMAT(T8,E15.8,T25,E15.8,T48,F11.8,T59,F11.8)
      GO TO 119
  118 WRITE(6,185)XBUFF2,YBUFF2,XBUFF1,YBUFF1
  119 WRITE(13,199)XBUFF1,YBUFF1
  199 FORMAT(2020)
  200 CONTINUE
  210 FLAG3=.T.
      IF(JO.NE.3)GO TO 212
      WRITE(NFILE,242)N,XSHIFT,YSHIFT,XEXPAND,YEXPAND
  242 FORMAT(*NORMALIZATION PARAMETERS:*,T27,I2,* POINTS*,/,
     +*XSHIFT=*,E12.6,*YSHIFT=*,E12.6,* XEXP.=*,E12.6,
     +* YEXP.=*,E12.6)
      GO TO 213
  212 WRITE(6,230)
      WRITE(6,240)N,XSHIFT,YSHIFT,XEXPAND,YEXPAND
  213 NBP=N
      RETURN
  112 CALL TIME(ITIME)
      WRITE(17,132) ITIME
      IABORT=.T.
      RETURN
  114 CALL TIME(ITIME)
      WRITE(17,134) ITIME,XBUFF1
      IABORT=.T.
      RETURN
    8 FORMAT(/,T6,A10,5X,A10,T47,*---DATA IDENTIFICATION = *,
     +A10,*---*,T114,*ABTRANS 1*)
   63 FORMAT(A10,T15,*NON-RECOGNIZABLE CHARACTER-*,A1,*- IN DATA.*,T67,
     +*DATA.*)
   64 FORMAT(A10,T15,*BUFFER OVERFLOW ON INPUT.*,T67,*DATA.*,/,A10,T21,*
     +X-BUFFER = *,15A1,T67,*DATA.*,/,A10,T21,*Y-BUFFER = *,15A1,T67,
     +*DATA.*)
   65 FORMAT(A1,A10)
   66 FORMAT(A10,T15,*DATA IDENT = *,A10,T67,*DATA.*)
   67 FORMAT(A10,T15,*MISSING IDENT ON INPUT DATA.*,T67,*DATA.*)
  132 FORMAT(A10,T15,*INSUFFICIENT DATA FOR IMPLIED SEPARATION MODE.*,
     +T67,*DATA.*)
  134 FORMAT(A10,T15,*MISSING ORDINATE FOR ABSCISSA = *,E18.10,T67,
     +*DATA.*)
  150 FORMAT(/,T58,*---INPUT DATA---*,/,T44,*REAL*,T85,*NORMALIZED*,
     +/,T32,*ABSCISSA*,T53,*ORDINATE*,T78,*ABSCISSA*,T95,*ORDINATE*,/)
  185 FORMAT(1H ,21X,E15.8,6X,E15.8,12X,F11.8,6X,F11.8)
  230 FORMAT(/,T49,*---DATA NORMALIZATION PARAMETERS---*,/)
  240 FORMAT(T47,*NUMBER OF DATA POINTS = *,I2,/,T47,*SHIFT FACTORS*,/,
     +T60,*ABSCISSA = *,E15.8,/,T60,*ORDINATE = *,E15.8,/,T47,
```

```
     +*EXPANSION FACTORS*,/,T60,*ABSCISSA = *,E15.8,/,T60,
     +*ORDINATE = *,E15.8)
      END
      SUBROUTINE PINTA
      COMMON/ALPHA/ISD,NBP,TSW,NO,N,M,NTS,BPS
     +/BETA/IDATE,ITIME,IDENT,IABORT,FLAG1,FLAG2,FLAG3,ABORTF,
     +NFILE,NFILE,X(50),F(50)
     +/GAMMA/JO
      LOGICAL FLAG2
      DATA MESSA,MESSB,MESSC/10HUSER DEFND,10HIMPLIED VL,10HPROGM CALC/
      BPS=1./FLOAT(NBP-1)
      SSW=(1.)/FLOAT(ISD)
      SSN=BPS/SSW
      NTS=(IFIX(SSN/2.))*2
      TSW=BPS/(FLOAT(NTS))
      NO=((NBP-1)*NTS)+1
      IF(JO.NE.3)GO TO 5
      WRITE(NFILE,31)ISD,SSN,NBP,NTS,BPS,TSW,SSW,NO
   31 FORMAT(*INTEGRATION PARAMETERS:*,/,*INT. STRIP DENSITY =*,T25,
     +I4,T40,*SET STRIPS/BASE POINT=*,T65,E14.6,/,*NO. BASE POINTS*
     +* REQD.=*,T25,I4,T40,*REAL STRIPS/BASE POINT=*,T65,I4,/,
     +*BASE POINT SEP.=*,T25,E14.6,T40,*REAL INT. STRIP WIDTH=*,
     +T65,E14.6,/,*SET INT. STRIP WIDTH=*,T25,E14.6,T40,*TOTAL NO.*,
     +* ORDINATES=*,T65,I4)
      RETURN
    5 IF(FLAG2) GO TO 20
      WRITE(6,10) TSW,NO
   10 FORMAT(/,T51,*INTEGRATION PARAMETERS (B)*,/,T11,
     +*REAL INTEGRATION STRIP WIDTH*,T48,E15.8,T11,
     +*TOTAL NUMBER OF ORDINATES*,T48,I4)
      RETURN
   20 WRITE(6,30)ISD,MESSA,NBP,MESSA,BPS,MESSB,SSW,MESSB,SSN,MESSB,
     +NTS,MESSC,TSW,MESSC,NO,MESSC
   30 FORMAT(/,T48,*---INTEGRATION PARAMETERS---*,/,T11,
     +*INTEGRATION STRIP DENSITY*,T48,*ISD*,T56,I4,T101,A10,/,T11,
     +*NUMBER OF BASE POINTS REQUIRED*,T48,*NBP*,T56,I4,T101,A10,/,T11,
     +*SEPARATION BETWEEN BASE POINTS*,T48,*BPS*,T56,E15.8,T101,A10,/,
     +T11,*SET INTEGRATION STRIP WIDTH*,T48,*SSW*,T56,E15.8,T101,A10,/,
     +T11,*NUMBER OF SET STRIPS /BASE POINT*,T48,*SSN*,T56,E15.8,T101,
     +A10,/,T11,*NUMBER OF REAL STRIPS/BASE POINT*,T48,*NTS*,T56,I4,T101
     +,A10,/,T11,*REAL INTEGRATION STRIP WIDTH*,T48,*TSW*,T56,E15.8,
     +T101,A10,/,T11,*TOTAL NUMBER OF ORDINATES*,T48,*NO*,T56,I4,T101,
     +A10)
      RETURN
      END
      SUBROUTINE PINTB(TSTART,XSHIFT,YSHIFT,XEXPND,YEXPND)
      COMMON AA(50,50),Q(50,50),WKS1(50),WKS2(50),DUMMY(10),PDSH(2000)
     +/ALPHA/ISD,NBP,TSW,NO,N,M,NTS,BPS
```

```
     +/BETA/ICATE,ITIME,IDENT,IABORT,FLAG1,FLAG2,FLAG3,ABORTF,
     +MFILE,NFILE,X(50),F(50)
     +/GAMMA/JO
      LOGICAL IABORT,FLAG4
      DATA PY /17216207732504205518/
      IF(JO.NE.3)GO TO 2
      WRITE(NFILE,8)IDENT
    8 FORMAT(*RESULT OF INVERSE ABEL TRANSFORM ON *,A10,/,
     +T5,*ABSCISSA*,T23,*ORDINATE*)
      GO TO 6
    2 WRITE(6,5) IDENT
    5 FORMAT(//,T35,*---RESULT OF INVERSE ABEL TRANSFORM ON *,
     +A10,*---*,/,T44,*ABSCISSA*,T71,*ORDINATE*,/)
    6 R=0.0
      FLAG4=.F.
      NPK=N+K
      DELTA=1.E-12
      NOP=1
   10 NOOF=NOP
      S=0.
      NOOFSN=1
      XA=R+DELTA
      XB=(XA*(1.-TSTART))+TSTART
      P=PVALUE(T,A,N,K,XB,1,NPK)
   20 DENOM=(XA*XA)-(R*R)
      IF(DENOM.LE.0.)GO TO 900
      DENOM=SQRT(DENOM)
      F1=P/DENOM
      IF((NOOF.GT.NOP).AND.(NOOF.LT.NO))GO TO 30
      S=S+F1
      IF(NOOF.EQ.NOP) GO TO 40
      GO TO 50
   30 IF(NOOFSN.LT.0) S=S+(F1*2.)
      S=S+(F1*2.)
   40 XA=XA+TSW
      NOOF=NOOF+1
      NOOFSN=-NOOFSN
      P=PDSH(NOOF)
      GO TO 20
   50 S=-(((TSW*S)/3.0)/PY)
      R2=(((R*(1.-TSTART))+TSTART)/XEXPAND)-XSHIFT
      S2=(S/YEXPAND)-YSHIFT
      IF(JO.NE.3)GO TO 60
      WRITE(NFILE,100) R2,S2
  100 FORMAT(F12.4,F18.4)
      GO TO 70
   60 WRITE(6,110) R2,S2
  110 FORMAT(T40,F16.12,T66,F16.12)
```

```
 70 NOR=NOR+NTS
    R=R+RPS
    IF(NOR.LT.NO) GO TO 10
    S=0.
    R2=(((R*(1.-TSTART))+TSTART)/XEXPAND)-XSHIFT
    IF(JO.NE.3) GO TO 80
    WRITE(NFILE,100) R2,S
    GO TO 90
 80 WRITE(6,110)R2,S
 90 WRITE(NFILE,120) NRP
120 FORMAT(T42,I4,* POINTS.*)
    RETURN
900 CALL OPUTM(14)
    IABORT=.T.
    RETURN
    END
    SUBROUTINE BANNA
    COMMON/BETA/IDATE,ITIME,IDENT,IABORT,FLAG1,FLAG2,FLAG3,ABORTF,
   +NFILE,NFILE,X(50),F(50)
   +/GAMMA/JO
    DIMENSION IBAN(10),ORGN(4)
    DATA ORGN    /6HSYSTEM,6HBATCH ,6HEXPORT,6HTELEX /
    WRITE(NFILE,10)
 10 FORMAT(1H1)
    IRET=1
    LC=20
    GO TO 200
 70 REWIND 17
    JB=JO+1
    WRITE(17,80)IDATE,ORGN(JB)
 80 FORMAT(A10,T60,*ORIGIN *,A6,/)
    RETURN
    ENTRY BANNB
    WRITE(NFILE,90)
 90 FORMAT(1H ,//)
    IRET=2
    LC=4
    GO TO 200
100 REWIND 17
105 READ(17,110)(IBAN(I),I=1,8)
110 FORMAT(7A10,A2)
    IF(EOF(17))140,120
120 WRITE(6,130) (IBAN(I),I=1,8)
130 FORMAT(1H ,T26,3H** ,7A10,A2,T103,2H**)
    GO TO 105
140 IRET=3
    LC=14
200 DO230 J=1,LC
```

```
      READ(18,210)(IBAN(I),I=1,5)
  210 FORMAT(5I15)
      READ(18,210)(IBAN(I),I=6,10)
      WRITE(NFILE,220) IBAN
  220 FORMAT(1H ,T25,10A8)
  230 CONTINUE
      GO TO (70,100,240),IRET
  240 RETURN
      END
      SUBROUTINE POLYFT(T,A,N,K,G,TAU,NPK,NERR)
      COMMON AA(50,50),Q(50,50),WKS1(50),WKS2(50),DUMMY(10),PDSH(2000)
      DIMENSION T(NPK),A(N),TAU(N),G(N)
      LN=(N-K)+1
      DELTAXI=1.0/FLOAT(LN)
      XI=0.0
      NP1=N+1
      DO 10 I=1,NPK
      IF((I.GT.K).AND.(I.LE.NP1)) XI=XI+DELTAXI
   10 T(I)=XI
      KM1=K-1
      NP2MK=N+2-K
      KPKM1=K+KM1
      DO 30 I=1,N
      DO 13 J=1,N
   13 Q(I,J)=0.0
      CALL INTERV(T(K),NP2MK,TAU(I),ILEFT,MFLAG)
      ILEFT=ILEFT+KM1
      IF(MFLAG)99,15,14
   14 IF(I.LT.N)GO TO 98
      ILEFT=N
   15 ILFTPK=ILEFT+K
      CALL BSPLVN(T,K,1,TAU(I),ILEFT,DUMMY,ILFTPK)
      L=ILEFT-K
      DO 16 J=1,K
      L=L+1
      IF(L.LT.1)L=1
   16 Q(I,L)=DUMMY(J)
   30 CONTINUE
      NERR=0
      IQ=50
      CALL F04ATF(Q,IQ,G,N,A,AA,IQ,WKS1,WKS2,NERR)
      RETURN
   98 NERR=4
      RETURN
   99 NERR=3
      RETURN
      END
      SUBROUTINE BSPLVN(T,JHIGH,INDEX,X,ILEFT,VNIKX,ILPJH)
```

```
C CALCULATES THE VALUE OF ALL POSSIBLY NON-ZERO B-SPLINES AT *X* OF
C ORDER MAX(JHIGH,(J+1)(INDEX-1)) ON *T*.
C DIMENSION T(ILEFT+JHIGH)
C
      DIMENSION T(ILPJH),VNIKX(JHIGH),DELTAM(20),DELTAP(20)
      DATA J/1/
      GO TO (10,20),INDEX
   10 J=1
      VNIKX(1)=1.0
      IF(J.GE.JHIGH)GO TO 99
   20 IPJ=ILEFT+J
      DELTAP(J)=T(IPJ)-X
      IMJP1=ILEFT-J+1
      DELTAM(J)=X-T(IMJP1)
      VMPREV=0.0
      JP1=J+1
      DO 26 L=1,J
      JP1ML=JP1-L
      VM=VNIKX(L)/(DELTAP(L)+DELTAM(JP1ML))
      VNIKX(L)=VM*DELTAP(L)+VMPREV
   26 VMPREV=VM*DELTAM(JP1ML)
      VNIKX(JP1)=VMPREV
      J=JP1
      IF(J.LT.JHIGH)GO TO 20
C
   99 RETURN
      END
      FUNCTION BVALUE(T,A,N,K,X,IDERIV,NPK)
C CALCULATES VALUE AT *X* OF *IDERIV*TH DERIVATIVE OF SPLINE FROM
C B-REPRESENTATION. DIMENSION T(N+K)
C
      DIMENSION T(NPK),A(N),AJ(20),DP(20),DM(20)
      BVALUE=0.0
      KMIDER=K-IDERIV
      IF(KMIDER.LE.0)GO TO 99
C
      KM1=K-1
      NP1=N+1
      CALL INTERV(T,NP1,X,I,MFLAG)
      IF(X.LT.T(K)) GO TO 99
      IF(MFLAG.EQ.0) GO TO 20
      IF(X.GT.T(I)) GO TO 99
   10 IF(I.EQ.K) GO TO 99
      I=I-1
      IF(X.EQ.T(I)) GO TO 10
C
   20 IMK=I-K
      DO 21 J=1,K
```

```
      IMKPJ=IMK+J
   21 AJ(J)=A(IMKPJ)
      IF(IDERIV.EQ.0) GO TO 30
   22 DO 23 J=1,IDERIV
      KMJ=K-J
      FKMJ=FLOAT(KMJ)
      DO 23 JJ=1,KMJ
      IHI=I+JJ
      IHMKMJ=IHI-KMJ
   23 AJ(JJ)=(AJ(JJ+1)-AJ(JJ))/(T(IHI)-T(IHMKMJ))*FKMJ
C
   30 IF(IDERIV.EQ.KM1) GO TO 39
      IP1=I+1
      DO 32 J=1,KMIDER
      IPJ=I+J
      DP(J)=T(IPJ)-X
      IP1MJ=IP1-J
   32 DM(J)=X-T(IP1MJ)
      IDERP1=IDERIV+1
      DO 33 J=IDERP1,KM1
      KMJ=K-J
      ILO=KMJ
      DO 33 JJ=1,KMJ
      AJ(JJ)=(AJ(JJ+1)*DM(ILO)+AJ(JJ)*DP(JJ))/(DM(ILO)+DP(JJ))
   33 ILO=ILO-1
   39 BVALUE=AJ(1)
C
   99 RETURN
      END
      SUBROUTINE INTERV(XT,LXT,X,ILEFT,MFLAG)
C
      DIMENSION XT(LXT)
      DATA ILO/1/
      IHI=ILO+1
      IF(IHI.LT.LXT) GO TO 20
      IF(X.GE.XT(LXT)) GO TO 110
      IF(LXT.LE.1) GO TO 90
      ILO=LXT-1
      IHI=LXT
   20 IF(X.GE.XT(IHI)) GO TO 40
      IF(X.GE.XT(ILO)) GO TO 100
C
   30 ISTEP=1
   31 IHI=ILO
      ILO=IHI-ISTEP
      IF(ILO.LE.1) GO TO 35
      IF(X.GE.XT(ILO)) GO TO 50
      ISTEP=ISTEP*2
```

```
      GO TO 31
   35 ILO=1
      IF(X.LT.XT(1)) GO TO 90
      GO TO 50
C
   40 ISTEP=1
   41 ILO=IHI
      IHI=ILO+ISTEP
      IF(IHI.GE.LXT) GO TO 45
      IF(X.LT.XT(IHI)) GO TO 50
      ISTEP=ISTEP*2
      GO TO 41
   45 IF(X.GE.XT(LXT)) GO TO 110
      IHI=LXT
C
   50 MIDDLE=(ILO+IHI)/2
      IF(MIDDLE.EQ.ILO) GO TO 100
      IF(X.LT.XT(MIDDLE)) GO TO 53
      ILO=MIDDLE
      GO TO 50
   53 IHI=MIDDLE
      GO TO 50
C
   90 MFLAG=-1
      ILEFT=1
      RETURN
  100 MFLAG=0
      ILEFT=ILO
      RETURN
  110 MFLAG=1
      ILEFT=LXT
      RETURN
      END
      SUBROUTINE OPUTM(MESSN)
      DIMENSION MES1(14),MES2(14)
      COMMON/BETA/IDATE,ITIME,IDENT,IABORT,FLAG1,FLAG2,FLAG3,ABORTF,
     +MFILE,NFILE,X(50),F(50)
     +/GAMMA/JO
      DATA MES1,MES2 /10HILLEGAL IN,
     +10HBAD ARGUME,10HDATA AREA,
     +10HREQUEST TO,10HNOT AVAILA,10HEND OF ABT,10HEND OF INF,
     +10HNO DATA FO,10H8 DATA FLA,10H8 JOB REPR,10H8 FATAL ER,
     +10HPOLYFIT FAI,10HITERATION ,10HINT DENOM ,10HSTRUCTION.,
     +3HNT.,9HDY READ.,8HO LARGE.,8HBLE YET.,5HRANS.,
     +9HORMATION.,4HUND.,10HG CLEARED.,6HIEVED.,4HROR.,
     +3HLS.,6HLIMIT.,5HLE 0./
      IF(JO.EQ.3) GO TO 20
      CALL TIME(ITIME)
```

```
      WRITE(17,10)ITIME,MES1(MESSN),MES2(MESSN)
10    FORMAT(A10,T15,2A10)
      RETURN
20    WRITE(6,30)MES1(MESSN),MES2(MESSN)
30    FORMAT(2A10)
      RETURN
      END
```

REFERENCES

1 Newton,Sir Isaac. Opticks or a treatise of the reflections,refractions,inflections and colours of light. G.Bell and Sons,Ltd. London 1931.

2 Kirchhoff,G. On the relations between the radiating and absorbing powers of different bodies for light and heat. Philosophical Magazine 20,1-21,(1860)

3 Kirchhoff,G. and Bunsen,R. Chemical analysis by spectrum-observations. Philosophical Magazine 20, 89-109,(1860)

4 Kirchhoff,G. and Bunsen,R. Chemical analysis by spectrum-observations.-Second memoir. Philosophical Magazine 22,329-349,(1861)

5 Hellund,E.J. The Plasma State. Reinhold Publishing Corporation,New York. (1961)

6 Thorne,A.P. Spectrophysics. Chapman&Hall and Science Paperbacks.London. (1974)

7 Parsonage,N.G. The Gaseous State. Pergamon Press.(1966)

8 Hittorf,W. Ueber die Electricitätsleitung der Gase. Annalen der Physik und Chemie.Neue Folge,XXI, 90-139,(1884)

9 Wiens,J.H. Production of Hg^{198}as a possible source of an improved wave-length standard. Physical Review 70, 910-914,(1946)

10 Meggers,W.F. A light wave of artificial mercury as the ultimate standard of length. J.Opt.Soc.Am. 38, 7-14,(1948)

11 Meggers,W.F.and Kessler,K.G. Wave-lengths of mercury 198. J.Opt.Soc.Am. 40,737-741,(1950)

12 Meggers,W.F.and Westfall,F.O. Lamps and wavelengths of mercury 198. Journal of Research of the National Bureau of Standards 44,447-455,(1950)

13 Winefordner,J.D.and Staab,R.A. Study of experimental parameters in atomic fluorescence flame spectrometry. Analytical Chemistry 36,1367-1369,(1964)

14 Bratzel,M.P.,Dagnall,R.M.and Winefordner,J.D.Evaluation of premixed flames produced using a total consumption nebulizer burner in atomic fluorescence spectrometry. Analytical Chemistry 41,1527-1535,(1969)

15 Hingle,D.N.,Kirkbright,G.F.,and West,T.S. The determination of beryllium by thermal-emission and atomic-fluorescence spectroscopy in a separated nitrous oxide-acetylene flame. Analyst 93,522-527,(1968)

16 Zacha,K.E.,Bratzel,M.P.,Winefordner,J.D.and Mansfield, J.M. Improvements in preparation and operation of electrodeless discharge lamps as high intensity sources in atomic fluorescence flame spectrometry.Analytical Chemistry 40,1733-1736,(1968)

17 Smith,R.,Stafford,C.M.and Winefordner,J.D. Some interference effects occurring in the hydrogen/argon /entrained-air flame. Anal.Chim.Acta 42,523-531,(1968)

18 Dagnall,R.M.,Kirkbright,G.F.,West,T.S.and Wood,R. Atomic fluorescence spectrometry of aluminium, molybdenum,titanium,vanadium and zirconium in inert gas separated nitrous oxide-acetylene flames. Analytical Chemistry 42,1029-1033,(1970)

19 Dagnall,R.M.,Kirkbright,G.F.,West,T.S.and Wood,R. The determination of silicon by flame photometry and atomic fluorescence spectroscopy with a separated nitrous oxide-acetylene flame. Anal.Chim.Acta 47, 407-413,(1969)

20 Ebdon,L.,Kirkbright,G.F.and West,T.S. Atomic-flourescence characteristics and analytical determination of manganese in an air-acetylene flame. Talanta 17,965-971,(1970)

21 Ebdon,L.,Kirkbright,G.F.and West,T.S. The determination of iron by atomic fluorescence spectroscopy with a modulated microwave-excited electrodeless discharge tube. Anal.Chim.Acta. 47,563-568,(1969)

22 Fleet,B.,Liberty,K.V.and West,T.S. The atomic fluorescence spectroscopy of cobalt with a high-intensity hollow cathode lamp and a microwave-excited electrodeless discharge tube as sources. Anal.Chim. Acta 45,205-211,(1969)

23 Mansfield,J.M.,Winefordner,J.D.and Veillon,C. High sensitivity determination of zinc,cadmium,mercury, thallium,gallium and indium by atomic fluorescence flame spectrometry. Analytical Chemistry 37,1049-1051, (1965)

24 Dagnall,R.M.,Kirkbright,G.F.,West,T.S.and Wood,R. An investigation of the determination of germanium by flame photometry and atomic flourescence spectroscopy by using a separated nitrous oxide-acetylene flame. Analyst 95,425-430,(1970)

25 Dagnall,R.M.,Thompson,K.C.and West,T.S. Studies in atomic-flourescence spectroscopy-VII Fluorescence and analytical characteristics of arsenic,with a microwave excited electrodeless discharge tube as source. Talanta 15,677-687,(1968)

26 Dagnall,R.M.,Thompson,K.C.and West,T.S. Studies in atomic-fluorescence spectroscopy - IV The atomic-fluorescence spectroscopic determination of selenium and tellurium. Talanta 14,557-563,(1967)

27 Azad,J.,Kirkbright,G.F.and Snook,R.D. The determination of selenium in soil digests by non-dispersive atomic fluorescence spectrometry using an argon-hydrogen flame and hydride generation technique. Analyst(in press)

28 L'Vov,B.V. in Atomic Absorption Spectroscopy.Editors: Dagnall,R.M.and Kirkbright,G.F. Butterworths, London (1970)

29 Browner,R.F.,Dagnall,R.M.and West,T.S. The determination of tin by atomic fluorescence spectroscopy,with an electrically modulated electrodeless discharge tube as source. Anal.Chim.Acta. 46,207-216,(1969)

30 Dagnall,R.M.,Thompson,K.C.and West,T.S. Studies in atomic-fluorescence spectroscopy - V The fluorescence characteristics and determination of antimony. Talanta 14,1151-1156,(1967)

31 Thompson,K.C. Atomic fluorescence determination of antimony,arsenic,selenium and tellurium by using the hydride-generation technique. Analyst 100,307-310,(1975)

32 Browner,R.F.,Dagnall,R.M.and West,T.S. Studies in atomic-fluorescence spectroscopy - VIII Atomic fluorescence and atomic absorption of thallium and mercury with electrodeless discharge tubes as sources. Talanta 16,75-81,(1969)

33 Kirkbright,G.F.,West,T.S.and Wilson,P.J. The direct determination of mercury by atomic fluorescence spectrometry in a nitrogen-separated air-acetylene flame with excitation at 184.9nm. Anal.Chim.Acta 66, 130-133,(1973)

34 Browner,R.F.,Dagnall,R.M.and West,T.S. The determination of lead by atomic fluorescence spectroscopy. Anal.Chim.Acta 50,375-381,(1970)

35 Dagnall,R.M.,Thompson,K.C.and West,T.S. Studies in atomic-fluorescence spectroscopy - VI The fluorescence characteristics and analytical determination of bismuth with an iodine electrodeless discharge lamp. Talanta 14,1467-1475,(1967)

36 Hobbs,R.S.,Kirkbright,G.F.and West,T.S. Spectroscopy in separated flames - VII Determination of bismuth by atomic-fluorescence spectroscopy in a separated air-acetylene flame with electronically modulated electrodeless discharge tube sources. Talanta 18, 859-864,(1971)

37 Thompson,K.C.and Wildy,P.C. The use of electronically modulated microwave-excited discharge tubes in atomic spectrometry. Analyst 95,776-780,(1970)

38 Browner,R.F.,Dagnall,R.M.and West,T.S. Electronically modulated microwave excited electrodeless discharge tubes as sources in atomic absorption spectroscopy. Anal.Chim.Acta 45,163-170,(1969)

39 Headridge,J.B.and Richardson,J. A comparison of electrodeless discharge tubes and hollow cathode lamps in atomic absorption spectroscopy. Laboratory Practice 19,372-373,(1970)

40 Kirkbright,G.F.and Marshall,M. Direct determination of phosphorus by atomic absorption flame spectrometry. Analytical Chemistry 45,1610-1613,(1973)

41 Kirkbright,G.F.and Marshall,M. Direct determination of sulfur by atomic absorption spectrometry in a nitrogen separated nitrous oxide-acetylene flame. Analytical Chemistry 44,1288-1290,(1972)

42 Dagnall,R.M.,Thompson,K.C.and West,T.S. The use of microwave excited electrodeless discharge tubes as spectral sources in atomic absorption spectroscopy. Atomic Absorption Newsletter 6,117-120,(1967)

43 Kirkbright,G.F.and Ranson,L. Use of the nitrous oxide-acetylene flame for determination of arsenic and selenium by atomic absorption spectrometry. Analytical Chemistry 43,1238-1241,(1971)

44 Kirkbright,G.F.,West,T.S.and Wilson,P.J. The direct determination of iodine by atomic absorption spectroscopy in a nitrogen separated nitrous oxide-acetylene flame. Atomic Absorption Newsletter 11, 53-56,(1972)

45 Thompson,K.C. A cold vapour mercury atomic fluorescence detector. Laboratory Practice 21,645-647,(1972)

46 Kirkbright,G.F.,West,T.S.and Wilson,P.J.The direct determination of mercury by atomic-absorption spectrophotometry at 184.9nm by using a nitrogen-separated nitrous oxide-acetylene flame. Analyst 98, 49-52,(1973)

47 Browner,R.F.and Winefordner,J.D. Optimization of thermostated electrodeless discharge lamps for analytical atomic spectrometry. Spectrochim.Acta 28B, 263-288,(1973)

48 Browner,R.F.,Patel,B.M.,Glenn,T.H.,Rietta,M.E.and Winefordner,J.D. A device for precise temperature control of electrodeless discharge lamps. Spectrosc.Lett. 5,311-318,(1972)

49 Patel,B.M.,Browner,R.F.and Winefordner,J.D. Design and operation of temperature-controlled multiple element electrodeless discharge lamps for atomic fluorescence spectrometry. Analytical Chemistry 44, 2272-2277,(1972)

50 Haarsma,J.P.S.,deJong,G.J.and Agterdenbos,J. The preparation and operation of electrodeless discharge lamps- A critical review. Spectrochim.Acta 29B,1-18,(1974)

51 L'Vov,B.V. Atomic absorption spectrochemical analysis.Hilger,London.(1970)

52 Brewer,R.G. High intensity low noise rubidium light source. Review of Scientific Instruments 32,1356-1358,(1961)

53 Avni,R.and Winefordner,J.D. Some considerations on the microwave electrodeless discharge.Plasma diagnostics in argon,helium or nitrogen atmospheres. Spectrochim.Acta 30B,281-303,(1975)

54 Busch,K.W.and Vickers,T.J. Fundamental properties characterizing low-pressure microwave-induced plasmas as excitation sources for spectroanalytical chemistry. Spectrochim.Acta 28B,85-104,(1973)

55 Kawaguchi,H.,Atsuya,I.and Vallee,B.L. Interelement effects and a possible excitation mechanism in a low-pressure microwave induced helium plasma. Analytical Chemistry 49,266-270,(1977)

56 Brassem,P.and Maessen,F.J.M.J. Electron temperatures and electron concentrations at low pressure in microwave induced plasmas. Spectrochim.Acta 29B, 203-210,(1974)

57 Aldous,K.M.,Dagnall,R.M.,Pratt,S.J.and West,T.S. Microwave excited electrodeless discharge tubes containing organo-sulfur and phosphorus compounds. Analytical Chemistry 41,1851-1853,(1969)

58 van Sandwijk,A.,van Montfort,P.F.E.and Agterdenbos,J. Trace analysis by microwave excitation of sealed samples- I Preliminary investigations. Talanta 20,495-499,(1973)

59 van Sandwijk,A.and Agterdenbos,J. Trace analysis by microwave excitation of sealed samples- II Determination of 4-100pg of cadmium,indium and thallium in 0.5ml of aqueous solution. Talanta 21,360-362,(1974)

60 van Montfort,P.F.E.and Agterdenbos,J. Trace analysis by microwave excitation of sealed samples- III Determination of 0.005-25ng of tellurium and 0.25-25ng of selenium in 0.5ml of aqueous solution. Talanta 21,660-663,(1974)

61 van Montfort,P.F.E.,Agterdenbos,J.,Denissen,R.,Piet,M. and van Sandwijk,A. Picogram analysis by microwave excitation from sealed atomization cells. Spectrochim.Acta 33B,47-52,(1978)

62 Eckert,H.U. Detection of trace metals in RF-heated electrodeless lamps by emission spectroscopy. ICP Information Newsletter 2,327-353,(1977)

63 Babat,G.I. Pecularities of the induction heating of steel. J.Techn.Phys.,U.S.S.R. 10,19,1604-1618,(1940)

64 Babat,G.I. Electrodeless discharges and some allied problems. J.Instn.Elect.Engrs.Part III,94,27-37,(1947)

65 Reed,T.B. Induction-coupled plasma torch. Journal of Applied Physics 32,821-824,(1961)

66 Greenfield,S.,Jones,I.L.and Berry,C.T. High pressure plasmas as spectroscopic emission sources. Analyst 89,713-720,(1964)

67 Greenfield,S.,Jones,I.L.W.,Berry,C.T.and Bunch,L.G. The high-frequency torch: some facts,figures and thoughts. Proc.Soc.Anal.Chem. 2,111-113,(1965)

68 Greenfield,S.,Smith,P.B.,Breeze,A.E.and Chilton,N.M.D. Atomic absorption with an electrodeless high-frequency plasma torch. Anal.Chim.Acta 41,385-387,(1968)

69 Wendt,R.H.and Fassel,V.A. Induction-coupled plasma spectrometric excitation source. Analytical Chemistry 37,920-922,(1965)

70 Wendt,R.H.and Fassel,V.A. Atomic absorption spectroscopy with induction-coupled plasmas. Analytical Chemistry 38,337-338,(1966)

71 Barnett,W.B.,Fassel,V.A.and Kniseley,R.N. Theoretical principles of internal standardization in analytical emission spectroscopy. Spectrochim.Acta 23B, 643-664,(1968)

72 Fassel,V.A.and Dickinson,G.W. Continuous ultrasonic nebulization and spectrographic analysis of molten metals.Analytical Chemistry 40,247-249,(1968).

73 Dickinson,G.W.and Fassel,V.A. Emission spectrometric detection of the elements at the nanogram per milliliter level using induction-coupled plasma excitation. Analytical Chemistry 41,1021-1024,(1969)

74 Dagnall,R.M.,Smith,D.J.and West,T.S. Emission spectroscopy of trace impurities in powdered samples with a high-frequency argon plasma torch. Anal.Chim.Acta 54,397-406,(1971)

75 Kirkbright,G.F.,Ward,A.F.and West,T.S. The determination of sulphur and phosphorus by atomic emission spectrometry with an induction-coupled high-frequency plasma source. Anal.Chim.Acta. 62,241-251,(1972)

76 Kirkbright,G.F.,Ward,A.F.and West,T.S. Atomic emission spectrometry with an induction-coupled high-frequency plasma source. The determination of iodine,mercury, arsenic and selenium. Anal.Chim.Acta 64,353-362,(1973)

77 Souilliart,J.C.and Robin,J.P. Quelques exemples d'applications du chalumeau a plasma inductif a l'analyse élémentaire. Analusis 1,427-433,(1972)

78 Boumans,P.W.J.M.and deBoer,F.J. Studies of flame and plasma torch emission for simultaneous multi-element analysis- I Preliminary investigations. Spectrochim.Acta 27B,391-414,(1972)

79 Alder,J.F.and Mermet,J.M. A spectroscopic study of some radio frequency mixed gas plasmas. Spectrochim.Acta 28B,421-433,(1973)

80 Scott,R.H.,Fassel,V.A.,Kniseley,R.N.and Nixon,D.E. Inductively coupled plasma-optical emission analytical spectrometry. A compact facility for trace analysis of solutions. Analytical Chemistry 46,75-80,(1974)

81 Kornblum,G.R.and deGalan,L. Arrangement for measuring spatial distributions in an argon induction coupled RF plasma. Spectrochim.Acta 29B,249-261,(1974)

82 Kirkbright,G.F.and Ward,A.F. Atomic-emission spectrometry with an induction-coupled high-frequency plasma source. Comparison with the inert-gas shielded premixed nitrous oxide-acetylene flame for multi-element analysis. Talanta 21,1145-1165,(1974)

83 Boumans,P.W.J.M.and deBoer,F.J. Studies of an inductively-coupled high-frequency argon plasma for optical emission spectrometry- II. Compromise conditions for simultaneous multi-element analysis. Spectrochim.Acta 30B,309-334,(1975)

84 Boumans,P.W.J.M.,deBoer,F.J.,Dahmen,F.J.,Hoelziel,H.and Meier,A. A comparative investigation of some analytical performance characteristics of an inductively-coupled RF plasma and a capacitively-coupled microwave plasma for solution analysis by emission spectrometry. Spectrochim.Acta 30B,449-469,(1975)

85 Mermet,J.M. Comparaison des températures et des densités électroniques mesurees sur le gaz plasmagène et sur des éléments excites dans un plasma h.f. Spectrochim.Acta 30B,383-396,(1975)

86 Barnes,R.M.and Schleicher. Computer simululation of RF induction-heated argon plasma discharges at atmospheric pressure for spectrochemical analysis- I. Preliminary investigations. Spectrochim.Acta 30B, 109-134,(1975)

87 Kalnicky,D.J.,Kniseley,R.N.and Fassel,V.A. Inductively coupled plasma - optical emission spectroscopy. Excitation temperatures experienced by analyte species. Spectrochim.Acta 30B,511-525,(1975)

88 Greenfield,S.,Jones,I.L.,McGeachin,H.McD.and Smith,P.B. Automatic multi-sample simultaneous multi-element analysis with a H.F. plasma torch and direct reading spectrometer. Anal.Chim.Acta 74,225-245,(1975)

89 Kniseley,R.N.,Amenson,H.,Butler,C.C.and Fassel,V.A. An improved pneumatic nebulizer for use at low nebulizing gas flows. Applied Spectroscopy 28, 285-286,(1974)

90 Barnett,W.B.,Fassel,V.A.and Kniseley,R.N. An experimental study of internal standardization in analytical emission spectroscopy. Spectrochim.Acta 25B, 139-161,(1970)

91 Mermet,J.M.and Robin,J. Etude des interférences dans un plasma induit par haute fréquence. Anal.Chim.Acta 70,271-279,(1975)

92 Greenfield,S.,McGeachin,H.McD.and Smith,P.B. Plasma emission sources in analytical spectroscopy- I. Talanta 22,1-15,(1975)

93 Boumans,P.W.J.M.and deBoer,F.J. Studies of a radio frequency inductively coupled argon plasma for optical emission spectrometry- III. Interference effects under compromise conditions for simultaneous multi-element analysis. Spectrochim.Acta 31B,355-375, (1976)

94 Visser,K.,Hamm,F.M.and Zeeman,P.B. Temperature determination in an inductively coupled RF plasma. Applied Spectroscopy 30,34-38,(1976)

95 Human,H.G.C.and Scott,R.H. The shapes of spectral lines emitted by an inductively coupled plasma. Spectrochim.Acta 31B,459-473,(1976)

96 Montaser,S.and Fassel,V.A. Inductively coupled plasmas as atomization cells for atomic fluorescence spectrometry. Analytical Chemistry 48,1490-1499,(1976)

97 Abdallah,M.H.,Mermet,J.M.and Trassy,C. Etude spectrometrique d'un plasma induit par haute fréquence. II Différents types d'effects interéléments observés. Anal.Chim.Acta 87,329-339,(1976)

98 Greenfield,S.,McGeachin,H.McD.and Smith,P.B. Nebulization effects with acid solutions in I.C.P. spectrometry. Anal.Chim.Acta 84,67-78,(1976)

99 Abdallah,M.H.,Diemiaszonek,R.,Jarosz,J.,Mermet,J.M., Robin,J.and Trassy,C. Etude spectrométrique d'un plasma induit par haute fréquence.Partie I: Performances analytiques.Anal.Chim.Acta 84,271-282, (1976)

100 Mermet,J.M.and Jacquinot,P. Spectroscopie atomique.- Sur les méchanismes d'excitation des éléments introduits dans un plasma HF d'argon. Compres Rendus Acad.Sc. Paris. 281,Série B,273-275,(1975)

101 Mermet,J.M.and Trassy,C. A plasma torch configuration for inductively coupled plasma as a source in optical emission spectroscopy and atomic absorption spectroscopy. Applied Spectroscopy 31,237-239,(1977)

102 Jarosz,J.and Mermet,J.M. A spectroscopic study of a high-frequency inductively-coupled Ar-H_2S plasma. J.Quant.Spectrosc.Radiat.Transfer 17, 237-246,(1977)

103 Edmonds,T.E.and Horlick,G. Spatial profiles of emission from an inductively coupled plasma source using a self-scanning photodiode array. Applied Spectroscopy 31,536-541,(1977)

104 Winge,R.K.,Fassel,V.A.,Kniseley,R.N.,DeKalb,E.and Haas,W.J.Jr. Determination of trace elements in soft, hard and saline waters by the inductively coupled plasma,multi-element atomic emission spectroscopic (ICP-MAES) technique. Spectrochim.Acta 32B,327-345, (1977)

105 Kornblum,G.R.and deGalan,L. A study of the interference of cesium and phosphate in the low power inductively coupled radiofrequency argon plasma using spatially resolved emission and absorption measurements. Spectrochim.Acta 32B,455-478,(1977)

106 Kornblum,G.R.and deGalan,L. Spatial distribution of the temperature and the number densities of electrons and atomic and ionic species in an inductively coupled RF argon plasma. Spectrochim.Acta 32B, 71-96,(1977)

107 Boumans,P.W.J.M.and DeBoer,F.J. An experimental study of a 1-kW,50-MHz RF inductively coupled plasma with pneumatic nebulizer,and a discussion of experimental evidence for a non-thermal mechanism. Spectrochim.Acta 32B,365-395,(1977)

108 Dahlquist,R.L.and Knoll,J.W. Inductively coupled plasma-atomic emission spectrometry: Analysis of biological materials and soils for major,trace,and ultra-trace elements. Applied Spectroscopy 32, 1-29,(1978)

109 Abdallah,M.H.and Mermet,J.M. The behavior of nitrogen excited in an inductively coupled argon plasma. J.Quant.Spectrosc.Radiat.Transfer 19,83-91,(1978)

110 Jarosz,J.,Mermet,J.M.and Robin,J.P. A spectrometric study of a 40-MHz inductively coupled plasma- III. Temperatures and electron number density. Spectrochim.Acta 33B,55-78,(1978)

111 Kalnicky,D.J.,Fassel,V.A.and Kniseley,R.N. Excitation temperatures and electron number densities experienced by analyte species in inductively coupled plasmas with and without the presence of an easily ionized element. Applied Spectroscopy 31,137-150,(1977)

112 Barnes,R.M.and Nikdel,S. Temperature and velocity profiles and energy balances for an inductively coupled plasma discharge in nitrogen. J.Applied Physics 47,3929-3934,(1976)

113 Barnes,R.M.and Nikdel,S. Computer simulation of inductively coupled plasma discharge for spectrochemical analysis.II. Comparison of temperature and velocity profiles,and particle decomposition for inductively coupled plasma discharges in argon and nitrogen. Applied Spectroscopy 30,310-320,(1976)

114 Fassel,V.A.and Kniseley,R.N. Inductively coupled plasmas. Analytical Chemistry 46,1155A-1164A,(1974)

115 Greenfield,S.,McGeachin,H.McD.and Smith,P.B. Plasma emission sources in analytical spectroscopy - III. Talanta 23,1-14,(1976)

116 Kuhn,H.G. Atomic Spectra. Longmans.(1969)

117 Drawin,H.W.and Felinboch,P. Data for Plasmas in L.T.E. Gauthier-Villers,Paris.(1965)

118 Fabry,C.and Perot,A. Sur les franges des lames minces argentées et leur application a la mesure de petites épaisseurs d'air. Annales de Chimie et de Physique 7È Série XII,459-501,(1897)

119 Tolansky,S. High Resolution Spectroscopy. Methuen London.(1947)

120 Tolansky,S. An Introduction to Interferometry. Longmans,London.(1955)

121 Francon,M. Optical Interferometry. Academic Press, London.(1966)

122 Jacquinot,P. New Developments in Interference Spectroscopy. Rep.Prog.Phys. 23,267,(1960)

123 Jacquinot,P.and Dufour,C. Conditions optiques d'emploi des cellules photo-életriques dans les spectrographes et les interféromètres. J.Rech.Cent.Nat.Rech.Scient. 2,91-103,(1948)

124 Bousquet,P. Spectroscopy and its Instrumentation. Adam Hilger,London.(1971)

125 Chabbal,R. Recherche des meilleurs condition d'utilisation d'un spectromètre photoélectrique Fabry-Perot. J.Rech.Cent.Nat.Rech.Scient. 5, 138-186,(1953)

126 Sargent,M. Ph.D. Thesis.University of London.(1970)

127 Cooper,J.and Greig,J.R. Rapid scanning of spectral line profiles using an oscillating Fabry-Perot interferometer. J.Sci.Instrum. 40,433-437,(1963)

128 Mack,J.E.,McNutt,D.P.,Roesler,F.L.and Chabbal,R. The pepsios purely interferometric high-resolution scanning spectrometer.I. The pilot model. Applied Optics 2,873-887,(1963)

129 Hernandez,G. Analytical description of a Fabry-Perot photoelectric spectrometer.Applied Optics 5,1745-1748,(1966)

130 Hernandez,G. Analytical description of a Fabry-Perot photoelectric spectrometer.II.Numerical results. Applied Optics 9,1591-1596,(1970)

131 Ballik,E.A. The response of scanning Fabry-Perot interferometers to atomic transition profiles. Applied Optics 5,170-172,(1966)

132 Bruce,C.F.and Hannaford,P. On the widths of atomic resonance lines from hollow-cathode lamps. Spectrochim.Acta 26B,207-235,(1971)

133 Posener,D.W. The shape of spectral lines:Tables of the Voigt profile. Austral.J.Phys. 12,184-196,(1959)

134 Armstrong,B.H. Spectrum line profiles:the Voigt function. J.Quant.Spectrosc.Radiat.Transfer 7, 61-88,(1967)

135 Minkowski,R.and Bruck,H. Wahre und scheinbare Breite von Spektrallinien. ZS.Physik 95,299-301,(1935)

136 Danos,M.and Geschwind,S. Broadening of microwave absorption lines due to wall collisions. Physics Review 91,1159-1162,(1953)

137 Cooper,J.and Greig,J.R. An ultra-rapid scanning Fabry-Perot interferometer. Nature 195,371-372,(1962)

138 Bartley,D.F. Ph.D.Thesis,University of London.(1975)

139 Mansfield,J.M.,Bratzel,M.P.,Norgordon,H.O.,Knapp,D.O., Zacha,K.E.and Winefordner,J.D. Experimental investigation of electrodeless discharge lamps as excitation sources for atomic fluorescence flame spectrometry. Spectrochim.Acta 23B,389-402,(1968)

140 Aldous,K.M.,Dagnall,R.M.and West,T.S. The preparation of electrodeless discharge tubes for some alkali and alkaline earth elements. Anal.Chim.Acta 44,457-460,(1969)

141 Dagnall,R.M.and West,T.S. Some applications of microwave-excited electrodeless discharge tubes in atomic spectroscopy.Applied Optics 7,1287-1294,(1968)

142 Kirkbright,G.F.and Sargent,M. Atomic absorption and fluorescence spectroscopy. Academic Press,London.(1974)

143 Dagnall,R.M.,Silvester,M.D.and West,T.S. Electronic modulation of microwave-excited electrodeless discharge lamps for use in atomic-fluorescence spectrometry. Talanta 18,1103-1109,(1971)

144 Gleason,W.S.and Pertel,R. High stability electrodeless discharge lamps. Rev.Sci.Instrum. 42,1638-1643,(1971)

145 Kleiman,H.and Davis,S.P. Hyperfine structures,isotope shifts,and nuclear moments of Hg^{195},Hg^{195m},and Hg^{194}. J.Opt.Soc.Am. 53,822-827,(1963)

146 Silvester,M.D.and McCarthy,W.J. The intensity of electrodeless discharge lamps containing cadmium, mercury and manganese. Spectrochim.Acta 25B,229-243, (1970)

147 Oliver,D.,Electromedical Supplies (Greenham)Limited. Private communication.(1977)

148 Human,H.G.C.and Butler,L.R.P. High frequency excitation of vapours produced by hollow cathode sputtering. Spectrochim.Acta 25B,647-656,(1970)

149 Mounce,R.P. Ph.D.Thesis,University of London.(1975)

150 Meggers,W.F.,Corliss,C.H. and Scribner,B.F. Tables of Spectral-line Intensities. N.B.S. Monograph 145, Parts 1and2,(1975)

151 Kirkbright,G.F.and Sargent,M. The application of a piezoelectric scanning Fabry-Perot interferometer to the study of atomic line sources.I. Assembly and general application of the instrumental system. Spectrochim.Acta 25B,577-596,(1970)

152 Mitchell,A.C.G.and Zemansky,M.W. Resonance radiation and excited atoms. Cambridge University Press.(1934)

153 Clemmow,P.C.and Dougherty,J.P. Electrodynamics of particles and plasmas. Addison-Wesley,London.(1969)

154 Johnson,C.C. Field and wave electrodynamics. McGraw-Hill,New York.(1965)

155 Stark,J.G.and Wallace,H.G. Chemistry Data Book. John Murray,London.(1970)

156 Gunn,A.M.,Kirkbright,G.F.and Opheim,L.N. Determination of phosphorus in milk powders by optical emission spectrometry with a high frequency inductively-coupled argon plasma source. Analytical Chemistry 49,1492-1493,(1977)

157 Zhiglinskii,A.G.and Kund,G.G. On the spectral determination of the isotopic composition of strontium. Optics and Spectroscopy 7,490,(1959)

158 Heyden,M.and Kopfermann,H. Über die Kernspinänderung beim radioaktiven β-Zerfallsprozess Rb87→Sr87. ZS.Physik 108,232-243,(1938)

159 Shpenik,O.B.,Ovchinnikov,V.L.and Zapesochny,I.P. Resonance radiation excitation with low energy collisions between alkali-earth ions and rare gas atoms. Ukrains'kii Fizichnii Zhurnal 19,1943-1948, (1974)

160 Bombelka,R.M. Ph.D.Thesis,University of London.(1978)

161 Cremers,C.J.and Birkebak,R.C. Application of the Abel integral equation to spectrographic data. Applied Optics 5,1057-1064,(1966)

162 Boumans,P.W.J.M. Theory of Spectrochemical Excitation. Hilger and Watts,London.(1966)

163 Bracewell,R.N. Strip integration in radio astronomy. Aust.J.Phys. 9,198-217,(1956)

164 Bockasten,K. Transformation of observed radiances into radial distributions of the emission of a plasma. J.Opt.Soc.Am. 51,943-947,(1961)

165 Barr,W.L. Method for computing the radial distribution of emitters in a cylindrical source. J.Opt.Soc.Am. 52,885-888,(1962)

166 Lochte-Holtgreven,W. Plasma Diagnostics. North-Holland Publishing Company,Amsterdam.(1968)

167 Scheeline,A. and Walters,J.P. Considerations for implementing spatially-resolved spectrometry using the Abel inversion. Analytical Chemistry 48,1519-1530, (1976)

168 Carnahan,B.and Wilkes,J.O. Digital Computing and Numerical Methods,(with FORTRAN-IV,WATFOR,and WATFIV programming). Wiley,New York.(1973)

169 Schoenberg,I.J. Contributions to the problem of approximation of equidistant data by analytic functions. Quart.Appl.Math.,4,45-99,& 112-141,(1946)

170 deBoor,C. Package for calculating with B-splines. S.I.A.M. J.Numer.Anal., 14,441-472,(1977)

171 Michel,R.G.,Coleman,J.and Winefordner,J.D. A reproducible method for preparation and operation of microwave excited electrodeless discharge lamps: SIMPLEX optimization of experimental factors for a cadmium lamp. Spectrochim.Acta 33B,195-215,(1978)